Mars in the Late Noachian: evolution of a habitable surface environment

by

Sarah Stewart Johnson

M.Sc. Biology, University of Oxford, UK, 2005
B.A. Philosophy, Politics and Economics, University of Oxford, UK, 2003
B.A. Mathematics and Environmental Studies, Washington University in St. Louis, USA, 2001

Submitted to the Department of Earth, Atmospheric, and Planetary Sciences
in partial fulfillment of the requirements for the degree of

Doctor of Philosophy
at the
MASSACHUSETTS INSTITUTE OF TECHNOLOGY

June 2008

© Massachusetts Institute of Technology 2008. All rights reserved.

Author: .....
Department of Earth, Atmospheric, and Planetary Sciences
April 30, 2008

Accepted by: .....
Maria T. Zuber
E. A. Griswold Professor of Geophysics
Thesis Advisor

Accepted by: .....
Thomas A. Herring
Professor of Geophysics
Graduate Officer, Department of Earth, Atmospheric, and Planetary Sciences

[THIS PAGE INTENTIONALLY LEFT BLANK]

Mars in the Late Noachian:
evolution of a habitable surface environment

by

Sarah Stewart Johnson

Submitted to the Department of Earth, Atmospheric and Planetary Sciences
on April 30, 2008, in partial fulfillment of the requirements for the degree of
Doctor of Philosophy in Planetary Sciences

Abstract

This dissertation addresses whether simple life forms might have existed on Mars during the late Noachian epoch, and whether those life forms, or their traces, can be detected today. It begins by analyzing the ancient Martian climate in light of new evidence that sulfur chemistry played a prominent role in the planet's early evolution. It finds that sulfur-induced greenhouse warming could have periodically heated the planet enough to support liquid water, thereby creating warm, wet, clement conditions. Moreover, it finds that those warming pulses, while short-lived over geologic time, may have persisted for hundreds of years. If sulfur helped create environmental conditions capable of hosting life, however, it also created conditions that were adverse to sustaining it. In particular, dissipation of sulfur volatiles cooled the climate, and sulfur rainout contributed to the acidity of Martian surface waters. The dissertation therefore proceeds to analyze the potential for persistence and detection of life in terrestrial environments with Mars-like characteristics. It first investigates the potential for detecting ancient life by searching for lipid biomarkers in sulfur-rich acid salt lakes, concluding that a variety of biomarkers may be more resistant to decay than previously believed. It then analyzes soil samples from permafrost, discovering the oldest independently authenticated viable organisms ever found, and positing low-level metabolic activity and DNA repair as a survival mechanism in ancient cells. Finally, the dissertation uses deep sequencing to examine prokaryotic diversity in a terrestrial Mars-like river characterized by low pH and high concentrations of iron and sulfur, with results considered in light of the implications for life detection approaches incorporating new, *in situ* "PCR in a chip" technology. The dissertation concludes by proposing future work, including the ultimate goal of developing a life detection instrument for Mars.

Thesis Advisor: Maria T. Zuber, Ph.D.
Title: E. A. Griswold Professor of Geophysics

Acknowledgments

And suddenly we are back at Walden Pond, or on the tiny planet of the Little Prince, as poor as church mice and as rich as lords. I count every star in Sagittarius as mine.

-C. Raymo

I am deeply indebted to the following people: Emma Brunskill, a comrade without whom I cannot imagine MIT, Lisha Bai, and John Lavinsky, I stand in the sweep of their orbits; Jim Brennan, for nourishing a young mind; Jim Garvin, for his inspiriting love of planets; and especially Ray Arvidson, for first illuminating Mars; Michael Mischna, Alex Pavlov, Roger Summons, Eske Willerslev, Martin Bay Hebsgaard, Tom Gilbert, Ricardo Amils, and Chris Carr, for lending their acumen to the work that appears in this dissertation; and Roberta Allard, Maya Bhatia, Ying Wu, Deirdre Mask, Sarah Garson, Sinead English, Ingrid Barnsley, Anne Dodge, Chelsea Elander Bodnar, Lippy Goyal, Nanna Jumah, Trine Christensen, Jason Wasfy, Sherry Deckman, Ben Hurlbut, Bernard Mwangi, Scott Lee, Rex Malmstrom, Maurice Bulter, Roberta Bennett-Calorio, Vicki McKenna, Jacqui Taylor, Carol Sprague, Erwan Mazarico, James Dennedy-Frank, Chin-Wu Chen, Einat Lev, Ian Garrick-Bethell, Kyle Bradley, Will Ouimet, Mike Krawczynski, Jay Barr, Noah McLean, Anna Monders, Taylor Schildgen, Doug Jerolmack, Jeff Andrews-Hanna, Pete Girgius, and Lindy Elkins-Tanton, for causerie, and such meaningful support as friends and colleagues. In addition, I would like to thank the sagacious core of young scientists on MER with whom I worked, including Wes Watters, Dave Fike, and Bethany Ehlmann, as well as those who made fieldwork in Antarctica and Western Australia possible, among them, Donal Manahan, John Grotzinger, and Angus Turner. Finally, my humblest gratitude to Antje Duvekot, Aggrey Omondi, Kate Harris, Leslie Kendrick, Sven Birkerts, and Alan Lightman, six of the most astonishing people I know, for sounding the depths of experience and stirring me to do the same.

My greatest acknowledgments, however, go to my advisor, Maria Zuber, my unqualified ideal as a scientist and mentor, for whom I would need another thesis to express my boundless gratitude; Gary Ruvkun, Rick Binzel, Ben Weiss, and Tim Grove, who round out my discerning, generous committee; my illimitable grandmother, Jean Johnson; my treasured parents, John and Kate Johnson; and my sister Emily, who has my whole heart.

-S.S.J.

Table of Contents

Chapter 1 – Introduction

Chapter 2 – Sulfur-induced greenhouse warming on early Mars

Chapter 3 – Longevity of SO_2 in the ancient Martian atmosphere: implications for transient greenhouse warming

Chapter 4 – Biomarker preservation in ephemeral acid saline lakes: implications for Mars

Chapter 5 – Ancient bacteria show evidence of DNA repair

Chapter 6 – Prokaryotic diversity in Spain's Red River: lessons for life detection on the Red Planet

Chapter 7 – Conclusion

List of Tables and Figures

Chapter 1 – Introduction

Chapter 2 – Sulfur-induced greenhouse warming on early Mars

Chapter 3 – Longevity of SO_2 in the ancient Martian atmosphere: implications for transient greenhouse warming

Chapter 4 – Biomarker preservation in ephemeral acid saline lakes: implications for Mars

Chapter 5 – Ancient bacteria show evidence of DNA repair

Chapter 6 – Prokaryotic diversity in Spain's Red River: lessons for life detection on the Red Planet

Chapter 7 – Conclusion

No tables or figures.

[THIS PAGE INTENTIONALLY LEFT BLANK]

Chapter 1

Introduction

1.1 Context and chapter outline

This dissertation sits at the nexus of planetary science and biology, probing the prospects for habitability in the late Noachian epoch on Mars, and for the detection of life or its traces on Mars today. The first half of the dissertation draws upon petrology, geomorphology, radiative transfer and photochemistry to analyze the role the element of sulfur played in the late Noachian atmosphere. The second half of the dissertation scrutinizes habitability in the ancient Martian surface environment. From the sulfur-rich acid salt lakes of the Yilgarn Craton and the permafrost soils of the Kolyma Lowlands to the Rio Tinto Basin, an acidic river in the Iberian Pyritic Belt in Southwest Spain, the research examines the nature of life in Mars-like conditions, particularly its preservation, survival, and prospects for detection. Interwoven throughout the dissertation's seven chapters is the element of sulfur, fast emerging as a component of any comprehensive explanation of the ancient Martian atmosphere and surface environment, as well as the prospects for life therein.

1.1.1 A sulfur-rich environment on ancient Mars

For someone who hopes to find life on Mars to focus her research on the element of sulfur begets a certain irony: for much of history, sulfur has been associated not with life,

but with death. It was used as the base of a fumigant and bleaching agent in Pre-Roman civilizations, it appears in English translations of the Bible as "brimstone," and it was referenced in Homer's Odyssey as an insecticide and "purifier of sick rooms." This association started to fade in the late 19th Century, however, when one of the founders of microbiology, Sergei Winogradsky, demonstrated sulfur's life-sustaining role in certain classes of bacteria [*Ackert*, 2006]. In the 120 years since, as our understanding of microbial metabolism has advanced, sulfur has emerged as a multifaceted and far-reaching component of complex biological systems. Capable of existing in an exceptionally broad range of oxidized and reduced states, sulfur provides organisms with ample opportunities to harvest energy, the most elemental task for any life form. The element has proven to be particularly beneficial in anaerobic environments such as hydrothermal vents, deep marine sediments, and the subsurface biosphere. For example, there are clues suggesting that the biosphere flourishing deep in the Earth's crust, home to 10 to 66% of Earth's microbial population, may thrive off the reduction of sulfate via oxidation of iron [*D'Hondt, et al.*, 2004; *Schippers, et al.*, 2005]. Despite a century of research, however, the role of sulfur in sustaining simple life, both on Earth and possibly elsewhere, remains largely unexplained.

The data from recent NASA missions indicate that Mars is also an anaerobic, sulfur-rich world: a place that was periodically warm and wet in the late Noachian period of Martian history, roughly 3.7 to 4 billion years ago (see Figure 1.1). During that time period, the Martian hydrologic cycle radically altered the landscape: water flowed across the surface

of Mars, cutting the river valleys and outflow channels that are visible today. At present, however, the surface of Mars is dry, cold, and incapable of supporting liquid water. The mechanisms of this dramatic climate change remain uncertain. Many planetary scientists have tried to simulate early atmospheric conditions, but the most prominent models have failed to make the surface warm enough using carbon dioxide alone to sustain the liquid water necessary for the observed hydrology-related geologic features to form. Even when the models assume 1000 times the amount of CO_2 we have on Earth, they result in insufficient greenhouse warming, in part because Mars is farther from the sun and because the sun may have been less bright in the distant past [*Gulick*, 1997; *Kasting*, 1991; 1997; *Pollack*, 1987; *Postawko*, 1986].

There is, however, a growing body of evidence from recent Mars exploration missions suggesting that sulfur chemistry may have played a prominent role in the planet's early evolution. My thesis begins by integrating this evidence into previous efforts to explain the evidence for a warm, wet surface environment on ancient Mars. Although the thin Martian atmosphere contains virtually no sulfur species at present, both soils and rocks observed by landed missions have very high sulfur abundances. Isotopic analyses in Martian meteorites further support the idea that the sulfur detected at the surface first underwent atmospheric chemical reactions prior to surface deposition [*Farquhar*, 2000]. These recent discoveries are intriguing because sulfur volatiles emitted from volcanoes can act as powerful greenhouse gases, absorbing at wavelengths complimentary to CO_2

and driving climate change during periods of enhanced volcanic activity [*Postawko*, 1986].

My work hypothesizes that pulses of sulfur volatiles into the Martian atmosphere from volcanic activity could have given rise to short-lived periods of clement environmental conditions on late Noachian Mars. The possibility of these warm, wet periods is particularly intriguing because the late Noachian period on Mars coincides with a time period when the first protocells were evolving on Earth [*Knoll, et al.*, 2005]. Many have assumed that the physical similarity of Earth and Mars during this period, particularly the weakly reducing atmosphere, protective magnetic field and silicate mantle structure, are reasons to believe that Mars, too, may have hosted life; similarity of climate during the relevant time period would provide another such reason.

Chapters 2 and 3 address these topics. Using a theoretical model, Chapter 2 investigates the solubility of sulfur in Martian magma, which is directly tied to the amount of sulfur volatiles available for release to the atmosphere during volcanic degassing, and then proceeds to investigate the sulfur volatile levels that could be reached in the Martian atmosphere and the subsequent implications for greenhouse warming. Tremendous amounts of volcanism occurred before the end of the late Noachian, and the gases released from the magma associated with this volcanism certainly affected the early climate. Yet it remains unclear to what extent gases deep within igneous provinces could have been released to the atmosphere. For this reason, I explore the climatic

consequences of large, discrete, near-surface volcanic events. Orbital reconnaissance shows recognizable topographic features that correspond to places where magma was once rapidly emplaced near the surface [*Wilson*, 2002]. The associated volumes of magma are estimated after making some basic assumptions from geophysics. That amount of near-surface magma together with the amount of soluble sulfur in Martian magma gives an estimate of total sulfur volatiles that could have been directly released to the atmosphere. I further assume that these amounts will be well mixed over the planet within a short time in comparison to the lifetimes of the gases. This method allows me to take a "snapshot" of the atmosphere shortly after the volcanic event takes place and analyze the extra greenhouse warming caused by these pulses of sulfur volatiles. To calculate the magnitude of the warming, I use a three-dimensional global circulation model adapted for Martian conditions. Surface temperature results indicate extra heating from sulfur volatiles of up to 25 Kelvin, and even higher if water vapor feedback effects are included. The resulting surface temperatures on Mars create localized conditions conducive to the presence of liquid water.

Chapter 3 investigates how long these sulfur volatile warming pulses may have lasted in the early Martian atmosphere. I use a one-dimensional photochemical model adapted from a previous study of sulfur volatiles in Earth's early atmosphere. While photochemistry research to date has concentrated on current Martian conditions, my work examines the ancient Martian atmosphere, which was thicker, warmer, and more reducing than the current regime. After validating the model against other photochemical models,

I conclude that sulfur dioxide could have persisted in the ancient atmosphere for at least hundreds of years, generating short but potent warming episodes following an episode of volcanic activity.

1.1.2 Finding ancient life

If sulfur helped create environmental conditions capable of hosting life, it also created conditions that were adverse to sustaining it. As sulfur species were removed from the atmosphere, most likely in the form of SO_2 rainout, they would have strongly affected surface waters, generating highly acidic conditions and precluding the formation of carbonates. In addition, the warm, wet surface environment caused by sulfur-induced greenhouse warming may only have persisted for hundreds of years; at most, they lasted until the end of the late Noachian epoch, when Mars likely lost its core dynamo and protective magnetic field, and much of its volcanic activity subsided. By the Hesperian epoch, cold, dry steady state conditions dominated Mars' climate, and the atmosphere was slowly sputtered away by the solar wind. What remains is the planet we see today.

If life began but did not survive on Mars, it may still be detectable in the acidic, sulfur-rich surface environments predicted by sulfur-induced greenhouse warming. Of the many life detection techniques proposed for Mars, searching for organic material has emerged as one of the optimal methods for finding evidence of extinct life. This effort centers on the search for lipid biomarkers, which are organic compounds derived from living organisms found in rocks and sediments. Unlike other biomolecules that degrade

quickly, such as nucleic acids, traces of lipids from ancient organisms can be preserved over geologic time [*Brocks, et al.*, 1999]. Moreover, the majority of sedimentary organic matter reflects highly characteristic biological processes, lessening the difficulty presented by abiotic routes to these biomarkers.

A chief criticism of the lipid biomarker approach for Mars comes from the field of thermodynamics, which predicts poor preservation in acidic, oxidizing environments like that at Meridiani Planum, the Opportunity landing site. There, we see evidence for an ancient aqueous biosedimentary system that was characterized by high acidity and salinity in the late Noachian. To evaluate this criticism, I assay sediments from highly acidic natural salt lakes, which are rare in terrestrial settings, for their lipid biomarker compositions. My work suggests a variety of organic compounds, including those from dead organisms, remain in these environments, thereby furthering the debate about the search for organic matter in Martian evaporite deposits.

Chapter 4 begins by describing the sulfur-rich acid saline basins in the vicinity of Norseman, Western Australia. I use two independent analytical methods to extract and quantify lipid residues, both of which identify biomarkers from the indigenous microbial population as well as biomarkers from dead vascular plant material, swept in from the catchment areas associated with the lakes. Given that microbial and plant lipids have similar chemistries, it is unlikely that this outcome reflects a preservational bias. My

findings demonstrate that fossil lipids, in general, are surprisingly stable in the oxidizing and acidic saline sediments represented by these environments.

1.1.3 Survival under duress

Perhaps more intriguing than searching for signs of fleeting life on Mars, however, is the possibility that life survived long enough to begin adapting to the Martian environment. To do so, ancient organisms would have had to survive the long-lasting intervals of cold, dry conditions that would have prevailed between warming periods. Numerous scientists have posited long-term microbial survival, but they do not agree on the mechanism by which it can occur [*Cano*, 1995; *Fish*, 2002; *Vreeland*, 2000]. While the favored explanation for the survival of ancient cells has centered on dormancy, recent claims of cultivable ancient bacteria within sealed environments have highlighted our limited understanding of the mechanisms behind long-term cell survival. Specifically, it has remained unclear how processes like sporulation can cope with spontaneous genomic decay over geological timescales. My work with bacteria in Siberian permafrost suggests that low-level metabolic activity and DNA repair, as opposed to the alternative explanation that cells enter a state of dormancy under conditions of stress, allows cells to survive under cold, desiccated conditions for up to half a million years. This is of particular interest given that results from neutron and gamma-ray spectroscopy aboard the Mars Odyssey orbiter suggest that water ice is widespread on Mars, comprising several percent of at least top meter of the surface [*Feldman, et al.*, 2002; *Mitrofanov, et al.*, 2002].

Chapter 5 addresses the survival of life over geologic timescales. I use strict protocols and new metabolic methods to address the questionable existence of ancient cells in permanently frozen sediments here on the Earth. I find that ancient cells not only exist but also can remain in a metabolically active state repairing their DNA for at least 400,000 to 600,000 years. This work documents the oldest independently authenticated DNA ever reported from viable cells in isolated environments and suggests intriguing possibilities for the survival of life within permafrost and ice on Mars.

1.1.4 Finding existing life

While probing for lipid biomarkers is perhaps the most conservative way to look for life, a far greater scientific yield could come from the application of new, precision technologies to the search for life on Mars. One exciting new approach is a NASA instrument prototype being developed by the Search for Extraterrestrial Genomes (SETG) Project [*Ruvkun, et al.*, 2002] that incorporates genetic amplification, sequencing, and analysis technologies originally developed for the health sciences industry. If microbial life adapted to environmental change and is still present at low levels today, the SETG approach promises considerable gains in sensitivity and specificity for certain life detection approaches, and could greatly increase the chances of finding and identifying Martian life. This approach utilizes microfluidic "PCR in a chip" technology that enables hundreds of DNA fragments to be sequenced in wells only a few microns in width. By returning genetic sequences, the instrument could virtually eliminate false positive

results: sequence data from likely contaminates would be immediately identified, whereas any system of life isolated from that on Earth over geologic time would be evident from phylogenetic analysis. In addition, this technique is superior to others for its single molecule sensitivity and ability to recognize contamination. Moreover, the applicability of these techniques, which are useful only for RNA/DNA-based life forms, is consistent with an increasingly tenable "shared-ancestry" hypothesis.

Central to the use of the SETG approach is the hypothesis that life on Earth and Mars share a common ancestor. This hypothesis is not unlikely; indeed, the probability of a common ancestor seems at least as high, if not radically higher, than the alternative of two independent geneses. Evidence from magnetization studies increasingly shows that viable microbes could have been transferred well below sterilization temperatures to or from Mars during the late Noachian [*Weiss, et al.*, 2000]. Once life had evolved on one of the planets, the rate of material transfer makes it plausible that the adjacent planet could "catch" life rather than independently evolving it. Moreover, microbial life has been discovered here on Earth at extremes of temperature and radiation, demonstrating the significant adaptability of microbes and reducing the likelihood that extreme environmental stress would fully sterilize a planet.

In Chapter 6, I consider this new life detection approach vis-à-vis a "training set" of phylotypes detected in the Mars-like chemistry of the Rio Tinto Basin in southwestern Spain, a terrestrial analog for the sulfur-rich early Martian environment. Much as we

might expect for early Mars, the microbial population at Rio Tinto harvests energy from chemical gradients created by the elements iron and sulfur. I perform deep sequencing, collecting more sequence data from prokaryotic organisms than have been collected from any single sampling site at Rio Tinto before, and I discuss the implications of my results for the SETG instrument being pioneered for use in a life detection platform on a future Mars mission.

At different points, this dissertation draws upon the results of missions such as Mars Global Surveyor, the Mars Exploration Rovers, Mars Odyssey, Mars Reconnaissance Orbiter, and Mars Express. What has emerged from recent exploration is an entirely new vision of Mars in the ancient past. My work not only helps us understand the history of climate change and the evolution of the surface environment on early Mars, it prompts us to look forward to results from the next generation of Mars spacecraft. Perhaps what will emerge in coming years is yet another vision of our near neighbor, one more similar to Earth than we think… perhaps even one that harbors, or once harbored, life.

1.2 References

Ackert, L. (2006), The Role of Microbes in Agriculture: Sergei Vinogradskii's Discovery and Investigation of Chemosynthesis, 1880-1910, *Journal of the History of Biology*, *39*, 373-406.

Brocks, J. J., et al. (1999), Archean Molecular Fossils and the Early Rise of Eukaryotes, *Science*, *285*, 1033-1036.

Cano, R. J. a. M. K. B. (1995), Revival and identification of bacterial spores in 25-million-year-old to 40-million- year-old Dominican amber, *Science 268*, 1060–1064.

D'Hondt, S., et al. (2004), Distributions of Microbial Activities in Deep Subseafloor Sediments, *Science*, *306*, 2216-2221.

Farquhar, J., J. Savrino, T. L. Jackson, and M. H. Thiemnes (2000), Evidence of atmospheric sulphur in the Martian regolith from sulphur isotopes in meteorites, *Nature*, *404*, 50-52.

Feldman, W. C., et al. (2002), Global Distribution of Neutrons from Mars: Results from Mars Odyssey, *Science*, *297*, 75.

Fish, S. A., T. J. Shepard, T. J. McGenity and W. D. Grant (2002), Recovery of 16S ribosomal RNA gene fragments from ancient halite. , *Nature 417*, 432-436.

Gulick, V. C., D. Tyler, C. P. McKay, and R. M. Haberle (1997), Episodic ocean-induced CO_2 greenhouse on Mars: Implications for fluvial valley formation, *Icarus*, *130*, 68-86.

Kasting, J. F. (1991), CO_2 condensation and the climate of early Mars, *Icarus*, *94*, 1-13.

Kasting, J. F. (1997), Warming early Earth and Mars, *Science*, *276*, 1213-1215.

Knoll, A. H., et al. (2005), An astrobiological perspective on Meridiani Planum, *Earth and Planetary Science Letters*, *240*, 179-189.

Mitrofanov, I., et al. (2002), Maps of Subsurface Hydrogen from the High Energy Neutron Detector, Mars Odyssey, *Science*, *297*, 78.

Pollack, J. B., J. F. Kasting, S. M. Richardson, and K. Poliakoff (1987), The case for a wet, warm climate on early Mars, *Icarus*, *71*, 203-224.

Postawko, S. E., and W. R. Kuhn (1986), Effect of the greenhouse gases (CO_2, H_2O, SO_2) on Martian paleoclimate, *J. Geophys. Res.*, *91*, D431-438.

Ruvkun, G., et al. (2002), A Robotic-PCR Detector for DNA-based Life on Other Planets, in *Signs of Life: A Report based on the April 2000 Workshop on Life Detection Techniques*, edited, pp. 137-140, Space Sciences Board, The National Academies Press, Washington, DC.

Schippers, A., et al. (2005), Prokaryotic cells of the deep sub-seafloor biosphere identified as living bacteria, *Nature*, *433*, 861-864.

Vreeland, R. H., W. D. Rosenzweig, and D. W. Powers (2000), Isolation of a 250 million-year-old halo-tolerant bacterium from a primary salt crystal, *Nature 407*, 897-900.

Weiss, B. P., et al. (2000), A Low Temperature Transfer of ALH84001 from Mars to Earth, *Science*, *290*, 791-795.

Wilson, L., and J. W. Head, III (2002), Tharsis-radial graben systems as the surface manifestation of plume-related dike intrusion complexes: models and implications, *J. Geophys. Res.*, *107*, 5057.

1.3 Figures

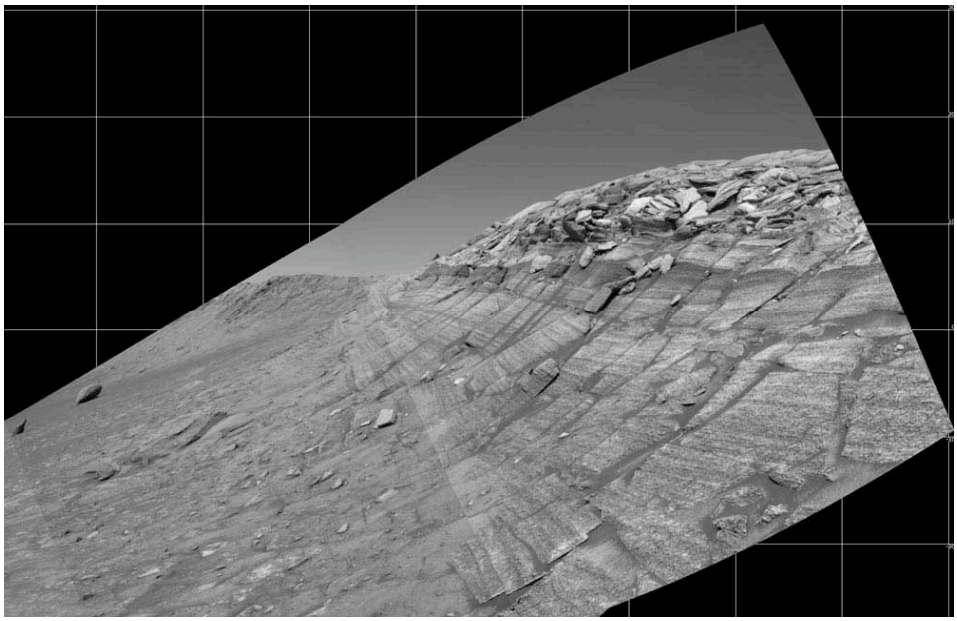

Figure 1.1. The Mars Exploration Rovers analyzed layered sedimentary rocks, such as this sulfate-rich section at Burns Cliff, to discover that Mars was characterized by ancient acidic aqueous weathering in at least some regions during the late Noachian.

[THIS PAGE INTENTIONALLY LEFT BLANK]

[THIS PAGE INTENTIONALLY LEFT BLANK]

Chapter 2

Sulfur-induced greenhouse warming on early Mars[1]

2.0 Abstract

Mineralogical, geological, geophysical and isotopic data recently returned from Mars suggest that the delivery of sulfur gases to the atmosphere may have played a significant role in the planet's early evolution. Using the Gusev Crater basalt composition and a batch melting model, we obtain a high sulfur solubility, approximately 1400 ppm, in Martian mantle melts. We proceed to explore different scenarios for the pulsed degassing of sulfur volatiles associated with the emplacement of near-surface dikes during the late Noachian or early Hesperian, when surface pressures are thought to be substantially higher than present. We investigate background Martian atmospheres of 50 and 500 mb CO_2 with varying abundances of H_2O and sulfur volatiles (H_2S and SO_2 mixing ratios of 10^{-3} to 10^{-6}). Results suggest that these sulfur volatile influxes, alone, could have been responsible for greenhouse warming up to 25 K above that caused by CO_2. Including additional water vapor feedback, this process could have raised the early surface temperature above the freezing point for brines and possibly allowed transient liquid

[1] This chapter was accepted at the *Journal of Geophysical Research – Planets* on February 28, 2008.

Johnson, S.S., M.A. Mischna, T.L. Grove, and M.T. Zuber, "Sulfur-related greenhouse warming on early Mars," Journal of Geophysical Research, *in press*.

water on the Martian surface. Each temperature rise was likely to have been short-lived, however, due to brief residence times for sulfur volatiles in an optically thin atmosphere.

2.1 Introduction

The present geology of Mars points to the existence of a thicker, warmer atmosphere in the past. Climate change is best evidenced by the early age and distribution of dendritic valley networks and interior channels within these valley networks as well as geologic indicators of much higher erosion rates in ancient Martian history, such as degraded Noachian-aged craters [*Fanale et al*., 1992; *Catling*, 2005]. Some have postulated the existence of a large ocean in the Northern Plains [*Baker et al*., 1991; *Clifford and Parker*, 2001]. Mars Orbiter Laser Altimeter data suggest that the innermost of two proposed shorelines forms an approximately equipotential surface [*Head et al.*, 1999], and *Perron et al.* [2007] propose that, coupled with the resistance of Mars' elastic crust, true polar wander over the past two to three billion years can account for much of the shorelines' topographic variation. The smoothness of the lowlands also may be explained by fluvially transported sediments [*Aharonson et al*., 1998]. Others suggest that more sporadic climate variations led only to ephemeral rivers and lakes, or simply near-surface groundwater with multiple recharge events [*Segura et al*., 2002]. At the Opportunity landing site, the sedimentary and mineralogical features associated with a sulfate-rich stratigraphic section at least seven meters in thickness suggest that water was present episodically for at least thousands of years [*Knoll et al.,* 2005], with no less than four

distinct recharge episodes [*McLennan et al.,* 2005]. Orbital data indicate that this geological unit, associated with aeolian and shallow water deposition, and likely to be late Noachian or early Hesperian in age, extends over several hundred thousand square kilometers and reaches up to 800 m in thickness [*Hynek et al.*, 2002; *Arvidson et al.*, 2003, 2005].

An increasing body of evidence from recent Mars exploration missions suggests that sulfur chemistry may have played an important role on early Mars. Although the Martian atmosphere contains virtually no sulfur species at present (upper limit = 0.1 ppm), all soils observed by landed missions have duricrust with enhanced sulfate abundances of 3-10% sulfate [*Maguire*, 1977; *Settle*, 1979; *Owen et al.*, 1992; *Squyres et al.*, 2004]. Sulfate abundances in outcrops have been detected at even higher levels. Mg-sulfates are estimated to constitute up to the 30% of the Meridiani Planum landing site outcrop [*Wänke et al.*, 2001; *Feldman*, 2004], and the OMEGA hyperspectral imager aboard Mars Express has identified kieserite, gypsum and polyhydrated sulfates on localized layered terrains that extend well beyond these landing sites [*Gendrin et al.*, 2005]. The visible/infrared spectrometer aboard Mars Reconnaissance Orbiter, CRISM, has targeted many of these hydrated sulfate deposits for further analyses [*Roach*, 2007; *Poulet*, in preparation]. Most sulfate-rich deposits correspond to freshly exhumed surfaces that can be dated to the Noachian and/or Hesperian epochs. The layered deposits where OMEGA sees evidence for hydrated sulfates occupy a few percent of the equatorial to mid-latitude

regions; these deposits are on the order of a few hundred meters thick, containing roughly 20 to 30 percent sulfate [*Arvidson*, 2006].

The SNC meteorites (shergottites, nakhilites and chassignites— basaltic, achondritic meteorites believed to have originated from Mars) contain sulfur, and isotopic sulfur data from the meteorites reflect deposition of sulfur species produced by atmospheric chemical reactions [*Farquhar et al.*, 2000]. Sulfur isotope measurements of oxidized and reduced sulfur reveal mass-independent fractionation, indicating that dynamic atmospheric chemistry has strongly contributed to the history of the Martian sulfur cycle and suggesting an important role for sulfur volatiles and sulfate aerosols in Martian history [*Farquhar et al.,* 2000].

Sulfur volatiles, in the form of SO_2 and H_2S, act as powerful greenhouse gases and may have been important atmospheric components during periods of enhanced volcanic activity on Mars [*Postawko and Kuhn*, 1986; *Settle*, 1979]. Sulfur volatiles have also been suggested as serving a useful secondary role in warming early Mars; the presence of small amounts of SO_2 in the middle atmosphere may have kept temperatures warm enough to prevent CO_2 condensation, allowing for both a thicker CO_2 atmosphere and less reflectance of solar energy back to space [*Yung et al.,* 1997]. Without sulfur volatiles, many atmospheric models have struggled with two related problems: 1) creating the necessary warming for liquid water stability with CO_2 alone, and 2) explaining the lack of carbonate deposition. Regarding the first problem, *Kasting* [1991]

finds that a dense early CO_2 atmosphere could not warm early Mars sufficiently to allow aqueous surface features without additional, complementary greenhouse gases, and *Postawko and Kuhn* [1986] found that even three bars of CO_2 would not provide sufficient warming to reach melting temperatures. Concerning the second problem, while carbonate platforms would be expected in abundance with a CO_2-rich atmosphere and an aqueous surface environment, none have been detected on the surface of the planet. Orbital Thermal Emission Spectrometer (TES) data constrain carbonate abundance in Martian dust to 1-2 wt% [*Bandfield*, 2002]. The discovery of the mineral jarosite, $(Na,K)Fe_3(SO_4)_2(OH)$, by Opportunity at Meridiani Planum indicates the presence of ancient acidic conditions on Mars, which could have prevented the deposition of carbonate, despite the fact that expected weathering reactions with widespread surface basalt layers would have served to buffer pH. This conclusion requires a source for surface acidity over Martian history.

It has been proposed that outgassed sulfur species, and the subsequent formation of sulfuric acid aerosols in the atmosphere, may have been responsible for, *inter alia*: 1) producing ubiquitous sulfur-rich dust and globally dispersed sulfate platforms, 2) creating the low pH levels of 2-4 that are suggested by the presence of jarosite, preventing carbonate deposition, and 3) generating relatively clement climatic conditions that allow for liquid water and brines at the surface of Mars via potent but short-lived greenhouse warming (see [*Settle*, 1979; *Postawko and Kuhn*, 1986; *Blaney,* 1996; *Halevy et al.*, 2007]). A Martian history with significant sulfur outgassing may explain recent mission

findings more comprehensively than theories in the literature which invoke: 1) an extremely thick (multiple bar) CO_2 atmosphere [*Pollack et al.,* 1997; *Gulick et al.,* 1997], a CH_4-rich atmosphere [*Kasting*, 1997] or an NH_3-rich atmosphere with shielding by an organic haze layer [*Sagan and Chyba*, 1997] as the source of greenhouse warming; 2) near global coverage of scattering CO_2 ice clouds [*Forget and Pierrehumbert,* 1997*; Mischna et al.,* 2000]; 3) impacts as the source of heat for short-lived aquifer recharge [*Segura et al.,* 2002]; 4) weathering without the presence of liquid water at the rock-atmosphere interface over hundreds of millions of years as the source of surface evaporites [*Banin*, 2005]; 5) mechanical mixing of subsurface salts, brines and ices from large impact events as the source of the Burns Formation material in Meridiani Planum [*Burt et al.,* 2005]; or 6) aqueous oxidation of volcanic iron sulfides pyrite and pyrrhotite as the source of sulfate minerals [*Zolotov and Shock*, 2005]. What follows is the first model that has been created to account for both sulfur delivery to the early atmosphere of Mars and its subsequent atmospheric warming effects. We show in a feasibility demonstration that sulfur volatiles may have been key to warming the early Martian atmosphere.

2.2 Sulfur solubility in Martian mantle melts

2.2.1 Batch melting model

A batch melting model, in which decompression melting of the mantle takes place with the solid residue staying with the melt during most of its ascent, is used to assess the

sulfur solubility in Martian silicate melts in equilibrium with metal sulfide. Regardless of ascent velocity and melt fraction volume, magma from mantle source regions in this model will arrive at the base of the lithospheric lid undersaturated in sulfur. This is due to the unique negative pressure dependence for sulfur solubility that dominates the positive temperature dependence in systems that contain FeO [*Holzheid and Grove*, 2002].

At the base of the lithospheric lid, a final equilibration will take place before the liquid melt is advected to the planet's surface. While significant cooling in passage through the crust would affect the Sulfur Solubility Limit (*SSL*), here we assume that chemical and thermal halo effects insulate the magma along cracks and in magma chambers.

To calculate the *SSL* in liquid silicate conditions, *Mavrogenes and O'Neill* [1999] used the equation:

(1) $$\ln(SSL) = \frac{A}{T} + B + C\left(\frac{P}{T}\right) + \ln a_{FeS}^{sulfide},$$

where $a_{FeS}^{sulfide}$ is the activity of FeS in metallic sulfide, and constants A, B and C are derived from a fit to experimental data. The sulfur content in the silicate liquid is in ppm, temperature, T, in Kelvin, and pressure, P, in bars. *Holzheid and Grove* [2002] adapted the equation from *Mavrogenes and O'Neill* [1999] by adding an additional parameter to assess the further dependence of sulfur solubility on the silicate liquid composition:

(2) $$\ln(SSL) = \frac{A}{T} + B + C\left(\frac{P}{T}\right) + D \cdot nbo / t + \ln a_{FeS}^{sulfide},$$

where *nbo*/*t* is the ratio of non-bridging oxygen anions to tetrahedrally coordinated cations in the silicate; it is a measure of the degree of polymerization in the silicate melt structure. The value of $a_{FeS}^{sulfide}$ is taken to be ~ 1 as metallic sulfides are close to stoichiometric FeS in the experimental data [*Holzheid and Grove*, 2002].

The empirically-derived parameters (*A*, *B*, *C* and *D*) are found by means of a nonlinear least squares regression of the sulfur solubility limits in liquid silicate from experimental data as a function of *T* (over the range 1573 to 1873 K), *P* (over the range 9 to 27 kbar) and *nbo*/*t* (over the range 0.46 to 1.62). These values in Equation 2 are found to be –7714, 11.90, -0.038 and 0.368 for *A*, *B*, *C* and *D*, with standard deviations of 2582, 1.65, 0.012 and 0.169, respectively [*Holzheid and Grove*, 2002].

2.2.2. Calculating sulfur solubility

Alpha Particle X-ray Spectrometer (APXS) data from abraded, dark, vesicular basaltic rocks at the Spirit landing site in Gusev Crater are consistent with primitive basalts, with an average of 11 wt% MgO [*McSween et al.*, 2006]. Furthermore, laboratory experiments performed by *Monders et al.* [2007] on a basalt of a composition averaged from the unaltered Gusev basalts document a three-phase multiple saturation of olivine + orthopyroxene + spinel near the liquidus at 10 kbar and 1583 K. This result, at a point

equivalent to a pressure depth of approximately 80 km, suggests the Gusev basalts either were generated or were last in equilibrium with mantle minerals not far below the approximately 50 km thick crust [*Zuber*, 2001].

The primitive mantle compositions derived from the unaltered Gusev basalt composition are given in Table 2.1 for APXS targets Adirondack, Humphrey and Mazatzal. The compositional results were originally reported by *Gellert et al.* [2004], but the percentages in Table 2.1 reflect corrections made subsequent to new instrument calibrations completed in early 2005 [*McSween et al.*, 2006].

We calculate an average value for *nbo/t* by using Equations 3, 4 and 5 [*Mills*, 1993; *Mysen*, 1988]:

(3) $$Y_{NB} = \sum \begin{bmatrix} x(\mathrm{SiO_2}) + x(\mathrm{TiO_2}) + x(\mathrm{Al_2O_3}) + x(\mathrm{Cr_2O_3}) \\ + x(\mathrm{FeO}) + x(\mathrm{MnO}) + x(\mathrm{MgO}) + x(\mathrm{CaO}) \end{bmatrix},$$

(4) $$X_T = \sum \left[\frac{x(\mathrm{SiO_2})}{2} + \frac{x(\mathrm{Al_2O_3})}{1.5} \right],$$

(5) $$nbo/t = \left(\frac{1}{X_T} \right) \left(2Y_{NB} - 4X_T \right),$$

where x is the mole fraction of the respective constituent.

The resulting *nbo*/*t* value, 1.26, can be substituted into Equation 2 along with the previously listed constants for A, B, C and D, and T = 1583 K and P = 10 kbar. The resulting sulfur solubility at the 80 km depth equilibration region, as suggested by the *Monders et al*. [2007] experiments, is 1407 ppm.

The 15 kbar anhydrous partial melting experiments of *Bertka and Holloway* [1994] at 1633 K on an iron-rich spinel lherzolite also simulated a Martian mantle composition as inferred from *Dreibus and Wänke* [1985]. Parallel calculations result in a broadly similar sulfur solubility of 1699 ppm. In addition, a number of effects not considered here may also serve to increase the release of sulfur volatiles and associated warming effects. Preliminary petrologic experiments suggest that the addition of a few weight percent of water to the melt could increase sulfur solubility by up to 50% [*Grove*, unpublished data].

The melting of metal sulfide, forming immiscible blebs of FeS, occurs approximately 400 K below the beginning of melting of the silicate mantle. Because the negative pressure dependence of sulfur solubility is more significant than its positive temperature dependence, adiabatic ascent will lead to sulfur undersaturation of a formerly sulfur-saturated magma [*Holzheid and Grove*, 2002]. When decompression melting commences in the batch-melting model, sulfur from these immiscible metal sulfide blebs will begin, and continue, dissolving directly into the silicate melt. The remaining metal sulfide will largely be left behind as the final equilibration takes place and melt is extracted at the

base of the lithospheric lid. As surface temperature and pressure conditions are well beneath the vapor saturation pressures for both H_2S and SO_2 [*Lemmon et al.*, 2005], we assume that all 1407 ppm of soluble sulfur are released from the magma directly to the atmosphere. With an estimate for the sulfur concentration in Martian magma, we proceed now to estimate the sulfur volatile amounts potentially released by volcanic degassing.

2.3 Volcanic release of sulfur volatiles

The Tharsis igneous province is estimated to contain $3x10^8$ km^3 of solidified magma. Volatile degassing associated with the formation, thought to be largely complete by the end of the Noachian, certainly affected the early Martian climate [*Phillips et al.,* 2001], yet it remains unclear to what extent the more deeply intruded magma in the Tharsis province may have communicated with the surface. Had magma been emplaced uniformly at a continuous rate, the impact of the sulfur species in the atmosphere is less likely to have had significant implications for warming over the late Noachian. Some abrupt, catastrophic volcanism events, however, are consistent with the current understanding of the surface geomorphology on Mars. For these reasons, we explore the consequences of sulfur volatiles on climate following large, discrete volcanic events associated with dike emplacement features as interpreted by orbital reconnaissance.

Analyzing near-surface dike intrusions associated with Tharsis-radial graben, *Wilson and Head* [2002] estimate that a single giant dike intruded radial to a Tharsis volcano could inject up to 60,000 km^3 of magma over a timescale on the order of days. Under a different set of assumptions, *Hanna and Phillips* [2006] and *Andrews-Hanna* [2007a] suggest a minimum emplacement volume of 1500 km^3 associated with some of these features. We examine volatile pulses associated with both a lower bound "Andrews-Hanna" model and an upper bound "Wilson" model. For the purposes of our model, we assume that sulfur volatile release occurs within the first few weeks of the simulation. Although the majority of this volcanism is intrusive, gases are thought to segregate up to the top of these dikes forming collapse craters and/or creating the necessary pressure to generate explosive eruptions, as was likely in the Memnonia Fossa region [*Scott and Wilson*, 2002]. Convective overturn in wide dikes (>100 m) is also thought to enhance this process of rapid volatile release. It is important to note that there would have certainly been flood basalt eruptions of similar magnitudes, presumably also driven by mantle plumes, on early Mars. We focus on giant dike swarm formation as it allows us estimate with more specificity the total magma emplacement in a single event. It is interesting to note that *Thordarson and Self* [2003] found that the largest lava flow in recorded history, the 1783-1784 flood basalt eruption associated with the Laki volcanic fissure in Iceland, released 15 km^3 of basalt and 122 megatons of SO_2 into the atmosphere over a period of 8 months, with nearly half released in the first six days. This proportion of sulfur release is within a factor of two of our estimate for Mars.

The density of the Gusev basalt magma is calculated to be 2820 kg/m^3 [*Greeley et al,* 2005], using the method of *Bottinga and Weill* [1970] with the parameters of *Mo et al.* [1982]. In our atmospheric calculations, we consider the range of exsolved volatiles associated with a pulse of 1500 km^3 to 60,000 km^3 of magma emplacement: 1.19x10^{13} to 4.76x10^{14} kg of SO_2 or 6.32x10^{12} to 2.53x10^{14} kg H_2S. These correspond to the mixing ratios listed in Table 2.2.

We examine both SO_2 and H_2S endmembers in our simulations of greenhouse warming. Analysis of shergottite meteorite data suggests that the mantle source of Martian basalts had a redox state within one log unit of the iron-wüstite buffer [*Wadhwa*, 2001]. As the magma may remain buffered by the mineral assemblages through its ascent to the surface, part of the sulfur could have been released to the atmosphere with an oxidation state of –2, forming H_2S. Yet, SO_2 is a likely intermediate in the process of sulfur volatile removal from the atmosphere, with reaction rates for liberated O and OH radicals in the pathway from H_2S to SO_2 (via HS and HSO or HS and SO) exceeding those in the pathway from SO_2 to sulfate (via SO_3) [*DeMore et al.*, 1997]. Although it should be noted that SO_2 disproportionation reactions are also possible, generating elemental sulfur and sulfate as products of atmospheric photochemistry [*Zahnle and Haberle*, 2006], our investigation primarily explores the exclusive volatile form of SO_2. At the beginning of the simulations, we assume either gas (H_2S or SO_2) to be uniformly mixed in the atmosphere.

2.4 Atmospheric warming

2.4.1 General circulation model

We use the Mars Weather Research and Forecasting (MarsWRF) general circulation model (GCM) as the basis for our atmospheric warming experiments [*Richardson et al.,* 2007]. The MarsWRF GCM solves the primitive equations using a finite difference model on an Arakawa-C grid, and is run with a lat x lon model resolution of 5° x 5.625° (36 x 64 grid points) and with 25 vertical levels on a modified sigma (terrain-following) vertical coordinate. The total present-day atmospheric CO_2 budget has been tuned to fit the Viking Lander annual pressure curves. We then scale the present-day annual and global average surface pressure (~6 mb) to either 50 or 500 mb, depending on the scenario being considered. Both surface albedo and thermal inertia are matched to present-day TES observations [*Christensen et al.*, 2001; *Putzig et al.*, 2005], and the present-day topography is used. Tests of the MarsWRF dynamical core [*Richardson et al.,* 2007] show that it produces results that compare favorably to the Held-Suarez "standard" [*Held and Suarez*, 1994] under terrestrial atmospheric conditions. Comparisons to existing Mars climate models and vertical profiles of TES data further show that MarsWRF is able to replicate key features of the Martian atmosphere quite well. At the Second International Workshop on Mars Atmosphere Modeling and Observations in Granada, Spain in March 2006, a broad model intercomparison was performed between seven independent Mars GCMs, including MarsWRF, to study their ability to reproduce observations of the Martian atmosphere. Sample results from this

(unpublished) intercomparison are shown in Figure 2.1. In each of the four comparisons, output from MarsWRF for its "best fit" to present-day temperature and zonal wind profiles is shown alongside the same field for both the GFDL Mars GCM [*Wilson and Hamilton,* 1996] and LMD/AOPP Mars GCM [*Forget et al.*, 1999]. For all four comparisons, atmospheric dust is set to a column opacity of 0.2. The intercomparison results are quite good at both solstice seasons, as well as during the equinoctial periods (not shown), and capture the winter zonal jets both in magnitude and location, as well as the zonal temperature gradient across the planet. Small differences between the simulations are due largely to differences in model architecture (i.e. different dynamical cores). These preliminary results provide confidence in the behavior of MarsWRF. Additional comparisons to TES temperature data [*Smith et al.*, 2001] further show a high degree of similarity to observations [*Richardson et al.*, 2007].

2.4.2 Radiation scheme

We have developed a new multi-gas, two-stream radiation code loosely based on the structure of the UK Hadley Centre Radiation Scheme [*Edwards and Slingo*, 1996], but modified to use the *k*-distribution radiative transfer method. This method retains much of the accuracy of line-by-line calculations, but is significantly faster, making it ideal for computationally expensive 3-D global models. Details about the *k*-distribution method can be widely found [*e.g.*, *Lacis and Oinas*, 1991; *Fu and Liou*, 1992], so only a brief summary of relevant points will be provided here.

The numerical scheme regarding the k-distribution method involves partitioning the solar/IR spectrum into distinct spectral bands, and re-sorting the individual lines, which are highly variable as a function of wavelength, within each band to produce a relatively smooth curve that is more conducive to numerical approximation. Each distinct band is both sufficiently narrow such that the Planck blackbody curve is approximately constant across the entire band and also sufficiently broad to encompass full absorption features of individual gases. In the present implementation of this k-distribution method, the entire solar/IR spectrum is partitioned into twelve bands (seven solar, five IR) of varying widths, following the partitioning employed by the Ames MGCM (versions 2.0 and greater) [*Haberle*, personal communication]. Errors introduced by variations in the Planck function across these spectral bands are quite nominal [*Haberle et al*., 2003]. Bands are prudently selected to ensure that individual absorption features are not bisected across two bands. Once band sizes are selected, the portion of the spectrum within each band is discretized at a sub-linewidth frequency, and these discrete intensities are sorted by magnitude. A before-and-after illustration of this type of line sorting is shown in Figure 2.2. The sorted curve in Figure 2.2b no longer maps line intensity directly to wavelength, but instead maps intensity to a cumulative probability function, i.e., what fraction of the intensities are smaller than the given intensity.

For a standard line-by-line calculation, the transmissivity, *Tr*, is calculated as

(6) $$Tr = \int_{\nu_{\min}}^{\nu_{\max}} \exp[-k_\nu u] d\nu ,$$

where k_ν is the absorption coefficient at frequency ν, and u is the mass of the absorbing gas. Following the resorting of this spectrum, transmissivity is calculated as

(7) $$Tr = \int_0^1 \exp\left[-k_g u\right] dg,$$

where now k_g is the absorption coefficient for the cumulative probability g (between zero and one).

Within each band, we perform the discretization and sorting to develop a smooth cumulative probability curve. We then fit this curve with 16 quadrature points at specified intervals along the distribution—eight points in the lowest 95% of the distribution and eight points in the upper 5%. These intervals were selected because experimentation has shown that the strongest absorption, which occurs at the cores of individual spectral lines, takes place in the top 5% of the distribution, so extra precision is warranted. From this, we can obtain a numerical approximation to the transmissivity for a given atmospheric layer of mass u

(8) $$Tr = \sum_{i=1}^{16} a_i e^{-k_i u},$$

where k_i is the absorption coefficient chosen at quadrature point i, and a_i is the assigned weight (where $\Sigma\, a_i$=1).

Absorption coefficients vary according to both temperature and pressure. To maintain the best accuracy possible in our absorption calculations, we have assembled, off-line, a

series of databases containing the *k*-distribution absorption coefficients for the full range of *p,T* conditions expected in the atmospheres used for this study (T = 50-400 K in 1 K increments; $p = 10^{-4}$-10^{6} Pa with log(p) spacing of 0.2). The most basic database is for a pure CO_2 atmosphere. Here, and in all other databases in this study, the CO_2 mixing ratio is fixed at 0.953. Spectral line data are obtained from the HITRAN database [*Rothman et al.*, 2005] and internal partition sum data of *Fischer et al.* [2003]. The Humlícek approximation to a Voigt lineshape is used to obtain the pressure and temperature dependent line shape [*Humlícek*, 1982]. A second database was assembled for a dual-gas (CO_2+H_2O) atmosphere over the same pressure/temperature conditions as above, but also across a range of putative water vapor mixing ratios (q, where q=10^{-7} to 10^{-2} by decade). The water vapor foreign continuum, which represents the net contribution of the distant tails of water vapor absorption lines, is parameterized [*Mlawer et al.*, in preparation] and included in this and any other databases containing water.

Two databases were assembled for each of the two-gas mixtures (SO_2+CO_2) and (H_2S+CO_2), at both the upper and lower bound values of the sulfur species. Rather than calculating *k*-coefficient data over a range of SO_2 or H_2S mixing ratios as was done for H_2O, we use the fixed sulfur species abundances found in Table 2.2 to build the database. This reduces the overall size of the database, and simplifies its construction, but also reduces the relevant parameter space to only those atmospheres with these precise sulfur species mixing ratios. For an investigation such as this, where specific atmospheric compositions are being considered, such an approach is acceptable. Lastly, a series of

databases were assembled for all three-gas (SO_2/H_2S+CO_2+H_2O) permutations, covering the same parameter space as the others. In total, 16 databases were required for the present study.

To assemble a database, the raw (unsorted) spectra are calculated for each *p,T,q* triad and then partitioned into 12 spectral bands where they are discretized and sorted by strength as noted above. Within each of the 12 bands and for each *p,T,q* combination, the 16 *k*-coefficients are obtained from the smoothed spectral curve and stored in the database (for a total of ~20 million coefficients per database). The weighting function for the *k*-coefficients is the same for all bands, and for all *p*,*T*,*q* triads.

These *k*-coefficient databases are then used by the two-stream radiation code as lookup tables, from which the appropriate *k*-coefficients are obtained for the specific *p,T,q* conditions at each model grid point, using the nearest neighbor in temperature and a linear interpolation in log space for both *p* and *q*. The corresponding radiative calculations are then performed to determine atmospheric heating rates. While such a process is, somewhat slower than current methods [e.g. *Hourdin*, 1992; *Forget et al.*, 1999], it is not unduly so. Because the *k*-coefficient databases are calculated directly from the HITRAN database, we are able to choose at the outset any arbitrary combination of atmospheric species to investigate and convolve their respective spectra into a single distribution, thus this method is not only very useful for investigating atmospheres with varying compositions but also generic enough to be used on virtually any planet with an

atmosphere. Currently, implementations of this code are being developed for the atmospheres of Titan and Venus.

Other radiation schemes commonly used for the Martian atmosphere have two major drawbacks that prevent their application to the present study. First, they are designed to best represent the present Martian climate, and are thus designed for compositionally pure CO_2 model atmospheres (since H_2O is radiatively negligible in the current Martian atmosphere). Second, they are tuned for atmospheres having surface pressures similar to present day (6-10 mb) and not for thick atmospheres. Above ~100 mb, for example, the model of *Hourdin* [1992] has been shown to become increasingly unreliable, making it impossible to investigate the model atmospheres we present here.

2.4.3 Water cycle

The model is initialized with a globally uniform 10^{-6} water vapor mixing ratio and is free to evolve without additional external adjustments. The MarsWRF water cycle provides a simple mechanism for the transport, sedimentation, and exchange of water between the vapor and ice phases. For each model time step, both water vapor and water ice (treated independently in the model) are advected by the local wind field and diffused down the local vapor/ice gradient. At the conclusion of each model time step, the ice sediments at a pressure-dependent velocity according to the Stokes-Cunningham slip-flow equation [*Conrath*, 1975; *Haberle et al.*, 1982], assuming uniform 10 μm radius particles.

The primary source of water for the atmosphere is from surface ice. Exchange of water vapor with the surface in MarsWRF follows the classical equation of *Flasar and Goody* [1976] and used in *Montmessin et al*. [2004]

(9) $$F_w = \rho C_d u_* (q_{sat} - q_v),$$

[*Forget et al*. 1999], u_* is the friction velocity, set to the horizontal wind in the lowest model layer, q_{sat} is the water vapor saturation mixing ratio at the surface temperature and q_v is the local atmosphere water vapor mixing ratio. The resulting flux determines the magnitude of vapor flowing into/out of the atmosphere, and is proportional to the difference in humidity between the surface and atmosphere.

2.4.4 Dust and solar luminosity

For present-day conditions, MarsWRF generally uses a time- and space-varying dust distribution modeled on MGS observations [*Montmessin et al*., 2004], but test cases have been run with no dust, or with a fixed global abundance. It's not evident whether any of these specific distributions can be translated to higher pressure regimes with any physical basis. For this reason, radiatively active dust was excluded in the present simulations, though the presence of atmospheric dust would likely cause additional warming in our model. Future investigations may gauge the impact of a simplified dust scheme on the dynamics of the system. The incoming solar luminosity is chosen to be conservative: 75% of the modern value, as has been traditionally demanded by solar evolution models [*Gough*, 1981].

2.5 Results

Water vapor and the sulfur species each contribute a fraction of the total greenhouse warming in the system (above that generated by CO_2 itself). To identify the magnitude of warming produced by water vapor alone, we have run a series of 'control' simulations at both surface pressures to quantify the effect of water vapor in the atmosphere. Results from all simulations in this work are shown for the third year, when the atmospheric vapor distribution has reached an approximate steady state. Figures 2.3a and 2.3b show annually averaged surface temperatures at 50 mb and 500 mb CO_2, respectively, without water vapor. Figures 2.3c and 2.3d show their water vapor-inclusive counterparts. The temperature difference between the two panels of like pressure shows the warming contribution of water vapor. At 50 mb (left column) water vapor plays only a minor role in atmospheric warming, generally enhancing temperatures by <5 K. There is little water vapor in this atmosphere due to low (<170K) surface temperatures in the polar regions (particularly the north polar region where the residual water ice cap resides). Vapor flux is highly sluggish at the temperatures.

In contrast, polar temperatures are substantially warmer in the 500 mb scenario, and polar ice sublimation is more vigorous. During summer, when nearly all sublimation occurs, the disparity between the two pressure scenarios is significant. Annual maximum temperatures at the North Pole at 50 mb rise to only 170 K, while at 500 mb, annual maxima approach 230 K. The vapor holding capacity is a factor of 10,000 greater at the

polar temperatures in the 500 mb simulation, permitting a vastly greater quantity of vapor to flow into the atmosphere. Additionally, the larger thermal inertia of the thicker atmosphere prevents nighttime temperatures from dipping to the low values in the 50 mb simulation, allowing a greater amount of water to remain in the atmosphere. The end result of this greater vapor content at 500 mb is a surface that is ~40 K warmer than its water-free counterpart, including some tropical locations with mean temperatures above the water ice melting point (Figure 2.3d).

It should be noted that the present implementation of MarsWRF does not account for the radiative effects of water ice clouds, which are believed to have an overall cooling effect. In these humid atmospheres, thick, low (and bright) convective clouds will likely be present, raising the planetary albedo, reducing the amount of insolation at the surface, and lowering surface temperatures. We do not consider this negative radiative feedback cycle at present in MarsWRF (although we do model the opacity and distribution of water ice clouds), thus the temperature results may be upper limits depending on the abundance of clouds and their specific distribution both horizontally and vertically.

In parallel with Figure 2.3's depiction of the extent of greenhouse warming by H_2O, Figure 2.4 shows the warming by "Wilson" upper and "Andrews-Hanna" lower bound amounts of SO_2 in a dry (no H_2O) CO_2 atmosphere. For the 50 mb "Andrews-Hanna" lower bound atmosphere, annual average warming by SO_2 is generally of the order of 7-15 K (Figure 2.4a), while for the "Wilson" upper bound, this warming increases to 15-25

K (Figure 2.4c). There is a noticeable hemispheric dichotomy present in both panels, mirroring the lower altitude and greater atmospheric mass present in the north. For a fixed SO_2 mixing ratio, there is more SO_2 present in an overhead column in the Northern Lowlands, and hence more greenhouse warming. The magnitude of warming introduced by the presence of SO_2 in the atmosphere is in line with the estimates of *Postawko and Kuhn* [1986]. Simulations involving H_2S show it is a less efficient greenhouse gas than SO_2. The results of these simulations are shown in Table 2.3.

In the 500 mb scenario, there is approximately the same level of warming as in the 50 mb scenarios, which is expected. The magnitude of greenhouse warming is largely a consequence of the mass of the species, as opposed to its mixing ratio. In both scenarios, the atmospheres have the same total mass of SO_2, and hence have similar greenhouse effects. The magnitude of warming is slightly greater in the 500 mb scenario. This small increase is a consequence of greater absorption caused by increased pressure broadening of the spectral lines in the thicker 500 mb atmosphere.

Figure 2.5 shows the result of combining both H_2O and SO_2 greenhouse warming in each of our two pressure scenarios. In Figure 2.5, the 'control' scenario is "wet" and contains both CO_2+H_2O (*cf.* Figures 2.3c-d). This is different from Figure 2.4, where the 'control' is "dry" (*cf.* Figures 2.3a-b). In each of the four scenarios presented in Figure 2.5, the same amount of SO_2 is present in the atmosphere as for the respective scenarios in Figure 2.4; thus, at first guess, one might assume the same level of warming (i.e. 7-25 K) by SO_2

here, above the "wet" control run, as in Figure 2.4 above the "dry" control run. Instead, we find the temperature differences in Figure 2.5 to be not only larger than in Figure 2.4, but also increasingly large as we move from "Andrews-Hanna" lower to "Wilson" upper bound values and from 50 mb to 500 mb (e.g. Figure 2.5a shows only slightly more warming than Figure 2.4a, while Figure 2.5d shows substantially more warming than Figure 2.4d.) Since this added warming is not produced by the SO_2 or CO_2, both of which have fixed abundances, it must be obtained from atmospheric water vapor. This is a clear demonstration of the positive feedback between SO_2 and H_2O greenhouse warming in the atmosphere. The addition of SO_2 provides a 'boost' in temperature, permitting even more water vapor into the atmosphere, further augmenting the already significant greenhouse effect. In the "Wilson" upper bound SO_2 500 mb case, this corresponds to additional warming by H_2O vapor of 25 K. For cooler scenarios, or those with a smaller SO_2 'boost,' the additional H_2O increase is correspondingly less.

An underlying objective of this work is to explore regions on the surface where enhanced greenhouse warming may provide conditions for liquid water to be present at the surface. This requires satisfying both atmospheric pressure and temperature restrictions [*Richardson and Mischna*, 2005]. For these thick atmospheres, the pressure restriction is fully satisfied, which means that the potential for liquid water is constrained only by temperature. This temperature constraint is nominally 273 K, but may be several tens of degrees lower depending on the salinity of the water. Figure 2.6 maps the fraction of the year when temperatures at each surface location exceed the nominal liquid water melting

temperature of 273 K under the listed atmospheric compositions, thus suggesting those places where the potential for liquid water would be greatest.

At 50 mb, much of the planet can sustain liquid for at least a portion of the year, Generally, between 1-30% of the year reaches temperatures >273 K, with these times occurring during the warmest periods—summertime, and in the mid-afternoon hours. The exception is the Northern Hemisphere, where summertime temperatures are colder, and over Tharsis when the SO_2 abundance is too low. This dichotomy is a direct result of the orbit chosen for this particular simulation, which is the same as present-day. For a different orbital configuration (e.g. if perihelion occurred during northern summer), summertime temperatures would be warmer in the north and cooler in the south, and the distribution would be different than shown in Figure 2.6, though the overall magnitudes would remain roughly the same. The situation is more favorable at 500 mb, where a majority of the planet is >273 K for at least half of the year, and much of the planet is permanently above this value.

Tying this all together, Figure 2.7 illustrates the maximum potential warming made possible by mixtures of SO_2+H_2O above the baseline temperature of a "dry" CO_2 atmosphere. These magnitudes range from 10-20 K for "Andrews-Hanna" lower bound SO_2 at 50 mb to over 100 K for the warmest, "Wilson" upper bound SO_2 at 500 mb scenario. Once again, these values will not be typically obtained due to the negative feedbacks imposed by the water cycle itself. It is interesting, however, to note that the

greatest warming occurs over the cold North Polar Cap where the summertime vapor concentration is the highest anywhere on the planet, and thus the potential for enhanced warming is greatest.

Table 2.3 provides a summary of conditions found for each of the simulations run, including those in Figures 2.3-2.6. Additional surveys of global average temperatures, including those for H_2S, are listed, along with measures of frequency of time above 260 K (a nominal brine melting temperature) and 273 K and the magnitude of greenhouse warming introduced by sulfur volatiles and water vapor.

2.6 Discussion

Our results suggest that volcanic release of sulfur volatiles in the early Martian atmosphere may have generated significant additional warming by trapping heat in wavelength-dependent atmospheric windows different from those of CO_2 and H_2O. Alone, SO_2 pulses may have generated up to 25 K of warming. In combination with water vapor feedbacks, surface temperatures after an SO_2 pulse may have risen 50-70 K or more above a steady state CO_2 atmosphere, creating widespread surface conditions conducive to the presence of transient liquid water. Furthermore, as we have already noted, freezing points can be depressed by salt composition in brines [*Clark and Van Hart*, 1981]. Although the most logical choice of salt under these conditions—sulfate—is a poor freezing-point depressor, high levels of chlorine have

been detected in soils at the landing sites for Spirit, Opportunity, Pathfinder and the Viking Landers, and salts may have been mobilized and concentrated by repeated wetting and evaporation events in ephemeral saline pans [*Yen et al.*, 2005; *Rutherford at al.*, 2001]. In his work on the stability of brines on Mars, *Brass* [1980] suggested a freezing point depression that easily allows for liquid phases within the upper range of our model results.

The length of time that sulfur-related greenhouse warming persists in the atmosphere is a key area for additional work. Although sulfur volatiles are converted to sulfate aerosols within days in the Earth's current oxidizing atmosphere (often creating a global cooling effect following sulfur-rich volcanic eruptions, as in the 1991 eruption of Mount Pinatubo). A study of sulfur photochemistry in the current Martian regime reveals a 600-day lifetime for SO_2 [*Wong et al.,* 2004, 2005]. However, this lifetime will change significantly under the weakly reducing atmospheric conditions that likely characterized early Mars. We have begun photochemical modeling using an adaptation for Mars of a one-dimensional photochemical model developed for sulfur chemistry simulations in the Earth's Archean atmosphere [*Pavlov and Kasting*, 2002]. Our results suggest that the warming associated with these pulses is on the order of at least hundreds of years [*Johnson et al.,* 2007a,b].

Inputs of sulfur volatiles to the early Martian atmosphere are consistent with the evolution of early Mars proposed by *Bibring et al.* [2005, 2007], in which the planet

experienced an early wet period of phyllosilicate formation followed by an arid, acidic period under which evaporitic sulfate deposits formed; this model invokes a surge in Tharsis outgassing near the end of the late Noachian to explain the transition from phyllosilicate to sulfate formation. However, evidence suggests that Tharsis was largely emplaced prior to the end of the late Noachian [*Phillips et al.,* 2001], and we show calculations that support the notion that sulfur volatiles in the atmosphere may prove necessary to create early warm, wet surface conditions. *Andrews-Hanna et al.* [2007b,c] argue that surface runoff and shallow subsurface hydrology dominated aqueous geochemistry during this early period, with the combination of mildly acidic precipitation (a result of dissolved atmospheric sulfur volatiles) and weathering of surface basalts producing the observed early Noachian phyllosilicates (see also [*Halevy et al.*, 2007]). This model suggests that sulfate evaporite deposition during the late Noachian or early Hesperian resulted not from a late-stage injection of volcanic gases into the atmosphere but rather from a change in global hydrology in response to either a decrease in the total water inventory or an increase in the storage capacity of the crustal aquifers. The water table would have then dropped deep below the surface, and evaporation and precipitation rates would have become dictated by deep global-scale groundwater flow rates. As a result, mildly oxidizing fluids in deep basaltic aquifers would have reacted with pyrrhotite, creating significant acidity and liberating dissolved ferrous sulfate, and evaporite deposition would have become limited to isolated regions of groundwater upwelling, such as Meridiani Planum. A lessening of volcanic activity at the close of the

late Noachian, and subsequent arid, low-temperature surface conditions in the absence of sulfur-related greenhouse warming, would have been part of this process.

Large, sulfur-rich volcanic eruptions likely continued to occur through the Hesperian and into the Amazonian, though at a much lower rate than in the Noachian. Presumably, the thinner atmosphere resulted in cooler temperatures despite the added volcanic greenhouse effect (as in our 50 mb simulations); nevertheless, later in Martian history there is evidence for the occurrence of transient warm climatic conditions, with valley network formation in the Hesperian and possibly Amazonian in some places [*Carr and Chuang*, 1997].

2.7 Conclusion

There is substantial evidence for stable liquid water on the past surface of Mars, but the requisite environmental conditions are incompatible with the present climate. We hypothesize that large, episodic releases of sulfur volatiles early in the history of the planet could have generated up to 25 K of additional greenhouse warming, alone, over a large enough portion of the surface to drive, in tandem with water vapor feedbacks, dramatic climate fluctuations on early Mars. Degassing events of this magnitude could plausibly have occurred hundreds of times within the late Noachian. This scenario accords well with recent Mars mission findings, accounting for widespread geologic evidence for past stability of liquid water on early Mars, generation of surface acidity,

preclusion of carbonate deposition, and high sulfur abundances as detected from orbit and at landing sites.

2.8 References

Aharonson, O., M. T. Zuber, G. A. Neumann, and J. W. Head, III (1998), Mars: Northern Hemisphere slopes and slope distributions. *Geophys. Res. Lett., 25*, 4413-4416.

Andrews-Hanna, J. C., (2007a) *personal communication*.

Andrews-Hanna, J. C., R. J. Phillips, and M. T. Zuber (2007b), Meridiani Planum and the global hydrology of Mars, *Nature, 446*, 163-166.

Andrews-Hanna, J. C., M. T. Zuber, and R. J. Phillips (2007c), Meridiani Planum: Implications for the hydrologic and climatic evolution of Mars, paper presented at Seventh International Conference on Mars, Pasadena, California, Abstract #3173.

Arvidson, R. E., F. P. Seelos, IV, K. S. Deal, W. C. Koeppen, N. O. Snider, J. M. Kieniewicz, B. M. Hynek, M. T. Mellon, and J. B. Garvin (2003), Mantled and exhumed terrains in Terra Meridiani, Mars, *J. Geophys. Res.*, *108*(E12), 8073, doi:10.1029/2002JE001982.

Arvidson, R. E., F. Poulet, J.-P. Bibring, M. Wolff, A. Gendrin, R. V. Morris, J. J. Freeman, Y. Langevin, N. Mangold, and G. Bellucci (2005), Spectral reflectance and morphologic correlations in Eastern Terra Meridiani, Mars, *Science, 307*, 1591-1594.

Baker, V. R., R. G. Strom, V. C. Gulick, J. S. Kargel, G. Komatsu, and V. S. Kale (1991), Ancient oceans, ice sheets and the hydrologic cycle on Mars, *Nature*, 352, 589-594.

Bandfield, J. L. (2002), Global mineral distributions on Mars, *J. Geophys. Res.*, *107*(E6), 5042, doi:10.1029/2001JE001510.

Banin, A. (2005), The enigma of the Martian soil, *Science*, *309*, 888-889.

Benison, K. C., R. H. Goldstein, B. Wopenka, R. C. Burruss, and J. D. Pasteris (1998), Extremely acid Permian lakes and ground waters in North America, *Nature, 392*, 911-914.

Bertka, C. M., and Holloway, J. R. (1994), Anhydrous partial melting of an iron-rich mantle II: Primary melt compositions at 15 kbar, *Contrib. Mineral. Petrol., 115*, 323-328.

Bibring, J.-P. *et al*. (2005), Mars surface diversity as revealed by the OMEGA/Mars Express observations, *Science, 307,* 1576-1581.

Bibring, J.-P. *et al*. (2007), Mars climatic and geological history, derived from the OMEGA/MEX data, paper presented at Seventh International Conference on Mars, Pasadena, California, Abstract #3234.

Blaney, D. L. (1996), Sulfate Formation on Mars by Volcanic Aerosols: A New Look, paper presented at Lunar and Planetary Science Conference XXVII, League City, Texas, 123.

Bottinga, Y., and D. F. Weill (1970), Densities of liquid silicate systems calculated from partial molar volumes of oxide components, *Am. J. Sci*., *269*, 169–182.

Brass, G. W. (1980), Stability of brines on Mars, *Icarus*, *42*, 20-28.

Burt, D. M., L. P. Knauth, and K. H. Wohletz (2005), Origin of layered rocks, salts and spherules at the Opportunity landing site on Mars: No flowing or standing water evident or required, paper presented at Lunar and Planetary Science Conference XXXVI, League City, Texas, Abstract #1527.

Carr, M.H. and F. C. Chuang (1997), Martian drainage densities. *J. Geophys. Res., 102* 9145-9152.

Catling, D. C., Atmospheric evolution of Mars, in *Encyclopedia of Paleoclimatology and Ancient Environments*, edited by V. Gornitz, Kluwer Academic Publishers, New York, *in press*.

Christensen, P. R., *et al.* (2001), Mars Global Surveyor Thermal Emission Spectrometer experiment: Investigation description and surface science results, *J. Geophys. Res.*, *106*, 23,823-23,871.

Clifford, S. M., and T. J. Parker (2001), The evolution of the Martian hydrosphere: Implications for the fate of a primordial ocean and the current state of the Northern Plains, *Icarus*, *154*, 40-79.

Conrath, B. J. (1975), Thermal structure of the Martian atmosphere during the dissipation of the dust storm of 1971, *Icarus*, *24*, 36-46.

DeMore, W. B., S. P. Sander, D. M. Golden, R. F. Hampson, M. J. Kurylo, C. J. Howard, A. R. Ravishankara, C. E. Kolb, and M. J. Molina (1997), *Chemical kinetics and photochemical data for use in stratospheric modeling,* Evaluation 12, 269 pp., JPL Publication 97-4, Jet Propulsion Laboratory, Pasadena, California.

Edwards, J. M., and A. Slingo (1996), Studies with a flexible new radiation code. I: Choosing a configuration for a large-scale model, *Q.J.R. Meteorol. Soc., 122*, 689–719.

Fanale, F. P., S. E. Postawko, J. B. Pollack, and M. H. Carr (1992), Mars: Epochal climate change and volatile history, in *Mars*, edited by H. Kieffer, B. Jakosky, C. Snyder, and M. Matthews, pp. 1135-1179, University of Arizona Press, Tucson.

Farquhar, J., J. Savrino, T. L. Jackson, and M. H. Thiemnes (2000), Evidence of atmospheric sulphur in the Martian regolith from sulphur isotopes in meteorites, *Nature*, *404,* 50-52.

Feldman, W. C., *et al*. (2004), Hydrated states of $MgSO_4$ at equatorial latitudes on Mars, *Geophys. Res. Lett.*, *31*, L16702, doi:10.1029/2004GL020181.

Fischer, J., R. R. Gamache, A. Goldman, L. S. Rothman, and A. Perrin, Total internal partition sums for molecular species in the 2000 edition of the HITRAN database. *J. Quant. Spect. Rad. Trans.*, 82, 401-412, 2003.

Flasar, F. M. and R. M. Goody, (1976), Diurnal behavior of water on Mars, *Planet. Space Sci., 24*, 161-181.

Forget, F., and R. T. Pierrehumbert (1997), Warming early Mars with carbon dioxide clouds that scatter infrared radiation, *Science, 278*, 1273-1276.

Forget, F., F. Hourdin, R. Rournier, C. Hourdin, O. Talagrand, M. Collins, S. R. Lewis, P. L. Read, and J.-P. Huot (1999), Improved general circulation models of the Martian atmosphere from the surface to above 80 km, *J. Geophys. Res.*, *104*, 24,155-24,175.

Fu, Q., and K. N. Liou (1992), On the correlated k-distribution method for radiative transfer in nonhomogeneous atmospheres, *J. Atmos. Sci., 49*, 2139-2156.

Gendrin, A., *et al*. (2005), Sulfates in Martian layered terrains: The OMEGA/Mars Express view, *Science, 307*, 1587-1591.

Gough, D. O. (1981), Solar interior structure and luminosity variations, *Solar Phys.*, *74*, 21-34.

Greeley, R., B. H. Foing, H. Y. McSween, G. Neukum, P. Pinet, M. van Kan, S. C. Werner, D. A. Williams, and T. E. Zegers (2005), Fluid lava flows in Gusev Crater, Mars, *J. Geophys Res. 110*, E05008, doi:10.1029/2005JE002401.

Gulick, V. C., D. Tyler, C. P. McKay, and R. M. Haberle (1997), Episodic ocean-induced CO_2 greenhouse on Mars: Implications for fluvial valley formation, *Icarus*, *130*, 68-86.

Haberle, R. M., C. B. Leovy, and J. B. Pollack (1982), Some effects of global dust storms on the atmospheric circulation of Mars, *Icarus*, *50*, 322-367.

Haberle, R. M., H. C. Houben, R. Hertenstein, and T. Herdtle (1993), A boundary layer for Mars: Comparison with Viking lander and entry data, *J. Atmos. Sci.*, *50*, 1544 -1559.

Halevy, I., M. T. Zuber, and D. P. Schrag (2007), A sulfur dioxide climate feedback on early Mars, *in review*.

Haberle, R.M., J.L. Hollingsworth, A. Colaprete, A.F.C. Bridger, C.P. McKay, J.R. Murphy, J. Schaeffer and R. Freedman (2003), The NASA Ames Mars General Circulation Model: Model improvements and comparison with observations, Mars Atmospheric Modeling and Observations Workshop, Granada, Spain.

Hanna, J.C. and R.J. Phillips (2006), Tectonic pressurization of aquifers in the formation of Mangala and Athabasca Valles, Mars, *J. Geophys. Res.*, *111*, E03003, doi:10.1029/2005JE002546.

Head, J.W. 3rd, H. Hiesinger, M.A. Ivanov, M.A. Kreslavsky, S. Pratt, and B.J. Thomson (1999), Possible ancient oceans on Mars: evidence from Mars Orbiter Laser Altimeter data, *Science*, *286*, 2134-2137.

Held, I. M., and Suarez, M. J. (1994), A proposal for the intercomparison of the dynamical cores of atmospheric general circulation models, *Bull. Amer. Met. Soc.*, *72*, 1825-1830.

Holzheid, A., and T. L. Grove (2002), Sulfur saturation limits in silicate melts and their implications for core formation scenarios for terrestrial planets, *American Mineralogist*, *87*, 227–237.

Hourdin, F. (1992), A new representation of the absorption by the CO_2 15-μm band for a Martian general circulation model, *J. Geophys. Res.*, *97*, 18,319-18,335.

Humlícek, J. (1982), Optimized computation of the Voigt and complex probability functions, *J. Quant. Spectrosc. Radiat. Transfer*, *27*, 437-444.

Hynek, B. M., R. E. Arvidson, and R. J. Phillips (2002), Geologic setting and origin of Terra Meridiani hematite deposit on Mars, *J. Geophys. Res.*, *107*(E10), 5088, doi:10.1029/2002JE001891.

Jakosky, B. M., and R. J. Phillips (2001), Mars' volatile and climate history, *Nature*, *412*, 237-244.

Johnson, S. S., M. T. Zuber, T. L. Grove, A. A. Pavlov, and M. A. Mischna (2007a), Sulfur volatiles in the early Martian atmosphere, paper presented at Lunar and Planetary Science XXXVIII, League City, Texas, Abstract #1754.

Johnson, S. S., A. A. Pavlov, and M. A. Mischna (2007b), Longevity of SO_2 in the ancient Martian atmosphere: implications for transient greenhouse warming, *submitted to Geophys. Res. Lett.*

Kasting, J. F. (1991), CO_2 condensation and the climate of early Mars, *Icarus, 94*, 1-13.

Kasting, J. F. (1997), Warming early Earth and Mars, *Science*, *276*, 1213-1215.

Knoll, A. H., *et al*. (2005), An astrobiological perspective on Meridiani Planum, *Earth & Planet. Sci. Lett., 240*, 179-189.

Lacis, A. A., and V. Oinas (1991), A description of the correlated *k* distribution method for modeling nongray gaseous absorption, thermal emission and multiple scattering in vertically inhomogeneous atmospheres, *J. Geophys. Res., 96*, 9027-9063.

Lemmon, E. W., M. O. McLinden, and D. G. Friend (2005), Thermophysical properties of fluid systems, in *NIST chemistry WebBook*, NIST Standard Reference Database Number 69, edited by P.J. Linstrom and W.G. Mallard, National Institute of Standards and Technology, Gaithersburg, Maryland.

Mavrogenes, J. A., and H. St. C. O'Neill (1999), The relative effects of pressure, temperature and oxygen fugacity on the solubility of sulfide in mafic magmas, *Geochim. et Cosmochim. Acta*, *63*, 1173–1180.

Maguire, W. S. (1977), Martian isotopic ratios and upper limits for possible minor constituents as derived from Mariner 9 infrared spectrometer data, *Icarus*, *32*, 85-97.

McLennan, S. M., *et al*. (2005), Provenance and diagenesis at Meridiani Planum, *Earth & Planet. Sci. Lett.*, *240*, 95-121.

McEwen A. S., M. C. Malin, M. H. Carr, and W. K. Hartmann (1999), Voluminous volcanism on early Mars revealed in Valles Marineris, *Nature*, *397*, 584-586.

McSween H. Y., Jr., *et al*. (2006), Characterization and petrologic interpretation of olivine-rich basalts at Gusev crater, Mars. *J. Geophys. Res., 111*, E02S10, doi:10.1029/2005JE002477.

Mills, K. C. (1993), The influence of structure on the physico-chemical properties of slags, *ISIJ Int., 33*, 148-155.

Mischna, M. A., J. F. Kasting, A. Pavlov, and R. Freedman (2000), Influence of carbon dioxide clouds on early Martian climate, *Icarus, 145*, 546-554.

Mo, X., I. S. E. Carmichael, M. Rivers, and J. Stebbins (1982), The partial molar volume of Fe_2O_3 in multicomponent silicate liquids and the pressure dependence of oxygen fugacity in magmas, *Mineral. Mag.*, *45*, 237-245.

Monders, A. G., E. Medard, and T. L. Grove (2007), Phase equilibrium investigations of the Adirondack class basalts from the Gusev plains, Gusev crater, Mars, *Meteoritics & Planetary Science, 42*, 131–148.

Montmessin, F., F. Forget, P. Rannou, M. Cabane, and R.M. Haberle (2004), Origin and role of water ice clouds in the Martian water cycle as inferred from a general circulation model. *J. Geophys. Res. 109*, E10004, doi:10.1029/2004JE002284.

Mysen, B. O. (1988), Structure and properties of silicate melts, *Developments in Geochemistry*, vol. 4, 368 pp. Elsevier Publishing.

Owen, T. (1992), The composition and early history of the atmosphere of Mars, in *Mars*, edited by H. Kieffer, B. Jakosky, C. Snyder, and M. Matthews, pp. 818-834, University of Arizona Press, Tucson.

Pavlov, A. A. and J. F. Kasting (2002), Mass-independent fractionation of sulfur isotopes in Archean sediments: Strong evidence for an anoxic Archean atmosphere, *Astrobiology*, *2*, 27-41.

Perron, J. T., J. X. Mitrovica, M. Manga, I. Matsuyama, and M. A. Richards (2007), Evidence for an ancient Martian ocean in the topography of deformed shorelines, *Nature, 447*, 840-843.

Phillips, R. J., *et al.* (2001), Ancient geodynamics and global-scale hydrology on Mars, *Science, 291*, 2587-2591.

Pollack, J. B., J. F. Kasting, S. M. Richardson, and K. Poliakoff (1987), The case for a wet, warm climate on early Mars, *Icarus*, *71*, 203-224.

Postawko, S. E., and W. R. Kuhn (1986), Effect of the greenhouse gases (CO_2, H_2O, SO_2) on Martian paleoclimate, *J. Geophys. Res., 91,* D431-438.

Putzig, N. E., M. T. Mellon, K. A. Kretke, and R. E. Arvidson (2005), Global thermal inertia and surface properties of Mars from the MGS mapping mission, *Icarus*, *173*, 325-341.

Richardson, M.I., A.D. Toigo and C.E. Newman (2007), PlanetWRF: A general purpose, local to global numerical model for planetary atmospheric and climate dynamics, *J. Geophys. Res., 112*, E09001, doi:10.1029/2006JE002825.

Roach, L. H., *et al.* (2007), CRISM spectral signatures of the north polar gypsum dunes, paper presented at Lunar and Planetary Science Conference XXXVIII, League City, Texas, Abstract #1970.

Rothman, L. S., *et al.* (2005), The HITRAN 2004 molecular spectroscopic database, *J. Quant. Spectrosc. Radiat. Transfer*, *96*, 139-204.

Rutherford, M. J., M. Minitti, and C. M. Weitz (2001), Compositions of Mars rocks: SNC meteorites, differentiates and soils, paper presented at Workshop on Mars 2001: Integrated science in preparation for sample return and human exploration, Houston, Texas, Abstract #2528.

Segura, T. L., O. B. Toon, A. Coloprete, and K. Zahnle (2002), Environmental effects of large impacts on Mars, *Science*, *298*, 1977-1980.

Settle, M. (1979), Formation and deposition of volcanic sulfate aerosols on Mars, *J. Geophys. Res*., *84*, 8343-8354.

Smith, M. D., J. C. Pearl, B. J. Conrath, and P. R. Christensen (2001), Thermal Emission Spectrometer results: Mars atmospheric thermal structure and aerosol distribution, *J. Geophys. Res., 106*, 23,929-23,945.

Squyres, S. W., *et al.* (2004), The Opportunity Rover's Athena science investigation at Meridiani Planum, Mars, *Science, 306*, 1698-1703.

Thordason, T. and S. Self (2003), Atmospheric and environmental effects of the 1783-1784 Laki eruption: A review and reassessment, J. Geophys. Res., 108 (D1), AAC7.1-AAC7.29.

Wadhwa, M. (2001), Redox states of Mars' upper mantle and crust from Eu anomalies in shergottite pyroxenes, *Science*, *291*, 1527-1530.

Wänke, H., J. Bruckner, G. Dreibus, R. Rieder, and I. Ryanchikov (2001), Chemical composition of rocks and soils at the Pathfinder site, *Space Sci. Rev*., *96*, 317-330.

Wilson, R. J., and K. Hamilton (1996), Comprehensive model simulation of thermal tides in the Martian atmosphere, *J. Atmos. Sci.*, *53*, 1290-1326.

Wilson, L., and J. W. Head, III (1994), Mars: review and analysis of volcanic eruption theory and relationships to observed landforms, *Rev. Geophys*., *32*, 221-264.

Wilson, L., and J. W. Head, III (2002), Tharsis-radial graben systems as the surface manifestation of plume-related dike intrusion complexes: models and implications, *J. Geophys. Res*., *107*(E8), 5057, doi:10.1029/2001JE001593.

Wong, A.-S., S. K. Atreya, and T. Encrenaz (2004), Correction to "Chemical markers of possible hot spots on Mars," *J. Geophys. Res.*, *109,* E01007.

Wong, A.-S., S. K. Atreya, and T. Encrenaz (2005), Correction to and updated reaction in "Chemical markers of possible hot spots on Mars," *J. Geophys. Res.*, *110* (E4), E10002.

Yen, A. S., *et al.* (2005), An integrated view of the chemistry and mineralogy of Martian soils, *Nature, 436*, 49-54.

Yung Y., H. Nair, and M. E. Gerstell (1997), CO_2 greenhouse in the early Martian atmosphere: SO_2 inhibits condensation, *Icarus*, *130*, 222-224.

Zahnle, K. J., and R. M. Haberle (2006), Atmospheric sulfur chemistry on ancient Mars, paper presented at Workshop on Martian Sulfates as Recorders of Atmospheric-Fluid-Rock Interactions, Houston, Texas, Abstract #7046.

Zolotov, M. Y., and E. L. Shock (2005), Formation of jarosite-bearing deposits through aqueous oxidation of pyrite at Meridiani Planum, Mars, *Geophys. Res. Lett., 32*, L21203, doi:10.1029/2005GL024253.

Zuber, M. T. (2001), The crust and mantle of Mars, *Nature*, *412*, 220-227.

2.9 Tables

	Adirondack	Humphrey	Mazatzal
Oxides (wt %)			
SiO_2	45.30	45.85	45.55
TiO_2	0.49	0.58	0.57
Al_2O_3	10.42	10.40	10.72
Fe_2O_3	3.63	3.36	2.11
Cr_2O_3	0.62	0.67	0.59
FeO	15.71	15.67	16.83
MnO	0.42	0.42	0.43
MgO	11.90	10.67	10.34
CaO	7.76	8.15	8.23
Na_2O	2.09	2.35	2.62
K_2O	0.03	0.09	0.11
P_2O_5	0.54	0.59	0.63
FeS	0.83	0.83	0.83
Total	***99.81***	***99.79***	***99.63***

Table 2.1 Extrapolated rock end-member chemical compositions for the Gusev basalts.

	50mb	500mb
Mixing Ratios		
SO_2	6.14×10^{-5} / 2.45×10^{-3}	6.14×10^{-6} / 2.45×10^{-4}
H_2S	3.26×10^{-5} / 1.30×10^{-3}	3.26×10^{-6} / 1.30×10^{-4}
Partial Pressures (in bars)		
SO_2	2.11×10^{-6} / 8.40×10^{-5}	2.11×10^{-6} / 8.40×10^{-5}
H_2S	2.11×10^{-6} / 8.40×10^{-5}	2.11×10^{-6} / 8.40×10^{-5}

Table 2.2 Prescribed mixing ratios and partial pressures. Format of each entry is *Andrews-Hanna (lower bound) / Wilson (upper bound).*

	Avg T (K)	Max >260K (%)	Max >273K (%)	Max ΔT [a] (K)
50mb without water				
SO_2 Upper Bound	214	35	29	27
SO_2 Lower Bound	204	21	12	18
H_2S Upper Bound	198	17	9	9
H_2S Lower Bound	196	16	9	5
Control ("Dry")	195	16	9	--
50mb with water				
SO_2 Upper Bound	225	48	38	43
SO_2 Lower Bound	208	25	14	21
H_2S Upper Bound	199	18	10	7
H_2S Lower Bound	198	17	10	5
Control ("Wet")	197	16	9	--
500mb without water				
SO_2 Upper Bound	237	53	32	27
SO_2 Lower Bound	226	30	12	17
H_2S Upper Bound	232	36	18	29
H_2S Lower Bound	219	17	9	10
Control ("Dry")	215	16	8	--
500mb with water				
SO_2 Upper Bound	315	100	100	70
SO_2 Lower Bound	283	100	100	31
H_2S Upper Bound	264	100	99	9
H_2S Lower Bound	259	100	89	1
Control ("Wet")	258	100	87	--

[a] versus control run for matching pressure/water vapor configuration

Table 2.3 Sensitivity analysis for warming results. Average temperatures are global, annual average surface temperatures. Max > 260 K shows the fraction of the year for which the warmest surface location has a surface temperature > 260 K (a reasonable brine

freezing point). Max > 273 K is the same, but for the pure water freezing point. Max ΔT shows the maximum temperature deviation of the warmest surface location from the same point in the control run.

2.10 Figures

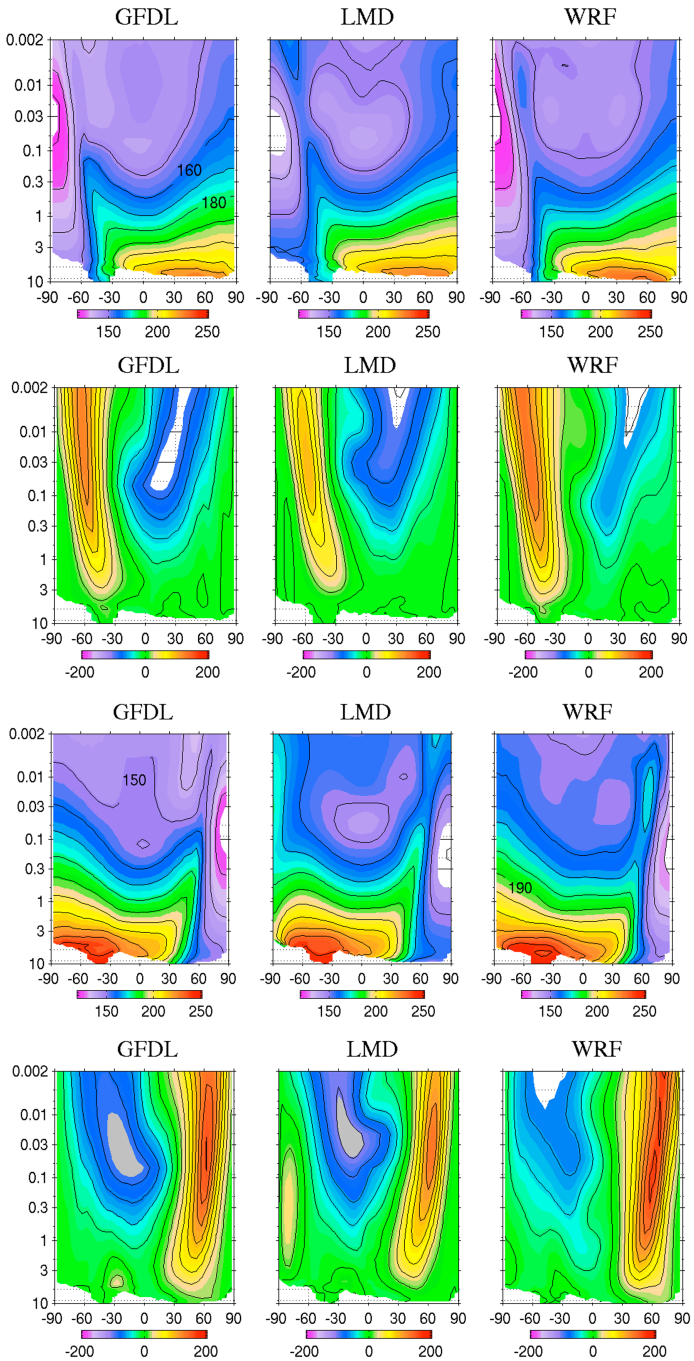

Figure 2.1 Comparison of MarsWRF output to model output from the GFDL Mars GCM and the LMD/AOPP Mars GCM. (top panel) Zonal mean temperature for L_s=90°,

(second panel) Zonal mean zonal wind for L_s=90°, (third panel) Same as top panel but at L_s=270°, (bottom panel) Same as second panel but at L_s=270°. All models have τ=0.2 column dust opacity. Abscissa units are millibars.

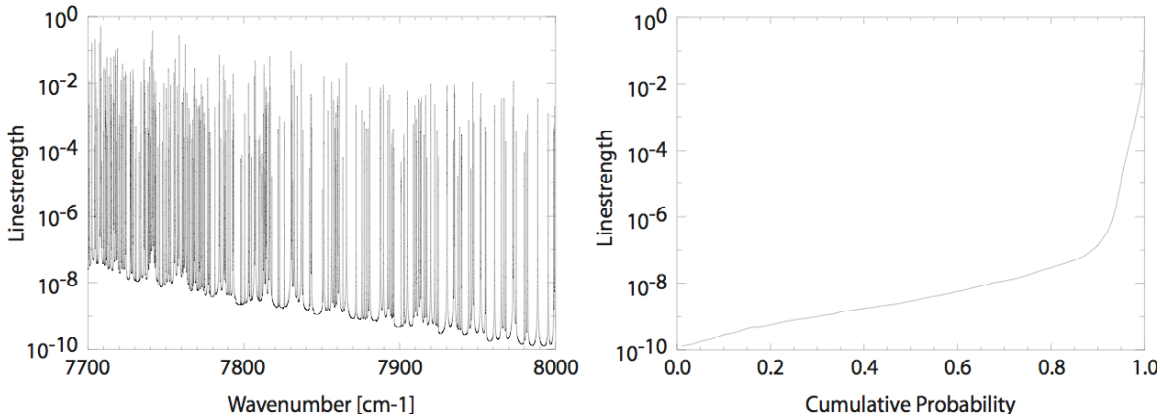

Figure 2.2 Comparison of a portion of the CO_2 spectrum both unsorted (left) and sorted by strength as a *k*-distribution (right). The sorted spectrum is substantially smoother than the unsorted spectrum, and the curve can be well approximated by few points. The elbow in the sorted curve marks the beginning of the contribution of the strong line cores in the distribution versus the relatively weaker line wings.

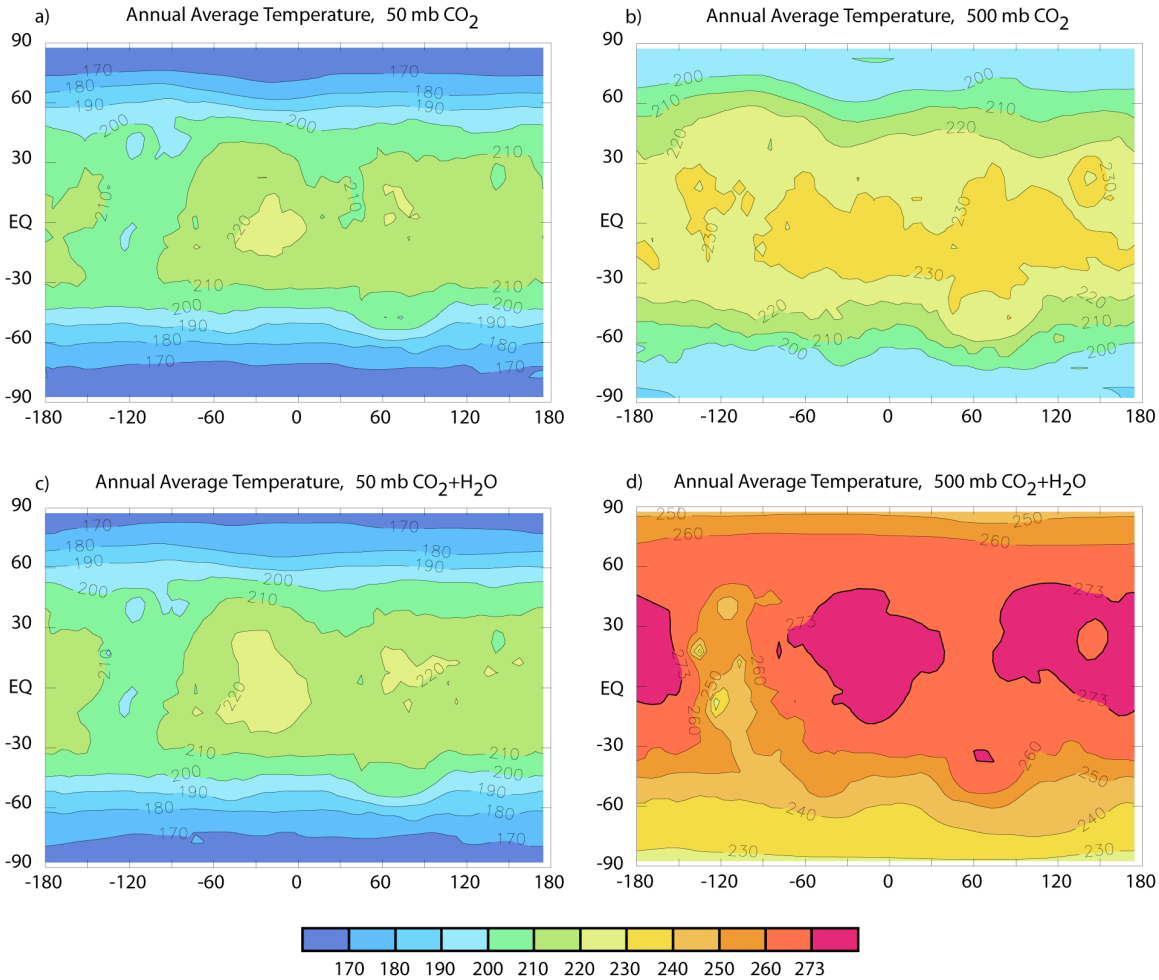

Figure 2.3 Annual average surface temperatures (in Kelvin) for control simulations: a) 50 mb atmosphere, CO_2 only, b) 500 mb atmosphere, CO_2 only, c) 50 mb atmosphere with CO_2+H_2O, and d) 500 mb atmosphere with CO_2+H_2O.

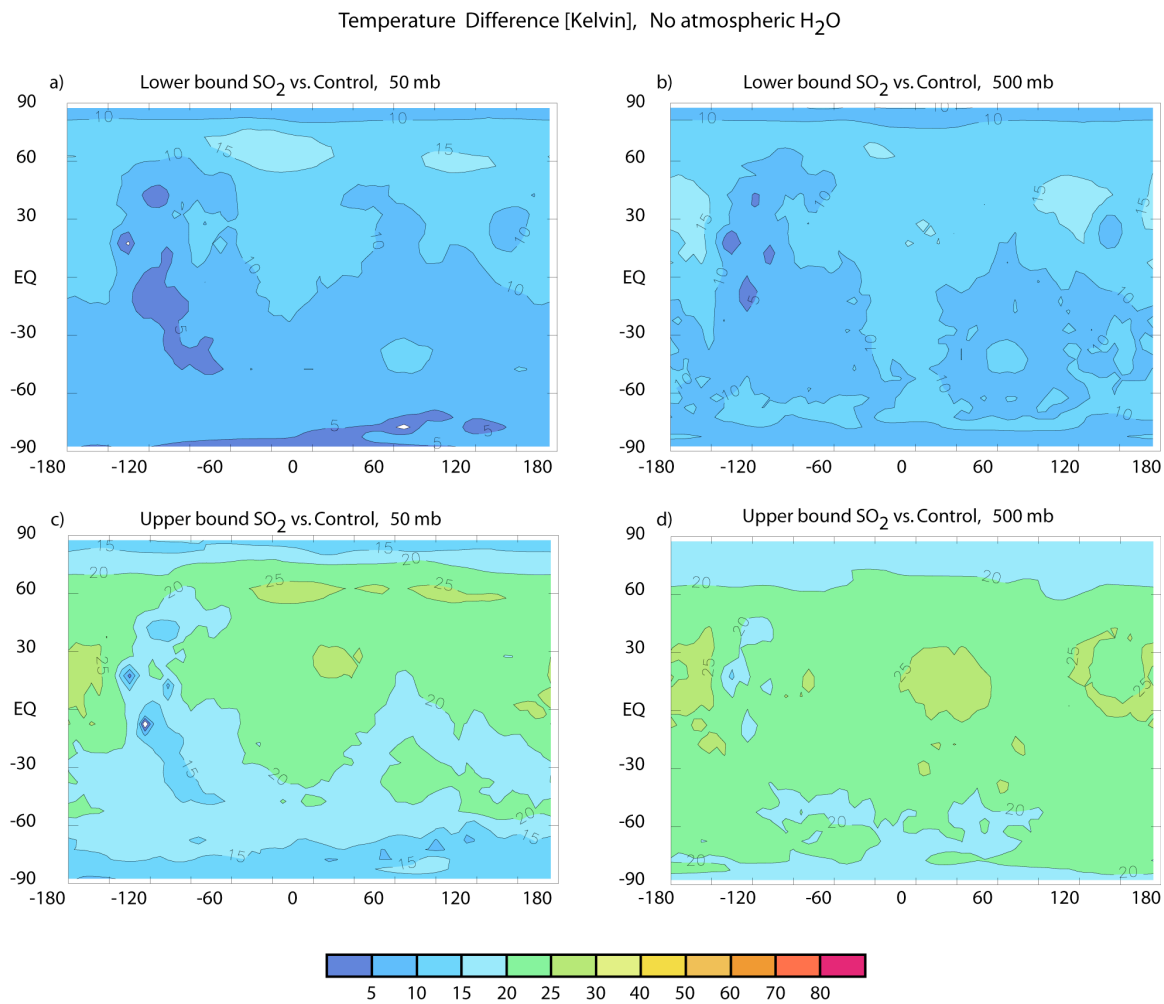

Figure 2.4 Difference (in Kelvin) in annual average surface temperature between the "dry" control simulations and SO_2 pulse simulations, *without* the effects of water vapor included, illustrating the magnitude of warming from SO_2 alone. a) Lower bound SO_2 abundance in 50 mb atmosphere, b) Lower bound SO_2 abundance in 500 mb atmosphere, c) Upper bound SO_2 abundance in 50 mb atmosphere, and d) Upper bound SO_2 abundance in 500 mb atmosphere. 'Control' simulation for left column is that in Figure 2.3a, and for right column, Figure 2.3b.

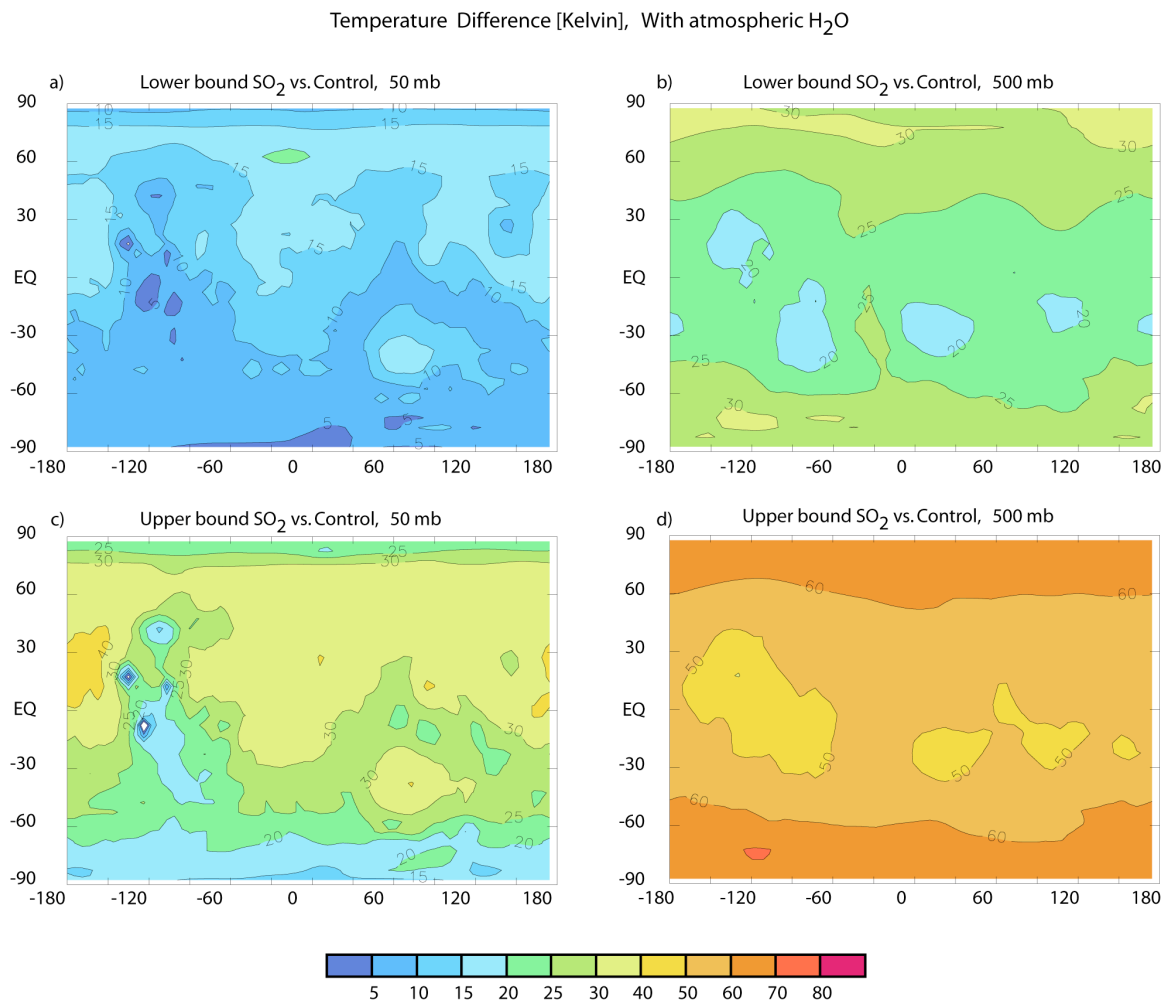

Figure 2.5 Difference (in Kelvin) in annual average surface temperature between the "wet" control simulations and SO_2 pulse simulations, *with* the effects of water vapor, depicting the combined warming from SO_2 and water vapor feedbacks. a) Lower bound SO_2 abundance in 50 mb atmosphere, b) Lower bound SO_2 abundance in 500 mb atmosphere, c) Upper bound SO_2 abundance in 50 mb atmosphere, and d) Upper bound SO_2 abundance in 500 mb atmosphere. 'Control' simulation for left column is that in Figure 2.3c, and for right column, Figure 2.3d.

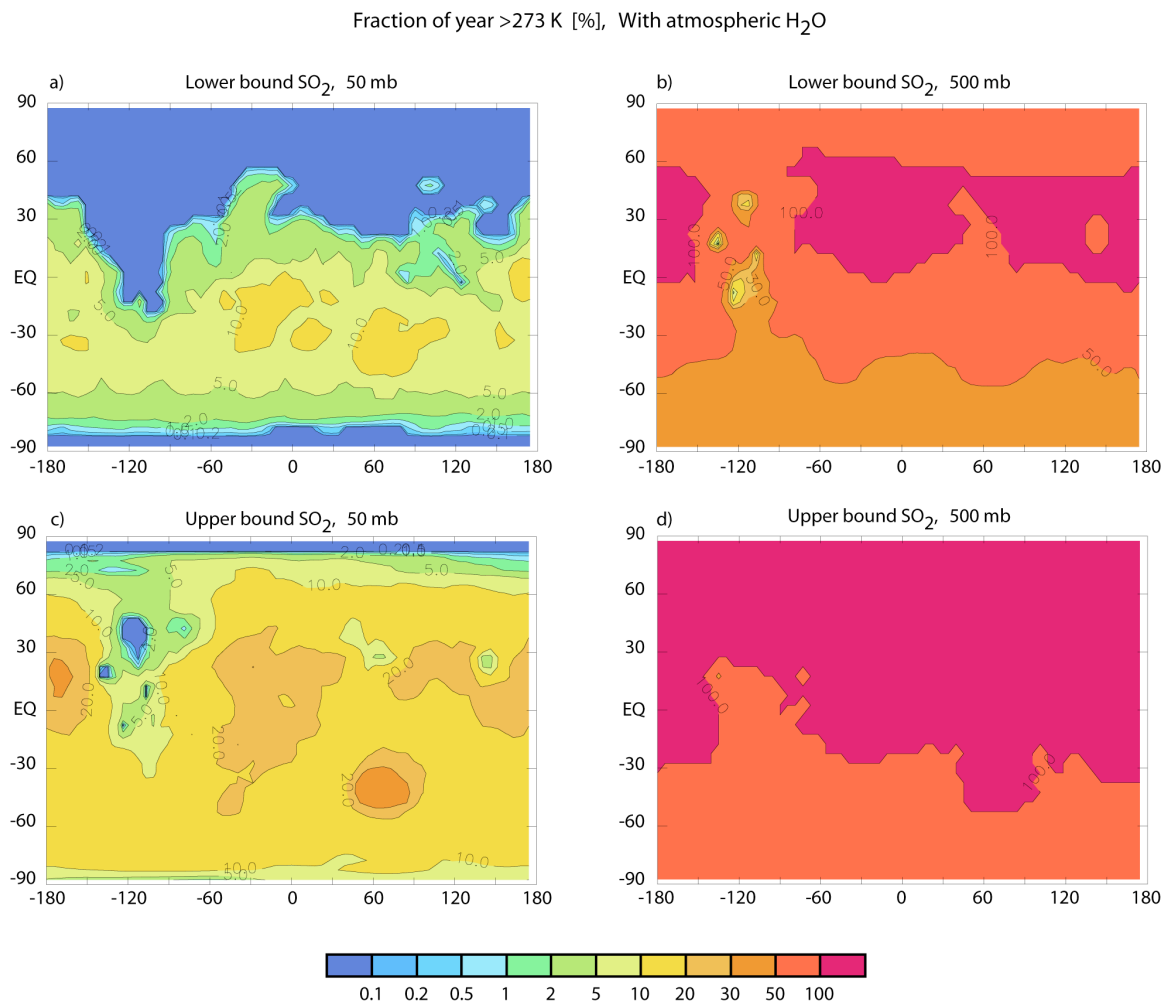

Figure 2.6 For the same configurations as Figure 2.5, fraction of the year (in percentage) that surface temperatures are >273 K at each model gridpoint. a) Lower bound SO_2 abundance in 50 mb atmosphere, b) Lower bound SO_2 abundance in 500 mb atmosphere, c) Upper bound SO_2 abundance in 50 mb atmosphere, and d) Upper bound SO_2 abundance in 500 mb atmosphere.

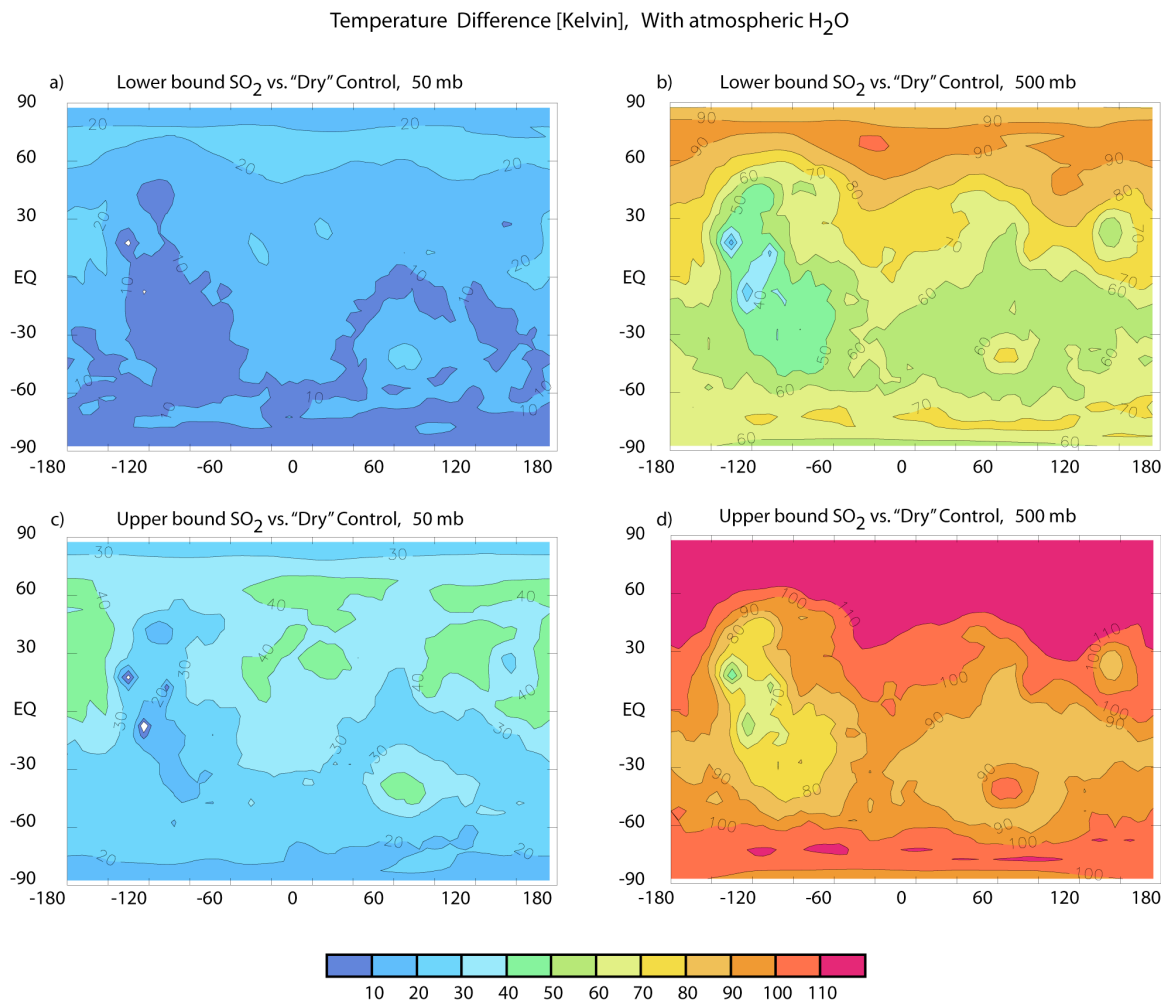

Figure 2.7 Difference (in Kelvin) in annual average surface temperature between the "dry" control simulations (CO_2 only) and SO_2 pulse simulations, *with* the effects of water vapor, depicting the total warming from H_2O and CO_2. a) Lower bound SO_2 abundance in 50 mb atmosphere, b) Lower bound SO_2 abundance in 500 mb atmosphere, c) Upper bound SO_2 abundance in 50 mb atmosphere, and d) Upper bound SO_2 abundance in 500 mb atmosphere. This should be seen as an upper extreme in the absence of negative feedback mechanisms such as cloud cover.

[THIS PAGE INTENTIONALLY LEFT BLANK]

Chapter 3

Longevity of SO_2 in the ancient Martian atmosphere: implications for transient greenhouse warming[1]

3.0 Abstract

There is increasing evidence that sulfur played an important role on early Mars. Sulfur is distributed ubiquitously on the Martian surface, and sulfur in Martian meteorites carries the signature of atmospheric interactions. Recent work suggests that the radiative properties of sulfur volatiles that were degassed into the Martian atmosphere may have caused a greenhouse effect early in the planet's history. It remains unclear, however, over what timescales these warming pulses would have persisted, and consequently how significant these pulses may have been. While photochemistry research to date has concentrated on current Martian conditions, the ancient Martian atmosphere was thicker, warmer, and more reducing than the current regime. Here we investigate sulfur photochemistry in a 500-mb ancient Martian atmosphere. After adapting a model used to study sulfur photochemistry on Earth during the Archaean, we find a short lifetime for SO_2 in the current Martian atmosphere, similar to results of other photochemical studies. Our simulations then suggest that moderate mixing ratios of SO_2 ($10^{-8} \leq f(SO_2) \leq 10^{-6}$)

[1] This chapter has been submitted to *Geophysical Research Letters*.

Johnson, S.S., A.A. Pavlov, and M.A. Mischna, "Longevity of SO_2 in the ancient Martian atmosphere: implications for transient greenhouse warming," *Geophys. Res. Lett.* submitted.

could have persisted in the ancient atmosphere for at least hundreds of years, generating short but potent warming episodes following an episode of volcanic activity.

3.1 Introduction

The element sulfur may be key to unlocking many of the questions associated with early geologic and climate history of Mars. Because degassed SO_2 can act as a powerful greenhouse gas, it has been suggested as an important atmospheric component during periods of enhanced volcanic activity on Mars [*Postawko and Kuhn*, 1986; *Settle*, 1979]. Isotopic analyses in Martian meteorites further support this view, reflecting deposition of sulfur species created by atmospheric chemical reactions [*Farquhar et al.,* 2000]. A recent investigation has indicated high sulfur solubility in Martian magmas, which, after a volcanic event, can generate a greenhouse warming effect of up to 25 K from SO_2 alone, and an even more potent effect if water vapor feedbacks are considered [*Johnson et al.,* 2007a, *Johnson et al.*, 2007b]. Therefore, despite Mars' greater distance from the sun than the Earth, and the likelihood of a less luminous sun early in solar system history [*Gough*, 1981], a greenhouse "boost" from SO_2 appears to have been capable of generating significant warming in the ancient Martian environment.

To estimate how long these warming pulses may have lasted, it is important to understand the fate of sulfur volatiles under these atmospheric conditions. Two investigations of sulfur photochemistry under current Martian conditions predict a

relatively brief photochemical lifetime to SO_2: *Settle* [1979] and *Wong et al.* [2003, 2004, 2005], the latter specifying a lifetime up to 600 days at high mixing ratios ($f(SO_2)=10^{-4}$). *Bullock and Moore* [2007] do address the ancient atmosphere with a set of calculations, but assume copious amounts of odd-hydrogen. Sulfur photochemistry studies have yet to sufficiently consider the differences between the current Martian atmosphere and a significantly denser, warmer atmospheric regime on ancient Mars. Here we explore a weakly reducing atmospheric regime, as has been suggested for early Earth and is further supported by the reduced state of the Martian mantle in comparison to Earth (near the iron-wustite buffer as opposed to the quartz-fayalite-magnetite buffer), and present results fully integrating sulfur photochemistry in the ancient Martian atmosphere. First, we present a validation of our model under the present-day Martian regime, and find results consistent with *Nair et al.,* [1994] and *Yung et al.* [1998]. Second, we proceed to our investigation of sulfur in the ancient Martian atmosphere and demonstrate sulfur volatile lifetimes could have been at least hundreds of years, representing a significantly longer lifetime than currently theorized for Mars. Our results suggest that under these conditions, SO_2 warming may have lasted long enough to allow liquid water to begin generating fluvial geologic features.

3.2 Photochemical model

To investigate sulfur chemistry, we use a horizontally averaged one-dimensional model adapted from a previous study of sulfur in the terrestrial Archean atmosphere [*Pavlov and*

Kasting, 2002]. The same base code has been used robustly in numerous studies, among them, investigations of NO_x photochemistry [*Kasting and Ackerman*, 1985] and chlorine-hydrocarbon photochemistry [*Singh and Kasting*, 1987] in the present-day Earth atmosphere, as well as NH_3 photochemistry [*Kasting*, 1982; *Pavlov, et al.,* 2001], CH_4 photochemistry [*Kasting, et al.*, 1983; *Pavlov, et al.,* 2000], and O_2 photochemistry [*Pavlov, et al.,* 2001] in the early Earth atmosphere. The one-dimensional model we use adapts this base code, carefully considering sulfur chemistry and incorporating the formation and diffusion of sulfate and elemental sulfur aerosols. In total, the model contains 359 chemical reactions involving 72 chemical species, including 16 sulfur species involved in 74 chemical reactions (see Figure 3.1 and Table 3.1). The model includes complexity, but this complexity is often necessary to resolve the chemistry of the system, as in the case of SO_2 recycling, and where it is not, as in the case of higher hydrocarbons, our results are not sensitive to the complexity of the model. Reactions and rate constants are adopted from *Pavlov et al.* [2001] and *Pavlov and Kasting* [2002] (see Table 3.1). For current Martian simulations, the model atmosphere is divided into 100 layers, each 1 km in height. At each layer, the continuity equation is solved for long-lived species, including transport by eddy and molecular diffusion. The combined equations are cast in centered, finite difference form. Boundary conditions are applied at the top and bottom of the atmosphere for each chemical species as in *Pavlov et al.* [2002]. At the upper boundary, zero flux is assumed for most species, and escape of H and H_2 is simulated by assuming a diffusion-limited upward flux [*Walker*, 1977; *Kasting and*

Brown, 1998]. As in *Nair et al.* [1994] and *Wong et al.* [2003], a fixed flux of atomic oxygen of 10^8 cm^{-2} s^{-1} is assumed for the upper boundary to balance hydrogen loss.

Two adjustments have been made to the model to enhance numerical stability. First, ten higher hydrocarbons have been eliminated from some of the simulations, all of which are organic molecules higher than C_2. Given the CO_2 rich atmosphere, we do not expect any hydrocarbon haze to form [*Pavlov et al.*, 2001; *Trainer et al.,* 2006]. In all output files, C_2H_6 mixing ratios are extremely small ($<10^{-30}$), thereby confirming that higher hydrocarbons would be even less significant. Second, N_2H_3 and N_2H_4 are removed from some simulations, as the mixing ratios for both species in previous output files are $<10^{-25}$.

The resulting set of coupled ordinary differential equations is integrated to steady state using the reverse Euler method. Once steady state is reached, sources and sinks for all chemical species are in balance and all major atmospheric species have converged. The model reaches this point after 10^8 model years (~500-2000 time steps). To explore dissipation of sulfur volatiles after an influx from a volcanic event, we take several snapshots of the atmosphere after a specified number of model years (e.g. 1, 10, 100, 1000, etc.).

3.3 Present-day Mars

We have performed an important set of simulations to validate our photochemistry model with previous studies of Martian photochemistry. A small number of adaptations are necessary to simulate the current Martian atmosphere. We assign the gravity for Mars at 373 cm s^{-2}, the albedo at 0.215, and the altitude of the tropopause at 15km. Due to the increased distance from the Sun, we assign the solar flux scaling for Mars as 0.43 of that incident upon Earth. We fix the CO_2 level at 6mb, and assign a fixed N_2 mixing ratio of 0.027 at the lower boundary of the model. Rainout rates in the model (determined using the method of *Giorgi and Chameides* [1986]) are adjusted to zero for current Martian conditions. For these simulations, we adopt a temperature profile and an eddy profile matching that of *Nair et al*. [1994]. Within the lower 20km of the atmosphere, water abundance is specified at a mixing ratio of 1.5×10^{-4}, as in *Wong et al.,* [2003, 2004, 2005], and is allowed to evolve photochemically at higher altitudes. A small amount of volcanic SO_2 production (10^6 molecules cm^{-2} s, approximately $1/1000^{th}$ of the current terrestrial SO_2 flux [*Holland*, 2002]) is also incorporated into the simulations.

Without imposing any additional constraints or boundary conditions, our results are exceptionally consistent with those of *Nair et al*. [1994]/*Yung and Demore* [1999]. The vertical profiles of major atmospheric constituents (O, H_2, CO and O_2) and radicals (HO_2, OH, H_2O_2 and H) are shown in Figures 3.2 and 3.3. For reference, the vertical profile of SO_2 is also included in Figure 3.3.

Even at moderate atmospheric loading levels, the lifetime of SO_2 under current Martian conditions is very short, consistent with prior studies. As a test case, we assign a moderate fixed mixing ratio of SO_2 ($f(SO_2)=10^{-7}$) in the lowermost level of the atmosphere in accordance with Model A of *Wong et al.* [2003, 2004, 2005]. We find broadly consistent chemistry (similar mixing ratios and column abundances at 10km altitude) as *Wong et al.* [2003, 2004, 2005]. We find the lifetime of SO_2 against photolysis for this scenario to be 18.23 days.

We note that our model incorporates more sophisticated sulfur photochemistry than previous models, including the formation of S_8 aerosols and a more nuanced scheme of H_2SO_4 condensation that allows for sulfur atoms incorporated into H_2SO_4 to be recycled back to SO_2. Thus, instead of considering a rate-determined lifetime against only SO_2 destruction via photolysis, we opt to consider *e*-folding times for SO_2 residence in the atmosphere in our work on ancient Mars.

3.4 Ancient Mars

For our simulations of the ancient Martian atmosphere, we extend our model atmosphere to 200 km to account for the higher-pressure regime. We set the atmospheric pressure of CO_2 and N_2 to 500 mb and 100 mb, respectively. For CO, we employ a fixed deposition velocity of 10^{-9} cm s^{-1}, in accordance the abiotic rate determined by *Kasting and Catling*

[2003]. We scale the solar UV flux up by a factor of five to account for higher Lyman-α UV fluxes in the Late Noachian [*Ribas et al.*, 2005]. We specify water vapor at the saturation vapor pressure (although it should be noted that sulfur lifetime is relatively insensitive to changes in water vapor in the troposphere in this temperature range; simulations at 77% relative humidity, Earth's global average, extend SO_2 persistence by less than 2%). Our vertical temperature profile, spanning from 258 K at the surface to 168 K in the upper atmosphere, is taken from radiative transfer steady state simulation results for a "wet" 500 mb CO_2 ancient Martian atmosphere [*Johnson et al.,* 2007b]. Our precipitation scheme is designed to mimic the hyperarid core of the Atacama Desert, as recent studies suggest that the geomorphology of Late Noachian basins on Mars are dominated by equal or greater aridity [*Stepinski and Stepinski*, 2005]. For our simulations, precipitation (as calculated by the terrestrial parameterization of *Giorgi and Chameides* [1986]) is reduced by a factor of 500. To take into account higher atmospheric pressure, we employ a terrestrial eddy diffusion profile scaled by the square root of density for the Martian atmosphere.

To study photochemical behavior, we begin from a steady-state atmosphere containing very little SO_2 ($f(SO)_2)<10^{-10}$). At the beginning of each simulation, we assign a starting SO_2 mixing ratio between 10^{-8} and 10^{-6}. Higher mixing ratios impose too large a disequilibrium on the system to generate model convergence under our 500 mb regime. The initial SO_2 mixing ratios are only assigned to the lower 20 km of the atmosphere,

simulating a Plinian eruption [see *Glaze and Baloga*, 2002]. We then take snapshots of the atmosphere after several different time steps as the atmosphere returns slowly to steady state. As oxidant rates change minimally from time step to time step, numerical noise is small, thereby enabling our use of the reverse Euler method for time-marching solutions.

In our model, no additional CO_2 is injected in association with the eruption because of its negligible mass compared to the background atmosphere. We predict that excess water vapor released with the eruption will condense quickly in the lower atmosphere, well before significant amounts of SO_2 (with a relatively low Henry constant) could be converted to H_2SO_4 (with a much higher Henry constant) and entrained. To test this, we simulated three days of rainout following the eruption at rates characteristic of the terrestrial tropics (an extreme overestimate, in part because much of the initial water vapor would have formed ice crystals). Even so, our initial $f(SO_2)$ of 10^{-6} only fell by 16%.

Figure 3.4 demonstrates the decline of SO_2 mixing ratios with time, as recorded in the lowermost layer of the atmosphere.

3.5 Sensitivity studies

We have completed a number of sensitivity studies on our simulations involving an initial SO_2 mixing ratio of 10^{-6}. First, we consider a higher-temperature regime, consistent with a 25 K greenhouse warming effect from a pulse of SO_2 in the atmosphere. This vertical temperature profile, spanning from 283 K at the surface to 180 K in the upper atmosphere, is taken from radiative transfer steady state simulation results for a "wet" 500 mb CO_2 ancient Martian atmosphere within three years of a 1.2×10^{13} kg SO_2 pulse (giving rise to a SO_2 mixing ratio of 6.14×10^{-6}) [*Johnson et al.,* 2007b].

Second and third, we explore the effects of a different hydrologic scheme. One set of simulations with a higher rate of precipitation is designed to mimic the rainout regime under conditions an order of magnitude more moist by reducing the *Giorgi and Chameides* parameterization by a factor of 50 (consistent with a few centimeters of precipitation per year). Another set considers even more arid conditions, reducing the *Giorgi and Chameides* parameterization by a factor of 1000. Finally, a last set of simulations studies the role of atmospheric mixing by scaling the eddy diffusion coefficient (*K*) profile scaled by a factor of five. The results of these sensitivity studies are shown in Figure 3.5 and Table 3.2.

3.6 Discussion

Our study shows that SO_2 is likely to persist much longer than has previously been assumed under ancient Martian conditions. Sulfur can leave the atmosphere in three primary ways: as S_8 aerosols, as SO_4 aerosols, and as SO_2 rainout (See Figure 3.1). The efficiency of these processes ultimately determines the lifetime of SO_2 in the atmosphere. As shown in Figure 3.6, the SO_2 photolysis rate decreases linearly with decreasing altitude in the current Martian atmosphere. In the ancient Martian regime, however, the SO_2 photolysis rate drops off dramatically in the lower atmosphere at moderate mixing ratios of SO_2. Furthermore, SO_2 photolysis alone cannot be considered as a loss of sulfur from the atmosphere, as recycling reactions may convert sulfur atoms back to SO_2.

The deposition of reduced sulfur is impeded by inefficient photolysis, which limits effective conversion of SO_2 to elemental S and on to S_8 aerosols (See Figure 3.7). Simultaneously, near-surface SO_2 becomes a significant sink for oxidants and, although mixing ratios of H_2O reach 10^{-2} near the bottom of the atmosphere in many simulations, a lack of oxidants precludes effective conversion of SO_2 to sulfate aerosols (Figure 3.8). Figure 3.9 shows that oxidants, particularly odd hydrogen, are highly depleted below the tropopause at a moderate SO_2 mixing ratio. In our simulations, there are simply too few oxidants per second to counter the increasing levels of SO_2. Thus, the abundance of aerosols, which tend to cool the atmosphere by reflecting incoming sunlight back to space, remain limited in the model atmosphere.

The major remaining loss process for sulfur is SO_2 rainout, and when rainout is small, SO_2 remains in the atmosphere. Over time, however, SO_2 rainout is the dominant mechanism for the destruction of sulfur in the ancient Martian atmosphere, as most of the initial influx of sulfur is lost as dissolved SO_2.

The reduced efficiency on ancient Mars of the processes that destroy atmospheric SO_2 results in a longer lifetime for SO_2 than previously assumed. Our findings suggest that SO_2 lifetime is highly dependent on oxidant availability, which cannot be properly modeled if the fates of non-sulfur atmospheric species are neglected. Our investigation indicates that the *e*-folding time for initial influxes of SO_2 is on the order of hundreds of years for moderate atmospheric loadings ($10^{-8} \leq f(SO_2) \leq 10^{-6}$). A lifetime of hundreds of years has important implications for understanding the ancient Martian atmosphere given recent studies assessing the potential for sulfur-induced greenhouse warming. Johnson et al. [2007b] report significant greenhouse warming at higher SO_2 mixing ratios, in the range of 10^{-6} to 10^{-4}. Although simulations at higher SO_2 mixing ratios impose too large an initial discontinuity in the system for model convergence, *e*-folding times for SO_2 only increase as additional sulfur is loaded into the atmosphere, as shown in Table 3.2 and Figure 3.4. Our results therefore suggest that transient greenhouse warming, arising from the degassing of SO_2 volatiles, likely persisted for at least hundreds of years, allowing for the stability of liquid water in the form of near-surface groundwater, lakes and streams capable of mediating debris flow and generating water-lain sedimentary deposits.

Not only would sulfur in the form of SO_2 have had strong atmospheric effects, the deposition of SO_2 (eventually oxidized to sulfate at the surface-atmosphere interface) would have generated potent acidity on the ancient Martian terrain. Indeed, extremely low pH levels are recorded in the mineral jarosite, recently discovered in Martian outcrop that dates to the Late Noachian [*Squyres et al.*, 2004]. Sulfuric acid can drastically depress the freezing point of water; for instance, a eutectic aqueous solution of 39% H_2SO_4 does not freeze until 200 K [*Clark*, 1999]. It is thus likely that sulfur played a dual role in the early history of the Mars: primarily as a potent greenhouse gas, and secondarily as an agent allowing sulfate-charged waters to remain in liquid form even after surface temperatures dropped below 273 K.

3.7 Conclusion

The element sulfur may have played an important role in the evolution of early Mars. In this study, we investigate the photochemical longevity of SO_2 in the ancient Martian atmosphere. Unlike simple models that render SO_2 photolysis as a final loss from the atmosphere, we consider nuanced recycling reactions, multiple sulfur species and associated reactions, as well as reduced sulfur chemistry and S_8 aerosols. We validate our model by fully replicating the present-day atmospheric results of *Nair, et al.* [1994]/*Yung* [1999], which no other model of sulfur photochemistry on Mars has done. We then load a model ancient atmosphere at moderate mixing ratios ($10^{-8} \leq f(SO_2) \leq 10^{-6}$)

to simulate volcanic degassing, and find *e*-folding times on the order of hundreds of years. Our results provide new insights to previous analyses [*Johnson et al.*, 2006; *Halevy, et al*. 2007; *Postawko and Kuhn*, 1986; *Bullock and Moore*, 2007] that suggest atmospheric SO_2 helped generated periods of transient warm, wet conditions, conditions that may have been conducive to the survival of simple life forms.

3.8 References

Adachi, H., N. Basco, and D. G. L. James (1981), The acetyl radicals CH_3CO and CD_3CO studied by flash photolysis and kinetic spectroscopy, *Int. J. Chem. Kinet., 13*, 1251–1276.

Albers, E. A., K. K. Hoyermann, H. G. G. Wagner, and J. Wolfrum (1969), Study of the reaction of ammonia with oxygen atoms, Symp. *Int. Combust. Proc., 12th*, 313– 320.

Allen, M., and J. E. Frederick (1982), Effective photodissociation cross sections for molecular oxygen and nitric oxide in the Schumann-Runge bands, *J. Atmos. Sci., 39,* 2066– 2075.

Allen, M., J. P. Pinto, and Y. L. Yung (1980), Titan: Aerosol photochemistry and variations related to the sunspot cycle, *Astrophys. J., 242*, L125– L128.

Allen, M., Y. L. Yung, and G. R. Gladstone (1992), The relative abundance of ethane to acetylene in the Jovian stratosphere, *Icarus, 100*, 527– 533,

Ashfold, M. N. R., M. A. Fullstone, G. Hancock, and G. W. Ketley (1981), Singlet methylene kinetics, *Chem. Phys., 55*, 245– 257.

Back, R. A. D., and W. L. Griffiths (1967), Flash photolysis of ethylene*, J. Chem. Phys., 46,* 4839– 4843.

Banyard, S. A., C. E. Canosa-Mas, M. D. Ellis, H. M. Frey, and R. Walsh (1980), Ketene photochemistry: Some observations on the reactions and reactivity of triplet methylene*, J. Chem. Soc. Chem. Commun., 1980,* 1156–1157.

Barassin, J., and J. Combourieu (1974), Etude cinètique des réaction entre l'oxygèn et les dèrivès chlorès du methane, *Bull. Soc. Chim. Fr., 1–2, part 1*, 1 –5.

Baughcum, S. L., and R. C. Oldenburg (1984), Measurement of the $C_2(a^3P_u)$ and $C_2(x\ ^1Sg^+)$ disappearance rates with O_2 from 298 to 1300 K, in *The Chemistry of Combustion Processes*, edited by T. M. Sloane, pp. 257–266, Am. Chem. Soc., Washington, D. C.

Baulch, D. L., D. D. Drysdale, and D. G. Horne (1973*), Evaluated Kinetic Data for High Temperature Reactions,* vol. 2, Butterworths, London.

Baulch, D. L., D. D. Drysdale, J. Duxbury, and S. J. Grant (1976), *Evaluated Kinetic Data for High Temperature Reactions,* vol. 3, Butterworths, London.

Becker, K. H., B. Engelhardt, P. Wiesen, and K. D. Bayes (1989), Rate constants for CH(x ^2P) reactions at low total pressures, *Chem. Phys. Lett., 154,* 342–348.

Benson, S. W., and G. R. Haugen (1967), The mechanism of the high temperature reaction of atomic hydrogen with acetylene over an extended pressure and temperature range, *J. Chem. Phys., 71*, 4404– 4411.

Berman, M. R., J. W. Fleming, A. B. Harvey, and M. C. Lin (1982), Temperature dependence of CH radical reactions with O_2, NO, CO, and CO_2, *Symp. Int. Combust. Proc., 19th*, 73– 85.

Bohland, T., S. Dóbé, F. Temps, and H. G.Wagner (1985), Kinetics of the reactions between CH_2(x $^3B_1$)-radicals and saturated hydrocarbons in the temperature range 296 K _ T _ 707 K, *Ber. Bunsen Ges. Phys. Chem., 89,* 1110–1116.

Bohren, C. F., and D. R. Huffman (1998)*, Absorption and Scattering of Light by Small Particles*, 479 pp., John Wiley, New York.

Brouard, M., M. T. Macpherson, and M. J. Pilling (1989), Experimental and RRKM modeling study of the CH_3 + H and CH_3 + D reactions*, J. Phys. Chem., 93,* 4047– 4059.

Brown, R. L., and A. H. Laufer (1981), Calculation of the activation energies for hydrogen-atom extinction reactions by radicals containing triple bonds, *J. Phys. Chem., 85,* 3826–3828.

Bullock, M. A., and H. J. Moore (2007), Atmospheric conditions on early Mars and the missing layered carbonates, *Geophys. Res. Lett.*, *43,* L19201.

Calvert, J. G., and J. N. Pitts, Jr. (1966), *Photochemistry*, John Wiley, New York.

Campbell, J. M., and B. A. Thrush (1967), The association of oxygen atoms and their combination with nitrogen atoms, *Proc. R. Soc. London, Ser. A, 296*, 222–232.

Cieslik, S., and M. Nicolet (1973), The aeronomic dissociation of nitric oxide, *Planet. Space Sci., 21*, 925– 939.

Clark, B. C. (1999), On the non-observability of carbonates on Mars. Paper presented at the Fifth International Mars Science Conference, Pasadena, California. Abstract # 6214.

Cox, R. A. (1974), *The photolysis of gaseous nitric acid—A technique for obtaining kinetic data on atmospheric photooxidation reactions, paper presented at the LODATA symposium on chemistry of the lower atmosphere,* Am. Chem. Soc., Warrenton, Va.

DeAlemeida, A. A., and P. D. Singh (1986), Photodissociation lifetimes of $^{32}S_2$ molecule in comets, *Earth Moon Planets, 36*, 117– 125.

Demerjian, K. L., J. A. Kerr, and J. G. Calvert (1974), The mechanism of photochemical smog formation, *Adv. Environ. Sci. Technol., 4,* 1– 262.

DeMore, W. B., J. J. Margitan, M. J. Molina, R. T. Watson, D. M. Golden, R. F. Hampson, M. J. Kurylo, C. J. Howard, and A. R. Ravishankara (1985), Chemical kinetics and photochemical data for use in stratospheric modeling, in *Evaluation 7, JPL Publ.*, 85-37.

DeMore, W. B., D. M. Golden, R. F. Hampson, C. J. Howard, M. J. Kurylo, M. J. Molina, A. R. Ravishankara, and S. P. Sander (1992), Chemical kinetics and photochemical data for use in stratospheric modeling, in *Evaluation 10, JPL Publ.*, 92-20.

Donovan, R. J., and D. Hussain (1970), Recent advances in the chemistry of electronically excited atoms, *Chem. Rev.*, 70, 489– 516.

Fahr, A., A. Laufer, R. Klein, and W. Braun (1991), Reaction rate determination of vinyl radical reactions with vinyl, methyl, and hydrogen atoms, *J. Phys. Chem., 95*, 3218–3224.

Farquhar, J., J. Savrino, T. L. Jackson, and M. H. Thiemnes (2000), Evidence of atmospheric sulphur in the Martian regolith from sulphur isotopes in meteorites, *Nature*, *404,* 50-52.

Fenimore, C. P. (1969), Destruction of methane in water gas by reaction of CH_3 with OH radicals, *Symp. Int. Combust. Proc., 12th*, 463– 467.

Gehring, M., G. Hoyermann, H. G. Wagner, and J. Wolfrum (1969), Reaction of atomic hydrogen with hydrazine, *Ber. Bunsen Ges. Phys. Chem., 73*, 956– 959.

Gendrin, A., *et al.* (2005), Sulfates in Martian layered terrains: The OMEGA/Mars Express view, *Science, 307*, 1587-1591.

Giguere, P. T., and W. F. Huebner (1978), A model of comet comae, *Astrophys. J., 223*, 638– 654.

Giorgi, F. and W. L. Chameides (1986), Rainout lifetimes of highly soluble aerosols and gases as inferred from simulations with a general circulation model, *J. Geophys. Res.*, *91*, 14,367-14,376

Gladstone, G. R. (1983), Radiative transfer and photochemistry in the upper atmosphere of Jupiter, Ph.D. thesis, Calif. Inst. of Technol., Pasadena.

Glaze, L. S. and S. M. Baloga (2002), Volcanic plume heights on Mars: Limits of validity for convective models, *J. Geophys. Res*, *107*(E10), 5086.

Gordon, S., W. Mulac, and P. Nangia (1971), Pulse radiolysis of ammonia gas, II, Rate of disappearance of the NH_2 (x $^2B_1$) radical, *J. Phys. Chem., 75*, 2087– 2093.

Gough, D. O. (1981), Solar interior structure and luminosity variations, *Solar Phys.*, *74*, 21-34.

Hampson, R. F., and D. Garvin (1977), Reaction rate and photochemical data for atmospheric chemistry, *Natl. Bur. Stand. Spec. Publ., 513*, 107 pp.

Herron, J. T., and R. E. Huie (1980), Rate constants at 298 K for the reactions SO + SO + M $(SO)_2$ + M and SO + $(SO)_2$ SO_2 + S_2O, *Chem. Phys. Lett., 76*, 322– 324.

Hills, H. A., R. J. Cicerone, J. G. Calvert, and J. W. Birks (1987), Kinetics of the reaction of S_2 with O, O_2, O_3, N_2O, NO, and NO_2, *J. Phys. Chem., 91*, 1199–1204.

Hochanadel, C. J., T. J. Sworski, and P. J. Ogren (1980), Ultraviolet spectrum and reaction kinetics of the formyl radical, *J. Phys. Chem., 84*, 231– 235.

Holland, H. D. (2002) Volcanic gases, black smokers, and the great oxidation event, *Geochim. Cosmochim. Ac., 66,* 3811-3826.

Homan, K. H., and H. Schweinfurth (1981), Kinetics and mechanism of hydrocarbon formation in the system C_2H_2/O/H, *Ber. Bunsen Ges. Phys. Chem., 85*, 569–577.

Houghton, J. T., et al. (1994), *Climate Change, 1994: Radiative Forcing of Climate Change and an Evaluation of the IPCC IS92 Emission Scenarios*, Cambridge Univ. Press, New York.

Hoyermann, K., N. S. Loftfield, R. Sievert, and H. G. Wagner (1981), Mechanisms and rates of the reactions of CH_3 and CH_2OH radicals with H atoms, *Symp. Int. Combust. Proc., 18th*, 831–842.

Huebner, W. F., and P. T. Giguere (1980), A model of comet comae, *Astrophys. J., 238,* 753-762.

Johnson, S. S., M. T. Zuber, T. L. Grove, A. A. Pavlov, and M. A. Mischna (2007a), Sulfur volatiles in the early Martian atmosphere, paper presented at Lunar and Planetary Science XXXVIII, League City, Texas, Abstract #1754.

Johnson, S. S., M. A. Mischna, M. T. Zuber, and T. L. Grove (2007b), Sulfur-induced Greenhouse Warming on Early Mars. *J. Geophys. Res.*, in press.

Kasting, J. F. (1982), Stability of ammonia in the primitive terrestrial atmosphere, *J. Geophys. Res., 87,* 3091– 3098.

Kasting, J. F., K. J. Zahnle, and J. C. G. Walker (1983), Photochemistry of methane in the Earth's early atmosphere, *Precambrian Res., 20*, 121– 148.

Kasting, J.F, and T.P. Ackerman (1985), High atmospheric NOx levels and multiple photochemical steady states. *J. Atmos. Chem. 3:* 321-340.

Kasting, J. F. (1990), Bolide impacts and the oxidation state of carbon in the Earth's early atmosphere, *Origins Life Evol. Biosphere, 20,* 199– 231.

Kasting, J.F. and L.L. Brown (1998), Setting the Stage: The Early Atmosphere as a Source of Biogenic Compounds. Brack A. "The Molecular Origins of Life: Assembling the Pieces of the Puzzle." Cambridge University Press, New York, 35–56.

Kasting, J. and Catling, D. (2003), Evolution of a Habitable Planet, *Annu. Rev. Astron. Astr., 41*, 429-463.

Kuhn, W. R., and S. K. Atreya (1979), Ammonia photolysis and the greenhouse effect in the primordial atmosphere of the Earth, *Icarus, 37*, 207– 213.

Lander, D. R., K. G. Unfried, G. P. Glass, and R. F. Curl (1990), Rate constant measurements of C_2H with CH_4, C_2H_6, C_2H_4, D_2, and CO, *J. Phys. Chem., 94*, 7759–7763.

Langford, R. B., and G. A. Oldershaw (1972), Flash photolysis of H_2S, J. *Chem. Soc. Faraday Trans. 1, 68*, 1550–1558.

Langford, A. D., H. Petek, and C. B. Moore (1983), Collisional removal of $CH_2(^1A_1)$: Absolute rate constants for atomic and molecular collisional partners at 295 K, *J. Chem. Phys., 78,* 6650– 6659.

Laufer, A. H. (1981), Kinetics of gas phase reactions of methylene, *Rev. Chem. Intermed., 4,* 225–257.

Laufer, A. H., E. P. Gardner, T. L. Kwok, and Y. L. Yung (1983), Computations and estimates of the rate coefficients for hydrocarbon reactions of interest to the atmosphere of the outer solar system, *Icarus, 56*, 560– 567.

Lee, L. C. (1980), CN(A^2P_i x $^2S^+$) and CN(B^2S^+ x $^2S^+$) yields from HCN photodissociation, *J. Chem. Phys., 72,* 6414–6421.

Lenzi, M., J. R. McNesby, A. Mele, and C. Nguyen Xuan (1972), Collisional deactivation of NH_2 (A^2A_1), *J. Chem. Phys., 57*, 319– 323.

Levine, J. S. (1985*), The photochemistry of the early atmosphere,* in The Photochemistry of Atmospheres, Earth, the Other Planets and Comets, edited by J. S. Levine, pp. 3– 38, Academic, San Diego, Calif.

Lightfoot, P. D., and M. J. Pilling (1987), Temperature and pressure dependence of the rate constant for the addition of H to C_2H_4, *J. Phys. Chem., 93*, 3373–3379.

McElroy, M. B., S. C. Wofsy, and N. D. Sze (1980), Photochemical sources for atmospheric H_2S, *Atmos. Environ., 14*, 159– 163.

McEwan, M. J., and L. F. Phillips (1975), *Chemistry of the Atmosphere*, John Wiley, New York.

McGovern, W. (1969), The primitive Earth: Thermal models of the upper atmosphere for a methane-dominated environment*, J. Atmos. Sci., 26*, 623–635.

Messing, I., S. V. Filseth, C. M. Sadowski, and T. Carrington (1981), Absolute rate constants for the reactions of CH with O and N atoms, *J. Chem. Phys., 74*, 3874– 3881.

Michael, J. V., D. F. Nava, W. A. Payne, and L. J. Stief (1979), Absolute rate constants for the reaction of atomic hydrogen with ketene from 298 to 500 K, *J. Chem. Phys., 70,* 5222–5228.

Miller, J. A., R. E. Mitchell, M. D. Smooke, and R. J. Kee (1982), Toward a comprehensive chemical kinetic mechanism for the oxidation of acetylene, *Symp. Int. Combust. Proc., 19th,* 181.

Mordaunt, D. H., I. R. Lambert, G. P. Morley, M. N. R. Ashfold, R. N. Dixon, and C. M. Western (1993), Primary product channels in the photodissociation of methane at 121.6 nm*, J. Chem. Phys., 98*, 2054– 2065.

Nair, H., M. Allen, A. D. Anbar, Y. L. Yung, and R. T. Clancy (1994), A photochemical model of the Martian Atmosphere. *Icarus, 111*, 124-150.

Nakayama, T., and K. Watanabe (1964), Absorption and photoionization coefficients of acetylene, propyne, and 1-butyne, *J. Chem. Phys., 40*, 558–561.

Niki, H., P. D. Maker, C. M. Savage, and L. P. Breitenbach (1978), Relative rate constants for the reaction of hydroxyl radicals with aldehydes, *J. Phys. Chem., 82*, 132–134.

Okabe, H. (1971), Fluorescence and predissociation of sulfur dioxide, *J. Am. Chem. Soc., 93,* 7095– 7096.

Okabe, H. (1978), *Photochemistry of Small Molecules*, John Wiley, New York.

Okabe, H. (1981), Photochemistry of acetylene at 1470 A ° , *J. Chem. Phys., 75*, 2772–2778.

Okabe, H. (1983), Photochemistry of acetylene at 1849 A ° , J. Chem. Phys., 78, 1312–1317.

Parkes, D. A., D. M. Paul, C. P. Quinn, and R. C. Robson (1973), The ultraviolet absorption by alkylperoxy radicals and their mutual reactions, *Chem. Phys. Lett., 23*, 425–429.

Pavlov, A. A., J. F. Kasting, L. L. Brown, K. A. Rages, and R. Freedman (2000), Greenhouse warming by CH_4 in the atmosphere of early Earth, *J. Geophys. Res., 105*, 11,981-11,990.

Pavlov, A. A., L. L. Brown, and J.F. Kasting (2001), UV shielding of NH_3 and O_2 by organic hazes in the Archean atmosphere, *J. Geophys. Res., 106* (E10) 23,267-23,288.

Pavlov, A. A. and J. F. Kasting (2002), Mass-independent fractionation of sulfur isotopes in Archean sediments: Strong evidence for an anoxic Archean atmosphere, *Astrobiology*, *2*, 27-41.

Parkes, D. A., D. M. Paul, C. P. Quinn, and R. C. Robson (1973), The ultraviolet absorption by alkylperoxy radicals and their mutual reactions, *Chem. Phys. Lett., 23*, 425–429.

Perry, R. A., and D. Williamson (1982), Pressure and temperature dependence of the OH radical reaction with acetylene, *Chem. Phys. Lett., 93*, 331– 332.

Pinto, J. P., C. R. Gladstone, and Y. L. Yung (1980), Photochemical production of formaldehyde in the Earth's primitive atmosphere, *Science, 210*, 183–185.

Pitts, W. M., L. Pasternack, and J. R. McDonnald (1982), Temperature dependence of the C_2(x $^1S\pm$) reaction with H_2 and CH_4 and C_2(x $^1S\pm$ and a^3 P_u equilibrated states) with O_2, *Chem. Phys., 68*, 417–422.

Postawko, S. E., and W. R. Kuhn (1986), Effect of the greenhouse gases (CO_2, H_2O, SO_2) on Martian paleoclimate, *J. Geophys. Res., 91,* D431-438.

Prasad, S. S., and W. T. Huntress (1980), A model for gas phase chemistry in interstellar clouds, *Astrophys. J. Suppl. Ser., 43*, 1–35.

Pratt, G. L., and S. W. Wood (1984), Kinetics of the reaction of methyl radicals with oxygen*, J. Chem. Soc. Faraday Trans., 80,* 3419–3427.

Rabalais, J. W., J. M. McDonald, V. Scherr, and S. P. McGlynn (1971), Electronic spectroscopy of isoelectronic molecules, *Chem. Rev., 71,* 73– 108.

Ribas, I., E. F. Guinan, M. Güdel, and M. Audard (2005), Evolution of the Solar Activity over Time and Effects on Planetary Atmospheres. I. High-Energy Irradiances (11700 Å), *Astrophysical J., 622*, 680-694.

Romani, P. N., J. Bishop, B. Beézard, and S. Atreya (1993), Methane photochemistry on Neptune: Ethane and acetylene mixing ratios and haze production, *Icarus, 106*, 442– 463.

Settle, M. (1979), Formation and deposition of volcanic sulfate aerosols on Mars*, J. Geophys. Res., 84,* 8343-8354.

Shemansky, D. E. (1972), CO_2 extinction coefficient 1700 – 3000 A °*, J. Chem. Phys., 56,* 1582– 1587.

Singh, H.B. and J.F. Kasting (1987). Chlorine-hydrocarbon photochemistry in the marine troposphere and lower stratosphere. *J. Atmos. Chem., 7*, 261-285.

Stephens, J. W., J. L. Hall, H. Solka, W.-B. Yan, R. F. Curl, and G. P. Glass (1987), Rate constant measurements of reactions of C_2H with H_2, O_2, C_2H_2, and NO using color center laser kinetic spectroscopy, *J. Phys. Chem., 91*, 5740–5743.

Stepinski, T.F. and A. P. Stepinski (2005), Morphology of Drainage Basins as an Indicator of Climate on Early Mars. *J. Geophys. Res., 110*, E12S12

Stief, L. J., and W. A. Payne (1976), Absolute rate parameter for the reaction of atomic hydrogen with hydrazine*, J. Chem. Phys., 64*, 4892– 4897.

Squyres, S. W., *et al.* (2004), The Opportunity Rover's Athena science investigation at Meridiani Planum, Mars, *Science, 306*, 1698-1703.

Sullivan, J. O., and A. C. Holland (1966), *A congeries of absorption cross sections for wavelengths less than 3000 A* °, NASA Tech Rep., CR371.

Sworski, T. J., C. J. Hochanadel, and P. J. Ogren (1980), Flash photolysis of H_2O vapor in CH_4, *J. Phys. Chem., 84*, 129–134.

Thompson, B. A., P. Harteck, and R. R. Reeves (1963), Ultraviolet absorption coefficients of CO_2, CO, O_2, H_2O, N_2O, NH_3, NO, SO_2 and CH_4 between 1850 and 4000 A °, *J. Geophys. Res., 68*, 6431–6436.

Toublanc, D., J. P. Parisot, J. Brillet, D. Gautier, F. Raulin, and C. P. McKay (1995), Photochemical modeling of Titan's atmosphere, *Icarus, 113*, 2 –26.

Trainer, M. G., A. A. Pavlov, H. L. DeWitt, J. L. Jimenez, C. P. McKay, O. B. Toon, and M. A. Tolbert (2006), Organic haze on Titan and the early Earth, *Proc. Nat. Acad. Sci. 103*, 18035-18042.

Tsang, W., and R. F. Hampson (1986), Chemical kinetic database for combustion chemistry, part 1, Methane and related compounds, *J. Phys. Chem. Ref. Data, 15*, 1087–1279.

Turco, R. P., P. Hamill, O. B. Toon, R. C. Whitten, and C. S. Kiang (1979), A onedimensional model describing aerosol formation and evolution in the stratosphere, I, Physical processes and mathematical analogs, *J. Atmos. Sci., 36*, 699– 717.

Turco, R. P., R. C. Whitten, and O. B. Toon (1982), Stratospheric aerosols: Observation and theory, *Rev. Geophys., 20,* 233– 279.

Veyret, B., and R. Lesclaux (1981), Absolute rate constants for the reactions of HCO with O_2 and NO 298 to 503K, *J. Phys. Chem., 85*, 1918–1922,

Von Wagner, H. G., and R. Zellner (1971), Reaktionen von Wasserstoffatomen mit ungesättigten C3-Kohlenwasserstoffen, II, Die Reaktion von H-Atomen mit Methylacetylen, *Ber. Bunsen Ges. Phys. Chem., 76*, 518– 525.

Wagner, A. F., and D. M. Wardlaw (1988), Study of the recombination reaction CH_3 + CH_3 = C_2H_6, 2, Theory, *J. Phys. Chem., 92,* 2462–2471.

Walker, J. C. G. (1977), *Evolution of the Atmosphere*, Macmillan, Old Tappan, N. J.

Warnatz, J. (1984*), Rate coefficients in the C/H/O system,* in Combustion Chemistry, edited by W. C. Gardiner Jr., pp. 197– 360, Springer-Verlag, New York.

Warneck, P., F.F. Marmo, and J. O. Sullivan (1964), Ultraviolet absorption of SO_2: Dissociation energies of SO_2 and SO*, J. Chem. Phys., 40,* 1132–1136.

Washida, N. (1981), Reaction of ethanol and $CH_3CH(OH)$ radicals with atomic molecular oxygen, *J. Chem. Phys., 75,* 2715– 2722.

Watkins, K. W., and W. W. Word (1974), Addition of methyl radicals to carbon monoxide, *Int. J. Chem. Kinet., 6*, 855–866.

Wen, J.-S., J. P. Pinto, and Y. L. Yung (1989), Photochemistry of CO and H_2O: Analysis of laboratory experiments and applications to the prebiotic Earth's atmosphere, *J. Geophys. Res., 94*, 14,957–14,970.

Whytock, D. A., W. A. Payne, and L. J. Stief (1976), Rate of the reaction of atomic hydrogen with propyne over an extended pressure and temperature range*, J. Chem. Phys., 65*, 191– 195.

Wong, A.-S., S. K. Atreya, and T. Encrenaz (2003), Chemical markers of possible hot spots on Mars, *J. Geophys. Res.*, *108* (E4), 5026.

Wong, A.-S., S. K. Atreya, and T. Encrenaz (2004), Correction to "Chemical markers of possible hot spots on Mars," *J. Geophys. Res.*, *109,* E01007.

Wong, A.-S., S. K. Atreya, and T. Encrenaz (2005), Correction to and updated reaction in "Chemical markers of possible hot spots on Mars," *J. Geophys. Res.*, *110* (E4), E10002.

World Meteorological Organization (WMO) (1985), *Atmospheric Ozone*, vol. 1, WMO Rep. 16, Geneva, Switzerland.

Yung, Y. L., and W. B. DeMore (1982), Photochemistry of the stratosphere of Venus: Implications for atmospheric evolution, Icarus, 51, 199–247.

Yung, Y. L., M. Allen, and J. P. Pinto (1984), Photochemistry of the atmosphere of Titan: Comparison between model and observations, *Astrophys. J. Suppl. Ser., 55*, 465– 506

Yung Y., H. Nair, and M. E. Gerstell (1997), CO_2 greenhouse in the early Martian atmosphere: SO_2 inhibits condensation, *Icarus*, *130*, 222-224.

Yung, Y.L., and W. B. Demore (1999), Photochemistry of Planetary Atmospheres, Oxford University Press: New York.

Zabarnick, S., J. W. Fleming, and M. C. Lin (1986), Kinetic study of the reaction CH(x ^2P) +H_2 _ CH_2(x $^3B_1$) + H in the temperature range 372 to 675 K, *J. Chem. Phys., 85*, 4373– 4376.

Zahnle, K. J. (1986), Photochemistry of methane and the formation of hydrocyanic acid (HCN) in the Earth's early atmosphere, *J. Geophys. Res., 91*, 2819–2834.

Zelikoff, M., and K. Watanabe (1953), Absorption coefficients of ethylene in the vacuum ultraviolet, *J. Opt. Soc. Am., 43*, 756–759.

3.9 Tables

No.	*Reaction*	*Rate Constant (cm^3/s^{-1})*	*Reference/Notes*
R1	$H_2O + O(^1D) \rightarrow 2\ OH$	2.2×10^{-10}	*DeMore et al.* [1992]
R2	$H_2 + O(^1D) \rightarrow OH + H$	1.0×10^{-10}	*DeMore et al.* [1992]
R3	$H_2 + O \rightarrow OH + H$	$3.0 \times 10^{-14} T \exp(-4480/T)$	*Hampson and Garvin* [1977]
R4	$H_2 + OH \rightarrow H_2O + H$	$5.5 \times 10^{-12} \exp(-2000/T)$	*DeMore et al.* [1992]
R5	$H + O_3 \rightarrow OH + O_2$	$1.4 \times 10^{-10} \exp(-470/T)$	*DeMore et al.* [1992]
R6	$H + O_2 + M \rightarrow HO_2 + M$	$k_0 = 5.7 \times 10^{-32} (300/T)^{1\ 6}$ $k_\infty = 7.5 \times 10^{-11}$	*DeMore et al.* [1992]
R7	$H + HO_2 \rightarrow H_2 + O_2$	$8.1 \times 10^{-11} \times (0.08)$	*DeMore et al.* [1992]
R8	$H + HO_2 \rightarrow H_2O + O$	$8.1 \times 10^{-11} \times (0.02)$	*DeMore et al.* [1992]
R9	$H + HO_2 \rightarrow OH + OH$	$8.1 \times 10^{-11} \times (0.90)$	*DeMore et al.* [1992]
R10	$OH + O \rightarrow H + O_2$	$2.2 \times 10^{-11} \exp(120/T)$	*DeMore et al.* [1992]
R11	$OH + HO_2 \rightarrow H_2O + O_2$	$4.8 \times 10^{-11} \exp(250/T)$	*DeMore et al.* [1992]
R12	$OH + O_3 \rightarrow HO_2 + O_2$	$1.6 \times 10^{-12} \exp(-940/T)$	*DeMore et al.* [1992]
R13	$HO_2 + O \rightarrow OH + O_2$	$3.0 \times 10^{-11} \exp(200/T)$	*DeMore et al.* [1992]
R14	$HO_2 + O_3 \rightarrow OH + 2O_2$	$1.1 \times 10^{-14} \exp(-500/T)$	*DeMore et al.* [1992]
R15	$HO_2 + HO_2 \rightarrow H_2O_2 + O_2$	$2.3 \times 10^{-13} \exp(600/T)\ [M] + 1.7 \times 10^{-33} \exp(1000/T)\ [M]$	*DeMore et al.* [1992]
R16	$H_2O_2 + OH \rightarrow HO_2 + H_2O$	$2.9 \times 10^{-12} \exp(-160/T)$	*DeMore et al.* [1992]
R17	$O + O + M \rightarrow O_2 + M$	$2.76 \times 10^{-34} \exp(710/T)\ [M]$	*Campbell and Thrush* [1967]
R18	$O + O_2 + M \rightarrow O_3 + M$	$k_0 = 6.0 \times 10^{-34} (300/T)^{2\ 3}$ $k_\infty = 1 \times 10^{-10}$	*DeMore et al.* [1992]
R19	$O + O_3 \rightarrow 2O_2$	$8 \times 10^{-12} \exp(-2060/T)$	*DeMore et al.* [1992]
R20	$OH + OH \rightarrow H_2O + O$	$4.2 \times 10^{-12} \exp(-240/T)$	*DeMore et al.* [1992]
R21	$O(^1D) + M \rightarrow O + M$	$1.8 \times 10^{-11} \exp(110/T)$	*DeMore et al.* [1992]
R22	$O(^1D) + O_2 \rightarrow O + O_2$	$3.2 \times 10^{-11} \exp(70/T)$	*DeMore et al.* [1992]
R23	$O_2 + h\nu \rightarrow O + O(^1D)$	$2.51 \times 10^{-6}\ s^{-1}$	*Thompson et al.* [1963]
R24	$O_2 + h\nu \rightarrow O + O$	$4.81 \times 10^{-8}\ s^{-1}$	*Allen and Frederick* [1982]
R25	$H_2O + h\nu \rightarrow H + OH$	$7.83 \times 10^{-6}\ s^{-1}$	*Thompson et al.* [1963]
R26	$O_3 + h\nu \rightarrow O_2 + O(^1D)$	$5.81 \times 10^{-3}\ s^{-1}$	*WMO* [1985]
R27	$O_3 + h\nu \rightarrow O_2 + O$	$1.48 \times 10^{-3}\ s^{-1}$	*WMO* [1985]
R28	$H_2O_2 + h\nu \rightarrow 2OH$	$8.41 \times 10^{-5}\ s^{-1}$	*DeMore et al.* [1985]
R29	$CO2 + h\nu \rightarrow CO + O(3P)$	$1.35 \times 10^{-9}\ s^{-1}$	*Shemansky* [1972]
R30	$CO + OH \rightarrow CO_2 + H$	$1.5 \times 10^{-13} (1 + 0.6\ P_{atm})$	*DeMore et al.* [1992]
R31	$CO + O + M \rightarrow CO_2 + M$	$6.5 \times 10^{-33} \exp(-2180/T)\ [M]$	*Hampson and Garvin* [1977]
R32	$H + CO + M \rightarrow HCO + M$	$2.0 \times 10^{-33} \exp(-850/T)\ [M]$	*Baulch et al.* [1976]
R33	$H + HCO \rightarrow H_2 + CO$	1.2×10^{-10}	*Hochanadel et al.* [1980]
R34	$HCO + HCO \rightarrow H_2CO + CO$	2.3×10^{-11}	*Hochanadel et al.* [1980]
R35	$OH + HCO \rightarrow H_2O + CO$	5.0×10^{-11}	*Baulch et al.* [1976]

No.	*Reaction*	*Rate Constant (cm^3/s^{-1})*	*Reference/Notes*	
R36	$O + HCO \rightarrow H + CO_2$	1.0×10^{-10}	*Hampson and Garvin* [1977]	
R37	$O + HCO \rightarrow OH + CO$	1.0×10^{-10}	*Hampson and Garvin* [1977]	
R38	$H_2CO + h\nu \rightarrow H_2 + CO$	$4.85 \times 10^{-5}\ s^{-1}$	*DeMore et al.* [1985]	
R39	$H_2CO + h\nu \rightarrow HCO + H$	$5.85 \times 10^{-5}\ s^{-1}$	*DeMore et al.* [1985]	
R40	$HCO + h\nu \rightarrow H + CO$	$1 \times 10^{-2}\ s^{-1}$	*Pinto et al.* [1980]	1
R41	$H_2CO + H \rightarrow H_2 + HCO$	$2.8 \times 10^{-11} \exp(-1540/T)$	*DeMore et al.* [1985]	
R42	$CO_2 + h\nu \rightarrow CO + O(^1D)$	$1.48 \times 10^{-7}\ s^{-1}$	*Thompson et al.* [1963]	
R43	$H + H + M \rightarrow H_2 + M$	$1.5 \times 10^{-29}\ T^{-1.3}$	*Tsang and Hampson* [1986]	
R44	$HCO + O_2 \rightarrow HO_2 + CO$	$5.5 \times 10^{-11}\ T^{-0\ 4}$	*Veyret and Lesclaux* [1981]	
R45	$H_2CO + OH \rightarrow H_2O + HCO$	1×10^{-11}	*DeMore et al.* [1992]	
R46	$H + OH + M \rightarrow H_2O + M$	$6.1 \times 10^{-26}\ T^{-2}\ [M]$	*McEwan and Phillips* [1975]	
R47	$OH + OH + M \rightarrow H_2O_2 + M$	$k_0 = 6.9 \times 10^{-31}\ (300/T)^{0.8}$ $k_\infty = 1.5 \times 10^{-11}$	*DeMore et al.* [1992]	
R48	$H_2CO + O \rightarrow HCO + OH$	$3.4 \times 10^{-11} \exp(-1600/T)$	*DeMore et al.* [1992]	
R49	$H_2O_2 + O \rightarrow OH + HO_2$	$1.4 \times 10^{-12} \exp(-2000/T)$	*DeMore et al.* [1992]	
R50	$HO_2 + h\nu \rightarrow OH + O$	$5.46 \times 10^{-4}\ s^{-1}$	*DeMore et al.* [1985]	
R51	$CH_4 + h\nu \rightarrow {}^1CH_2 + H_2$	$1.38 \times 10^{-6}\ s^{-1}$, Ly α: 0.24; other: 1	*Mordaunt et al.* [1993]	
R52*	$C_2H_6 + h\nu \rightarrow 2\,{}^3CH_2 + H_2$	0		
R53*	$C_2H_6 + h\nu \rightarrow CH_4 + {}^1CH_2$	$6.35 \times 10^{-7}\ s^{-1}$, Ly α: 0.25; other: 0.02	*Yung et al.* [1984]	
R54	$HNO_2 + h\nu \rightarrow NO + OH$	$1.7 \times 10^{-3}\ s^{-1}$	*Cox* [1974]	
R55	$HNO_3 + h\nu \rightarrow NO_2 + OH$	$1.15 \times 10^{-4}\ s^{-1}$	*DeMore et al.* [1985]	
R56	$NO + h\nu \rightarrow N + O$	$1.84 \times 10^{-6}\ s^{-1}$	*Cieslik and Nicolet* [1973]	
R57	$NO_2 + h\nu \rightarrow NO + O$	$5.81 \times 10^{-3}\ s^{-1}$	*DeMore et al.* [1985]	
R58	$CH_4 + OH \rightarrow CH_3 + H_2O$	$2.9 \times 10^{-12} \exp(-1820/T)$	*DeMore et al.* [1992]	
R59	$CH_4 + O(^1D) \rightarrow CH_3 + OH$	1.4×10^{-10}	*DeMore et al.* [1992]	
R60	$CH_4 + O(^1D) \rightarrow H_2CO + H_2$	1.4×10^{-11}	*DeMore et al.* [1992]	
R61	${}^1CH_2 + CH_4 \rightarrow 2\ CH_3$	6.0×10^{-11}	*Bohland et al.* [1985]	
R62	${}^1CH_2 + O_2 \rightarrow HCO + OH$	3.0×10^{-11}	*Ashfold et al.* [1981]	
R63	${}^1CH_2 + M \rightarrow {}^3CH_2 + M$	8.8×10^{-12}	*Ashfold et al.* [1981]	
R64	${}^3CH_2 + H_2 \rightarrow CH_3 + H$	0		
R65	${}^3CH_2 + CH_4 \rightarrow 2\ CH_3$	0		
R66	${}^3CH_2 + O2 \rightarrow HCO + OH$	1.5×10^{-12}	*Prasad and Huntress* [1980]	
R67	$CH_3 + O_2 + M \rightarrow H_2CO + OH$	$k_0 = 4.5 \times 10^{-31}\ (300/T)^{3.0}$ $k_\infty = 1.8 \times 10^{-12}\ (300/T)^{1.7}$	*DeMore et al.* [1992]	
R68	$CH_3 + OH \rightarrow H_2CO + H_2$	9.3×10^{-11}	*Sworski et al.* [1980]	
R69	$CH_3 + O \rightarrow H_2CO + H$	1.1×10^{-10}	*DeMore et al.* [1992]	

No.	*Reaction*	*Rate Constant (cm^3/s^{-1})*	*Reference/Notes*	
R70	$CH_3 + O_3 \rightarrow H_2CO + HO_2$	$5.4 \times 10^{-12} \exp(-220/T)$	*DeMore et al.* [1992]	
R71*	$CH_3 + CH_3 + M \rightarrow C_2H_6 + M$	$F_C = 0.381 \exp(-T/73.2)$ + $0.619 \exp(-T/1180)$ $k_0 = 8.76 \times 10^{-7}\ T^{-7.03} \exp(-1390/T)\ [M]$ $k_\infty = 1.50 \times 10^{-7}\ T^{-1.18} \exp(-329/T)$	*Wagner and Wardlaw* [1988]	
R72	$CH_3 + h\nu \rightarrow {}^1CH_2 + H$	$1.87 \times 10^{-4}\ s^{-1}$	*Parkes et al.* [1973] and *Allen et al.* [1980]	
R73	$CH_3 + H + M \rightarrow CH_4 + M$	$F_C = 0.902 - (1.03 \times 10^{-3} T)$ $k_0 = 4.0 \times 10^{-29}\ [M]$ $k_\infty = 4.7 \times 10^{-10}$	*Brouard et al.* [1989]	2
R74	$CH_3 + HCO \rightarrow CH_4 + CO$	8.2×10^{-11}	*Hochanadel et al.* [1980]	
R75	$CH_3 + HNO \rightarrow CH_4 + NO$	3.0×10^{-14}	*Zahnle* [1986]	
R76	$CH_3 + H_2CO \rightarrow CH_4 + HCO$	$2.8 \times 10^{-11} \exp(-1540/T)$	*Zahnle* [1986]	
R77	$H + NO + M \rightarrow HNO + M$	$2.1 \times 10^{-32} \exp(-300/T)[M]$	*Hampson and Garvin* [1977]	
R78	$N + N + M \rightarrow N_2 + M$	0		
R79	$N + O_2 \rightarrow NO + O$	$1.5 \times 10^{-11} \exp(-3600/T)$	*DeMore et al.* [1992]	
R80	$N + O_3 \rightarrow NO + O_2$	0		
R81	$N + OH \rightarrow NO + H$	5.3×10^{-11}	*Baulch et al.* [1973]	
R82	$N + NO \rightarrow N_2 + O$	3.4×10^{-11}	*DeMore et al.* [1992]	
R83	$NO + O_3 \rightarrow NO_2 + O_2$	$2.0 \times 10^{-12} \exp(-1400/T)$	*DeMore et al.* [1992]	
R84	$NO + O + M \rightarrow NO_2 + M$	$k_0 = 9.0 \times 10^{-32}(300/T)^{1.5}$ $k_\infty = 3.0 \times 10^{-11}$	*DeMore et al.* [1992]	3
R85	$NO + HO_2 \rightarrow NO_2 + OH$	$3.7 \times 10^{-12} \exp(250/T)$	*DeMore et al.* [1992]	
R86	$NO + OH + M \rightarrow HNO_2 + M$	$k_0 = 7.0 \times 10^{-31}(300/T)^{2.6}$ $k_\infty = 1.5 \times 10^{-11}(300/T)^{0.5}$	*DeMore et al.* [1992]	3
R87	$NO_2 + O \rightarrow NO + O_2$	$6.5 \times 10^{-12} \exp(120/T)$	*DeMore et al.* [1992]	
R88	$NO_2 + OH + M \rightarrow HNO_3 + M$	$k_0 = 2.6 \times 10^{-30}(300/T)^{3.2}$ $k_\infty = 2.4 \times 10^{-11}(300/T)^{1.3}$	*DeMore et al.* [1992]	3
R89	$NO_2 + H \rightarrow NO + OH$	$4.0 \times 10^{-10} \exp(-340/T)$	*DeMore et al.* [1992]	
R90	$HNO_3 + OH \rightarrow H_2O + NO_2 + O$	$k_0 = 7.2 \times 10^{-15} \exp(785/T)$ $k_2 = 4.1 \times 10^{-16}\ (1440/T)$ $k_3 = 1.9 \times 10^{-33} \exp(725/T)[M]$	*DeMore et al.* [1992]	4
R91	$HCO + NO \rightarrow HNO + CO$	$1.2 \times 10^{-10}\ T^{-0.4}$	*Veyret and Lesclaux* [1981]	
R92	$HNO + h\nu \rightarrow NO + H$	$(= J_{HNO2})$	See (R54)	1
R93	$H + HNO \rightarrow H_2 + NO$	$5 \times 10^{-13} T^{0.5} \exp(-1200/T)$	*Baulch et al.* [1973]	
R94	$O + HNO \rightarrow OH + NO$	$(= k_{258})$		1

No.	*Reaction*	*Rate Constant (cm^3/s^{-1})*	*Reference/Notes*	
R95	$OH + HNO \rightarrow H_2O + NO$	6×10^{-11}	*Baulch et al.* [1973]	
R96	$HNO_2 + OH \rightarrow H_2O + NO_2$	$1.8 \times 10^{-11} \exp(-390/T)$	*DeMore et al.* [1992]	
R97	$CH_4 + O \rightarrow CH_3 + OH$	$5.8 \times 10^{-11} \exp(-4450/T)$	*Barassin and Combourie* [1974]	
R98	$^1CH_2 + H_2 \rightarrow CH_3 + H$	9.24×10^{-11}	*Allen et al.* [1992], *Langford et al.* [1983], *Ashfold et al.* [1981], and *Braun et al.* [1970]	
R99	$^1CH_2 + CO_2 \rightarrow H_2CO + CO$	1×10^{-12}	*Zahnle* [1986]	
R100	$^3CH_2 + O \rightarrow HCO + H$	1×10^{-11}	*Huebner and Giguere* [1980]	
R101	$^3CH_2 + CO_2 \rightarrow H_2CO + CO$	3.9×10^{-14}	*Laufer* [1981]	
R102*	$C_2H_6 + OH \rightarrow C_2H_5 + H_2O$	$8.7 \times 10^{-12} \exp(-1070/T)$	*DeMore et al.* [1992]	
R103*	$C_2H_6 + O \rightarrow C_2H_5 + OH$	$4.1 \times 10^{-11} \exp(-3200/T)$	*Hampson and Garvin* [1977]	
R104*	$C_2H_6 + O(^1D) \rightarrow C_2H_5 + OH$	$(=k_{111})$		1
R105*	$C_2H_5 + H \rightarrow CH_3 + CH_3$	$7.95 \times 10^{-11} \exp(-127/T)$	*Pratt and Wood* [1984]	
R106*	$C_2H_5 + O \rightarrow CH_3 + HCO + H$	$(=k_{98})$		1
R107*	$C_2H_5 + OH \rightarrow CH_3 + HCO + H_2$	$(=k_{98})$		1
R108*	$C_2H_5 + HCO \rightarrow C_2H_6 + CO$	5×10^{-11}		1
R109*	$C_2H_5 + HNO \rightarrow C_2H_6 + NO$	3×10^{-14}		1
R110*	$C_2H_5 + O_2 + M \rightarrow CH_3 + HCO + OH$	$k_0 = 1.5 \times 10^{-28}(300/T)^{3.0}$ $k_\infty = 8.0 \times 10^{-12}$	*DeMore et al.* [1992]	3
R111	$SO + h\nu \rightarrow S + O$	0		
R112	$SO_2 + h\nu \rightarrow SO + O$	$1.34 \times 10^{-4}\ s^{-1}$	*Warneck et al.* [1964] and *Okabe* [1971]	
R113	$H_2S + h\nu \rightarrow HS + H$	$2.20 \times 10^{-4}\ s^{-1}$	*Sullivan and Holland* [1966]	
R114	$SO + O_2 \rightarrow O + SO_2$	$2.6 \times 10^{-13} \exp(-2400/T)$	*DeMore et al.* [1992]	
R115	$SO + HO_2 \rightarrow SO_2 + OH$	2.8×10^{-11}	*DeMore et al.* [1992]	5
R116	$SO + O + M \rightarrow SO_2 + M$	$6.0 \times 10^{-31}\ [M]$	*Kasting* [1990]	1
R117	$SO + OH \rightarrow SO_2 + H$	8.6×10^{-11}	*DeMore et al.* [1992]	
R118	$SO_2 + OH + M \rightarrow HSO_3 + M$	$k_0 = 3.0 \times 10^{-31}\ (300/T)^{3.3}$ $k_\infty = 1.5 \times 10^{-12}$	*DeMore et al.* [1992]	3
R119	$SO_2 + O + M \rightarrow SO_3 + M$	$3.4 \times 10^{-32} \exp(-1130/T)[M]$	*Turco et al.* [1982]	
R120	$SO_3 + H_2O \rightarrow H_2SO_4$	6.0×10^{-15}	*DeMore et al.* [1992]	
R121	$HSO_3 + O_2 \rightarrow HO_2 + SO_3$	$1.3 \times 10^{-12} \exp(-330/T)$	*DeMore et al.* [1992]	

No.	*Reaction*	*Rate Constant (cm^3/s^{-1})*	*Reference/Notes*	
R122	$HSO_3 + OH \rightarrow H_2O + SO_3$	1×10^{-11}	*Kasting* [1990]	1
R123	$HSO_3 + H \rightarrow H_2 + SO_3$	1×10^{-11}	*Kasting* [1990]	1
R124	$HSO_3 + O \rightarrow OH + SO_3$	1×10^{-11}	*Kasting* [1990]	1
R125	$H_2S + OH \rightarrow H_2O + HS$	$6 \times 10^{-12} \exp(-75/T)$	*DeMore et al.* [1992]	
R126	$H_2S + H \rightarrow H_2 + HS$	$1.3 \times 10^{-11} \exp(-860/T)$	*Baulch et al.* [1976]	
R127	$H_2S + O \rightarrow OH + HS$	$9.2 \times 10^{-12} \exp(-1800/T)$	*DeMore et al.* [1992]	
R128	$HS + O \rightarrow H + SO$	1.6×10^{-10}	*DeMore et al.* [1992]	
R129	$HS + O_2 \rightarrow OH + SO$	4.0×10^{-19}	*DeMore et al.* [1992]	
R130	$HS + HO_2 \rightarrow H_2S + O_2$	3×10^{-11}	*McElroy et al.* [1980]	
R131	$HS + HS \rightarrow H_2S + S$	1.2×10^{-11}	*Baulch et al.* [1976]	
R132	$HS + HCO \rightarrow H_2S + CO$	5×10^{-11}	*Kasting* [1990]	1
R133	$HS + H \rightarrow H_2 + S$	1.0×10^{-11}	*Langford and Oldershaw* [1972]	
R134	$HS + S \rightarrow H + S_2$	$2.2 \times 10^{-11} \exp(120/T)$	*Kasting* (1990)	1
R135	$S + O_2 \rightarrow SO + O$	2.3×10^{-12}	*DeMore et al.* [1992]	
R136	$S + OH \rightarrow SO + H$	6.6×10^{-11}	*DeMore et al.* [1992]	
R137	$S + HCO \rightarrow HS + CO$	5×10^{-11}	*Kasting* [1990]	1
R138	$S + HO_2 \rightarrow HS + O_2$	1.5×10^{-11}	*Kasting* [1990]	1
R139	$S + HO_2 \rightarrow SO + OH$	1.5×10^{-11}	*Kasting* [1990]	1
R140	$S + S \rightarrow S_2$	$2.76 \times 10^{-34} \exp(710/T)$		
R141	$S_2 + OH \rightarrow HSO + S$	0		
R142	$S_2 + O \rightarrow S + SO$	1.1×10^{-11}	*Hills et al.* [1987]	
R143	$HS + H_2CO \rightarrow H_2S + HCO$	$1.7 \times 10^{-11} \exp(-800/T)$	*DeMore et al.* [1992]	
R144	$SO_2 + hv \rightarrow {}^1SO_2$	$1.59 \times 10^{-3}\ s^{-1}$	*Warneck et al.* [1964] and *Okabe* [1971]	
R145	$SO_2 + hv \rightarrow {}^3SO_2$	$8.69 \times 10^{-7}\ s^{-1}$	*Warneck et al.* [1964] and *Okabe* [1971]	
R146	$S_2 + hv \rightarrow S + S$	$9.74 \times 10^{-4}\ s^{-1}$	*DeAlmeida and Singh* [1986]	
R147	$S_2 + hv \rightarrow S_2^*$	0		
R148	$H_2SO_4 + hv \rightarrow SO_2 + 2OH$	$8.74 \times 10^{-7}\ s^{-1}$	*Turco et al.* [1979]	6
R149	$SO_3 + hv \rightarrow SO_2 + O$	0		
R150	${}^1SO_2 + M \rightarrow {}^3SO_2 + M$	1×10^{-12}	*Turco et al.* [1982]	
R151	${}^1SO_2 + M \rightarrow SO_2 + M$	1×10^{-11}	*Turco et al.* [1982]	
R152	${}^1SO_2 \rightarrow {}^3SO_2 + hv$	$1.5 \times 10^{3}\ s^{-1}$	*Turco et al.* [1982]	
R153	${}^1SO_2 \rightarrow SO_2 + hv$	$2.2 \times 10^{4}\ s^{-1}$	*Turco et al.* [1982]	
R154	${}^1SO_2 + O_2 \rightarrow SO_3 + O$	1×10^{-16}	*Turco et al.* [1982]	
R155	${}^1SO_2 + SO_2 \rightarrow SO_3 + SO$	4×10^{-12}	*Turco et al.* [1982]	
R156	${}^3SO_2 + M \rightarrow SO_2 + M$	1.5×10^{-13}	*Turco et al.* [1982]	
R157	${}^3SO_2 \rightarrow SO_2 + hv$	$1.13 \times 10^{3}\ s^{-1}$	*Turco et al.* [1982]	
R158	${}^3SO_2 + SO_2 \rightarrow SO_3 + SO$	7×10^{-14}	*Turco et al.* [1982]	
R159	$SO + NO_2 \rightarrow SO_2 + NO$	1.4×10^{-11}	*DeMore et al.* [1992]	
R160	$SO + O_3 \rightarrow SO_2 + O_2$	$3.6 \times 10^{-12} \exp(-1100/T)$	*DeMore et al.* [1992]	
R161	$SO_2 + HO_2 \rightarrow SO_3 + OH$	0		
R162	$HS + O_3 \rightarrow HSO + O_2$	$9.0 \times 10^{-12} \exp(-280/T)$	*DeMore et al.* [1992]	
R163	$HS + NO_2 \rightarrow HSO + NO$	$2.9 \times 10^{-11} \exp(240/T)$	*DeMore et al.* [1992]	
R164	$S + O_3 \rightarrow SO + O_2$	1.2×10^{-11}	*DeMore et al.* [1992]	

No.	*Reaction*	*Rate Constant (cm^3/s^{-1})*	*Reference/Notes*	
R165	$SO + SO \rightarrow SO_2 + S$	8.3×10^{-15}	*Herron & Huie* [1980]	
R166	$SO_3 + SO \rightarrow SO_2 + SO_2$	2×10^{-15}	*Yung & DeMore* [1982]	
R167	$S + CO_2 \rightarrow SO + CO$	1×10^{-20}	*Yung & DeMore* [1982]	1
R168	$SO + HO_2 \rightarrow HSO + O_2$	0		
R169	$SO + HCO \rightarrow HSO + CO$	$5.5 \times 10^{-11}\ T^{-0.4}$	*Kasting* [1990]	1
R170	$H + SO + M \rightarrow HSO + M$	$K_0 = 5.7 \times 10^{-32}\ (300/T)^{1.6}$ $K_\infty = 7.5 \times 10^{-11}$	*Kasting* [1990]	1
R171	$HSO + hv \rightarrow HS + O$	$5.46 \times 10^{-4}\ s^{-1}$ ($=J_{HO2}$)	*DeMore et al.* [1985]	1
R172	$HSO + NO \rightarrow HNO + SO$	$3.7 \times 10^{-12} \exp(250/T)$	*Kasting* [1990]	1
R173	$HSO + OH \rightarrow H_2O + SO$	$4.8 \times 10^{-11} \exp(250/T)$	*Kasting* [1990]	1
R174	$HSO + H \rightarrow HS + OH$	$8.1 \times 10^{-11} \times (0.90)$	*Kasting* [1990]	1
R175	$HSO + H \rightarrow H_2 + SO$	$8.1 \times 10^{-11} \times (0.08)$	*Kasting* [1990]	1
R176	$HSO + HS \rightarrow H_2S + SO$	1×10^{-12}	*Kasting* [1990]	1
R177	$HSO + O \rightarrow OH + SO$	$3.0 \times 10^{-11} \exp(200/T)$	*Kasting* [1990]	1
R178	$HSO + S \rightarrow HS + SO$	1×10^{-11}	*Kasting* [1990]	1
R179	$S + S_2 + M \rightarrow S_3 + M$	$2.8 \times 10^{-32}\ [M]$	*Kasting* [1990]	1
R180	$S_2 + S_2 + M \rightarrow S_4 + M$	$2.8 \times 10^{-31}\ [M]$	*Baulch et al.* [1976]	7
R181	$S + S_3 + M \rightarrow S_4 + M$	($= k_{61}$)	*Kasting* [1990]	1
R182	$S_4 + S_4 + M \rightarrow S_8(AER) + M$	($= k_{61}$)	*Kasting* [1990]	1
R183	$S_4 + hv \rightarrow S_2 + S_2$	($=J_{S2}$)	See (R146)	1
R184	$S_3 + hv \rightarrow S_2 + S$	($=J_{S2}$)	See (R146)	1
R185	$NH_3 + hv \rightarrow NH_2 + H$	$8.29 \times 10^{-5}\ s^{-1}$	*Kasting* [1985] and *Levine* [1985]	
R186	$NH_3 + OH \rightarrow NH_2 + H_2O$	$1.7 \times 10^{-12} \exp(-710/T)$	*DeMore et al.* [1992]	
R187	$NH_3 + O(^1D) \rightarrow NH_2 + OH$	2.5×10^{-10}	*DeMore et al.* [1992]	
R188	$NH_2 + H + M \rightarrow NH_3 + M$	$(6 \times 10^{-30}\ [M])/(1 + 3 \times 10^{-20}\ [M])$	*Gordon et al.* [1971]	
R189	$NH_2 + NO \rightarrow N_2 + H_2O$	$3.8 \times 10^{-12} \exp(450/T)$	*DeMore et al.* [1992]	8
R190*	$NH_2 + NH_2 + M \rightarrow N_2H_4 + M$	1×10^{-10}	*Gordon et al.* [1971]	
R191	$NH_2 + O \rightarrow NH + OH$	5×10^{-12}	*Albers et al.* [1969]	
R192	$NH_2 + O \rightarrow HNO + H$	5×10^{-12}	*Albers et al.* [1969]	
R193	$NH + NO \rightarrow N_2 + O + H$	4.9×10^{-11}	*DeMore et al.* [1992]	8
R194	$NH + O \rightarrow N + OH$	1×10^{-11}	*Kasting* [1982]	1
R195*	$N_2H_4 + hv \rightarrow N_2H_3 + H$	$1.52 \times 10^{-4}\ s^{-1}$	*Kasting* [1982]	
R196*	$N_2H_4 + H \rightarrow N_2H_3 + H_2$	$9.9 \times 10^{-12} \exp(-1200/T)$	*Stief and Payne* [1976]	
R197*	$N_2H_3 + H \rightarrow 2NH_2$	2.7×10^{-12}	*Gehring et al.* [1969]	
R198*	$N_2H_3 + N_2H_3 \rightarrow N_2H_4 + N_2 + H_2$	6×10^{-11}	*Kuhn and Atreya* [1979]	
R199	$NH + H + M \rightarrow NH_2 + M$	($=k_{263}$)	*Kasting* [1982]	1
R200	$NH + hv \rightarrow N + H$	($=J_{NH3}$)	see (R185)	1
R201	$NH_2 + hv \rightarrow NH + H$	($=J_{NH3}$)	see (R185)	1
R202	$NH_2 + hv \rightarrow NH_2^*$	$3.8 \times 10^{-3}\ s^{-1}$	*Kasting* [1982]	1
R203	$NH_2^* \rightarrow NH_2 + hv$	$1.2 \times 10^{-5}\ s^{-1}$	*Lenzi et al.* [1972]	
R204	$NH_2^* + M \rightarrow NH_2 + M$	3×10^{-11}	*Kasting* [1982]	1
R205	$NH_2^* + H_2 \rightarrow NH_3 + H$	3×10^{-11}	*Kasting* [1982]	1
R206	$NH_2 + HCO \rightarrow NH_3 + CO$	1×10^{-11}		9

No.	*Reaction*	*Rate Constant (cm^3/s^{-1})*	*Reference/Notes*	
R207	$NH + HCO \rightarrow NH_2 + CO$	1×10^{-11}		9
R208	$^1CH_2 + O_2 \rightarrow H_2CO + O$	0		
R209	$^3CH_2 + O_2 \rightarrow H_2CO + O$	0		
R210*	$C_2H_2 + h\nu \rightarrow C_2H + H$	2.86×10^{-6} s^{-1}, Ly α: 0.3; other: 0.06	*Nakayama and Watanabe* [1964]	10
R211*	$C_2H_2 + h\nu \rightarrow C_2 + H_2$	1.10×10^{-6} s^{-1}, Ly α: 0.10; other: 0.10	*Okabe* [1981, 1983a]	10
R212*	$C_2H_4 + h\nu \rightarrow C_2H_2 + H_2$	$(0.51) \times 3.37 \times 10^{-5}$ s^{-1}	*Zelikoff and Watanabe* [1953]	
R213*	$^3CH_2 + CH_3 \rightarrow C_2H_4 + H$	7.0×10^{-11}	*Tsang and Hampson* [1986]	
R214*	$C_2H_5 + CH_3 + M \rightarrow C_3H_8 + M$	$k_0 = 2.519 \times 10^{-16}/(T)^{2.458}$ $k_\infty = 8.12 \times 10^{-10}/(T)^{0.5}$		
R215*	$C_3H_8 + OH \rightarrow C_3H_7 + H_2O$	$1.1 \times 10^{-11} \exp(-700/T)$	*DeMore et al.* [1992]	
R216*	$C_3H_8 + O \rightarrow C_3H_7 + OH$	$1.6 \times 10^{-11} \exp(-2900/T)$ $+ 2.2 \times 10^{-11} \exp(-2250/T)$	*Hampson and Garvin* [1977]	
R217*	$C_3H_8 + O(^1D) \rightarrow C_3H_7 + OH$	$(=k_{111})$		1
R218*	$C_3H_7 + H \rightarrow CH_3 + C_2H_5$	$(=k_{151})$		1
R219*	$^3CH_2 + {}^3CH_2 \rightarrow C_2H_2 + H + H$	0		
R220*	$C_2H_2 + OH \rightarrow CO + CH_3$	$2 \times 10^{-12} \exp(-250/T)$	*Hampson and Garvin* [1977]	
R221*	$C_2H_2 + H + M \rightarrow C_2H_3 + M$	$k_0 = 2.6 \times 10^{-31}$ $k_\infty = 3.8 \times 10^{-11} \exp(-1374/T)$	*Romani et al.* [1993]	2
R222*	$C_2H_3 + H \rightarrow C_2H_2 + H_2$	2×10^{-11}	*Warnatz* [1984]	
R223*	$C_2H_3 + H_2 \rightarrow C_2H_4 + H$	$2.6 \times 10^{-13} \exp(-2646/T)$	*Allen et al.* [1992]	
R224*	$C_2H_3 + CH_4 \rightarrow C_2H_4 + CH_3$	$2.4 \times 10^{-24} T^{4.02} \exp(-2754/T)$	*Tsang and Hampson* [1986]	
R225*	$C_2H_3 + C_2H_6 \rightarrow C_2H_4 + C_2H_5$	$3.0 \times 10^{-13} \exp(-5170/T)$	*Kasting et al.* [1983]	
R226*	$C_2H_4 + OH \rightarrow H_2CO + CH_3$	$2.2 \times 10^{-12} \exp(385/T)$	*Hampson and Garvin* [1977]	
R227*	$C_2H_4 + O \rightarrow HCO + CH_3$	$5.5 \times 10^{-12} \exp(-565/T)$	*Hampson and Garvin* [1977]	
R228*	$C_2H_4 + H + M \rightarrow C_2H_5 + M$	$k_0 = 2.15 \times 10^{-29} \exp(-349/T)$ $k_\infty = 4.95 \times 10^{-11} \exp(-1051/T)$	*Lightfoot and Pilling* [1987]	
R229*	$C_2H + O_2 \rightarrow CO + HCO$	2×10^{-11}	*Brown and Laufer* [1981]	
R230*	$C_2H + H_2 \rightarrow C_2H_2 + H$	$5.58 \times 10^{-11} \exp(-1443/T)$	*Stephens et al.* [1987] and *Allen et al.* [1992]	
R231*	$C_2H + CH_4 \rightarrow C_2H_2 + CH_3$	$6.94 \times 10^{-12} \exp(-250/T)$	*Lander et al.* [1990] and *Allen et al.* [1992]	

No.	*Reaction*	*Rate Constant (cm^3/s^{-1})*	*Reference/Notes*	
R232*	$C_2H + C_2H_6 \rightarrow C_2H_2 + C_2H_5$	3.6×10^{-11}	*Lander et al.* [1990]	
R233*	$C_2H + H + M \rightarrow C_2H_2 + M$	$k_0 = 1.26 \times 10^{-18}\ T^{-3.1} \exp(-721/T)$ $k_\infty = 3.0 \times 10^{-10}$	*Tsang and Hampson* [1986]	2
R234*	$C_3H_8 + h\nu \rightarrow C_3H_6 + H_2$	$4.31 \times 10^{-6}\ s^{-1}$, Ly α: 0.33; other: 0.94	*Yung et al.* [1984]	10
R235*	$C_3H_8 + h\nu \rightarrow C_2H_6 + {}^1CH_2$	$7.42 \times 10^{-7}\ s^{-1}$, Ly α: 0.09; other: 0.0	*Calvert and Pitts* [1966]	
R236*	$C_3H_8 + h\nu \rightarrow C_2H_4 + CH_4$	$3.21 \times 10^{-6}\ s^{-1}$, Ly α: 0.39; other: 0.0		
R237*	$C_3H_8 + h\nu \rightarrow C_2H_5 + CH_3$	$1.75 \times 10^{-6}\ s^{-1}$, Ly α: 0.20; other: 0.06		
R238*	$C_2H_6 + h\nu \rightarrow C_2H_2 + H_2 + H_2$	$7.70 \times 10^{-7}\ s^{-1}$, Ly α: 0.25; other: 0.27	*Yung et al.* [1984]	10
R239*	$C_2H_6 + h\nu \rightarrow C_2H_4 + H + H$	$8.25 \times 10^{-7}\ s^{-1}$, Ly α: 0.30; other: 0.14	*Yung et al.* [1984]	
R240*	$C_2H_6 + h\nu \rightarrow C_2H_4 + H_2$	$6.27 \times 10^{-7}\ s^{-1}$, Ly α: 0.13; other: 0.56	*Yung et al.* [1984]	
R241*	$C_2H_6 + h\nu \rightarrow 2CH_3$	$2.05 \times 10^{-7}\ s^{-1}$, Ly α: 0.08; other: 0.01	*Yung et al.* [1984]	
R242*	$C_2H_4 + h\nu \rightarrow C_2H_2 + H + H$	$(0.49) \times 3.37 \times 10^{-5}\ s^{-1}$	*Back and Griffiths* [1967]	
R243*	$C_3H_6 + h\nu \rightarrow C_2H_2 + CH_3 + H$	$(0.34) \times 3.37 \times 10^{-5}\ s^{-1}$	assumed to equal J_{C2H4}	1, 10
R244	$CH_4 + h\nu \rightarrow {}^3CH_2 + 2H$	$1.12 \times 10^{-6}\ s^{-1}$, Ly α: 0.25; other: 0	*Toublanc et al.* [1995]	
R245	$CH_4 + h\nu \rightarrow CH_3 + H$	$2.29 \times 10^{-6}\ s^{-1}$, Ly α: 0.51; other: 0		
R246	$CH + h\nu \rightarrow C + H$	$3.37 \times 10^{-5}\ s^{-1}$	assumed to equal J_{C2H4}	1, 11
R247	$CH_2CO + h\nu \rightarrow {}^3CH_2 + CO$	$2.44 \times 10^{-4}\ s^{-1}$	*Okabe* [1978]	
R248*	$CH_3CHO + h\nu \rightarrow CH_3 + HCO$	$(0.50) \times 1.29 \times 10^{-4}\ s^{-1}$	*Demerjian et al.* [1974]	
R249*	$CH_3CHO + h\nu \rightarrow CH_4 + CO$	$(0.50) \times 1.29 \times 10^{-4}\ s^{-1}$	*Calvert and Pitts* [1966]	
R250*	$C_2H_5CHO + h\nu \rightarrow C_2H_5 + HCO$	$1.29 \times 10^{-4}\ s^{-1}$	assumed to equal J_{Ch3cho}	1
R251*	$C_3H_3 + h\nu \rightarrow C_3H_2 + H$	$3.37 \times 10^{-5}\ s^{-1}$	assumed to equal J_{C2H4}	1
R252*	$CH_3C_2H + h\nu \rightarrow C_3H_3 + H$	$(0.40) \times 2.44 \times 10^{-5}\ s^{-1}$	*Nakayama and Watanabe* [1964]	10
R253*	$CH_3C_2H + h\nu \rightarrow C_3H_2 + H_2$	$(0.15) \times 2.44 \times 10^{-5}\ s^{-1}$	*Yung et al.* [1984]	
R254*	$CH_3C_2H + h\nu \rightarrow CH_3 + C_2H$	$(0.02) \times 2.44 \times 10^{-5}\ s^{-1}$		
R255*	$CH_2CCH_2 + h\nu \rightarrow C_3H_3 + H$	$(0.40) \times 5.34 \times 10^{-11}\ s^{-1}$	*Rabalais et al.* [1971]	10

No.	*Reaction*	*Rate Constant (cm^3/s^{-1})*	*Reference/Notes*	
R256*	$CH_2CCH_2 + h\nu \rightarrow C_3H_2 + H_2$	(0.15) x 5.34 x 10^{-11} s^{-1}	*Yung et al.* [1984]	
R257*	$CH_2CCH_2 + h\nu \rightarrow C_2H_2 + {}^3CH_2$	(0.06) x 5.34 x 10^{-11} s^{-1}		
R258*	$C_3H_6 + h\nu \rightarrow CH_2CCH_2 + H_2$	(0.57) x 3.37 x 10^{-5} s^{-1}		
R259*	$C_3H_6 + h\nu \rightarrow C_2H_4 + {}^3CH_2$	(0.02) x 3.37 x 10^{-5} s^{-1}		
R260*	$C_3H_6 + h\nu \rightarrow C_2H + CH_4 + H$	(0.05) x 3.37 x 10^{-5} s^{-1}		
R261	$C + OH \rightarrow CO + H$	4 x 10^{-11}	*Giguere and Huebner* [1978]	
R262	$C + H_2 + M \rightarrow {}^3CH_2 + M$	k_0 = 8.75 x 10^{-31} exp(524/*T*) k_∞ = 8.3 x 10^{-11}	*Zahnle* [1986]	2, 12
R263	$C + O_2 \rightarrow CO + O$	3.3 x 10^{-11}	*Donovan and Hussain* [1970	
R264	$CH + H \rightarrow C + H_2$	1.4 x 10^{-11}	*Becker et al.* [1989]	
R265	$CH + O \rightarrow CO + H$	9.5 x 10^{-11}	*Messing et al.* [1981]	
R266	$CH + H_2 \rightarrow {}^3CH_2 + H$	2.38 x 10^{-10} exp(–1760/*T*)	*Zabarnick et al.* [1986]	
R267	$CH + H_2 + M \rightarrow CH_3 + M$	k_0 = 8.75 x 10^{-31} exp(524/*T*) k_∞ = 8.3 x 10^{-11}	*Romani et al.* [1993]	2
R268	CH + O2 → CO + OH	5.9 x 10^{-11}	*Butler et al.* [1981]	
R269	$CH + CO_2 \rightarrow HCO + CO$	5.9 x 10^{-12} exp(–350/*T*)	*Berman et al.* [1982]	
R270*	$CH + CH_4 \rightarrow C_2H_4 + H$	min{2.5 x 10^{-12} exp(200/*T*); 1.7 x 10^{-10}}	*Romani et al.* [1993]	
R271*	$CH + C_2H_2 \rightarrow C_3H_2 + H$	min{1.75 x 10^{-10} exp(61/*T*); 5.3 x 10^{-10}}	*Romani et al.* [1993]	
R272*	$CH + C_2H_4 \rightarrow CH_3C_2H + H$	min{5.5 x 10^{-11} exp(173/*T*); 3.55 x 10^{-10}}	*Romani et al.* [1993]	
R273*	$CH + C_2H_4 \rightarrow CH_2CCH_2 + H$	(= k_{76})	*Romani et al.* [1993]	
R274	${}^3CH_2 + O \rightarrow CH + OH$	8 x 10^{-12}	*Huebner and Giguere* [1980]	
R275	${}^3CH_2 + O \rightarrow CO + H + H$	8.3 x 10^{-11}	*Homan and Schweinfurth* [1981]	
R276	${}^3CH_2 + H + M \rightarrow CH_3 + M$	k_0 = 3.1 x 10^{-30} exp(457/*T*) k_∞ = 1.5 x 10^{-10}	*Gladstone* [1983]	2
R277	${}^3CH_2 + H \rightarrow CH + H_2$	4.7 x 10^{-10} exp(–370/*T*)	*Zabarnick et al.* [1986]	
R278*	${}^3CH_2 + CO + M \rightarrow CH_2CO + M$	k_0 = 1.0 x 10^{-28} k_∞ = 1.0 x 10^{-15}	*Yung et al.* [1984]	2
R279*	${}^3CH_2 + {}^3CH_2 \rightarrow C_2H_2 + H_2$	5.3 x 10^{-11}	*Banyard et al.* [1980] and *Laufer* [1981	

No.	*Reaction*	*Rate Constant (cm^3/s^{-1})*	*Reference/Notes*	
R280*	$^3CH_2 + C_2H_2 + M \rightarrow CH_3C_2H + M$	$k_0 = 3.8 \times 10^{-25}$ $k_\infty = 2.2 \times 10^{-12}$	*Laufer et al.* [1983] and *Laufer* [1981]	2
R281*	$^3CH_2 + C_2H_3 \rightarrow CH_3 + C_2H_2$	3.0×10^{-11}	*Tsang and Hampson* [1986]	
R282*	$^3CH_2 + C_2H_5 \rightarrow CH_3 + C_2H_4$	3.0×10^{-11}	*Tsang and Hampson* [1986]	
R283	$CH_2CO + H \rightarrow CH_3 + CO$	$1.9 \times 10^{-11} \exp(-1725/T)$	*Michael et al.* [1979]	
R284	$CH_2CO + O \rightarrow H_2CO + CO$	3.3×10^{-11}	*Miller et al.* [1982] and *Lee* [1980]	
R285*	$CH_2CCH_2 + H + M \rightarrow CH_3 + C_2H_2 + M$	$k_0 = 8.0 \times 10^{-24} \exp(-1225/T)$ $k_\infty = 9.7 \times 10^{-13} \exp(-1550/T)$	*Yung et al.* [1984]	2
R286*	$CH_2CCH_2 + H + M \rightarrow C_3H_5 + M$	$k_0 = 8.0 \times 10^{-24} \exp(-1225/T)$ $k_\infty = 1.4 \times 10^{-11} \exp(-1000/T)$	*Yung et al.* [1984]	
R287	$CH_3 + O_2 + M \rightarrow CH_3O_2 + M$	0		
R288	$CH_3 + CO + M \rightarrow CH_3CO + M$	$1.4 \times 10^{-32} \exp(3000/T)[M]$	*Watkins and Word* [1974]	
R289	$CH_3 + H_2CO \rightarrow CH_4 + HCO$	0		
R290	$CH_3 + OH \rightarrow CO + H_2 + H_2$	6.7×10^{-12}	*Fenimore* [1969]	
R291*	CH3 + C2H3 → C3H5 + H	2.4×10^{-13}		
R292	$CH_3O_2 + H \rightarrow CH_4 + O_2$	1.4×10^{-11}		
R293	$CH_3O_2 + H \rightarrow H_2O + H_2CO$	1×10^{-11}		
R294	$CH_3O_2 + O \rightarrow H_2CO + HO_2$	1×10^{-11}		
R295	$CH_3CO + H \rightarrow CH_4 + CO$	1×10^{-10}	*Zahnle* [1986]	
R296	$CH_3CO + O \rightarrow H_2CO + HCO$	5×10^{-11}	*Zahnle* [1986]	
R297*	$CH_3CO + CH_3 \rightarrow C_2H_6 + CO$	5.4×10^{-11}	*Adachi et al.* [1981]	
R298	$CH_3CO + CH_3 \rightarrow CH_4 + CH_2CO$	8.6×10^{-11}	*Adachi et al.* [1981]	
R299*	$CH_3CHO + H \rightarrow CH_3CO + H_2$	$2.8 \times 10^{-11} \exp(-1540/T)$	*Zahnle* [1986]	
R300*	$CH_3CHO + O \rightarrow CH_3CO + OH$	5.8×10^{-13}	*Washida* [1981]	
R301*	$CH_3CHO + OH \rightarrow CH_3CO + H_2O$	1.6×10^{-11}	*Niki et al.* [1978]	

No.	*Reaction*	*Rate Constant (cm^3/s^{-1})*	*Reference/Notes*	
R302*	$CH_3CHO + CH_3 \rightarrow CH_3CO + CH_4$	$2.8 \times 10^{-11} \exp(-1540/T)$	*Zahnle* [1986]	
R303*	$CH_3C_2H + H + M \rightarrow CH_3 + C_2H_2 + M$	$k_0 = 8.0 \times 10^{-24} \exp(-1225/T)$ $k_\infty = 9.7 \times 10^{-12} \exp(-1550/T)$	*Whytock et al.* [1976] and *Von Wagner and Zellner* [1972]	2
R304*	$CH_3C_2H + H + M \rightarrow C_3H_5 + M$	$(= k_{165})$	*Yung et al.* [1984]	
R305*	$C_2 + O \rightarrow C + CO$	5×10^{-11}	*Prasad and Huntress* [1980]	
R306*	$C_2 + O_2 \rightarrow CO + CO$	$1.5 \times 10^{-11} \exp(-550/T)$	*Baughcum and Oldenburg* [1984]	
R307*	$C_2 + H_2 \rightarrow C_2H + H$	$1.77 \times 10^{-10} \exp(-1469/T)$	*Pitts et al.* [1982]	
R308*	$C_2 + CH_4 \rightarrow C_2H + CH_3$	$5.05 \times 10^{-11} \exp(-297/T)$	*Pitts et al.* [1982]	
R309*	$C_2H + O \rightarrow CO + CH$	$1 \times 10^{-10} \exp(-250/T)$	*Zahnle* [1986]	
R310*	$C_2H + C_3H_8 \rightarrow C_2H_2 + C_3H_7$	1.4×10^{-11}		
R311*	$C_2H_2 + O \rightarrow {}^3CH_2 + CO$	$2.9 \times 10^{-11} \exp(-1600/T)$	*Zahnle* [1986]	
R312*	$C_2H_2 + OH \rightarrow C_2H_2OH$	$k_0 = 5.5 \times 10^{-30}$ $k_\infty = 8.3 \times 10^{-13} \exp(300/T)^2$		
R313*	$C_2H_2 + OH + M \rightarrow CH_2CO + H + M$	$k_0 = 5.8 \times 10^{-31} \exp(-1258/T)$ $k_\infty = 1.4 \times 10^{-12} \exp(388/T)$	*Perry and Williamson* [1982]	2
R314*	$C_2H_2OH + H \rightarrow H_2O + C_2H_2$	5.0×10^{-11}	*Miller et al.* [1982]	
R315*	$C_2H_2OH + H \rightarrow H_2 + CH_2CO$	$3.3 \times 10^{-11} \exp(-2000/T)$	*Miller et al.* [1982]	
R316*	$C_2H_2OH + O \rightarrow OH + CH_2CO$	$3.3 \times 10^{-11} \exp(-2000/T)$	*Miller et al.* [1982]	
R317*	$C_2H_2OH + OH \rightarrow H_2O + CH_2CO$	$1.7 \times 10^{-11} \exp(-1000/T)$	*Miller et al.* [1982]	
R318*	$C_2H_3 + O \rightarrow CH_2CO + H$	5.5×10^{-11}	*Hoyermann et al.* [1981]	
R319*	$C_2H_3 + OH \rightarrow C_2H_2 + H_2O$	8.3×10^{-12}	*Benson and Haugen* [1967]	
R320*	$C_2H_3 + CH_3 \rightarrow C_2H_2 + CH_4$	3.4×10^{-11}	*Fahr et al.* [1991]	
R321*	$C_2H_3 + CH_3 + M \rightarrow C_3H_6 + M$	$k_0 = 1.3 \times 10^{-22}$ $k_\infty = 1.2 \times 10^{-10}$		
R322*	$C_2H_3 + C_2H_3 \rightarrow C_2H_4 + C_2H_2$	2.4×10^{-11}	*Fahr et al.* [1991]	
R323*	$C_2H_3 + C_2H_5 \rightarrow C_2H_4 + C_2H_4$	3.0×10^{-12}	*Laufer et al.* [1983]	
R324*	$C_2H_3 + C_2H_5 \rightarrow CH_3 + C_3H_5$	see reference	*Romani et al.i [1993]*	
R325*	$C_2H_4 + OH + M \rightarrow C_2H_4OH + M$	$k_0 = 1.0 \times 10^{-28} \exp(300/T)^{0.8}$ $k_\infty = 8.8 \times 10^{-12}$	*DeMore et al.* [1992]	
R326*	$C_2H_4OH + H \rightarrow H_2O + C_2H_4$	5×10^{-11}	*Miller et al.* [1982]	

No.	*Reaction*	*Rate Constant (cm^3/s^{-1})*	*Reference/Notes*	
R327*	$C_2H_4OH + H \rightarrow H_2 + CH_3CHO$	$3.3 \times 10^{-11} \exp(2000/T)$	*Zahnle* [1986]	
R328*	$C_2H_4OH + O \rightarrow OH + CH_3CHO$	$3.3 \times 10^{-11} \exp(2000/T)$	*Zahnle* [1986]	
R329*	$C_2H_4OH + OH \rightarrow H_2O + CH_3CHO$	$1.7 \times 10^{-11} \exp(-1000/T)$	*Zahnle* [1986]	
R330*	$C_2H_5 + OH \rightarrow CH_3CHO + H_2$	1.0×10^{-10}		
R331*	$C_2H_5 + O \rightarrow CH_3CHO + H$	1.0×10^{-10}		
R332*	$C_2H_5 + CH_3 \rightarrow C_2H_4 + CH_4$	$3.25 \times 10^{-11}\ T^{0.5}$	*Romani et al.* [1993]	13
R333*	$C_2H_5 + C_2H_3 \rightarrow C_2H_6 + C_2H_2$	6.0×10^{-12}	*Laufer et al.* [1983]	
R334*	$C_2H_5 + C_2H_5 \rightarrow C_2H_6 + C_2H_4$	2.3×10^{-12}	*Tsang and Hampson* [1986]	
R335*	$C_2H_5 + H + M \rightarrow C_2H_6 + M$	$k_0 = 5.5 \times 10^{-23}\ T^{-2} \exp(-1040/T)$ $k_\infty = 1.5 \times 10^{-13} \exp(-440/T)$	*Gladstone* [1983]	2
R336*	$C_2H_5 + H \rightarrow C_2H_4 + H_2$	3.0×10^{-12}	*Tsang and Hampson* [1986]	
R337*	$C_3H_2 + H + M \rightarrow C_3H_3 + M$	$k_0 = 1.7 \times 10^{-26}$ $k_\infty = 1.5 \times 10^{-10}$	*Yung et al.* [1984]	2
R338*	$C_3H_3 + H + M \rightarrow CH_3C_2H + M$	$k_0 = 1.7 \times 10^{-26}$ $k_\infty = 1.5 \times 10^{-10}$	*Yung et al.* [1984]	2
R339*	$C_3H_3 + H + M \rightarrow CH_2CCH_2 + M$	$k_0 = 1.7 \times 10^{-26}$ $k_\infty = 1.5 \times 10^{-10}$	*Yung et al.* [1984]	2
R340*	$C_3H_5 + H \rightarrow CH_3C_2H + H_2$	1.5×10^{-11}	*Yung et al* [1984]	
R341*	$C_3H_5 + H + M \rightarrow C_3H_6 + M$	$k_0 = 1.0 \times 10^{-28}$ $k_\infty = 1.0 \times 10^{-11}$	*Yung et al.* [1984]	2
R342*	$C_3H_5 + H \rightarrow CH_4 + C_2H_2$	1.5×10^{-11}	*Yung et al.* [1984]	
R343*	$C_3H_5 + CH_3 \rightarrow CH_3C_2H + CH_4$	4.5×10^{-12}	*Yung et al.* [1984]	
R344*	$C_3H_5 + CH_3 \rightarrow CH_2CCH_2 + CH_4$	4.5×10^{-12}	*Yung et al.* [1984]	
R345*	$C_3H_6 + OH \rightarrow CH_3CHO + CH_3$	$4.1 \times 10^{-12} \exp(-540/T)$	*Hampson and Garvin* [1977]	
R346*	$C_3H_6 + O \rightarrow CH_3 + CH_3 + CO$	$4.1 \times 10^{-12} \exp(-38/T)$	*Hampson and Garvin* [1977]	9
R347*	$C_3H_6 + H + M \rightarrow C_3H_7 + M$	$(= k_{147})$		1

No.	*Reaction*	*Rate Constant (cm^3/s^{-1})*	*Reference/Notes*	
R348*	$C_3H_7 + CH_3 \rightarrow C_3H_6 + CH_4$	$2.5 \times 10^{-12} \exp(-200/T)$	*Yung et al.* [1984]	
R349*	$C_3H_7 + OH \rightarrow C_2H_5CHO + H_2$	(= k_{98})		1
R350*	$C_3H_7 + O \rightarrow C_2H_5CHO + H$	(= k_{98})		1
R351*	$H + CH_2CCH_2 \rightarrow CH_3C_2H + H$	$1.0 \times 10^{-11} \exp(-1000/T)$		
R352	$O + H_2CO \rightarrow OH + HCO$	$3.4 \times 10^{-11} \exp(-1600/T)$	*DeMore et al.* [1992]	
R353*	$^3CH_2 + C_2H_2 + M \rightarrow CH_2CCH_2 + M$	$k_0 = 3.8 \times 10^{-25}$ $k_\infty = 3.7 \times 10^{-12}$	*Laufer et al.* [1983] and *Laufer* [1981]	2
R354*	$C_2H + C_2H_2 \rightarrow C_4H_2(AER) + H$	1.5×10^{-10}	*Stephens et al.* [1987]	
R355	$^1CH_2 + H_2 \rightarrow {}^3CH_2 + H_2$	1.26×10^{-11}	*Romani et al.* [1993]	
R356*	$C_3H_5 + H \rightarrow CH_2CCH_2 + H_2$	1.5×10^{-11}	*Yung et al.* [1984]	
R357	$HCO + H_2CO \rightarrow CH_3O + CO$	3.8×10^{-17}	*Wen et al.* [1989]	
R358	$CH_3O + CO \rightarrow CH_3 + CO_2$	$2.6 \times 10^{-11} \exp(-5940/T)$	*Wen et al.* [1989]	
R359	$C_2H + CH_2CCH_2 \rightarrow C_5H_4(AER) + H$	1.5×10^{-10}		2

Notes: 1, estimated; 2, rate constant given by $k(M, T) = [k_0(T)k_\infty(T)[M]]/[k_0(T)[M] + k_\infty(T)]$, unless a value of F_C is given, in which case, use $\log(k) = \log\{k_0/[1 + (k_0/k_\infty)]\} + \{\log(F_C)/[1 + \log(k_0/k_\infty)^2]\}$; 3, three-body rate constant given by $k(M, T) = [k_0(T)[M]/(1 + (k_0(T)[M])/k_\infty(T))]\ 0.6^{\{1 + [\log(k_0(T)[M]/k_\infty(T))]^2\}^{-1}}$; 4, products uncertain; rate constant given by $k(M, T) = k_0(T) + \{k_3(T)[M]/[1 + (k_3(T)[M]/k_2(T)]\}$; 5, assumed equal to rate for reaction of SO with ClO; 6, assumed equal to J_{HCl}; 7, no recommendation given; value based on measurement by *Langford and Oldershaw* [1972], 8, products uncertain; 9, by analogy to R35 and R37; 10, branching ratios from Yung et al. [1984]; 11, photolysis rates are calculated from solar fluxes [*WMO*, 1985] and cross sections, and rates shown are diurnally averaged values at the top of the atmosphere in the standard model; 12, assumed same as R267; 13, rate is 0.04 of k_∞ for $C_2H_5 + CH_3 + M \rightarrow C_3H_8 + M$ [*Romani et al.*, 1993, and references therein].

Table 3.1 Model reactions and rate constants. An asterisk in Column 1 denotes the reactions removed from ancient Martian simulations to promote numerical stability.

Initial $f(SO_2)$	*e*-folding time (in Earth years)
Base code calculations	
10^{-8}	333
10^{-7}	381
10^{-6}	793
Sensitivity studies	
10^{-6} (higher temperature)	751
10^{-6} (higher precipitation)	81
10^{-6} (lower precipitation)	1550
10^{-6} (higher K)	783

Table 3.2 *e*-folding times in Earth years for $f(SO_2)$ in the early Martian atmosphere, including sensitivity factors.

3.10 Figures

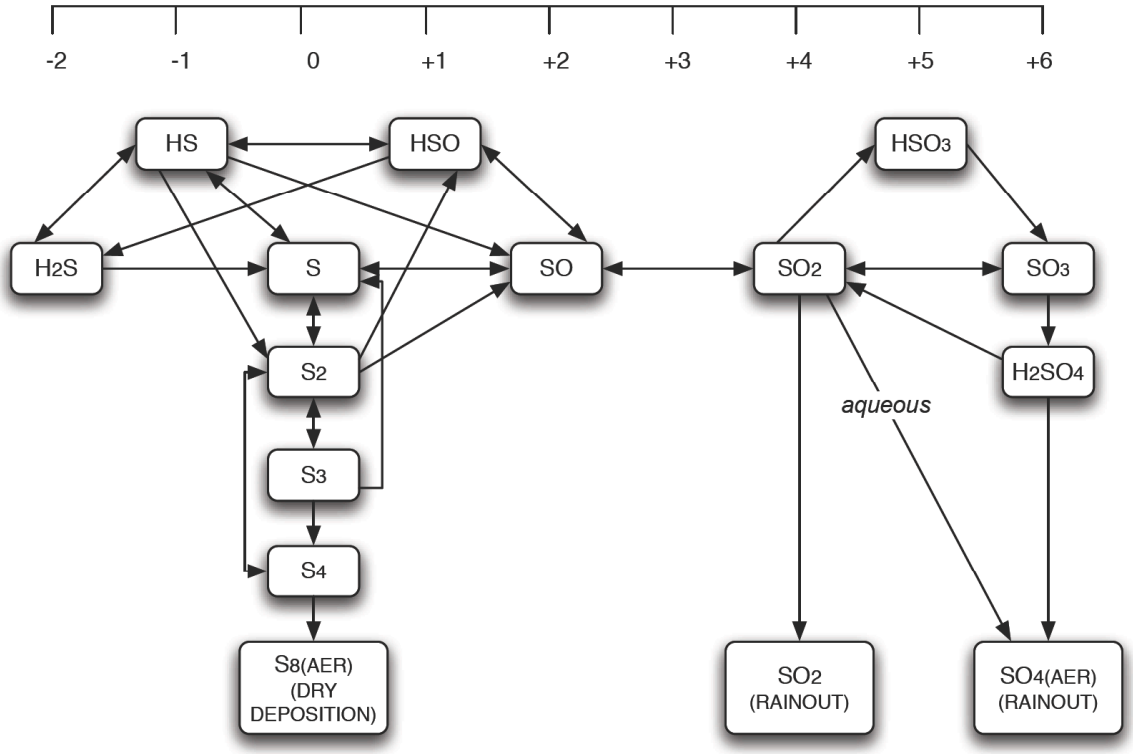

Figure 3.1 A schematic of the primary reactions involving sulfur species in the photochemical model, with oxidation state shown by the upper axis. All reactions in the gas phase with the exception of SO_2 to SO_4 aerosols, which occurs in the aqueous phase.

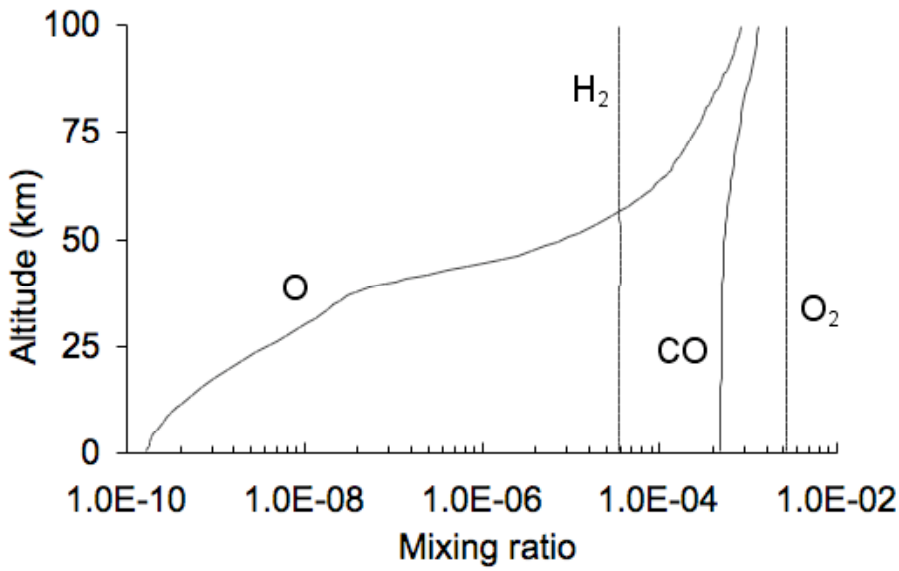

Figure 3.2 Profiles of major constituents (O, H_2, CO and O_2) in the current Martian atmosphere.

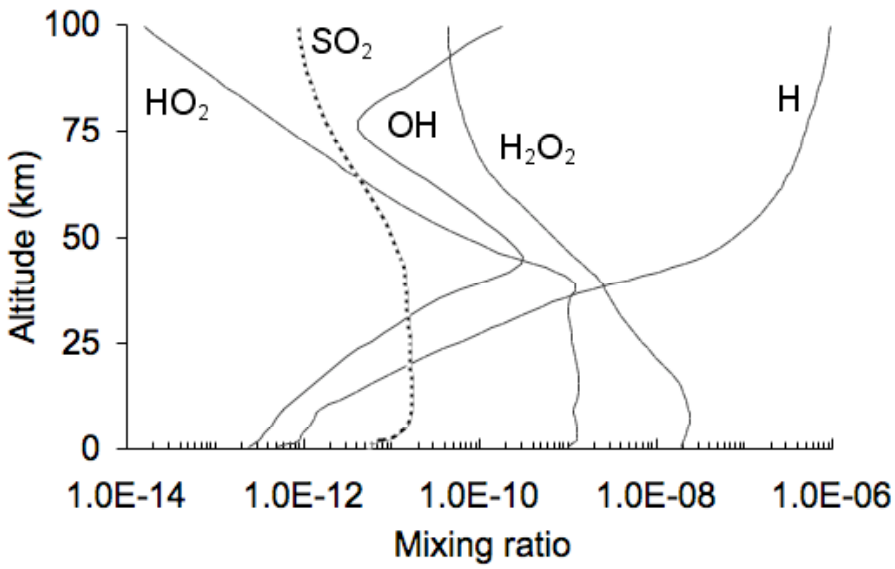

Figure 3.3 Profiles of radicals (HO_2, OH, H_2O_2 and H) in the current Martian atmosphere. For reference, a profile of SO_2 is also shown.

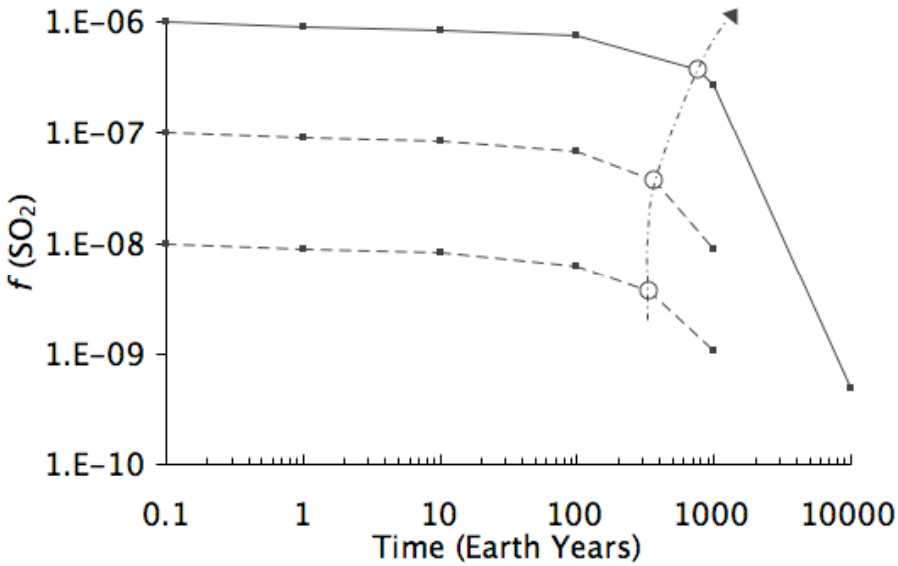

Figure 3.4 SO_2 longevity: $f(SO_2)$ versus time for three initial SO_2 mixing ratios. *e*-folding times for each simulation, marked by a circle, increase as initial SO_2 mixing ratios increase.

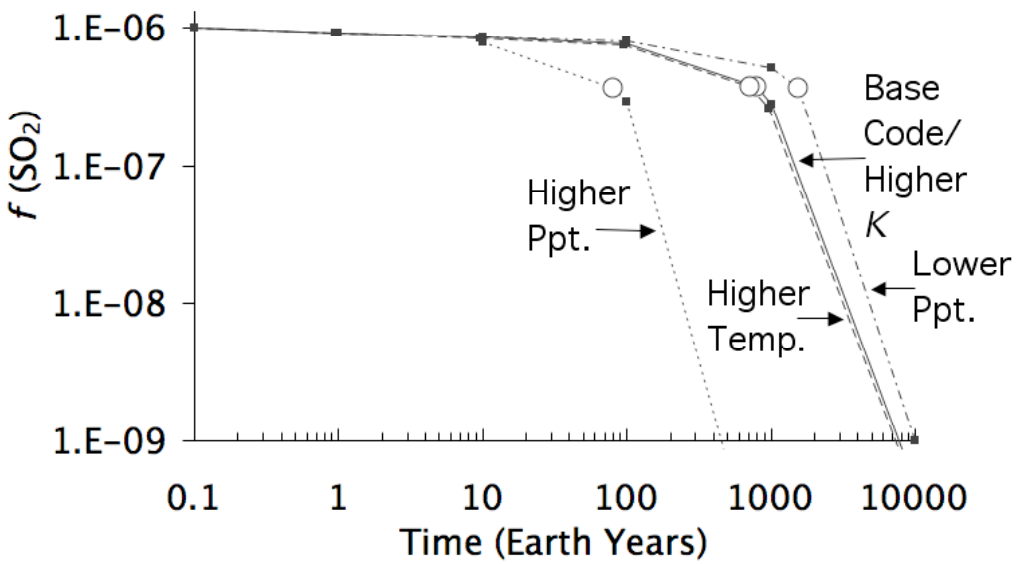

Figure 3.5 Sensitivity factors for SO_2 longevity: $f(SO_2)$ versus time for an initial SO_2 mixing ratio of 10^{-6}. *e*-folding times for the simulations are marked by a circle.

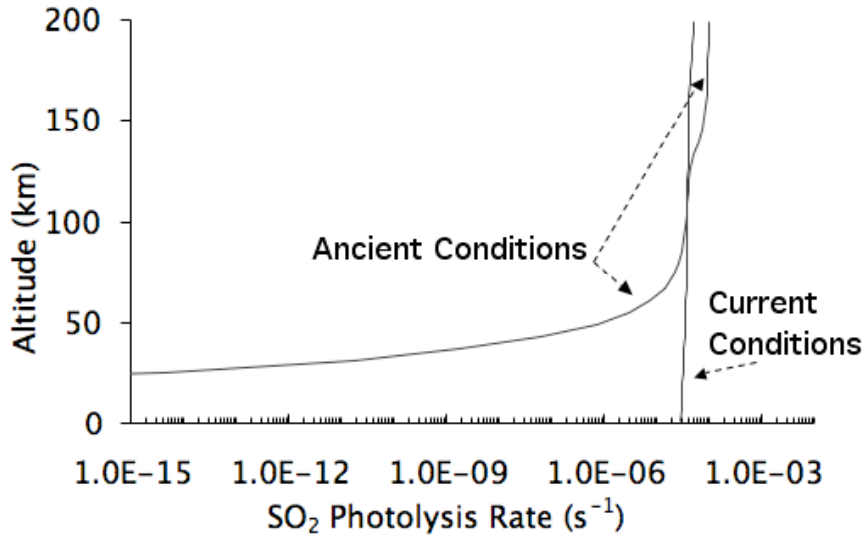

Figure 3.6 SO_2 photolysis rates decrease dramatically near the surface under ancient Martian conditions. The current Martian regime is shown in steady state at $f(SO_2)\sim10^{-12}$. The ancient Martian regime (initial $f(SO_2)=10^{-6}$) is shown at the *e*-folding time of 793 years ($f(SO_2)=3.67\text{x}10^{-7}$).

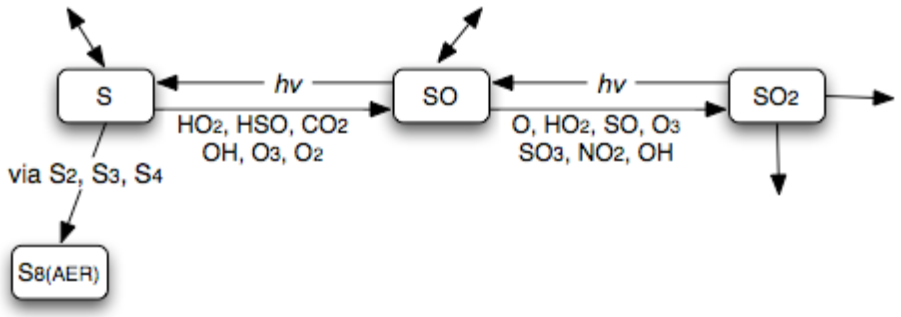

Figure 3.7 SO_2 is converted to elemental S, an important intermediate for S_8 aerosols, via photolysis. When photolysis is limited, the formation of elemental S is inhibited.

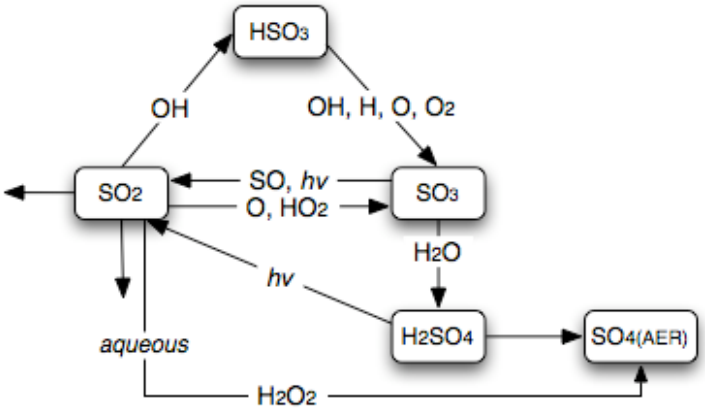

Figure 3.8 SO_2 is converted to sulfate aerosols via pathways involving radicals. When radicals are in short supply, the intermediates HSO_3 and SO_3 rarely form.

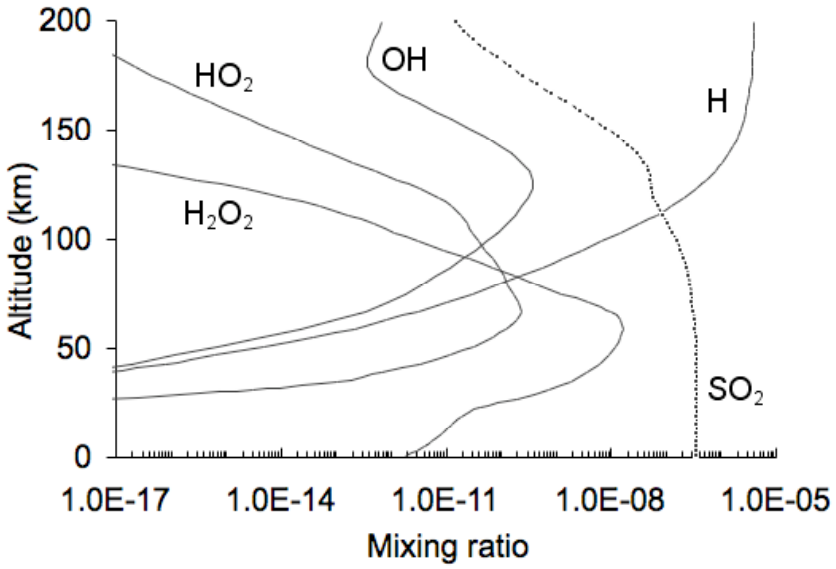

Figure 3.9 Profiles of radicals in ancient Martian regime (initial $f(SO_2)=10^{-6}$) at the *e*-folding time of 793 years ($f(SO_2)=3.67\text{x}10^{-7}$). For reference, a profile of SO_2 is also shown. Under these conditions, oxidants become scavenged near the surface.

[THIS PAGE INTENTIONALLY LEFT BLANK]

[THIS PAGE INTENTIONALLY LEFT BLANK]

Chapter 4

Biomarker preservation in ephemeral acid salt lakes: implications for Mars[1]

4.0 Abstract

The Mars Exploration Rover mission discovery of ancient aqueous biosedimentary systems that are characterized by high acidity and high salinity has recently shifted the focus of analog studies to similar environments here on Earth, and the possibility of biomarker preservation in these environments has strong implications for the search for life on Mars. To this end, lipid biomarker compositions of sediments from six highly acidic salt lakes on the Yilgarn Craton of Western Australia have been identified and quantified. Based on genetic community surveys using universal bacterial and archaeal primers, a predominance of short chain length *n*-alkanes, alcohols and acids, as well as monoether, diether and hopanoid lipids associated with organisms such as *Thermoplasma* and *Halobacteria* were expected. The GC-MS results of the lipid assay, however, revealed a strong signature of terrigenous plant debris. Two independent analytical methods were used to extract and quantify lipid residues, and both showed traces of the indigenous microbial population, including small quantities of bacterial glycerol monoethers and C_{15} and C_{17} iso- and anteiso- branched fatty acids, as well as the overprinting of biomarkers from vascular plants. Given that microbial and plant lipids

[1] Parts of this chapter have been adapted from work the author completed in MIT laboratories while a student at Oxford.

have similar chemistries, it is unlikely that this result reflects a preservational bias. Moreover, all traces of higher plants in the biosedimentary system are residues (i.e. unable to be seen material that is no longer living and was at some stage once washed into the catchment basin). Our findings demonstrating that lipids, in general, are surprisingly stable in the oxidizing and acidic saline sediments represented by these lakes.

4.1 Introduction

Biological signatures or biomarkers are organic compounds derived from living organisms found in rocks and sediments. While abiotic synthesis of some organic compounds may occur in hydrothermal settings [*Sumner*, 2004; *Simoneit*, 2004], the vast majority of sedimentary organic matter reflects highly characteristic biological processes. Biomarkers are particularly important in reconstructing Earth's biological history prior to the Cambrian radiation emergence of body fossils. Lipids are among the most resistant biological compounds to degradation [*Sumner*, 2004]. They have been found associated with some of the earliest life forms here on Earth and have been used to characterize both physical environments and primitive biological systems [*Brocks, et al.*, 1999]. As a result, much debate has taken place in the literature over the possibility of detecting similar biosignatures in the late Noachian/early Hesperian geological record on the surface of Mars. Aboard NASA's Mars Science Laboratory rover mission, scheduled for launch in 2009, is the Sample Analysis at Mars (SAM) instrument; the instrument

contains a Gas Chromatograph-Mass Spectrometer (GC-MS) capable of probing for lipid biomarkers [*Cabane, et al.*, 2004].

NASA's Mars Exploration Rover mission has recently revealed evidence for two key factors motivating this study: first, surface sediments at Meridiani Planum, the landing site of the Opportunity Rover, show strong signatures of aqueous cementation and diagenesis, suggesting the presence of at least episodic liquid water in physical settings analogous to inter-dune playa lakes on terrestrial continents [*Knoll, et al.*, 2005; *McLennan, et al.*, 2005]. The data further suggests that water may have either originated from groundwater flow or regional catchments and may have persisted for thousands and possibly millions of years [*Knoll et al*, 2005]. Second, compositional and mineralogical data from the Alpha-Particle X-ray Spectrometer and Moessbauer Spectrometer now point to the likelihood that strongly acidic conditions may have been present on parts of the surface of early Mars. For the first time, spacecraft have had the *in situ* capacity to detect characteristic minerals such as jarosite, ($KFe_3(SO_4)_2(OH)_6$), that only form at very low pH [*Klingelhofer, et al.*, 2004]. Based on geological, mineralogical and geochemical orbital data from Mars Express, Mars Odyssey and Mars Reconnaissance Orbiter, there is reason to believe that these conditions were not localized to the Opportunity landing site [*Arvidson*, 2005; *Gendrin, et al.*, 2005; *Roach*, 2007].

This evidence for highly acidic, saline surface conditions has reignited the debate about biosignatures being found in Martian evaporite sediments. *Sumner* [2004] suggests that

any organic compounds, even if present when the Meridiani sedimentary rocks were deposited, are unlikely to be preserved. Organic molecules are thermodynamically unstable in hot, oxidizing planetary surface environments but stable under cool to cold reducing conditions. Decay of organic matter should rapidly proceed as long as oxidants remain present, and Meridiani data points to an apparent abundance of Fe(III) minerals and apparent paucity of Fe(II) minerals. This suggests that the regional hematite-bearing sedimentary formation at Meridiani is composed of oxidized minerals and/or has had oxidized fluid flow through it [*Sumner*, 2004].

In the absence of fermentative or respiring organisms, reactions between sulfates and organic carbon may be unlikely to lead to significant abiotic decay over geologic time because of the necessary transfer of multiple electrons, stability relations of intermediate species and rate controls exerted by low temperature [*Sumner*, 2004; *Ohmoto, et al.*, 1992]. The reduction of Fe(III) to Fe(II), however, is strongly coupled to the oxidation of organic carbon because of the generation of free radicals and H_2O_2 on the surface of iron-bearing minerals. The calculations of Stumm and Morgan suggest that Fe(III)-bearing minerals are not stable at the low electron potentials necessary for organic carbon stability [*Stumm and Morgan*, 1996; *Sumner*, 2004].

Mineral stability fields, however, depend critically on ion pairing in solution. This in turn depends on brine compositions. Although significant progress has been made [*Tosca and McLennan*, 2005; *Tosca, et al.*, 2006)], these compositions are not fully

constrained for the early Martian surface. In addition, investigations on Earth of late Archaean and early Paleoproterozoic banded iron formations as well as the Gunflint Iron Formation (1.878 +/- 0.001 Ga) have shown at least some evidence of co-preservation of organics in the presence of iron oxides [*Fralick, et al.,* 2002]. In addition, lipid biomolecules adapted to protect cells living in harsh environments typically are particularly recalcitrant.

To this end, our study was undertaken to investigate the types of biomarkers and range of biomarker recovery in a modern biosedimentary terrestrial analog. Naturally acidic saline depositional environments are rare on Earth. However, much like Meridiani, the acidic salt lakes in the vicinity of Norseman, Western Australia, are characterized by: (1) ephemeral saline continental playas hosted by red siliciclastic sediments and oxidizing conditions, (2) abundant sulfate and iron oxide minerals, (3) Al-Fe-Si-rich waters with extremely low pH values, and (4) an absence of carbonates [*Benison and LaClair,* 2003; *Benison and Brown,* 2006]. The acid system is based within the Yilgarn Craton, which is composed of highly weathered Archaean rocks with little or no sedimentary cover, and owes its low pH to sulfide and sulfate weathering [*Anand and Paine*, 2002; *Benison, et al.,* 2007]. The lakes are supplied by a regional acid saline groundwater body throughout the Yilgarn and precipitate calcium and magnesium sulfates, chloride, hematite, a siliciclastic component, and, notably, the mineral jarosite [*Benison and Brown*, 2006]. In addition, their sedimentary characteristics and alteration features are strikingly similar to those of the Burns Formation at Meridiani Planum, including fine-medium sand-sized

and mud-sized grains, planar bedding, cross bedding, ripple marks, mudcracks, displacive crystal molds and concretions [*Benison and Brown*, 2006].

DNA community surveys were completed on the lake samples, and a lipid assay was done using gas chromatography-mass spectrometry (GC-MS). GC-MS data illuminates the chemical structure of biomolecules from characteristic fragment ions in their mass spectra. Lipids vary greatly in their structural detail although all are based on a stable, apolar hydrocarbon skeleton linked to a polar and less stable head group. The membrane phospholipids of bacteria and eukaryotes are fatty acid esters linked to an *sn*-glycerol-3-phosphate. In contrast, membrane phospholipids of archaea comprise distinctive isoprenoid ethers built on *sn*-glycerol-1-phosphate. Sterols comprise an essential component in the membranes of all eukaryotic organisms, regulating membrane fluidity and permeability [*Volkman*, 2002]. In bacteria, hopanoids are hypothesized to serve a similar purpose as eukaryotic sterols, and extremely few cases of sterol synthesis outside of the domain Eukarya can be identified (exceptions include the production of lanosterol and 4-methylsterols in some bacteria) [*Brocks and Summons*, 2004].

Though certain compounds like *n*-alkanes and *n*-alcohols are found ubiquitously in the biosphere, certain distinctions can be made in regard to carbon number size and the predominance of odd over even or even over odd carbon numbers. For instance, long *n*-alkanes with more than 27 carbon atoms and an odd over even carbon number majority are frequently derived from terrigenous plant waxes [*Brocks and Summons*, 2004].

Many lipids are highly specific for particular organisms below the domain level. Among these, 2-methylhopanes indicate cyanobacteria and/or strains of the anoxygenic phototroph *Rhodopseudomonas palustris* [Rashby, et al., 2007], 24-npropylcholestanes indicate pelagophyte algae, 24-isopropylcholestane indicates particular sponges, and the compound botryococcanes indicates a single taxon, the alga *Botryococcus braunii*. Other lipids are specific for particular environmental conditions. For example, high gammacerane and C_{21} to C_{25} regular isoprenoids enriched in ^{13}C are thought to correspond to hypersaline environments. 28,30-Dinorhopane and 25,28,30-trinorhopane suggest strongly anoxic conditions while 24-*n*-propylcholestane indicates marine depositional environments [*Brocks and Summons*, 2004].

4.2 Methods

4.2.1 Sample acquisition

In total, 99 sediment samples were taken using sterile procedures from twelve acid saline lakes in the vicinity of Norseman, Western Australia; of those, six samples were chosen for the lipid assay (see Figure 4.1, Table 4.1). The collection took place during in January 2005, during the austral summer when ambient temperatures and desiccation levels were high. Most lakes in the region are ephemeral; of those still containing surface water, lake diameters were typically less than a few hundred meters and never more than 30 cm deep. The pH levels ranged between 1.5 and 3.5 as measured in the field with pH

indicator strips. Samples from six of the lakes were chosen for genetic and lipid analyses to characterize the biology in the system. Samples were directly frozen on dry ice and were kept frozen until DNA extraction, lyophilization, and lipid extraction.

4.2.2 DNA analyses

Two DNA extractions were attempted on ten samples. The first attempt utilized a MoBio Soil Extraction kit and was unsuccessful (likely due to iron-related inhibition); the initial difficulty was overcome using a modification of the longer, three-day Bulat chemical extraction method [*Bulat, et al.,* 2000)]. Of the ten samples, DNA was successfully extracted and amplified from six.

Universal archaeal primers ARC344F-GC: 5' ACGGGGYGCAGCAGGCGCGA 3' and [*Raskin*, 1994] and ARC915R: 5' GTGCTCCCCCGCCAATTCCT 3' [*Stahl and Amann*, 1991], and universal bacterial primers 907F: 5'AAACTYAAAKGAATTGACGG-3' [*Muzyer,* 1995] and rP1: 5'ACGGTTACCTTGTTACGACTT-3' [*Weisberg, et al.*, 1991] were used to amplify 16S RNA (the 907F primer will pick up most known organisms; although Rp1 is largely oriented to bacteria, the combination of primers resulted in some archaeal matches). Standard cloning, sequencing, and BLAST matching gave identifications as presented in the phylogenic tree in Figure 4.2.

4.2.3 Lipid extraction

Sediment samples of 25-100g wet weight were freeze dried for 36 hours in precombusted

glass jars (550°C, 8 hours). Samples were then crushed to a fine powder using a solvent-washed (6x methanol alternating with dichloromethane) mortar and pestle. Lipids were extracted using a modification of the method of Bligh and Dyer [*Bligh and Dyer*, 1959]. Extractions took place in pre-washed 50 ml Teflon tubes that were ultra-cleaned through two sequential 30-minute sonications in methanol and dichloromethane. 19 ml of a 10:5:4 mixture of methanol: chloroform: dichloromethane-washed H_2O were added to each dry sample powder (of approximate weight 10 g) within the Teflon tubes.

The sample tubes were then vortexed for 5 minutes and sonicated for 20 minutes before centrifugation at 5000 rpm for 5 minutes. The liquid phase was transferred to a 60 ml precombusted glass vial and the process repeated four times with the remaining sediment. On the final extraction, 19 ml of a 10:5:4 mixture of methanol: chloroform: dichloromethane-washed H_2O with 1% TCA were used. 5 ml of chloroform were added to each of the four extraction vials per sample and gently shaken using a precombusted foil-lined cap. 5 ml of dichloromethane-washed H_2O were then added to aid in phase separation. The heavy phases containing the lipid extract from each of the four vials per sample were then combined in new 60 ml precombusted glass vial and blown down under N_2 gas. The total lipid extracts (TLE) were finally transferred to pre-weighed 4 ml precombusted glass vials and blown to dryness so a final TLE weight could be obtained.

4.2.4 Silica gel column separation

Acid-activated copper pellets were used to desulfurize samples dissolved in

dichloromethane before column separation. Approximately 2mg of total lipid extract was then applied to a 10-cm silica gel pipet column for each sample. Columns were sequentially eluted with 1.4 column-volumes of hexane and 2 column volumes of 8:2 hexane-dichloromethane to obtain the nonpolar fractions F1 and F2; this was followed by 2 column volumes of dichloromethane for fraction F3, 2 column volumes of 8:2 dichloromethane-ethyl acetate for fraction F4, and 3 column volumes of 7:3 dichloromethane-methanol for fraction F5.

4.2.5 Ether cleavage

4 ml autoclaved glass vials and an autoclaved glass syringe were kept at 130°C overnight to insure dryness for the ether cleavage procedure. 0.5 ml of CH_2Cl_2 was added to dissolve 5mg of the total lipid extract of each of the polar fractions. Vials were blown down briefly with argon gas. 40 µl of 1.0M BBr_3/CH_2Cl_2 solution were then added with a gas tight microliter syringe (Teflon plunger) and 5-inch SS, 18G needle through an Oxford valve under argon gas. Vials were sealed with Teflon caps and heated at 60°C for two hours. 0.5 ml of 1.0 M Super-Hydride (lithium triethylborohydride) in tetrahydrofuran was then added under argon gas once vials had cooled. Vials were sealed and heated at 70°C for two hours. The reaction was quenched by slowly adding 1ml of water. Cleaved lipids were extracted with hexane.

4.2.6 Base saponification

5mg of total lipid extract were added to a 12ml autoclaved glass vial and blown to dryness using N_2. 1 ml of 0.5N KOH in methanol was then added. The vials were sealed with Teflon caps and heated for 2 hours at 60°C. The saponified solution was then transferred to a new 12ml vial and checked with pH paper to ensure a strongly basic solution.

4.2.7 Base extraction

5ml of HCl-cleaned water and 2.5 ml of a 4:1 hexane:ether mix were then added and the vials gently shaken. The hexane:ether layer was transferred into a new vial and another 2.5 ml of hexane mix were added to the water fraction and the process repeated. A last 1ml of HCl-cleaned water were added to wash the hexane mix and returned to the aqueous fraction. Sodium sulfate was used to absorb traces of water in the hexane mix before the hexane layer was decanted off to attain the neutral fraction.

4.2.8 Acid extraction

4M HCl were added drop-wise to the aqueous fraction remaining after base extraction to attain a pH between 2 and 3. The extraction procedure was repeated as above with water and hexane:ether. The organics decanted off in the last step contained the free fatty acid fraction. An aliquot of this fraction was then derivatized with BF_3 methanol to create fatty acid methyl esters (FAMEs).

4.2.9 Derivatization for GC-MS

Approximately 20μg of the samples were used for GC-MS analysis. If less than 0.5mg of sample weight was returned after column separation, 20% of the total sample was used. Nonpolar fractions were transferred in 20μl of hexane to GC-MS vials and 50ng of the internal standard 5α-andostane were added. Trimethylsilyl (TMS) reagents were used to derivatize (reducing the polarity of) functional groups in polar fractions F3, F4 and F5 prior to GC-MS analysis. Polar fraction samples were transferred in 20μl of dicholoromethane and left to evaporate. Then 10μl of bis(trimethylsilyl)trifluoroacetamide (BSTFA) in 10μl of pyridine were used to prepare trimethylsilyl derivatives of alcohols, acids and amines; once added, samples were heated at 70 °C for 30 minutes. Prior to derivatization, 100ng of the internal standard epiandosterone were added to polar fractions. All polar fractions were run on the GC-MS within thirty-six hours of derivatization.

4.2.10 GC-MS conditions

An injection volume of 1ul from each fraction was analyzed on a gas chromatograph (GC) and GC-mass spectrometer (MS). The HP6890 Series II GC is equipped with a programmed-temperature vaporization (PTV) inlet, a 60 m Varian Chrompac CP-Sil 5 capillary column with 0.32 mm i.d. and 0.25 m film thickness and using helium as carrier gas, and a flame ionization detector (FID). The GC-MS has the same equipment except a

mass selective detector is used to replace the FID. The oven temperature column programs were different for various fractions. The programs are described below:

Inlet program: ini. 60 °C, 0.85 min hold, 720 °C/min to 320 °C, 2.35 min hold, 720 °C/min to 450 °C, 5 min hold, -100 °C/min to 50 °C, 0 min hold. Inlet Purge: 50ml/min at 2 minutes (splitless injection).

Column program A (for nonpolar fractions): ini. 60 °C, 2 min hold, 8 °C/min to 320 °C, 50 min hold.

Column program B (for polar fractions): ini. 60 °C, 2 min hold, 10 °C/min to 100 °C, 0 min hold. Ramp 4 °C/min to 320 °C, 30 min hold.

Column program C (for FAMEs): ini. 60 °C, 1 min hold, 10 °C/min to 150 °C, 0 min hold. 4 °C/min to 320 °C, 25 min hold.

4.2.11 Peak identifications

Chromatograms and the mass spectra for different compounds were viewed using Enhanced ChemStation G1701CA Version C, Agilent Technologies. Identifications were based on spectral reduction by AMDIS software followed by NIST Spectral Library software matches when available. Otherwise, spectra were identified based on derivations and similarities to a laboratory-acquired spectral library. Quantifications were based on integration under peaks and scaled to the known amount of internal standard added.

4.3 Results

4.3.1 DNA community survey

The results of the DNA community surveys for five of the six lakes are shown in the phylogenic tree in Figure 4.2. A total of 78 sequences were obtained, and non-overlapping sequences over 400bp are included in the phylogenic analysis. Based on the DNA survey, lipids associated with halophilic or acidophilic bacteria and archaea, especially *Thermaplasma* and *Halobacteria*, were expected.

4.3.2 Column-separated total lipid extract, fractions 1 – 5

Typical GC-MS chromatograms from the Bligh and Dyer extracted nonpolar fractions (F1 and F2) are presented in Figure 4.3 and polar (F3, F4, and F5) fractions are presented in Figures 4.4, 4.5, and 4.7. Identifications are noted in the associated tables in Appendix 4.10. Amounts are quantified in terms of internal standards: 50 ng of 5-α- andostane for the nonpolar fractions and 100 ng of epiandostane for the polar fractions.

4.4 Discussion

4.4.1 Terrigenous plant biomarkers

4.4.1.1 Long chain n-alkanes

n-Alkanes were identified in fractions F1 and F2 following Bligh-Dyer extractions and column separation. The *n*-alkanes range in carbon number from 21 to 33 while the most dominant homologues are the C_{27} - C_{33} *n*-alkanes (subscripts for carbon #s). No evidence

of cyanobacteria in short chain *n*-alkanes was seen. There is a strong odd over even carbon number predominance (See Figure 4.3). This indicates a terrigenous origin of the long-chain *n*-alkanes, probably in the primary form of cuticular waxes [*Eglinton and Hamilton*, 1967]. These have also been shown to be carried in eolian dust [*Gagosian, et al.,* 1981; *Gagosian, et al.,* 1987; *Simoneit, et al.* 1977].

4.4.1.2 Fatty acids and *n*-alcohols

Fatty acids in lake extracts range in carbon number from 16 to 31 and *n*-alcohols from 21 to 31. Like long-chain *n*-alkanes, even numbered carbon compounds dominate the distributions of fatty acids; the odd numbered compounds dominated the *n*-alcohols, both compounds again suggesting a strong terrigenous plant origin (See Figure 4.5). An algal origin of the long-chain fatty acids does, however, remain a possibility [*Volkmann, et al.,* 1998].

4.4.1.3 Sterols and higher plant leaf waxes

C_{29} sterols comprised approximately 90% of the total lipid residue for the lakes. The predominance of C_{29} sterols over C_{27} and C_{28} sterols again suggests a land plant source [*Brocks and Summons*, 2004]. Oleanic acid derivatives and betulin were also found in high levels in the polar fractions, indicative of higher plant leaf waxes (See Figures 4.5 and 4.7). The overall assemblage of saturated alkanes, alcohols fatty acids and sterols points strongly to the overprinting of plant debris.

4.4.2 Archael and bacterial lipids

4.4.2.1 Column separation method

Column-separated polar fractions F3, F4 and F5 from the Bligh-Dyer extractions for the six saline lakes revealed no correlating m/z peaks of 205 (diagnostic for glycerol monoethers), 130, 131 or 133 (diagnostic for glycerol diethers) or 191 (diagnostic for hopanoids). Specific microbial lipids were also probed for, including archaeol and hydroxyarchaeol (diagnostic m/z peaks at 143, 341), as well as the regular acyclic isoprenoids i_{21} to i_{30} thought to be a biomarker for halophilic archaea; none were found.

The BBr_3/Superhydride Ether Cleavage procedure was used on these fractions to probe for previously intact ether and tetraether lipids that might have been escaped GC-MS volatilization. Tetraethers, with two polar head groups and the glycerol moieties linked by two C_{40} isopreniod alykl components, have strikingly unique architecture among lipids and are very resistant to chemical attack. These molecular structures enable archaea to tolerate extremes of temperature as well as salinity and pH, and special procedures are required to break their ether bonds to enable analysis of the alkyl groups [*Christie*, 2003]. The procedure resulted in no detectable isoprenoid chains or isoprenoid chains with ringed carbon structures. If present, not only tetraether products but also the alkyl groups from any archaeal ether lipids should have been seen (see Figure 4.5). Evidence confirming the BBr_3 procedure worked can be seen in three respects: 1) the previous predominance of odd over even high carbon number alcohols was hydrolyzed to predominantly even over odd *n*-alkanes, 2) Br-derivatives are present in the spectra, and

3) multiple isoprenoid residues from a separate archaea-containing sample from Ojo Caliente, Yellowstone National Park were retrieved during the procedure.

4.4.2.2 Saponification method

The saponifcation method comprised a separate, independent analytical technique to extract and separate lipid residues at high resolution. Traces of non-isoprenoid glycerol monoethers (GMEs) were found in the neutral polar fractions from sediment samples 8_32 and 11_81 (see Figure 4.9 and 4.10). 1-*O*-alkylglycerols are formed by a very small subset of bacteria including *Aquifex, Ammonifex*, *Thermodesulfobacteria* and certain extremophilic δ-proteobacteria [*Pancost, et al*., 2005; *Huber, et al*., 1992; *Langworthy, et al*., 1982]. *Thermodesulfobacteria* were identified in Sample 11-81 in the DNA community survey.

4.4.3 C_{15} and C_{17} branched fatty acids

Branched fatty acids are often found in heterotrophic bacteria, and the branched fatty acids iso-15:0, anteiso-15:0, and iso-17:0 are considered diagnostic for sulfate reducing bacteria; iso- and anteiso-C15:0 acids are also thought to be abundant in sulfur-oxidizing bacteria (Taylor and Parkes, 1983; Taylor and Parkes, 1985). These fatty acids were detected in the FAME residues at low levels (see Figure 4.11). In the DNA community surveys, microbes such as the sulfur-reducing bacterium *Thermodesulfobacteria* and Gammaproteobacterium *Sulfur-oxidizing bacteria OBII5* were detected.

Again, the combined polar fraction from the second procedure of saponfication followed by acid/base extractions revealed no m/z peaks of 130,131 or 133 (diagnostic for glycerol diethers) or 191 (diagnostic for hopanoids). No archaeol or hydroxyarchaeol was detected (diagnostic m/z peaks at 143, 341), and no C_{20} - C_{30} isoprenoids were seen. Multiple diether and isoprenoid lipids were found in a positive control containing the archaeon *Ignicoccus* Kin4I.

4.5 Conclusion

A hypothesis was formed on the basis of DNA community surveys that a lipid assay of sediments from the Norseman Acid Salt Lakes would show short carbon number chain length *n*-alkanes, alcohols and acids, in addition to multiple monoether, diether and hopanoid lipids; however, the biomarker profiles were dominated by terrigenous plant debris from the sparse eucalyptus, wattle and saltbrush forests that exist on the Yilgarn Craton. Yet low abundance C_{15} and C_{17} iso and anteiso-branched fatty acids in addition to glycerol monoethers suggest an indigenous microbial population. Peaks comprising as little as 1/3000th of the overall GC-MS-detected lipid biomass per lake could be identified in the data. If a single isoprenoid ether lipid or hopanoid had been present at the level of at least 150 nanograms per gram wet weight (or ~200 mg dry weight) of sample, it is likely that it would be in the detectable range. It is probable that the indigenous microbial populations in the sediments of the ephemeral acidic salt lakes are limited, while the signature of terrigenous plant debris, in contrast, is sizeable due to the vast

quantity of plant biomass in the lakes' drainage basins. The particular plant biochemicals identified are recalcitrant, but importantly, there is no chemical reason for bacterial and archaeal lipids to be less stable than plant lipids. The results presented suggest surprising stability of lipid biomarkers in the modern biosedimentary system of the Norseman Acid Salt Lakes. They also motivate further studies of acid lakebeds preserved in the geologic record, particularly the ancient acid saline pans of the Permian Opeche Shale, Williston Basin, North Dakota. Here the oxidation of sulfide minerals along with other acidification processes, which may have been mediated by microbes, gave rise to extremely acidic waters (pH<1) in tectonically stable, closed-drainage basins [*Benison, et al.*, 1998; *Benison and Goldstein*, 2002]. These ancient sites precipitated evaporitic minerals in an arid climate characterized by abundant, carbonate-poor red siliciclastics, much like lithified strata that have been observed at Meridiani Planum; the discovery of lipid biomarkers in the Opeche Shale would further bolster the search for remnant organic matter on Mars.

4.6 References

Anand, R.R., and M.D. Paine (2002), Regolith geology of the Yilgarn Craton, *Australian Journal of the Earth Sciences, 49*, 3-62.

Arvidson, R.E., F. Poulet, J.-P. Bibring, M. Wolff, A. Gendrin, R.V. Morris, J.J. Freeman, Y. Langevin, N. Mangold, and G. Bellucci (2005), Spectral reflectance and morphologic correlations in Eastern Terra Meridiani, Mars, *Science, 307*, 1591-1594.

Benison, K.C., R.H. Goldstein, B. Wopenka, R.C. Burruss, and J.D. Pasteris (1998), Extremely acid Permian lakes and ground waters in North America, *Nature, 392*, 911-914.

Benison, K.C., and R.H. Goldstein (2002), Sedimentology of ancient saline pans: an example from the Permian Opeche Shale, Williston Basin, North Dakota, USA, *Sedimentary Geol., 151*, 177-185.

Benison, K., and D. LaClair (2003), Modern and Ancient Extremely Acid Saline Deposits: Terrestrial Analogs for Martian Environments? *Astrobiology*, *3,* 609-619.

Benison, K., and B. Brown (2006), Acid Saline lake systems give clues about past environments and the search for life on Mars, *Icarus, 183,* 225-229.

Benison, K. C., et al. (2007), Sedimentology of Acid Saline Lakes in Southern Western Australia: Newly Described Processes and Products of an Extreme Environment, *Journal of Sedimentary Research*, *77*, 366-388.

Bligh, E.G., and W.J. Dyer (1959), A rapid method of total lipid extraction and purification, *Can. J. Biochem. Physiol. 37*, 911-917.

Bulet S., M. Lübeck, I.A. Alekhina, D.F. Jensen, I.M.B. Knudsen, and P.S. Lübeck (2000), Identification of a Universally Primed-PCR-Derived Sequence-Characterized Amplified Region Marker for an Antagonistic Strain of Clonostachys rosea and Development of a Strain-Specific PCR Detection Assay, *Appl. Envir. Microbiol. 66*, 4758-4763.

Brocks, J.J., and R.E. Summons (2004), Sedimentary hydrocarbons, biomarkers for early life. In *Treatise in Geochemistry* (Eds. H.D. Holland and K. Turekian). Ch. 8.03, 65-115

Brocks, J. J., et al. (1999), Archean Molecular Fossils and the Early Rise of Eukaryotes, *Science, 285*, 1033-1036.

Cabane, M., P. Coll, C. Szopa, G. Israël, F. Raulin, R. Sternberg, P. Mahaffy, A. Person, C. Rodier, R. Navarro-Gonzàlez, f, H. Niemann, D. Harpold, and W. Brinckerhoff (2004) Did life exist on Mars? Search for organic and inorganic signatures, one of the goals for "SAM" (sample analysis at Mars). *Adv. Space Res., 33*, 2240-2245.

Christie, W. (2003), *Lipid Analysis*. The Oily Press, Bridgwater, UK.

Eglinton, G, and R.J. Hamilton (1967), Leaf epicuticular waxes. *Science*, *156*, 1322-1335.

Gagosian, R.B., E.T. Peltzer, and J.T. Merrill (1987), Long-range transport of terrestrially derived lipids in aerosols from the south Pacific. *Nature*, *325*, 800-803.

Gagosian, R.B., E.T. Peltzer, and O.C. Zafiriou (1981) Atmospheric transport of continentally derived lipids to the tropical North Pacific. *Nature*, *291*, 312-314.

Gendrin, A., *et al.* (2005), Sulfates in Martian layered terrains: The OMEGA/Mars Express view, *Science, 307*, 1587-1591.

Fralick, P., D.W. Davis, and S.A. Kissin (2002), The age of the Gunflint Formation, Ontario, Canada: Single zircon U – Pb age determinations from reworked volcanic ash, *Can. J. Earth Sci.*, *39*, 1085-1091.

Huber R., T. Wilharm, D. Huber, et al. (1992), *Aquifex pyrophilus* gen. nov., sp. nov., represents a novel group of marine hyperthermophilic hydrogen-oxidizing bacteria. *Syst. Appl. Microbiol. 15*, 340-351.

Klingelhöfer G., and MER Science Team (2004), Jarosite and Hematite at Meridiani Planum from Opportunity's Mössbauer Spectrometer *Science*, *306*, 1740-1745.

Knoll, A. H., et al. (2005), An astrobiological perspective on Meridiani Planum, *Earth and Planetary Science Letters*, *240*, 179-189.

Langworthy T.A., G. Holzer, J.G. Zeikus, and T.G. Tornabene (1983), Iso-and anteiso-branched glycerol diethers of the thermophilic aerobe *Thermodisulfotobacterium* commune system. *Appl. Microbiol. 101*, 1-17.

McLennan S. et al. (2005) Provenance and Diagenesis of Impure Evaporitic Sedimentary Rocks on Meridiani Planum, Mars 36th Annual Lunar and Planetary Science Conference, League City, Texas, abstract no.1884.

Muyzer G., S. Hottenträger, A. Teske, and C. Waver (1995), Denaturing gradient gel electrophoresis of PCR-amplified 16S rDNA - a new molecular approach to analyse the

genetic diversity of mixed microbial communities, In: *Molecular microbial ecology manual*, Akkermans, A., J. Van Elsas, and F. De Bruijn, (eds) 2nd edn. Kluwer, Dordrecht, 3.4.4.1–3.4.4.22.

Ohmoto, H., and A. C. Lasaga (1982), Kinetics of reactions between aqueous sulfates and sulfides in hydrothermal systems, *Geochim. Cosmochim. Acta.*, 46, 1727-1745.

Pancost, R.D., S. Pressley, J.M. Coleman, G.L. Benning, and B.W. Mountain (2005), Lipid biomolecules in silica sinters: indicators of microbial biodiversity. *Environmental Microbiology*, *7*, 66-77.

Rashby, S. E., et al. (2007), Biosynthesis of 2-methylbacteriohopanepolyols by an anoxygenic phototroph, *Proceedings of the National Academy of Sciences*, 104, 15099-15104.

Raskin, L., J.M. Stromley, B.E. Rittmann, and D.A. Stahl (1994), Group-specific 16S rRNA hybridization probes to describe natural communities of methanogens. *Appl Environ Microbiol, 60*, 1232–1240.

Roach, L. H., *et al.* (2007), CRISM spectral signatures of the north polar gypsum dunes, paper presented at Lunar and Planetary Science Conference XXXVIII, League City, Texas, Abstract #1970.

Simoneit, B.R.T., R. Chester, and G. Eglinton (1977), Biogenic lipids in particulates from the lower atmosphere over the eastern Atlantic. *Nature*, *267*, 682-685.

Stahl, D.A., and R. Amann (1991) Development and Application of Nucleic Acid Probes in Bacterial Systematics, in *Sequencing and Hybridization Techniques in Bacterial Systematics*, E Stackebrandt and M Goodfellow (eds.), John Wiley and Sons, Chichester, England, 205-248.

Stumm W., and J.J. Morgan (1996), *Aquatic Chemistry*, John Wiley, New York. pp. 19 – 27.

Sumner, D.Y. (2004), Poor preservation potential of organics in Meridiani Planum hematite bearing sedimentary rocks, *J. Geophys. Res.* 109 (E12), E12007. 10.1029/2004JE002321.

Taylor J., and R.J. Parkes (1983), The cellular fatty acids of the sulfate-reducing bacteria, *Desulfobacter* sp., *Desulfobulbus* sp. and *Desulfovibrio desulfuricans*. *J. Gen. Microbiol., 129*, 3303-3309.

Taylor J., and R.J. Parkes (1985) Identifying different populations of sulfate-reducing bacteria within marine sediment systems, using fatty acid biomarkers. *J. Gen. Microbiol.*, *131*, 631-642.

Tosca, N.J., McLennan, S.M., Clark, B.C., Grotzinger, J.P., Hurowitz, J.A., Knoll, A.H., Schröder, C., Squyres, S.W. (2005) Geochemical Modeling of Evaporation Processes on Mars: Insight from the Sedimentary Record at Meridiani Planum. *Earth Planet. Sci. Lett., 240*, 125-151.

Tosca, N.J., and McLennan, S.M. (2006), Chemical divides and evaporite mineral assemblages on Mars. *Earth Planet. Sci. Lett., 241*, 1-2, 21-31.

Volkman J.K., S.M. Barrett, S.I. Blackburn, M.P. Mansour, E.L. Sikes, and F. Gelin (1998), Microalgal biomarkers: a review of recent research developments. *Org. Geochem.*, *29*, 1163-1179.

Volkman, J.K. (2003), Sterols in Microorganisms. *Appl. Microbiol. Biotechnol., 60*, 495–506

Weisburg, W.G., S.M. Barns, D.A. Pelletier, and D.J. Lane (1991), 16S ribosomal DNA amplification for phylogenetic study, *J. Bacteriol., 173*, 697-703.

4.7 Tables

#	Lake	Coordinates	pH	Lake Comments	Sample Comments	Image
2_6	Lake Cowen, shoreline puddle	S 32 11.390', E 121 46.111'	1.8	In the vicinity of Norseman, visible microbial growth/streamers, most of the lake dry, some small puddles near the shoreline	Near surface layer from a small puddle along shoreline	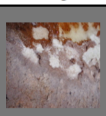
6_22	Lake Gilmore	S 32 36.566', E 121 33.534'	dry	Top sepia layer underlain by a black layer (1mm), brown-orange mud (hematite-coated gypsum, 25 cm), and sandy yellow dirt; cm-scale bright red patches at depth	Brown-orange mud layer	
8_32	Unnamed lake on abandoned farm	S 33 02.315', E 121 40.308'	1.5	Sulfur smell, yellow veneer on rocks, a thin layer of halite crystals underlain by thick mud with layers of crystals (with appearance like pyrite) about 2cm down	Thick mud layer	
9_49	Unnamed lake near Grass Patch	S 33 13.130', E 121 45.251'	2.3	Halite crust (1mm) underlain by tan top layer (3mm), underlain by dark brown sediment (hard and dry, 3cm), underlain to at least 12cm by a pinkish brown layer	Pinkish brown layer	
11_81	Unnamed lake near Salmon Gums	S 33 03.366', E 121 40.554'	2.6	Hard halite crust (3cm), underlain by brown siliciclastics (5mm), underlain by hematite mud (to 50 cm) w/ patches of white sediment (uncoated gypsum)	Deep hematite layer	
12_93 & 12_99	Unnamed lake near Salmon Gums (2)	S 33 02.923', E 121 43.532'	2.0	Dry surface crust underlain by a thin gooey golden layer (3mm), underlain by red clastic sandy mud to at least 15 cm in depth, trees noted nearby	Golden top layer	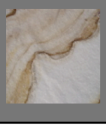

Table 4.1 Sample Information.

4.8 Figures

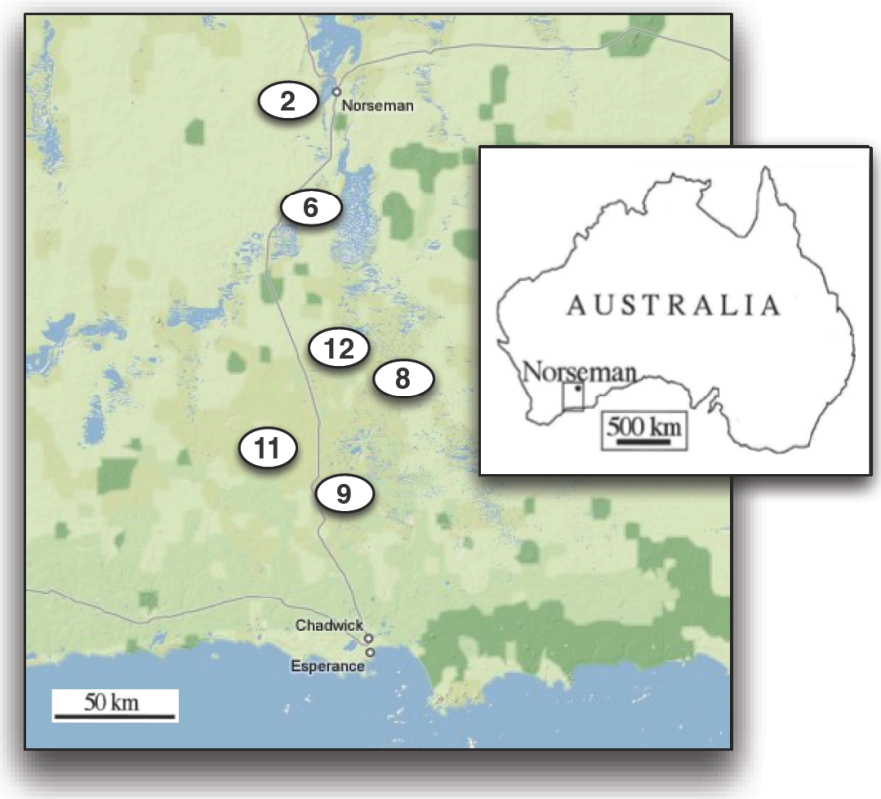

Figure 4.1 Sample sites.

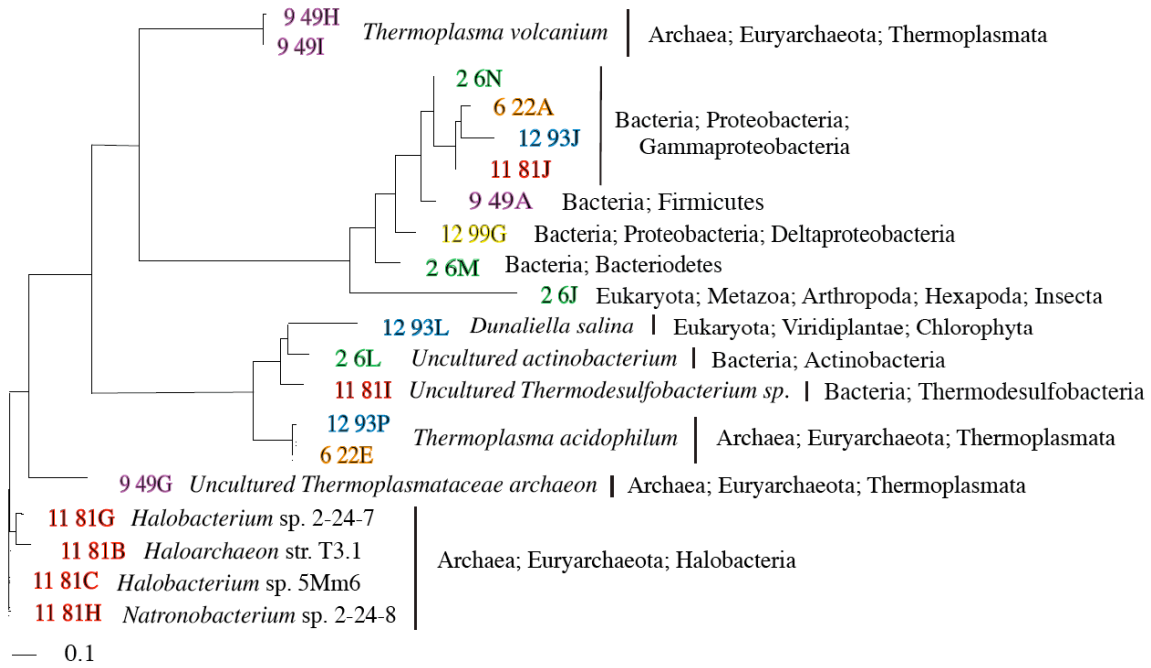

Figure 4.2 Prokaryotic diversity is shown in a phylogenic tree. Closest matches from BLAST are identified. The scale bar represents the number of nucleotide substitutions.

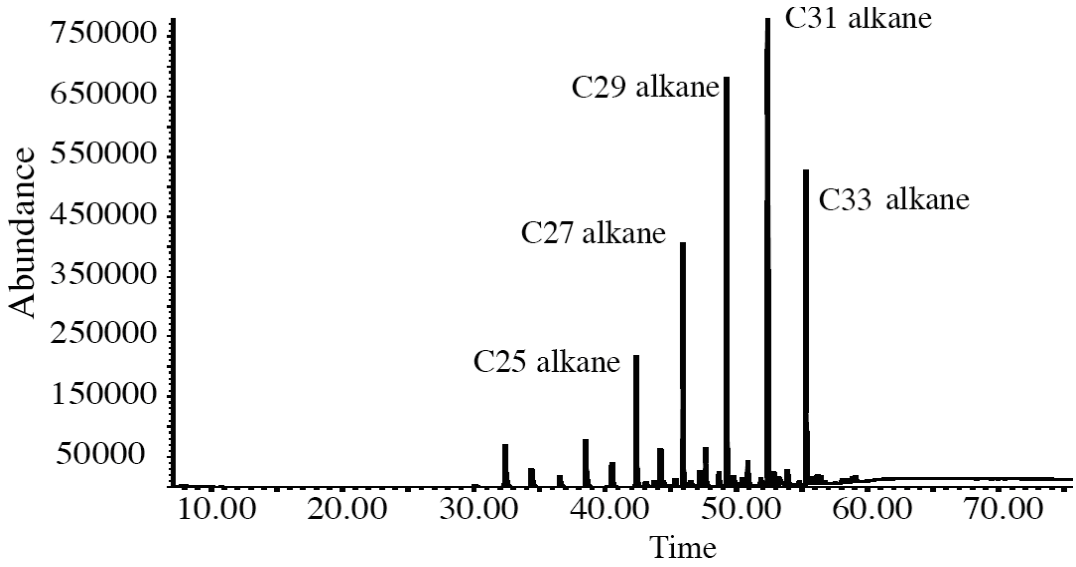

Figure 4.3 Sample 2_6 chromatogram, Fraction 2.

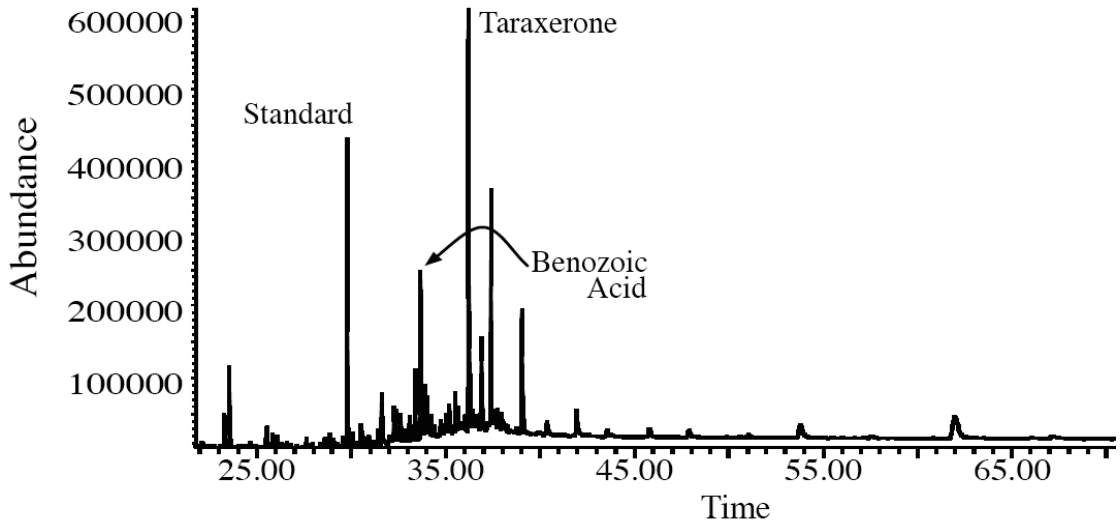

Figure 4.4 Sample 2_6 GC-MS spectrum, Fraction 3.

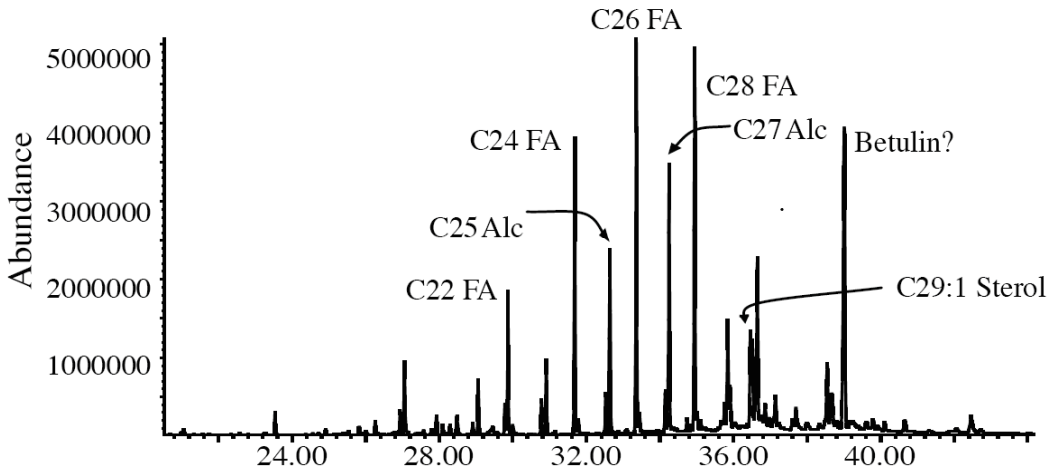

Figure 4.5 Sample 2_6 GC-MS chromatogram, Fraction 4.

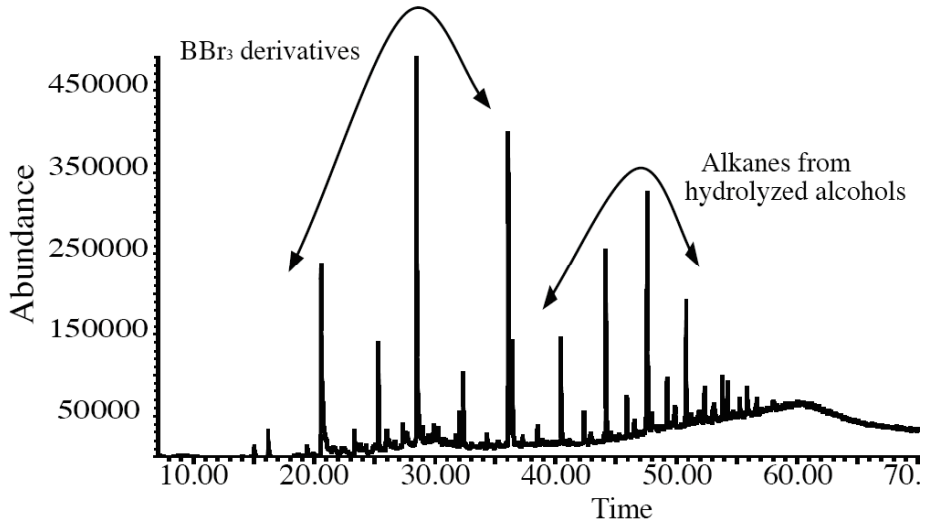

Figure 4.6 Sample 2_6 ether cleavage from column separation Fraction 4, BBr_3 derivatives and alkanes from hydrolyzed alcohols shown.

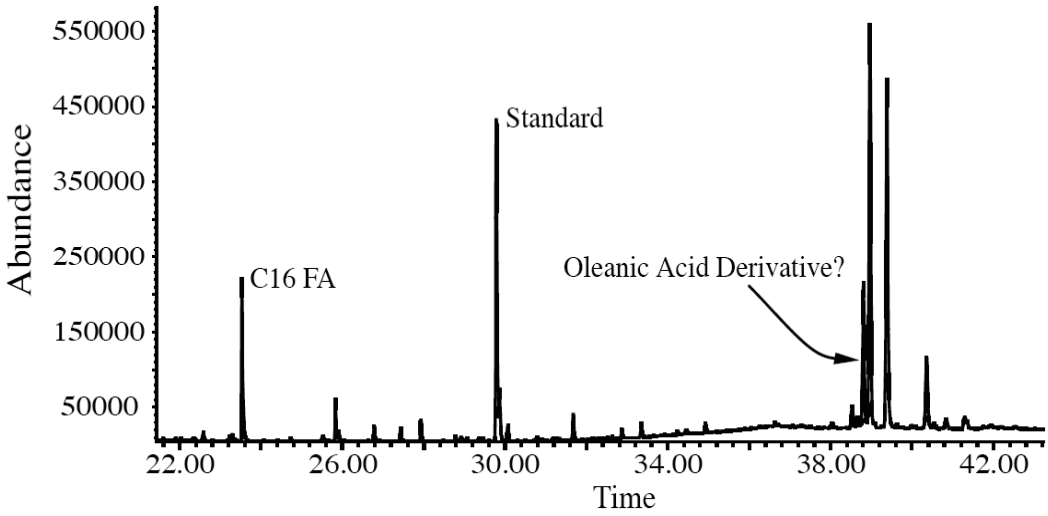

Figure 4.7 Sample 2_6 GC-MS chromatogram, Fraction 5.

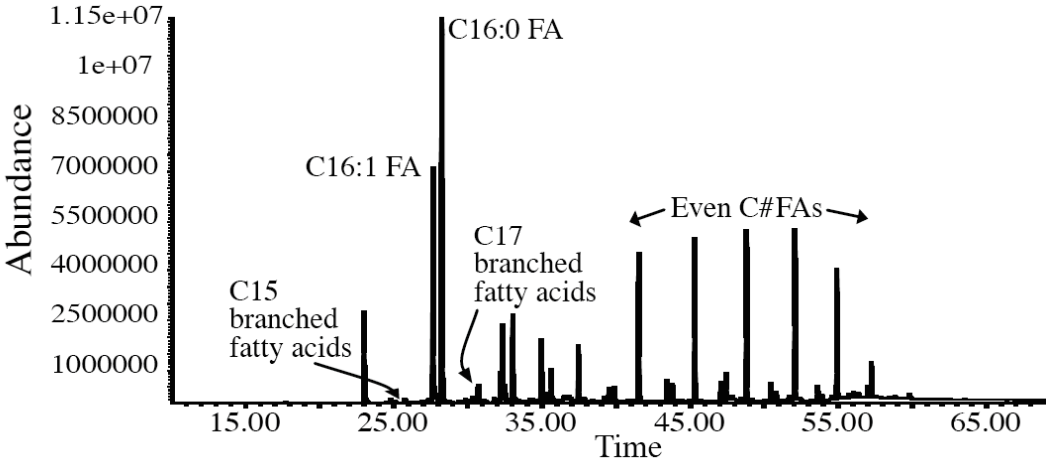

Figure 4.8 Sample 2_6 FAMEs.

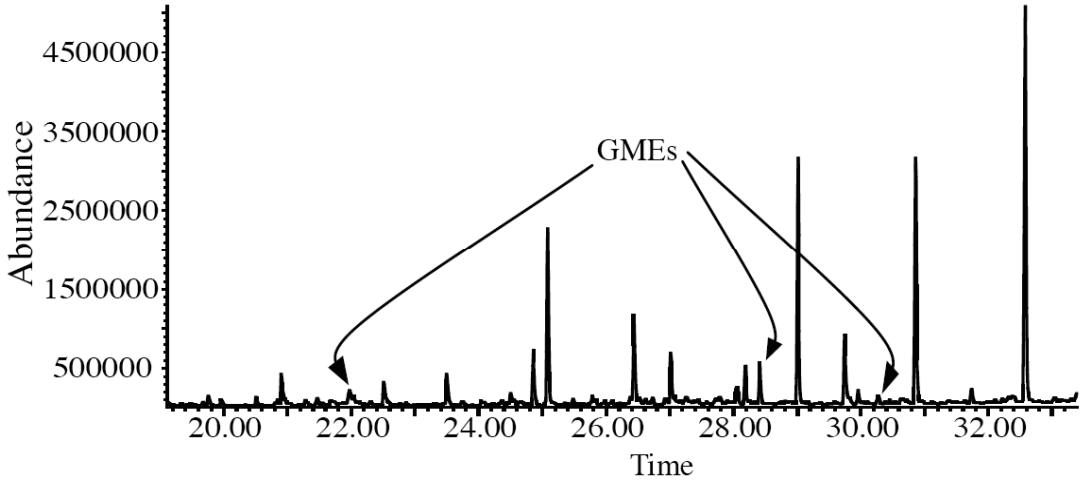

Figure 4.9 Glycerol monoethers (GMEs) identified in 8_32 neutral polar fraction chromotogram.

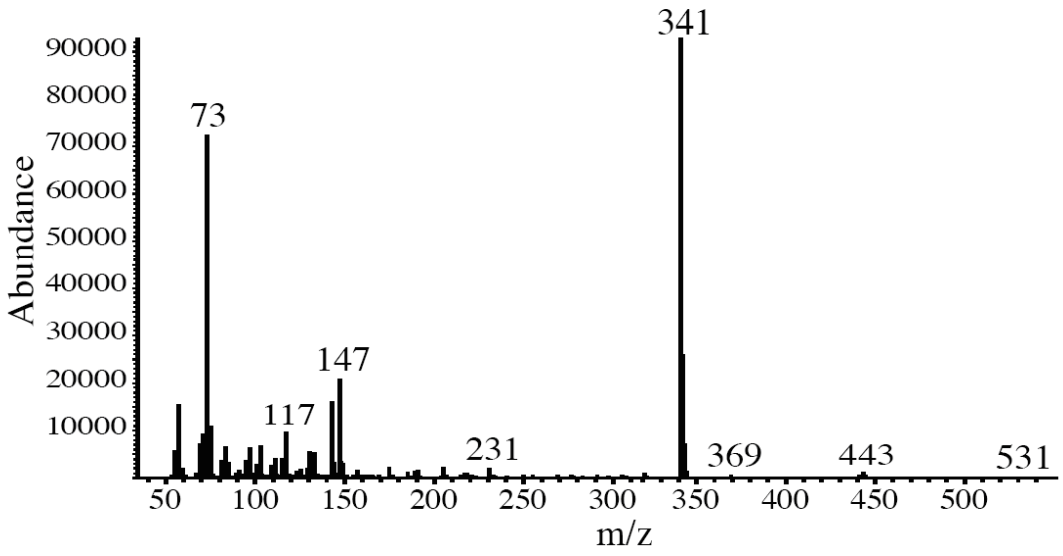

Figure 4.10 Mass spectrum of a 1-*O*-C16 GME from Sample 8_32.

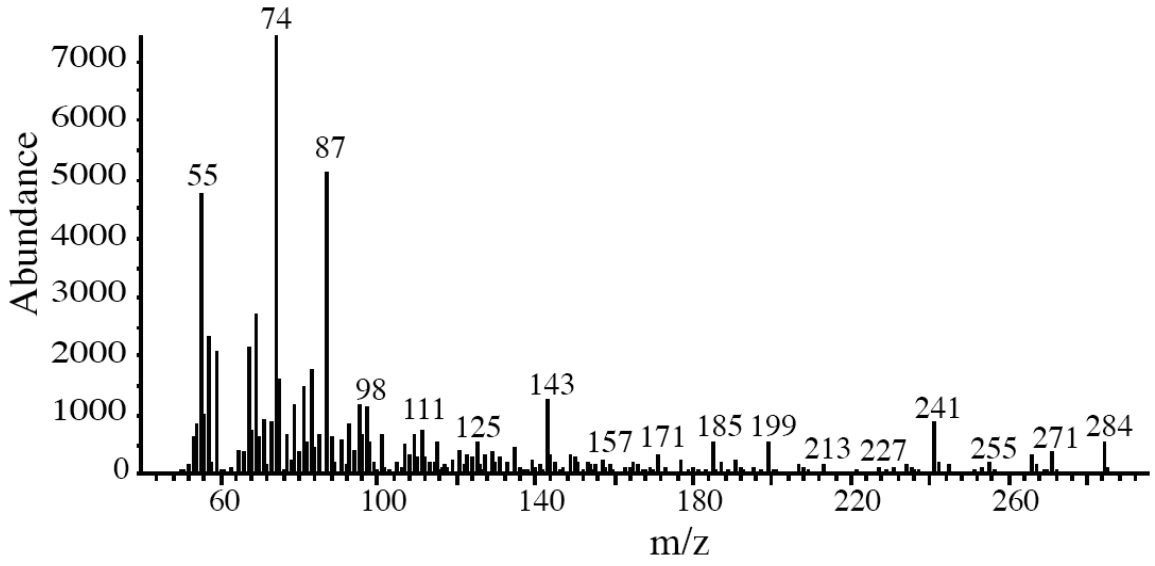

Figure 4.11 Mass spectrum for a C17 iso-branched fatty acid, indicative of sulfate-reducing bacteria.

4.9 Appendix

Sample 2 _6 F1

Peak #	R.T. min	Corrected Area	% of total	Nanograms	Identification
1	32.41	2709693	2.75	**50.00**	Standard
2	34.41	1604153	1.63	**29.60**	C21 alkane
3	38.54	3247538	3.30	**59.91**	C23 alkane
4	40.53	1561859	1.59	**28.82**	C24 alkane
5	42.38	7321484	7.43	**135.09**	C25 alkane
6	44.22	2194105	2.23	**40.47**	C26 alkane
7	45.95	13242805	13.44	**244.33**	C27 alkane
8	47.66	2277536	2.31	**42.02**	C28 alkane
9	49.28	21057677	21.37	**388.53**	C29 alkane
10	50.88	1269068	1.29	**23.42**	C30 alkane
11	52.40	24698528	25.06	**455.69**	C31 alkane
12	55.30	17360776	17.62	**320.31**	C33 alkane

	Even Alkanes	Odd Alkanes
Totals (ng):	**134.72**	**1633.46**

Appendix Table 4.1 Sample 2_6 Quantifications and Identifications, Fraction 1.

Sample 2 _6 F2

Peak #	R.T. min	Corrected Area	% of total	Nanograms	Identification
1	32.41	2957069	4.52	**50.00**	Standard
2	38.58	1102043	1.69	**18.64**	C23 alkane
3	42.39	3283366	5.02	**55.52**	C25 alkane
4	44.23	1286120	1.97	**21.75**	C26 alkane
5	45.95	7260189	11.10	**122.77**	C27 alkane
6	47.66	1760062	2.69	**29.77**	C28 alkane
7	49.28	13624698	20.83	**230.39**	C29 alkane
8	50.87	1541142	2.36	**26.06**	C30 alkane
9	52.39	18324945	28.01	**309.88**	C31 alkane
10	55.30	14277364	21.83	**241.43**	C33 alkane

	Even Alkanes	Odd Alkanes
Totals (ng):	**347.03**	**4245.53**

Appendix Table 4.2 Sample 2_6 Quantifications and Identifications, Fraction 2.

Sample 2 _6 F3					
Peak #	**R.T. min**	**Corrected Area**	**% of total**	**Nanograms**	**Identification**
1	29.792	10346895	17.571	**100.00**	Standard
2	33.673	4850695	8.238	**46.88**	Benzoic acid
3	36.221	16251577	27.599	**157.07**	Taraxerone (triterpene)
4	37.403	8990108	15.267	**86.89**	unknown
5	39.046	7305416	12.406	**70.60**	unknown

Appendix Table 4.3 Sample 2_6 Quantifications and Identifications, Fraction 3.

Sample 2 _6 F4

Peak #	R.T. min	Corrected Area	% of total	Nanograms	Identification
1	20.135	4197012	0.40	51.93	Weak Signal
2	23.53	5982551	0.58	74.04	C16 Fatty Acid
3	26.254	2978109	0.29	36.89	Weak Signal
4	26.942	8046263	0.77	99.49	Pimaric Acid
5	27.051	20520658	1.97	253.73	Isopimaric Acid
6	27.923	4556053	0.44	56.30	C20 Fatty Acid
7	28.484	5063840	0.49	62.60	
8	28.912	3557600	0.34	43.96	C21 Fatty Acid
9	29.063	13144590	1.27	162.60	C21 Alcohol
10	29.792	8084210	0.78	100.00	Standard
11	29.867	35939708	3.46	444.47	C22 Fatty Acid
12	30.781	9234454	0.89	114.27	C23 Fatty Acid
13	30.907	17407192	1.68	215.30	C23 Alcohol
14	31.678	71491957	6.88	884.19	C24 Fatty Acid
15	31.787	3949496	0.38	48.84	C24 Alcohol
16	32.524	10240572	0.99	126.61	C25 Fatty Acid
17	32.633	43832595	4.22	542.16	C25 Alcohol
18	33.363	95389455	9.18	1179.69	C26 Fatty Acid
19	33.446	6305675	0.61	78.02	C26 Alcohol
20	34.151	10340903	1.00	127.89	C27 Fatty Acid
21	34.251	65389850	6.29	808.74	C27 Alcohol
22	34.746	4326557	0.42	53.47	C27:1 Sterol
23	34.947	99947941	9.62	1236.12	C28 Fatty Acid
24	35.014	4539012	0.44	56.17	C28 Alcohol
25	35.76	8717303	0.84	107.84	C29 Fatty Acid
26	35.844	34362793	3.31	424.94	C29 Alcohol
27	35.911	14522524	1.40	179.56	C29:2 Sterol
28	36.464	31015600	2.98	383.55	C29:1 Sterol
29	36.514	28101135	2.70	347.56	Unknown
30	36.648	62516803	6.02	773.14	C30 Fatty Acid
31	36.858	10310066	0.99	127.51	Compounded Signal
32	37.143	13045459	1.26	161.31	Compounded Signal
33	37.612	4192947	0.40	51.80	C31 Fatty Acid
34	37.696	11868522	1.14	146.79	C31 Alcohol
35	38.551	28808655	2.77	356.30	Oleanic Acid Derivative?
36	38.677	21788807	2.10	269.54	Oleanic Acid Derivative?
37	39.021	24588963	11.99	1540.87	Betulin Derivative?
38	40.664	5545965	0.53	68.64	Unknown
39	42.457	10714079	1.03	132.52	Unknown

	Even Alcohols	Odd Alcohols	Even Fatty Acids	Odd Fatty Acids	C29 Sterols	Other Sterols
Totals (ng):	183.03	2300.51	4775.84	444.47	563.11	53.47

Appendix Table 4.4 Sample 2_6 Quantifications and Identifications, Fraction 4.

Sample 2 _6 F5					
Peak #	**R.T. min**	**Corrected Area**	**% of total**	**Nanograms**	**Identification**
1	20.144	866370	0.91	8.57	Unknown
2	23.53	4628994	4.84	45.80	C16 Fatty Acid
3	25.827	1006322	1.05	9.96	C18 Fatty Acid
4	27.931	573648	0.60	5.67	C20 Fatty Acid
5	29.792	10107606	10.56	100.00	Standard
6	29.867	1530440	1.60	15.14	C22 Fatty Acid
7	31.678	674341	0.71	6.67	C24 Fatty Acid
8	38.534	898716	0.94	8.89	Compounded Signal
9	38.811	5915004	6.18	58.52	Oleanic Acid Derivative?
10	38.97	16431591	17.17	162.56	Unknown
11	39.389	15423381	16.12	152.58	Unknown
12	40.362	3370582	3.52	33.35	Unknown

Appendix Table 4.5 Sample 2_6 Quantifications and Identifications, Fraction 5.

[THIS PAGE INTENTIONALLY LEFT BLANK]

[THIS PAGE INTENTIONALLY LEFT BLANK]

Chapter 5

Ancient bacteria show evidence of DNA repair[1]

5.0 Abstract

Recent claims of cultivable ancient bacteria within sealed environments highlight our limited understanding of the mechanisms behind long-term cell survival. It remains unclear how dormancy, a favored explanation for extended cellular persistence, can cope with spontaneous genomic decay over geological timescales. There has been no direct evidence in ancient microbes for the most likely mechanism, active DNA repair, or for the metabolic activity necessary to sustain it. In this paper we couple Polymerase Chain Reaction and enzymatic treatment of DNA with direct respiration measurements to investigate long-term survival of bacteria sealed in frozen conditions for up to one million years. Our results show evidence of bacterial survival in samples up to half a million years in age, making this the oldest independently authenticated DNA to date obtained from viable cells. Additionally, we find strong evidence that this long-term

---

[1] This chapter was originally published in the *Proceedings of the National Academy of Sciences*. It appeared in the print edition on September 4, 2007 (volume 104, issue number 36, pages 14401-14405), and its DOI reference is 10.1073/pnas.0706787104.

Johnson, S.S., M.B. Hebsgaard, T.R. Christensen, M. Mastepanov, R. Nielsen, K. Munch, T. Brand, M.T.P. Gilbert, M.T. Zuber, M. Bunce, R. Rønn, D. Gilichinsky, D. Froese, and E. Willerslev (2007), Ancient bacteria show evidence of DNA repair, *Proc. Nat. Acad. Sci., 104*, 14401-14405.

survival is closely tied to cellular metabolic activity and DNA repair that over time proves to be superior to dormancy as a mechanism in sustaining bacteria viability.

5.1 Introduction

In recent years, a number of studies have claimed that ancient bacterial cells and their DNA can survive for many millions of years within sediments, amber, and halite (*e.g.* [*Cano and Borucki*, 1995; *Vorobyova et al.*, 1997; *Vreeland et al.*, 2000; *Fish et al.*, 2002]). The most common explanation for these findings is that the microbes have remained in a stage of dormancy, known to be associated with high stress tolerance and resistance to adverse conditions. Although dormancy can be followed by special adaptations that reduce the rate of DNA damage, truly dormant cells, like the endospores of *Bacillus* and *Clostridium*, remain metabolically inactive and therefore have no active DNA repair [*Nicholson et al.*, 2000]. As a result, their genomes will degrade with time due to spontaneous chemical reactions like hydrolysis and oxidation [*Lindahl*, 1993] that finally become fatal, preventing the cell from germinating. Models suggest that unrepaired genomic DNA will be fragmented into small pieces less than 100 base-pairs (bp) in size or will become severely crosslinked within at most 100 thousand to 1 million years (100Kyr-1Ma) under optimal frozen conditions and much faster in warmer settings [*Lindahl*, 1993; *Poinar et al.*, 1996; *Osborne and Phillips,* 2000; *Smith et al.*, 2001; *Hansen et al.*, 2006]. Thus, the controversy of viable ancient bacteria is heightened by an absence of convincing evidence for mechanisms by which a cell can withstand damage to

DNA and other unstable molecules such as ATP over geological time scales [*Willerslev et al*., 2004a; *Willerslev et al*., 2004b; *Hebsgaard et al*., 2005; *Willerslev and Cooper*, 2005]. Even though there have been speculations and some indirect evidence of respiration in ancient microbes (*e.g.* [*Rivkina et al*., 2000; *Bakermans et al*., 2003; *Price and Sowers*, 2004; *Rivkina et al*., 2004; *Tung et al*., 2005; *Vishnivetskaya et al*., 2006; *Gilichinsky et al*., 2007]), so far there has been no direct evidence of active DNA repair. In this study, we used a combination of molecular biology techniques and direct measurement of CO_2 production from permanently frozen samples to show that dormancy is inferior to low-level metabolic activity with DNA repair as a long-term survival mechanism in ancient bacteria.

5.2 Results and discussion

We investigated samples from permafrost as these constant subzero temperature environments are considered among the best for long-term microbial and DNA survival [*Willerslev et al*., 2004b] (Table 5.1). Samples were drilled under strict conditions in northeastern Siberia, northwestern Canada, and Antarctica, and they were kept frozen until they were processed for DNA extraction in the laboratory. The cores were spiked on the surface with a recognizable contaminant during drilling as in [*Willerslev et al*., 2003; *Willerslev et al*., 2004a; *Willerslev et al*., 2004b], allowing us to test for penetration of contamination during collection, transport, and handling.

To ensure that DNA from dead cells was not included in the study, we attempted to amplify only 4 kilo-base (kb) bacterial ribosomal DNA fragments from our samples using universal bacterial primers. Previous studies have shown that fossil remains of dead organisms rarely produce endogenous amplification products longer than 100-500 bp in size [*Höss et al*., 1996], and no report has reproducibly generated amplicons >1042 bp from a dead specimen on ancient timescales [*Lambert et al.*, 2002]. The 4 kb amplicon length is both a factor of four beyond the longest fragment ever retrieved from the ancient DNA of dead cells and about twenty times longer than ancient DNA fragments recovered from plants and mammals in the same samples (88-230 bp, chemically similar to the DNA of microbes and certainly obtained from dead biomass) [*Willerslev et al*., 2003]. Although the successful culturing of microbes from ancient specimens could serve as direct evidence for life, this traditional tactic has been deliberately avoided as it suffers from two serious constraints. First, less than 1% of all cells are believed to be culturable using standard methods [*Torsvik et al*., 1996], severally restricting the applicability of the approach. Second, the long-term incubation times necessary for the detection of low-temperature growth greatly increase the risk of contamination [*Willerslev et al.,* 2004b].

Six samples dating up to 400-600Kyr yielded 4 kb amplicons of bacterial DNA while no amplification products were obtained from samples dated to be 740Kyr and ca. 1Ma, respectively (Table 5.1). Attempts to amplify 1 kb and 4 kb of rDNA from higher plant material in the samples failed. In order to exclude the possibility of false positive results due to intra-laboratory contamination, permafrost sub-samples were sent to Murdoch

University (Australia), where 4 kb amplifications of bacterial DNA were independently obtained (Table 5.1).

The successful and reproducible amplification of 4 kb bacterial DNA but not plant DNA suggests that viable bacterial cells are likely to be present in the permafrost core samples. Importantly, decreasing sequence diversity with age of the recovered bacterial DNA further supports the results' authenticity: this pattern has previously been seen in studies of ancient permafrost samples [*Willerslev et al.,* 2004a] and is unlikely to result from contamination (Figure 5.1, See Table 5.1 footnote and *Materials and Methods*). Together with near-constant levels of preserved cellular structures with sample age, the result is consistent with the view that ancient permafrost does not sustain a reproductive bacterial community [*Willerslev et al.,* 2004b].

Ancient viable bacteria may in principle exist in two different states: i) a dormant state, such as an endospore, which involves no metabolic activity and therefore no active DNA repair, or ii) a metabolically active state that may allow for some degree of DNA repair. One way to discriminate between these two states is through assessment of relative levels of DNA damage. The DNA molecule is susceptible to many forms of chemical modification [*Pääbo*, 1989; *Lindahl*, 1993]. One form commonly observed is the hydrolytic deamination of cytosine, generating uracil or its analogs. The subsequent pairing of uracil with adenine during polymerase amplification leads to the observation of characteristic C→T/G→A transitions [*Hansen et al*., 2001; *Binladen et al*., 2006]. In

order to identify metabolically active cells, we determined the relative levels of genetic damage by treating aliquots of the DNA extracts with uracil-*N*-glycosylase (UNG) prior to amplification of 4 kb rDNA bacterial fragments. UNG breaks the base-ribose bond in uracil (the product of cytosine deamination) and only allows undamaged DNA to be amplified (Figure 5.2; See *Materials and Methods*). Active *in vivo* systems can repair this damage; in dead or dormant cells (*i.e.* cells with no measurable metabolic activity), however, uracil residues will be expected to accumulate over time.

Our analyses of UNG-treated sequences revealed varying levels of DNA damage. In the 5-30Kyr age range, low-GC Gram positive bacteria with the capacity to form dormant endospores accumulated hydrolytic damage at the 99% confidence level (Fisher Exact Test, n= 95, p= 0.00008). No bacteria with a known capacity for dormancy were detected in the 400-600Kyr amplifications. Instead, members of high-GC Gram positive *Actinobacteria* largely related to the non-sporeforming *Arthrobacter* dominated the oldest intact DNA recovered (Figure 5.3).

Seeking evidence of the metabolic activity necessary for DNA repair, we directly tested the same frozen samples for respiration in the form of CO_2 production under close to ambient conditions. Using a highly sensitive technique (See *Materials and Methods*), we found mean rates of 0.142-0.794µg CO_2-C/g dw/day in samples less than 600Kyr but no CO_2 production above background in the 740Kyr sample or control blanks, which fits

with our inability to amplify long DNA amplification products from these samples (Figure 5.4).

Our respiration results together with the lack of DNA damage in high-GC Gram positive bacteria demonstrate evidence for long-term viability, metabolic activity, and DNA repair in ancient microbial cells. Many studies have suggested that dormancy is the most effective survival strategy for bacteria over long time periods (*e.g.* [*Kennedy et al*., 1994; *Cano and Borucki*, 1995; *Vorobyova et al*., 1997; *Vreeland et al*., 2000]); our data indicate that despite short-term robustness, however, dormant bacteria are unlikely to be the most persistent cells over thousand-year timescales in the cold and desiccated conditions represented by our samples. Instead, bacteria with an active DNA repair mechanism are most likely to persevere.

The long-term survival of bacteria within frozen environments provides a range of intriguing possibilities for DNA maintenance and recovery from subsurface environments. This study demonstrates that permafrost may harbor a subset of viable bacteria adapted to past paleoenvironments, some of which might have yet to be described. The long-term DNA survival observed in *Actinobacteria* warrants further research as components of these repair pathways could be enlisted for applications requiring maintenance of DNA integrity for extended periods of time. Finally, to the extent that extant life in permafrost and ice on Mars and Jupiter's moon Europa is thought to be similar to that on Earth, this study calls for further consideration of

metabolically active microbes at subzero temperatures in designing life detection strategies.

5.3 Materials and methods

All pre-PCR work was carried out in dedicated, isolated ancient DNA facilities (with separate ventilation systems, nightly UV-irradiation of surfaces and positive air pressure), and the research team adhered to strict protocols (with full bodysuits, facemasks, and gamma-sterilized gloves) [*Hebsgaard et al.*, 2005; *Willerslev and Cooper,* 2005]. Blank extraction and PCR-amplification controls were incorporated at ratios of 1:5 and 1:1, respectively. Primary analyses were performed in the Ancient DNA Laboratory at Centre for Ancient Genetics, University of Copenhagen, Denmark, and replication of the 4 kb PCR analyses were completed in the Ancient DNA Research Laboratory, Murdoch University, Australia (Table 5.1). The results from the independent laboratories showed an overlap of 83% between sequence groups (*i.e.* sequences that were ≥96% similar, accounting for intra-species heterogeneity in the 16S rDNA).

5.3.1 Sample acquisition

Samples were drilled in northwestern Canada, northeastern Siberia, and Antarctica from sections that have remained frozen since deposition [*Willerslev et al.,* 2003; *Willerslev et al.*, 2004a]. The drilling apparatus was spiked with recognizable bacterial cells or vector DNA for detection of contamination during sampling and handling as described in

Willerslev et al. [2003]; *Willerslev et al*. [2004a], and *Hansen et al.* [2006]. 2-4 cm of the contaminated surfaces were removed with a sterilized microtome knife as in [*Willerslev et al.,* 1999], and samples were dated using fission-track dating, tephrochronology, radiocarbon and argon dating [*Hansen et al*., 2001; *Willerslev et al.,* 2003; *Willerslev et al*., 2004a; *Froese et al.*, 2005]. A previous study of the same permafrost cores suggests that no leaching of free DNA or cells has taken place between the strata [*Hansen et al.,* 2006].

5.3.2 DNA extraction and amplification

DNA was extracted and purified (from 2 grams wet weight of sediment) using established protocols [*Willerslev et al.,* 2003; *Willerslev et al*., 2004a]. The primer pairs used for the 4 kb bacterial DNA amplifications were: 341F: 5'- CTCCTACGGGAGGCAGCAGTGGGGAATATTGC -3', located on the 16S rDNA and 2167R: 5'- GGTCGGAACTTACCCGACAAGGAATTTCGCTACCT -3', located on the 23S rDNA. The primer pairs used for 1 kb and 4 kb amplifications of plant DNA were: PL4000F: 5'- GTGGCAGAGTGGCCTTGCTGCCACGATCCACTGAG -3', located ETS region and PL4000R: 5'- CGTTTCTCAGGCTCCCTCTCCGGAATCGAACCCTA -3' located on the 18S rDNA as well as PL1000F: 5'- TGGTTGATCCTGCCAGTAGTCATATGC -3' located on the 26S rDNA and PL1000R: 5'- CCAAGAATTTCACCTCTGACTATGAAATAC -3' located on the 18S rDNA.

PCR amplifications were performed in 25µl reaction volumes: 9µl GATC mix (20mM/0.25µl dNTPs + ddH_2O), 2.5µl primer 341F, 2.5µl primer 2167R, 2.5µl $MgSO_4$, 0.2µl High Fidelity (HiFi) enzyme (Invitrogen) with 2.5µl HiFi buffer, in addition to 4µl BSA and 1.75µl DMSO (to aid the denaturing of GC-rich strands). PCR conditions for the non-UNG treated DNA extracts were: 2 min at 92°C initial; 10 cycles (2 min at 94°C, 1 min at 50°C, 3 min 40 sec at 72°C); 40 cycles (2 min at 94°C, 1 min at 50°C, 3 min 40 sec + 20 additional sec/cycle at 72°C); 10 min 72°C final. For UNG-treated extracts, 0.25µl of UNG (Nordic BioSite) and 2.5µl of UNG 10x buffer were added initially and allowed to incubate at 37°C for 30 min. An initial, one-time UNG activation step of 5 min at 50°C was added to the above PCR program. The initial denaturation step at 92°C was also lengthened from 2 to 5 min to completely deactivate the enzyme and prompt strand breaks in damaged templates. The efficacy of UNG for this purpose is supported by [*Pääbo*, 1989; *Hofreiter et al.*, 2001; *Gilbert et al.*, 2003]. It should be noted that UNG preferentially targets C-rich sequences, therefore there is less detection of damage in low-GC Gram positive bacteria than in high-GC Gram positive bacteria. The rate of damage in endospore-forming low-GC Gram positive bacteria may be even higher than reported, which adds further support to our conclusions.

5.3.3 Cloning and sequencing

From the 4 kb products amplified, 600 bp fragments were cut to enable cloning and sequencing using the following PCR primer pairs: 907F: 5'-AAACTYAAAKGAATTGACGG -3' and rP1: 5'- ACGGTTACCTTGTTACGACTT -3' [*Willerslev et al*., 2004a]. One to three amplifications per sample were pooled, cloned, purified and sequenced on both strands. The resulting sequences were aligned and investigated for possible recombination as in [*Willerslev et al*., 1999]. The sequences are deposited in GenBank under accession numbers EU083531–EU083798.

5.3.4 Sequence identification

Sequences were assigned to taxonomic groups using a Bayesian assignment criterion. For each sequence, a BLAST search was performed identifying the 50 sequences with the highest E-score. Sequences without a taxonomic identification in Genbank were not included. The sequences were first aligned using ClustalW [*Thompson et al*., 1994] and then analyzed using MrBayes [*Huelsenbeck and Ronquist*, 2001]. For each alignment, 1,000,000 iterations were performed in MrBayes under the default settings. The first 100,000 cycles were discarded as burn-in, and posterior probabilities of monophyly were inferred from the remaining 900,000 cycles. A sequence was then assigned to a particular taxonomic group if the probability that it was monophyletic with that group exceeded 90%. A sequence identification chart, including hyperlinks to GenBank and sequence distances, can be found online at:

http://www.binf.ku.dk/~kasper/taxonophy/bact_respiration/.

5.3.5 Metabolic activity

Past studies attempting to demonstrate viability and metabolic activity in ancient sealed environments have been prone to contamination, relying heavily on culturing, pulverization or thawing of samples [*Rivkina et al*., 2000; *Bakermans et al*., 2003; *Rivkina et al*., 2004; *Gilichinsky et al*., 2007]. For this reason, we employed a sensitive, low-temperature technique to conduct tests for microbial respiration on undisturbed permafrost cores.

Permafrost sub-samples from cores 25K, 500K and 740K (Table 5.1) were transferred into a cold incubation apparatus and incubated for nine months at –10°C in a CO_2-free atmosphere. Produced CO_2 was removed during incubation. The incubations were performed using a modified version of an experimental technique [*Panikov et al*., 2006] that reduces the slight possibility of CO_2 release from material of plastic (organic) origin. Hence, the incubation chambers and all connecting tubes were made of stainless steel. The CO_2 release was measured in a similar way to that described in [*Panikov et al*., 2006]; after an initial discharge of entrapped CO_2 for three months, the samples showed a constant level of daily CO_2 release during six months of incubation. Two control samples (without soil) were processed together with the permafrost samples. Respiration levels for controls as well as for Sample 740K were not distinct from zero, while Samples 25K and 500K showed significant relative CO_2 release.

The incubations were performed in anaerobic conditions, characteristic of subsurface permafrost environments from Siberia and Canada [*Willerslev et al*., 2004b]. While metabolic activity through chemoautotrophic pathways cannot be excluded in the older samples, our genetic findings (no viable bacteria in samples older than 600Kyr) parallel our respiration results (only CO_2 production in samples younger than 600 Kyr). Furthermore, it has been demonstrated that *Arthrobacter*, the most common genus we detected among the high-GC Gram positive bacteria, is capable of anaerobic metabolism [*Eschbach et al*., 2003].

5.4 References

Bakermans, C., A. I. Tsapin, V. Souza-Egipsy, D. A. Gilichinsky and K. H. Nealson (2003), Reproduction of metabolism at -10°C of bacteria isolated from Siberian permafrost. *Environ. Microbiol.*, *5*, 321-326.

Binladen, J., C. Wiuf, M. T. P. Gilbert, M. Bunce, R. Barnett, G. Larson, A. D. Greenwood, J. Haile, S. Y. W. Ho and A. J. Hansen, *et al.* (2006), Comparing miscoding lesion damage in mitochondrial and nuclear ancient DNA Genetics. *Genetics, 2*, 733-741.

Cano, R. J. and M. K. Borucki (1995), Revival and identification of bacterial spores in 25-million-year-old to 40-million- year-old Dominican amber. *Science, 268*, 1060–1064.

Eschbach, M., H. Möbitz, A. Rompf, and D. Jahn (2003), Members of the genus Arthrobacter grow anaerobically using nitrate ammonification and fermentative processes: anaerobic adaptation of aerobic bacteria abundant in soil. *FEMS Microbiol. Lett., 223*, 227-230.

Fish, S. A., T. J. Shepard, T. J. McGenity and W. D. Grant (2002), Recovery of 16S ribosomal RNA gene fragments from ancient halite. *Nature, 417*, 432-436.

Froese, DG, Westgate, JA & Alloway, BV. (2005) Field Trip Guide for the International Field Conference and Workshop of Tephrochronology and Volcanism: Dawson City, Yukon Territory, Canada. *Institute of Geological and Nuclear Sciences Science Report 2005/26* 132.

Gilbert, M. T. P., A. J. Hansen, E. Willerslev, L. Rudbeck, I. Barnes, N. Lynnerup and A. Cooper (2003), Characterisation of genetic miscoding lesions caused by post-mortem damage. *Am. J. Hum. Genet., 72*, 48-61.

Gilichinsky, D., G. S. Wilson, E. I. Friedmann, C. P. McKay, R. S. Sletton, E. M. Rivkina, T. A. Vishnivetskaya, L. G. Erokhina, N. E. Ivanushkina, and G. A. Kochkina, *et al.* (2007), Microbial populations in antarctic permafrost: biodiversity, state, age, and implication for astrobiology. *Astrobiology*, *7*, 275-311.

Hansen, A. J., E. Willerslev, C. Wiuf, T. Mourier and P. Arctander (2001), Statistical evidence for miscoding lesions in ancient DNA templates. *Mol. Biol. Evol., 18*, 262–265.

Hansen, A. J., D. L. Mitchell, C. Wiuf, L. Paniker, T. B. Brand, J. Binladen, D. A. Gilichinsky, R. Rønn and E. Willerslev (2006), Crosslinks Rather Than Strand Breaks

Determine Access to Ancient DNA Sequences From Frozen Sediments. *Genetics, 173*, 1175-1179.

Hebsgaard, M. B., M. J. Phillips and E. Willerslev (2005), Geologically ancient DNA: fact or artefact? *Trends Microbiol., 13*, 212-220.

Hofreiter, M., V. Jaenicke, D. Serre, A. von Haeseler and S. Pääbo (2001), DNA sequences from multiple amplifications reveal artifacts induced by cytosine deamination in ancient DNA. *Nucleic Acids Res., 29*, 4693-479.

Höss, M., P. Jaruga, A. T. H. Zastawny, M. Dizdarogluand and S. Pääbo (1996), DNA damage and DNA sequence retrieval from ancient tissues. *Nucleic Acids Res., 24*, 1304-1307.

Huelsenbeck, J. P. and F. Ronquist (2001), MRBAYES. Bayesian inference of phylogeny. *Bioinformatics, 17*, 754-755.

Lambert, D. M., P. A. Ritchie, C. D. Millar, B. Holland, A. J. Drummond and C. Baroni, (2002), Rates of Evolution in Ancient DNA from Adélie Penguins. *Science, 295*, 2270-2273.

Lindahl, T. (1993). Instability and Decay of the Primary Structure of DNA. *Nature, 362*, 709-715.

Kennedy, M. J., S. L. Reader, and L. M. Swierczynski (1994), Preservation records of microorganisms: evidence of the tenacity of life. *Microbiology, 140*, 2513–2529.

Marchant, D. R., A. R. Lewis, W. M. Phillips, E. J. Moore, R. A. Souchez, G. H. Denton, D. E. Sudgen, N. Potter and G. P. Landis (2002), Formation of patterned ground and sublimation till over Miocene glacier ice in Beacon Valley, southern Victoria Land Antarctica. *Geol. Soc. Am. Bull., 114*, 718-730.

Ng, F., B. Hallet, R. S. Sletton and J. O. Stone (2005), Fast growing till over ancient ice in Beacon Valley, Antarctica. *Geology, 33*, 121-124.

Nicholson, W. L., N. Munakata, G. Horneck, H. J. Melosh, and P. Setlow (2000), Resistance of Bacillus Endospores to Extreme Terrestrial and Extraterrestrial Environments. *Microbiol. Mol. Biol. Rev., 64*, 548–572.

Oberholzer, P., H. Baur, G. H. Denton, D. R. Marchant, J. M. Schafer, C. Schluchter, W. Rainer, and A. R. Lewis (2000), Minimum age and evolution of the buried ice in Beacon

Valley, Antarctica, derived from in-situ cosmogenic noble gases. *Journal of Conference Abstracts (Goldschmidt 2000, Oxford, UK) 5*, 747.

Osborne, M. R. and D. H. Phillips (2000), Preparation of a methylated DNA standard, and its stability on storage. *Chem. Res. Toxicol.*, *13*, 257-261.

Pääbo, S. (1989), Ancient DNA: Extraction, Characterization, Molecular Cloning, and Enzymatic Amplification. *Proc. Nat. Acad. Sci., 86*, 1939-1943.

Panikov, N. S., P. W. Flanagan, W. A. Oechel, M. A. Mastepanov, and T. R. Christensen (2006), Microbial activity in soils frozen to below -39ºC. *Soil Biol. Biochem., 38*, 785-794.

Poinar, H. N., M. Höss, J. L. Bada, and S. Pääbo (1996), Amino acid racemization and the preservation of ancient DNA. *Science, 272,* 864–866.

Price, P. B. and T. Sowers (2004), Temperature dependence of metabolic rates for microbial growth, maintenance, and survival. *Proc. Natl. Acad. Sci. USA, 101*, 4631-4636.

Rivkina, E. M., E. I. Friedmann, C. P. McKay, and D. A. Gilichinsky (2000), Metabolic activity of permafrost bacteria below the freezing point. *Appl. Environ. Microbiol., 66*, 3230-3233.

Rivkina, E., K. Laurinavichius, J. McGrath, J. Tiedje, V. Shcherbakova, and D. Gilichinsky (2004), Microbial life in permafrost. *Adv. Space Res., 33*, 1215-1221.

Schäfer, J. M., H. Baur, G. H. Denton, S. Ivy-Ochs, D. R. Marchant, C. Schluchter, and R. Wieler (2000), The oldest ice on Earth in Beacon Valley, Antarctica: New evidence from surface exposure dating. *Earth Planet. Sci. Lett., 179*, 91-99.

Smith, C. I., A. T. Chamberlain, M. S. Riley, A. Cooper, C. Stringer and M. J. Collins (2001), Neanderthal DNA: Not just old but old and cold? *Nature, 410*, 771–772.

Stone, J., R. S. Sletten, B. Hallet and M. Caffee (2000), Old ice, going fast: Cosmogenic isotope measurements on ice beneath the floor of Beacon Valley, Antarctica. *EOS Trans Am. Geophys. Union*, Fall 2000 meeting supplement.

Sugden, D. E., D. R. Marchant, N. Potter Jr., R. Souchez, G. H. Denton, C. C. Swisher, and J.-L. Tison (1995), Miocene glacier ice in Beacon Valley, Antarctica. *Nature, 376*, 412-416.

Thompson, J. D., D. G. Higgins, and T. J. Gibson (1994), CLUSTAL W: improving the sensitivity of progressive multiple sequence alignment through sequence weighting, position-specific gap penalties and weight matrix choice. *Nucleic Acids Res., 22*, 4673-4680.

Torsvik, V., R. Sørheim, and J. Goksøyr (1996), Total bacterial diversity in soil and sediment communities – a review. *J. Ind. Microbiol., 17*, 170-178.

Tung, H. C., N. E. Bramall and P. B. Price (2005), Microbial origin of excess greenhouse gases in glacial ice and implications for life on Mars. *Proc. Natl. Acad. Sci. USA, 102,* 18292-18296.

Vishnivetskaya, T. A., M. A. Petrova, J. Urbance, M. Ponder, C. L. Moyer, D. A. Gilichinsky, and J. M. Tiedje (2006), Bacterial Community in Ancient Siberian Permafrost as Characterized by Culture and Culture-Independent Methods. *Astrobiology, 6*, 400-414.

Vorobyova, E., V. Soina, M. Gorlenko, N. Minkovskaya, N. Zalinova, A. Mamukelashvili, D. Gilichinsky, E. Rivkina, and T. Vishnivetskaya (1997), The deep cold biosphere: facts and hypotheses. *FEMS Microbiol., 20*, 277–290.

Vreeland, R. H., W. D. Rosenzweig, and D. W. Powers (2000), Isolation of a 250 million-year-old halo-tolerant bacterium from a primary salt crystal. *Nature, 407*, 897-900.

Willerslev, E., A. J. Hansen, B. Christensen, J. P. Steffensen, and P. Arctander (1999), Diversity of Holocene life-forms in fossil glacier ice. *Proc. Natl. Acad. Sci. USA, 96*, 8017-8021.

Willerslev, E., A. J. Hansen, T. Brand, J. Binladen, M. T. P. Gilbert, B. A. Shapiro, C. Wiuf, D. A. Gilichinsky, and A. Cooper (2003), Diverse plant and animal DNA from Holocene and Pleistocene sedimentary records. *Science, 300*, 792-795.

Willerslev, E., A. J. Hansen, R. Rønn, T. B. Brand, C. Wiuf, I. Barnes, D. A. Gilichinsky, D. Mitchell, and A. Cooper (2004a), Long-term persistence of bacterial DNA. *Curr. Biol., 14*, R9-R10.

Willerslev, E., A. J. Hansen, and H. N. Poinar (2004b) Isolation of nucleic acids and cultures from ice and permafrost. *Trends Ecol. Evol., 19,* 141-147.

Willerslev, E. and A. Cooper (2005), Ancient DNA. *Proc. Royal Soc. Lon. B, 272*, 3-16.

5.5 Tables

Permafrost samples analyzed for 4kb amplification products				
Sample ID	Site	Age range	4kb Prod-ucts?	More Details
Sample 0K	Kolyma Lowland, Plakhin Jar (ca. 160° 50'E, 68° 40'N) Depth: up to 0.5m	Seasonally frozen modern tundra soil	√	--
° Sample 7K	Laptev Sea Coast, Cape Bykovskii (129° 30'E, 71° 40'N) Depth: 4.8m	Holocene 5-9Kyr	√	[*Willerslev et al.*, 2003; *Willerslev et al.*, 2004a; *Hansen et al.*, 2006]
° Sample 10K	Kolyma Lowland, Kon'kovaya River (158° 28'E, 69° 23'N) Depth: 4.0m	Holocene 10.425 ± 0.045Kyr	√	[*Willerslev et al.*, 2003; *Willerslev et al.*, 2004a; *Hansen et al.*, 2006]
Sample 21K	Ledovyi Obryv Exposure, Main River Ice Bluff, Southern Chukotka (171° 11'E, 64° 06'N) Depth: 6.0m	Late Pleistocene 20.900±0.110 Kyr	√	--
‡° Sample 25K	Kolyma Lowland, Chukochia River (156° 59'E, 69° 29'N) Depth: 14.8 m	Late Pleistocene 20-30Kyr	√	[*Willerslev et al.*, 2003; *Willerslev et al.*, 2004a]
‡° ∞ * Sample 500K	Khomus-Yuryakh River (153° 40'E, 70° 05'N) Depth: 41.6m	Middle Pleistocene 400-600Kyr	√	[*Willerslev et al.*, 2003; *Willerslev et al.*, 2004a; *Hansen et al.*, 2006]

continued…

Sample ID	Site	Age range	4kb Prod-ucts?	More Details
‡ Sample 740K	Dominion Creek, Yukon (138º 36'E, 63º 41'N) Depth: 10m	Middle Pleistocene 740 ± 60Kyr		[*Froese et al.,* 2005]
º Sample 1M	Beacon Valley, Antarctica (160° 36'E, 77° 50'S) Depth: 14.5m	≥1Ma*		[*Sugden et al*., 1995; *Nicholson et al.,* 2000; *Schäfer et al.*, 2000; *Stone et al*., 2000; *Oberholzer et al*., 2000; *Marchant et al*., 2002; *Ng et al*., 2005]

‡ Metabolic Activity experiments were conducted on these samples.
º Both DNA concentration and the frequency of interstrand crosslinks were assayed on these samples in [*Willerslev et al*., 2004a; *Hansen et al*., 2006]. Consistent with the DNA degradation undergone in dead cells, DNA concentration decreases with increasing age while the number of interstrand crosslinks increases. Additionally, cell counts from these samples changed little with increasing age. Observed cell counts for three other samples between 1.5 and 2Ma in age (all with no amplifiable DNA) were similar to these younger samples, thus suggesting that bacterial remnants are well preserved over these timescales [*Willerslev et al.,* 2004a]. This is expected as the DNA molecule is relatively unstable compared to other cellular components and consistent with the idea that few or no new cells arise.
∞ 4 kb amplification results were replicated on a duplicate sample of permafrost 500K in the Ancient DNA Research Laboratory, Murdoch University, Australia.
* Sample 1M was taken from beneath an 8.1Ma volcanic ash layer that has been interpreted as a direct air-fall deposit [*Sugden et al*., 1995]. The antiquity of Sample 1M is supported by a number of studies [*Oberholzer et al*., 2000; *Schäfer et al*., 2000; *Marchant et al*., 2002]. It should be noted, however, that a recent investigation has questioned age relations [*Ng et al*., 2005] and analyses are ongoing. Nevertheless, researchers at the University of Washington contend that our sample is at least 1Ma in age [*Stone et al*., 2000]. Thus, for our study we have assigned it an age that we think is cautious and accords with the available data, ≥1Ma.

Table 5.1

5.6 Figures

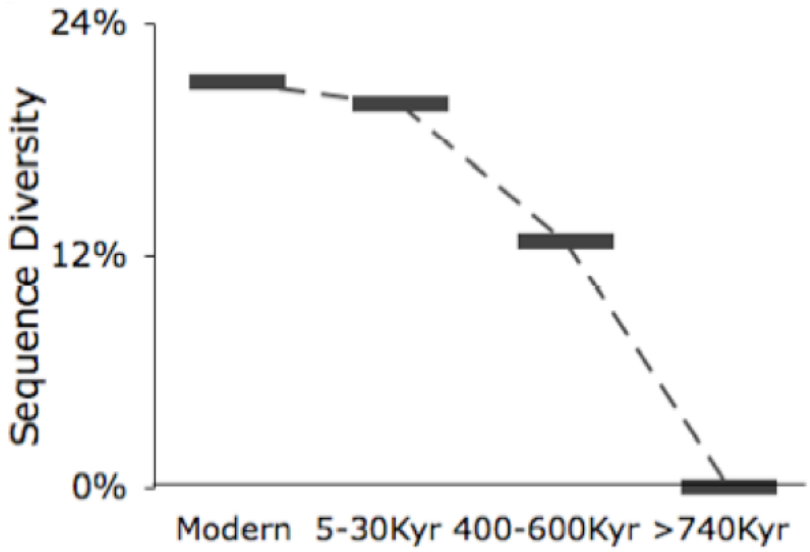

Figure 5.1 Sequence diversity (average percentage of non-matching nucleotides for sequence pairs within samples) as a function of permafrost age.

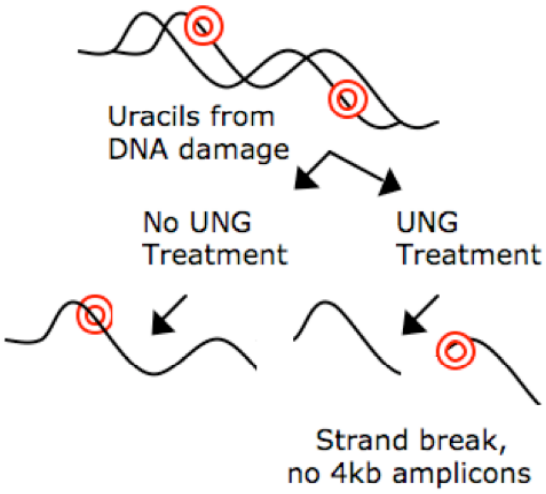

Figure 5.2 Uracil-*N*-glycosylase (UNG) treatment leads to strand breaks in damaged DNA during the Polymerase Chain Reaction (PCR) denaturation step.

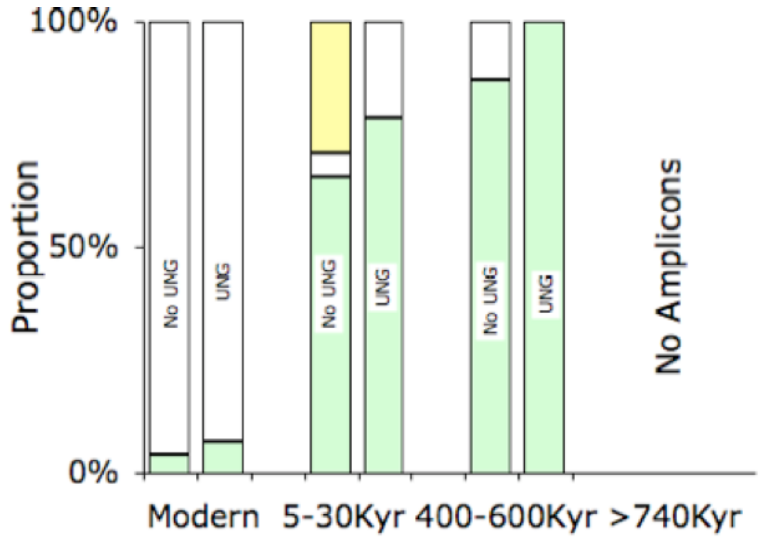

Figure 5.3 Proportion of clones before and after UNG treatment (see Figure 5.2). Low-GC Gram positive bacteria (yellow) such as the endospore-former *Clostridia* exhibited DNA damage. Gram negative bacteria (white) and high-GC Gram positive bacteria (green) such as *Actinobacteria* have no known capacity for dormancy.

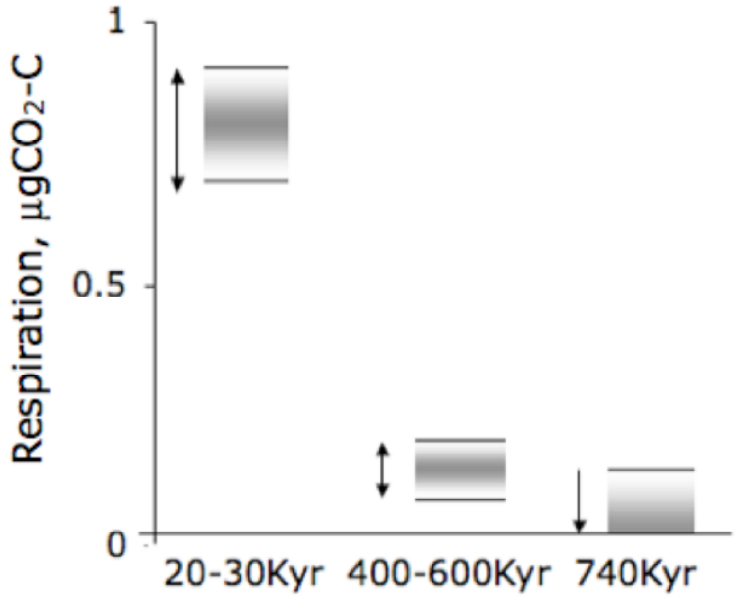

Figure 5.4 Respiration in µgCO_2-C per gram dry soil per day as a function of permafrost age; the range depicted represents the minimum detectable difference by this method.

[THIS PAGE INTENTIONALLY LEFT BLANK]

Chapter 6

Prokaryotic Diversity in Spain's Red River: lessons for life detection on the Red Planet

6.0 Abstract

Advances in genetics are paving the way for new methods to test the hypothesis that life on Mars, if it exists, shares a common ancestor with life on Earth. By returning DNA and RNA sequences, a new class of life detection instruments could virtually eliminate false positive results: genetic data from likely contaminates would be identified immediately, whereas any system of life isolated from Earth over geologic time would be evident from phylogenetic analysis. This new approach utilizes microfluidic "PCR in a chip" technology that enables hundreds of DNA fragments to be sequenced in wells only a few microns in width. Because this technology is capable of *in situ* DNA analysis, it is well-suited for deployment in Mars-like environments here on Earth, and perhaps, one day, on Mars itself. With an eye to potential applications for "PCR in a chip" technology, here we investigate prokaryotic diversity on sediment sampled from one such Mars-like environment, the Rio Tinto Basin in Southwest Spain, which is highly acidic and rich in iron and sulfur. We conclude that development and deployment of this new life detection technique can be informed by a "training set" of phylotypes detected in the Mars-like chemistry of the Rio Tinto, particularly by capitalizing on the benefits of deep sequencing, incorporating multiple primer pairs as allowed by a chip interface, and

sampling over a range of *in situ* micro-niches. Even if life is never found on Mars, the remotely sensed, biological data made possible by these techniques will expand our ability to observe and understand the vast microbial habitats on Earth that are not easy to reach: deserts and glaciers, the deep ocean, and our planet's subsurface.

6.1 Motivation

Following the dawn of the space age, satellite images and other remotely sensed data were generated from projects originally developed for the exploration of space. We reaped countless terrestrial benefits from these extraterrestrial efforts: among them, an array of technologies and techniques that allowed us to acquire data from the most inhospitable environments on Earth. At present, biology is poised for a similar revolution. Thanks to recent innovations in genetic and biosignature analysis, we are coming closer to unlocking the mysteries of some of the most inaccessible parts of the biosphere on our planet. In a fitting counterpoint to our earlier exploration foci, some of these terrestrial efforts focus on environments analogous to those on Mars, thereby contributing to an even more alluring objective: finding life on the Red Planet.

The data from recent NASA missions indicate that Mars is an anaerobic, carbonate-poor, sulfur-rich world, a place that was periodically warm and wet around the same time the first organisms were evolving on Earth [*Knoll, et al.*, 2005]. Many have theorized that the physical similarity of Earth and Mars during this period, in particular the weakly reducing atmosphere, protective magnetic field, and silicate mantle structure, are reasons

to believe that Mars, too, may have hosted life, and that life may have developed in a manner very similar to life on Earth.

Beyond this physical similarity, there is increasing evidence for the plausibility of biological material being transferred between the two planets. In the late 1990's, a series of theoretical studies demonstrated that Martian meteorites were transferred to the Earth at shortened time scales and with higher fluxes than previously believed [*Gladman and Burns*, 1996; *Gladman, et al.*, 1996; *Gladman, et al.*, 1997; *Mileikowsky, et al.*, 2000]. In fact, the final destination of 7.5% of all Martian meteorites is believed to be the Earth, delivering over one billion tons of meteoric debris [*Gladman and Burns*, 1996; *Gladman, et al.*, 1996]. Within this collection, numerous meteorites would have been delivered with interplanetary transit times on time scales of single to thousands of years. Several dozen SNC meteorites of Martian origin have been discovered here on Earth, and magnetic and thermochronological analyses indicate that ~20 wt% of Martian meteorites have only experienced mild heating (<100ºC, below sterilization temperatures) during ejection and impact [*Fritz, et al.*, 2005; *Shuster and Weiss*, 2005; *Weiss, et al.*, 2000]. The concept of lithopanspermia life had evolved on one of the planets, the rate of material transfer makes it plausible that the adjacent planet could "catch" life rather than independently evolving it. Indeed, the probability of the former seems at least as high, if not radically higher, than the probability of the latter.

In addition, microbial life is continually being discovered in Earth environments in exceedingly harsh conditions, demonstrating the surprising adaptability of microbes. Surveys of extreme environments have expanded what we recognize as potential habitable zones; for example, we now know that life can thrive in a range of temperatures from below 0°C to over 110°C, and in such hostile environments as acidic hot springs and highly radioactive nuclear reactor pools, including environments deep in the planet's crust [*Gross*, 1996]. It appears that life has colonized every habitat on Earth where biochemistry can operate, using almost every thermodynamically-favorable energy couple [*Fairen, et al.*, 2005].

Ventures such as the Search for Extra-Terrestrial Genomes (SETG) Project have been funded by NASA to develop life detection instrumentation for use on Mars based on the shared ancestry hypothesis [*Ruvkun, et al.*, 2002]. In searching for DNA and RNA molecules in iron- and sulfur-rich sediments, the SETG instrument is designed to deploy cutting-edge techniques for detecting and analyzing genetic material. These include microfluidic technology that allows DNA to be amplified in the tiny wells of a chip, single molecule sensitivity to detect life in low biomass samples, and serial dilution methods with sequencing-by-synthesis to circumvent the need for traditional cloning.

The Iberian Pyritic Belt in Southwest Spain is home to an iron and sulfur-rich, seasonally dry river, the Rio Tinto. The Rio Tinto has been the subject of multiple Martian analog studies because of its unique mineralogy, sedimentology, and geobiological

characteristics. As such, it provides an ideal context in which to consider the SETG approach and other similar approaches. Here we investigate prokaryotic diversity to gather insights for life detection from the "training set" of phylotypes we detect in the Mars-like chemistry of the Rio Tinto Basin.

6.2 Background

The waters of the Rio Tinto precipitate a diverse suite of iron sulfates and oxides, several of which resemble those found at the landing site of the Opportunity Rover on Mars. The Rio Tinto is home to multiple hydrated ferrous/ferric sulfates, ferrous/ferric hydroyxysulfates, and iron oxides [*Buckby*, 2003; *Roach, et al.,* 2006]. Near its source, ferric-iron enriched sediments are dominated by sulfate and oxihydride parageneses, resulting in goethite and hematite [*Fairen, et al.*, 2005]. Hematite was a major component of the Merdiani Planum site, where the Opportunity rover investigated Late Noachian/Early Hesperian formations. An aqueous hydrothermal origin is proposed for this section, at least seven meters in depth at the Meridiani site and mapped as spreading over the equatorial region of Mars.

Of particular note is the mineral jarosite, a ferric iron sulfate-hydroxide that only forms at extremely low pH (often <2.5) [*Bigham, et al.*, 1996]. The detection of jarosite by the Mars Exploration Rover, along with the recognition of several eolian and evaporite formations, have helped to characterize at least some portions of the early surface

environment as part of a periodically-wet world, one that was iron and sulfur-rich, and surprisingly, one that was subject to ancient acidic weathering.

Highly acidic conditions also dominate the Rio Tinto system; the average pH is only 2.3 [*Amils, et al.*, 2007]. At its headwaters, acid mine drainage mixes with natural sources of acidity. Although this area has been mined for ores for several thousands of years [*Davis*, 2000], there is evidence (in the form of ancient iron oxide terraces, for which isotopic evidence suggests an age of 2-6My [*Amils, et al.*, 2007; *Fernández-Remolar*, 2003; *Moreno*, 2003], and paleosols that predate the Pliocene) that the Rio Tinto system is also driven strongly by natural forces [*Fernandez-Remolar, et al.*, 2005].

Interestingly, the low pH of the Rio Tinto is not a product of the physical environment but rather a consequence of microbial metabolism [*Gonzalez-Toril, et al.*, 2003b]. While part of the acidity results from high evaporation rates, water chemistry is dominated by the biooxidation of pyrite, the most abundant sulfidic mineral in the system, by sulfur- and iron-oxidizing microorganisms via the following overall reaction [*Amils, et al.*, 2007]:

$$4FeS_2 + 14\ H_2O + 15O_2 \rightarrow 4Fe(OH)_3 + 8SO_4^{2-} + 16H^+$$

Meanwhile, the hydrolysis of ferric iron, which remains in solution due to acidic conditions, serves to buffer the nearly constant pH [*Fernandez-Remolar, et al.*, 2005]:

$$Fe^{3+} + 3H_2O \rightarrow Fe(OH)_3 + 3H^+$$

As [*Fernandez-Remolar and Knoll*, 2008] note, there remains an incompletely characterized diversity of acidophilic prokaryotic organisms living within the Rio Tinto system. In the past, the Rio Tinto has been noted for its unusual eukaryotic diversity [*Amaral Zettler, et al*., 2002; *Amaral Zettler*, 2003; *Amils, et al*., 2007; *López-Archilla*, 2001]. Despite the challenging environmental conditions, acidolphilic algae thrive in the Rio Tinto, along with ciliates, cercomonads, vahlkampfiid amoebae, stramenopiles and fungi [*Amaral Zettler, et al*., 2002]. Here we have chosen to focus on the river's simplest organisms, particularly archaea and bacteria that survive on energy from reduced mineral compounds.

6.3 Materials and methods

6.3.1 Sample collection and DNA extraction

Our work focuses on the Northern stretch of the river, where the most acidic conditions exist. Samples were collected in 50 ml Falcon tubes at the Salinas site (coordinates: 37°40'5" N, 6°32'54" W) at the confluence of multiple waterways in the Rio Tinto system (See Figure 6.1). Sampling conditions and DNA extraction were done as described in [*Gonzalez-Toril, et al*., 2006].

6.3.2 DNA amplification, cloning and sequencing

Universal primers 515F, 5'- GTGCCAGCMGCCGCGGTAA -3', and 1391R, 5'-GACGGGCGGTGWGTRCA -3', were chosen to recover maximum prokaryotic

diversity [*Baker, et al.*, 2003]. PCR was performed in 20µl reactions. Additives included: 10.75µl H_2O, 2µl Taq buffer (to 1.5mM $MgCl_2$), 2µl DNTPs (to 0.2mM), 2µl forward primer (to 1µM) (Integrated DNA Technologies), 2µl reverse primer (to 1µM) (Integrated DNA Technologies), 0.25µl Taq polymerase (1 U) (Sigma Aldrich).

Thermal cycling was completed under PCR conditions: 2 min initial denaturing at 95°, followed by 30 cycles of 5 s denaturing at 94°, 40 s annealing at 56°, and 1 min extension at 72°, followed by 10 min final extension at 72°. Products from four different PCR amplifications were pooled and then gel purified using the QIAquick Gel Extraction Kit (Qiagen).

The resulting 900bp PCR products were TOPO cloned (Invitrogen) for ABI sequencing using the Broad Institute's automated sequencing platform.

6.3.3 Phylogenic analysis

Sequences were aligned using ClustalX [*Thompson, et al.*, 1997] and the alignments adjusted by eye. Phylogenetic relationships were estimated using ClustalX, which uses the neighbor-joining algorithm [*Saitou and Nei*, 1987] with the Kimura two-parameter model, and confidence limits were estimated using bootstrap analyses. Phylogenetic trees were visualized using TreeView [*Page*, 1996].

6.4 Results

In sum, 480 clones were sequenced forward and backward, for a total of 960 sequences. Phylotypes include several species of *Acidobacteria, Alphaproteobacteria, Firmicutes, Gammaproteobacteria* (see Figure 6.2, Table 6.1 and Appendix Table 6.1).

6.5 Discussion

Another study of the Rio Tinto has found that the water column is dominated by three bacterial genera: *Leptosprillum* spp. *At. ferrooxidans* and *Acidophilium* spp [*Gonzalez-Toril, et al.*, 2003b]. Quantified by fluorescent *in situ* hybridization (FISH), these three genera alone are reported to represent up to 80% of the measured biomass [*Gonzalez-Toril, et al.*, 2003b]. In our study, we detect all the orders associated with all three genera as well as chloroplast DNA from eukaryotic algae, particularly *Euglena* and *Chlorella*, which survive via oxidative photosynthesis and contribute to primary production in the Rio Tinto System, along with several *Gammaproteobacteria*, including the families *Xanthomondaceae* and *Moraxellaceae*.

Several microhabitats appear to be present in the Northern regions of the river, primarily divided along the lines of the oxic zone and the anoxic zone. *Leptosprillum* spp. and *Ferroplasma* spp., for instance, can grow using ferrous iron as a sole source of energy while *Acidithiobacillus ferrooxidans* obtains energy from both ferrous iron and reduced sulfur compounds (it has been shown to attach preferentially to the less crystallized or

amorphous zones of pyrite substrates, increasing the availability of sulfide ions for bacterial oxidation) [*Amils, et al.*, 2007; *Sanhueza, et al.*, 1999]. Not surprisingly, molecular ecology analysis has shown higher proportions of *Leptospirillum ferrooxidans* (an iron-oxidizing bacterium) in the oxygenic part of the column, and higher proportions of *Acidithiobacillus ferrooxidans* (an iron-oxidizing and iron-reducing bacteria) under anaerobic and microaerobic conditions in the lower part of the column [*Gonzalez-Toril, et al.*, 2003b]. It appears that the combination of redox pathways in the Rio Tinto enable a self-sustaining ecosystem. Of particular importance in this system is iron, acting as a substrate for iron-oxidizing prokaryotes as well as an electron acceptor for anaerobic respiration in anoxic micro-niches [*Gonzalez-Toril, et al.*, 2003a]. In fact, the iron cycle can be completed by the metabolism of only three species, *Leptosprillum* spp., *Acidithiobacillus ferrooxidans,* and *Acidophilium* spp. [*Gonzalez-Toril, et al.*, 2003b].

6.6 Implications for life detection

6.6.1 Deep sequencing with multiple primer pairs

Several of the types of microbes detected in the community surveys only appeared once or twice within the group of 480 sequences, suggesting they may have been missed if fewer sequences had been returned. Among these were *Legionellales* (a *Gammaproteobacterium*), the *Firmicutes Ruminococcus* and *Alicyclobacillus acidocaldarius, Bradyrhizobiales* (an *Alphaproteobacterium*, which can be found in the roots of endemic plants in the Rio Tinto), as well as the *Bacteriodetes Candidatus*

cardinium, and *Acidocella* (an *Alphaproteobacterium*). Unclassified *Moraxellaceae* (a family of *Gammaproteobacteria*), were also detected at low levels. They have never been detected in any other acid mine site and are found deep underground in drilling samples from the Rio Tinto MARTE Project. The detection of *Arcobacteracae* (an *Epsilonproteobacterium*) is also intriguing, as it has never before been detected in any Rio Tinto sampling site.

Others groups were not detected at all. For instance, sulfate-reducing bacteria such as *Desulfosporosinus* are thought to play a role in cycling SO_4^{-2} to S^0/S^{2-} in the Rio Tinto system. Indeed, when three probes specific for sulfate-reducing bacteria were used on Salinas samples from October 1999 and May 2000, positive hybridization signals were detected [*Gonzalez-Toril, et al.*, 2003b]. Nevertheless, sulfate-reducing bacteria were not seen within our group of 480 sequences, suggesting that even deeper sequencing utilizing a wider range of primer pairs in different microhabitats may be necessary.

6.6.2 "PCR in a chip" deep sequencing technology

The "PCR in a chip" technology being developed for SETG enables the type of deep sequencing that may be necessary to fully characterize an environment like the Rio Tinto. The small mass and volume requirements for NASA space instruments require that SETG's detection, classification, and sequencing modules rely on handling small volumes of fluid. SETG is utilizing one of the most powerful microfluidic platforms, involving Multilayer Soft Lithography (MSL) [*Melin and Quake*, 2007; *Ng, et al.*, 2002;

Thorsen, et al., 2002; *Unger, et al.*, 2000; *Xia and Whitesides*, 1998], a technique in which polydimethylsiloxane (PDMS) or glass chips are etched with a number of interconnected microfluidic channels and fluid valves. Valves are then formed by the collapse of one channel by another channel maintained at a higher pressure (Figure 6.3, A-B). A chip capable of amplifying and sequencing DNA, designed by SETG team member Steven Quake, is shown in Figure 6.3 C; a more complex version of this chip, capable of handling hundreds of reactions, will be incorporated into the SETG flight instrument. Chip structures involving thousands of valves have now been manufactured [*Thorsen, et al.*, 2002], and valve density had risen rapidly to exceed 10,000 valves per square cm [*Hong and Quake*, 2003].

This chip density, allowing the analysis of samples from several micro-niches along with deep sequencing, will enable SETG to fully characterize a site like the Rio Tinto. Large amounts of sequence data will aid in analysis, particularly if some amount of contamination cannot be avoided. One of SETG's great advantages in comparison to other life detection techniques, such as seeking informational polymers, structures of biogenic origin, or chemical or isotopic signatures of enzymatic processes, is its definitive nature. While there are abiotic routes to other signatures, sequence information from a Mars system of life isolated from that on Earth over geologic time will be evident. Although rooting the tree of life is complex [*Poole and Willerslev*, 2007], phylogenetic analysis will reveal whether sequences found on Mars are similar to those on Earth and

are likely to represent contamination, or are phylogenetically isolated and indicative of extant Martian life that has been isolated from that on Earth for billions of years.

6.6.3 Future work

The SETG instrument also offers additional intriguing possibilities for investigating life in extreme settings like the Rio Tinto. Given the possibility that, on Mars, the 16S RNA gene may have evolved after the time of heavy meteorite exchange, or it might have diverged so much that, even if life on Mars was DNA or RNA based and ancestrally related to life on Earth, the SETG instrument is capable of finding life that would not be detectable using rRNA primers. However, using a slightly different set of reagents, SETG can also detect ancestrally related life that does not share these or other conserved genes. One standard method for general DNA amplification is isothermal, utilizing the phage ϕ29 DNA polymerase and very short random primers (hexamers of all 4^6 possible combinations). Our collaborators have already demonstrated microfluidic isothermal amplification [*Marcy, et al.*, 2007; *Zhang, et al.*, 2006], and we plan to show that it can be used to amplify and detect nucleic acids in environmental samples with Mars-like chemistry, including sites like the Rio Tinto. In addition, SETG may be able to utilize this capability as a preamplifier to 16S-based amplification, significantly increasing sensitivity. Soon, comparing sequences to our exponentially expanding metagenomic catalog of life will eliminate our current need to focus on highly conserved regions of the genome.

SETG is also being designed to survey for remnants of the RNA world on Mars as well as in terrestrial environments. The existence of an RNA world that predated the current DNA world was revealed by the discovery in 1989 of ribozymes, RNA-based informational molecules that also possess enzymatic activity on RNA [*Mojzsis, et al.*, 1999; *Pace, et al.*, 1999]. Although most of that RNA world has been displaced on Earth, ribozymes are living fossils of the RNA world that continue to exist inside modern DNA-based life. Nevertheless, if the RNA world dominated life on Earth 3.5-4 billion years ago, a time that is commonly inferred to be the beginning of life on Earth, also during which meteoritic bombardment of the inner solar system was much more intense than now, it is plausible that life on Mars diverged from life on Earth during the RNA world, rather than at the later point when DNA had evolved. To explore such a scenario, the SETG team is developing RT-PCR-based protocols to probe *in situ* for RNA-based life in extreme environments on Earth as well as Mars.

6.7 Conclusion

New life detection techniques involve adapting cutting-edge biological automation and miniaturization approaches for a Mars-compatible instrument that can, starting from a soil sample, isolate, amplify, detect, and classify DNA or RNA. Our analysis of genetic diversity in the Rio Tinto suggests these strategies should capitalize on the benefits of deep sequencing, incorporate multiple primer pairs as allowed by a chip interface, and

sample over a range of *in situ* micro-niches. Although instruments like SETG are being designed to attempt to detect life on Mars, the remotely sensed, telemetered technology they embrace can be utilized to ascertain biology's adaptability to hostile conditions - as well as the limits of life - in naturally-occurring extreme environments here on Earth.

6.8 References

Amaral Zettler, L. A., et al. (2002), Microbiology: Eukaryotic diversity in Spain's River of Fire, *Nature*, *417*, 137-137.

Amaral Zettler, L. A., M. A. Messerli, A. D. Laatsch, P. J. S. Smith, and M. L. Sogin (2003), From Genes to Genomes: Beyond Biodiversity in Spain's Rio Tinto *Biological Bulletin*, *204*, 205-209.

Amils, R., et al. (2007), Extreme environments as Mars terrestrial analogs: The Rio Tinto case, *Planetary and Space Science*, *55*, 370-381.

Baker, G. C., et al. (2003), Review and re-analysis of domain-specific 16S primers, *Journal of Microbiological Methods*, *55*, 541-555.

Bigham, J. M., et al. (1996), Schwertmannite and the chemical modeling of iron in acid sulfate waters, *Geochimica et Cosmochimica Acta*, *60*, 2111-2121.

Bourzac, K. (2007), Viewing Bacterial Dark Matter: a microfluidic chip lets researchers identify elusive human-dwelling microbes, *Technology Review*.

Buckby, T., S. Black, M.L. Coleman, and M.E. Hodson (2003), Fe-sulphate-rich evaporative mineral precipitates from the Rio Tinto, southwest Spain, *Mineral. Mag.*, *67*, 263-278.

Davis, R. A., A.T. Welty, J. Borrego, J.A. Morales, J.G. Pendon, and J.G. Ryan (2000), Río Tinto estuary (Spain): 5000 years of pollution, *Environ. Geol.* , *39* 1107–1116.

DeSantis, T. Z., et al. (2006), Greengenes, a Chimera-Checked 16S rRNA Gene Database and Workbench Compatible with ARB, *Appl. Environ. Microbiol.*, *72*, 5069-5072.

Fairen, A. G., et al. (2005), Prime candidate sites for astrobiological exploration through the hydrogeological history of Mars, *Planetary and Space Science*, *53*, 1355-1375.

Fernández-Remolar, D., N. Rodríguez, F. Gómez and R. Amils (2003), The geological record of an acidic environment driven by iron hydrochemistry: the Tinto River system, *J. Geophys. Res.* , *108*

Fernandez-Remolar, D. C., and A. H. Knoll (2008), Fossilization potential of iron-bearing minerals in acidic environments of Rio Tinto, Spain: Implications for Mars exploration, *Icarus*, *194*, 72-85.

Fernandez-Remolar, D. C., et al. (2005), The Rio Tinto Basin, Spain: Mineralogy, sedimentary geobiology, and implications for interpretation of outcrop rocks at Meridiani Planum, Mars, *Earth and Planetary Science Letters*, *240*, 149-167.

Fritz, J. r. g., et al. (2005), Ejection of Martian meteorites, *Meteoritics & Planetary Science*, *40*, 1393-1411.

Gladman, B. J., and J. A. Burns (1996), Mars Meteorite Transfer: Simulation, *Science*, *274*, 161b-165.

Gladman, B. J., et al. (1996), The Exchange of Impact Ejecta Between Terrestrial Planets, *Science*, *271*, 1387-1392.

Gladman, B. J., et al. (1997), Dynamical Lifetimes of Objects Injected into Asteroid Belt Resonances, *Science*, *277*, 197-201.

Gonzalez-Toril, E., et al. (2006), The Isolation and Study of Acidophilic Microorganisms, in *Methods in Microbiology*, edited, pp. 471-510, Academic Press.

Gonzalez-Toril, E., et al. (2003a), Geomicrobiology of the Tinto River, a model of interest for biohydrometallurgy, *Hydrometallurgy*, *71*, 301-309.

Gonzalez-Toril, E., et al. (2003b), Microbial Ecology of an Extreme Acidic Environment, the Tinto River, *Appl. Environ. Microbiol.*, *69*, 4853-4865.

Gross, M. (1996), *Life on the Edge*, Perseus Books, Cambridge.
Hong, J. W., and S. R. Quake (2003), Integrated nanoliter systems, *Nat Biotechnol*, *21*, 1179-1183.

Knoll, A. H., et al. (2005), An astrobiological perspective on Meridiani Planum, *Earth and Planetary Science Letters*, *240*, 179-189.

López-Archilla, A. I., I. Marín, and R. Amils (2001), Microbial community composition and ecology of an acidic aquatic environment: the Tinto River, Spain. , *Microbial Ecology*, *41*, 20–35.

Marcy, Y., et al. (2007), Nanoliter reactors improve multiple displacement amplification of genomes from single cells, *PLoS Genet*, *3*, 1702-1708.

Melin, J., and S. R. Quake (2007), Microfluidic large-scale integration: the evolution of design rules for biological automation, *Annu Rev Biophys Biomol Struct*, *36*, 213-231.

Mileikowsky, C., et al. (2000), Natural Transfer of Viable Microbes in Space: 1. From Mars to Earth and Earth to Mars, *Icarus*, *145*, 391-427.

Mojzsis, S. J., et al. (1999), Before RNA and After: Geophysical and Geochemical Constraints on Molecular Evolution, in *The RNA World, Second Edition*, edited by R. F. Gesteland, et al., pp. 1-48, Cold Spring Harbor Laboratory Press, Cold Spring Harbor, NY.

Moreno, C., M.A. Capitán, M. Doyle, J.M. Nieto, F. Ruiz and R. Sáez (2003), Edad mínima del gozan de Las Cruces: implicaciones sobre la edad de inicio de los ecosistemas extremos en la Faja Pirítica Ibérica, *Geogaceta*, *33*, 75–78.

Ng, J. M., et al. (2002), Components for integrated poly(dimethylsiloxane) microfluidic systems, *Electrophoresis*, *23*, 3461-3473.

Pace, N. R., et al. (1999), Probing RNA Structure, Function, and History by Comparative Analysis, in *The RNA World, Second Edition*, edited by R. F. Gesteland, et al., pp. 113-142, Cold Spring Harbor Laboratory Press, Cold Spring Harbor, New York.

Page, R. D. M. (1996), Tree View: An application to display phylogenetic trees on personal computers, *Comput. Appl. Biosci.*, *12*, 357-358.

Poole, A. M., and E. Willerslev (2007), Can identification of a fourth domain of life be made from sequence data alone, and could it be done on Mars?, *Astrobiology*, *7*, 801-814.

Roach, L. H., et al. (2006), Finding mineralogically interesting targets for exploration from spatially coarse visible and near IR spectra, *Earth and Planetary Science Letters*, *252*, 201-214.

Ruvkun, G., et al. (2002), A Robotic-PCR Detector for DNA-based Life on Other Planets, in *Signs of Life: A Report based on the April 2000 Workshop on Life Detection Techniques*, edited, pp. 137-140, Space Sciences Board, The National Academies Press, Washington, DC.

Saitou, N., and M. Nei (1987), The neighbor-joining method: a new method for reconstructing phylogenetic trees, *Molecular Biology and Evolution*, *4*, 406-425.

Sanhueza, A., et al. (1999), Attachment of Thiobacillus ferrooxidans on synthetic pyrite of varying structural and electronic properties, *Hydrometallurgy*, *51*, 115-129.

Shuster, D. L., and B. P. Weiss (2005), Martian surface paleotemperatures from thermochronology of meteorites, *Science*, *309*, 594-600.

Thompson, J. D., et al. (1997), The CLUSTAL_X windows interface: flexible strategies for multiple sequence alignment aided by quality analysis tools, *Nucl. Acids Res.*, *25*, 4876-4882.

Thorsen, T., et al. (2002), Microfluidic large-scale integration, *Science*, *298*, 580-584.

Tornos, F. (2006), Environment of formation and styles of volcanogenic massive sulfides: The Iberian Pyrite Belt, *Ore Geology Reviews*, *28*, 259-307.

Unger, M. A., et al. (2000), Monolithic microfabricated valves and pumps by multilayer soft lithography, *Science*, *288*, 113-116.

Weiss, B. P., et al. (2000), A Low Temperature Transfer of ALH84001 from Mars to Earth, *Science*, *290*, 791-795.

Xia, Y., and G. M. Whitesides (1998), SOFT LITHOGRAPHY, *Annual Review of Materials Science*, *28*, 153-184.

Zhang, K., et al. (2006), Sequencing genomes from single cells by polymerase cloning, *Nat Biotechnol*, *24*, 680-686.

6.9 Tables

	DIVISION	CLASS	ORDER	FAMILY	GENUS	SPECIES
Archaea	Euryarchaeota	Thermoplasmata	Thermoplasmatales	Ferroplasmaceae	Ferroplasma	
Bacteria	Acidobacteria	Acidobacteria	Acidobacteriales	Acidobacteriaceae	Acidobacterium	
				Unclassified		
				Bacterium Ellin337		
	Bacteroidetes	Bacteroidetes	Unclassified Bacteroidetes	Unclassified Bacteroidetes	Candidatus	cardinium
	Firmicutes	Bacilli	Bacillales	Alicyclobacillaceae	Alicyclobacillus	acidocaldarius
					Sulfobacillus	thermosulfidooxidans
						Mixotrophic Iron-Oxidizing Bacterium
		Clostridia	Clostridia	Clostridiaceae	Clostridium	quinii
			Clostridiales	Lachnospiraceae	Ruminococcus	
				Peptostreptococcaceae	Peptostreptococcus	anaerobius
				Unclassified		
	Nitrospirae	Nitrospira	Nitrospirales	Nitrospiraceae	Leptospirillum	Unclassified
	Planctomycetes					
	Proteobacteria	Alphaproteobacteria	Acetobacterales	Acetobacteraceae	Acidiphilium	
					Acidocella	
					Unclassified	
			Bradyrhizobiales	Methylobacteriaceae		
		Betaproteobacteria	Burkholderiales	Comamonadaceae	Variovorax	
					Unclassified	
		Deltaproteobacteria	Envir. Samples: BA18			
		Epsilonproteobacteria		Arcobacteraceae	Unclassified	
		Gammaproteobacteria	Acidithiobacillales	Acidithiobacillaceae	Acidithiobacillus	
			Envir. Samples: B2M28			
			Envir. Samples: CCD24	Envir. Samples: Ellin339	Envir. Samples: RCP1-57	
					Unclassified	
			Legionellales	Legionellaceae	Legionella	
				Unclassified		
			Pseudomonadales	Moraxellaceae		
			Unclassified Xanthomonadales			
Eukaryota (Chloroplasts)	*Viridiplantae*	*Chlorophyta*	*-*	*Chlorophyceae*	*Chlorella*	
	-	*Euglenida*	*Euglenales*	*-*	*Euglena*	*stellata*
						Unclassified
	Unclassified					

Table 6.1 Organisms detected at the Salinas site.

6.10 Figures

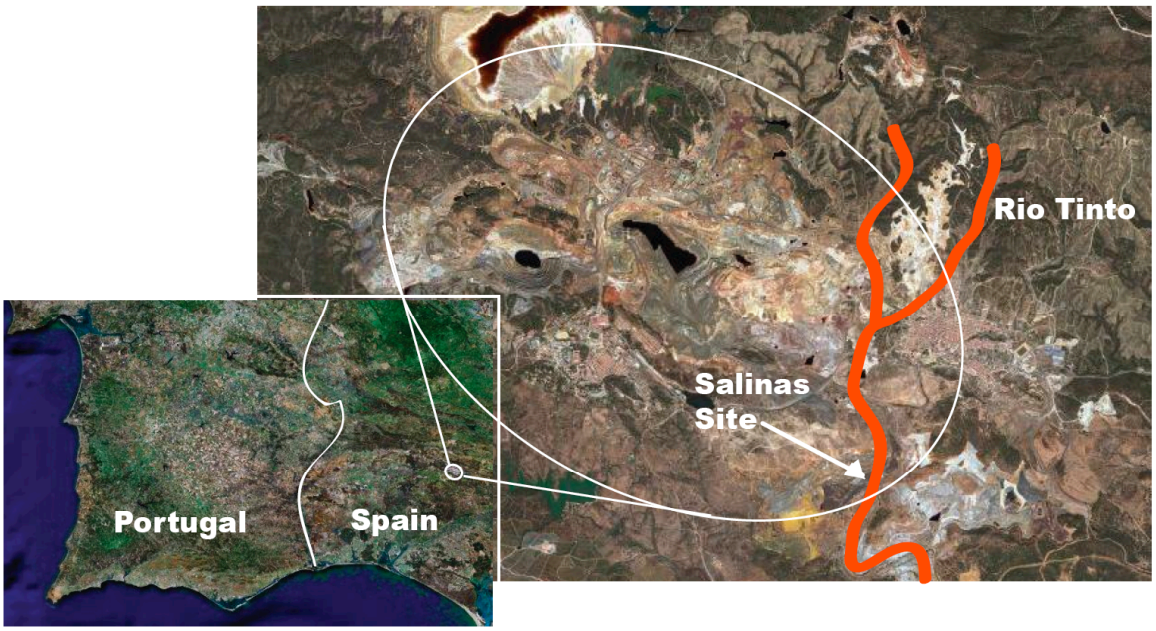

Figure 6.1 The Rio Tinto is located in the Iberian Pyrite Belt, a 250km long geologic structure emplaced by Late Paleozoic hydrothermal activity [*Fernandez-Remolar and Knoll*, 2008; *Tornos*, 2006], in Southwestern Spain.

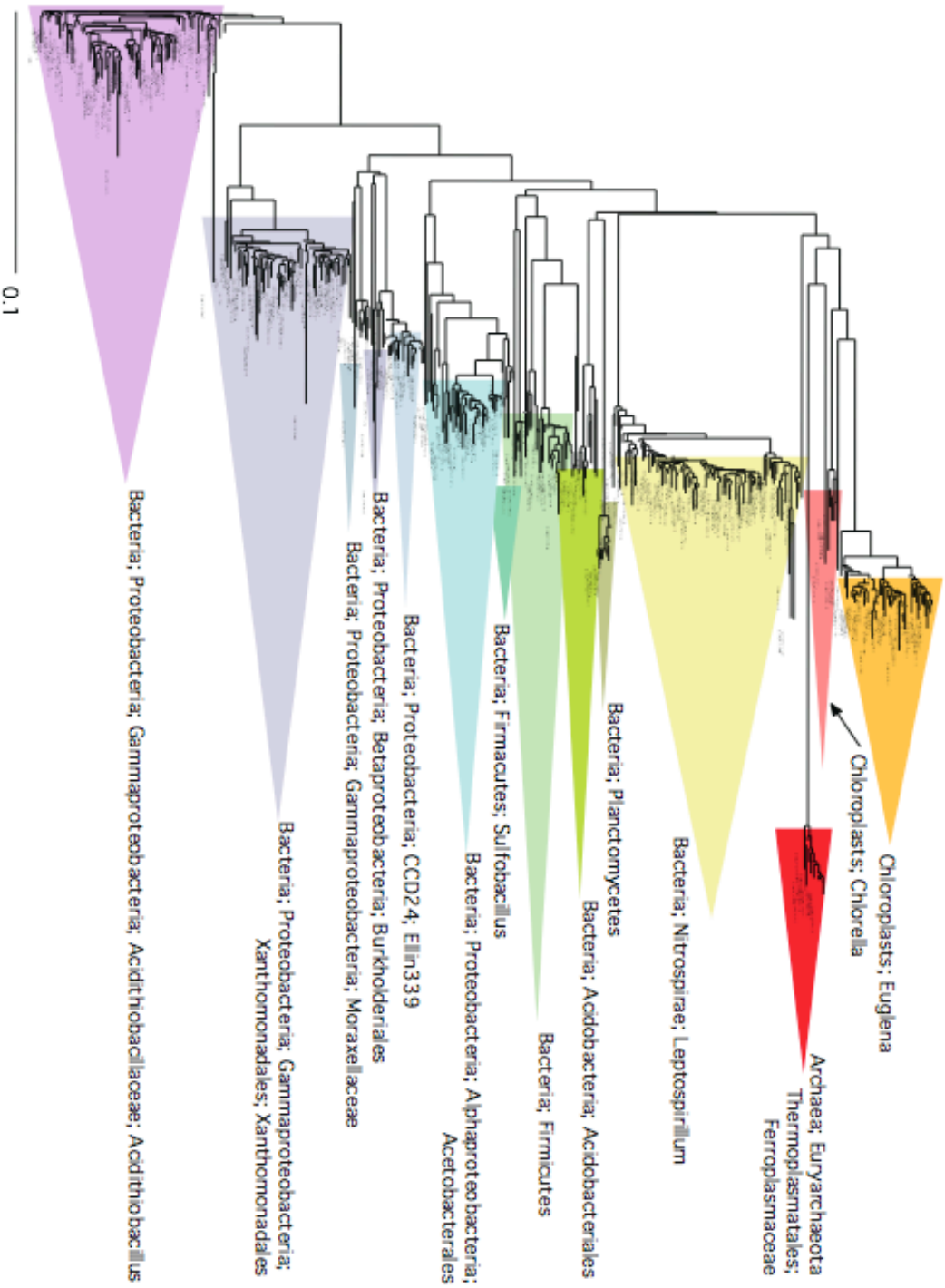

Figure 6.2 Phylogenic Tree showing prokaryotic diversity in the Rio Tinto. The scale bar denotes the number of nucleotide substitutions.

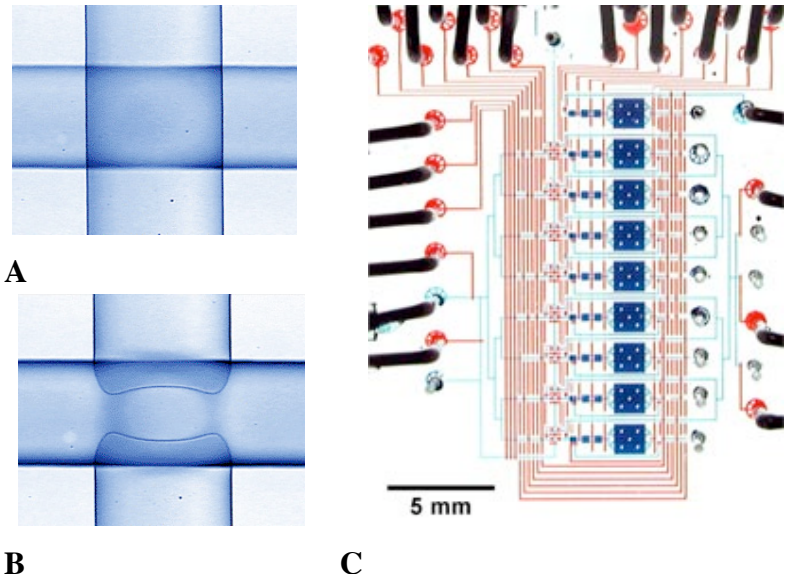

Figure 6.3 A. When the pressure in the horizontal control line is low, fluid can flow freely through the vertical sample line (Fludigm Corporation). **B.** Raising the control line pressure causes a deformation into the vertical sample line, creating a closed valve. **C.** New life detection techniques will employ microfluidic chips, such as the one shown here, to amplify the genome of single bacterial cells for sequencing (the channels and control lines on this chip are shown in blue and red, respectively [*Bourzac*, 2007]).

6.10 Appendix

Sequence	Hugenholtz Taxonomic String
D392P31FA10:	Bacteria; Cyanobacteria; Chloroplasts; Euglena; Unclassified; otu_763
D392P31FA11:	Bacteria; Firmicutes; Clostridia; Peptostreptococcaceae; Peptostreptococcus_anaerobius; Clostridium_bifermentans; AKIW475; otu_1214
D392P31FA12:	Bacteria; Proteobacteria; Alphaproteobacteria; Bradyrhizobiales; Methylobacteriaceae; otu_1587
D392P31FA13:	Archaea; Thermoplasmata_Eury; Thermoplasmatales; Thermoplasmatales; Ferroplasmaceae; Ferroplasma; otu_118
D392P31FA14:	Archaea; Thermoplasmata_Eury; Thermoplasmatales; Thermoplasmatales; Ferroplasmaceae; Ferroplasma; otu_118
D392P31FA15:	Bacteria; Proteobacteria; Gammaproteobacteria; Acidithiobacillaceae; Acidithiobacillus; otu_1857
D392P31FA16:	Bacteria; Nitrospirae; Leptospirillaceae; Leptospirillum; Unclassified; otu_1427
D392P31FA17:	Bacteria; Proteobacteria; Gammaproteobacteria; Acidithiobacillaceae; Acidithiobacillus; otu_1857
D392P31FA18:	Bacteria; Proteobacteria; Gammaproteobacteria; Acidithiobacillaceae; Acidithiobacillus; otu_1857
D392P31FA19:	Bacteria; Proteobacteria; Alphaproteobacteria; Acetobacterales; Acetobacteraceae; Acidiphilium; otu_1560
D392P31FA20:	Archaea; Thermoplasmata_Eury; Thermoplasmatales; Thermoplasmatales; Ferroplasmaceae; Ferroplasma; otu_118
D392P31FA21:	Bacteria; Proteobacteria; Gammaproteobacteria; Acidithiobacillaceae; Acidithiobacillus; otu_1857
D392P31FA22:	Bacteria; Proteobacteria; Gammaproteobacteria; Xanthomonadales; Xanthomonadales; gamma_proteobacterium_WJ2; otu_2136
D392P31FA23:	Bacteria; Acidobacteria; Acidobacteriales; Unclassified; otu_179
D392P31FA24:	Bacteria; Proteobacteria; Gammaproteobacteria; Xanthomonadales; Xanthomonadales; gamma_proteobacterium_WJ2; otu_2136
D392P31FA2:	Bacteria; Nitrospirae; Leptospirillaceae; Leptospirillum; Unclassified; otu_1427
D392P31FA3:	Bacteria; Nitrospirae; Leptospirillaceae; Leptospirillum; Unclassified; otu_1427
D392P31FA4:	Bacteria; Proteobacteria; Alphaproteobacteria; Acetobacterales; Acetobacteraceae; Unclassified; otu_1559
D392P31FA5:	Bacteria; Proteobacteria; Gammaproteobacteria; Acidithiobacillaceae; Acidithiobacillus; otu_1857
D392P31FA6:	Bacteria; Proteobacteria; Gammaproteobacteria; Acidithiobacillaceae; Acidithiobacillus; otu_1857
D392P31FA7:	Bacteria; Nitrospirae; Leptospirillaceae; Leptospirillum; Unclassified; otu_1427
D392P31FA8:	Bacteria; Firmicutes; Clostridia; Clostridiales; Unclassified; otu_1006
D392P31FA9:	Bacteria; Nitrospirae; Leptospirillaceae; Leptospirillum; Unclassified; otu_1427
D392P31FB10:	Bacteria; Proteobacteria; Gammaproteobacteria; Acidithiobacillaceae; Acidithiobacillus; otu_1857
D392P31FB11:	Bacteria; Nitrospirae; Leptospirillaceae; Leptospirillum; Unclassified; otu_1427
D392P31FB12:	Bacteria; Proteobacteria; Alphaproteobacteria; Acetobacterales; Acetobacteraceae; Acidiphilium; otu_1560
D392P31FB13:	Bacteria; Nitrospirae; Leptospirillaceae; Leptospirillum; Unclassified; otu_1427
D392P31FB14:	Bacteria; Nitrospirae; Leptospirillaceae; Leptospirillum; Unclassified; otu_1427
D392P31FB15:	Bacteria; Proteobacteria; Gammaproteobacteria; Acidithiobacillaceae; Acidithiobacillus; otu_1857
D392P31FB17:	Bacteria; Nitrospirae; Leptospirillaceae; Leptospirillum; Unclassified; otu_1427
D392P31FB18:	Bacteria; Proteobacteria; Gammaproteobacteria; CCD24; Ellin339; RCP1-57; otu_1973
D392P31FB19:	Bacteria; Nitrospirae; Leptospirillaceae; Leptospirillum; Unclassified; otu_1427
D392P31FB1:	Bacteria; Firmicutes; Clostridia; Peptostreptococcaceae; Peptostreptococcus_anaerobius; Clostridium_bifermentans; Unclassified; otu_1213
D392P31FB20:	Archaea; Thermoplasmata_Eury; Thermoplasmatales; Thermoplasmatales; Ferroplasmaceae; Ferroplasma; otu_118
D392P31FB21:	Bacteria; Proteobacteria; Gammaproteobacteria; Acidithiobacillaceae; Acidithiobacillus; otu_1857
D392P31FB22:	Bacteria; Firmicutes; Clostridia; Peptostreptococcaceae; Peptostreptococcus_anaerobius; Clostridium_bifermentans; Unclassified; otu_1213
D392P31FB24:	Bacteria; Proteobacteria; Gammaproteobacteria; Xanthomonadales; Xanthomonadales; gamma_proteobacterium_WJ2; otu_2136
D392P31FB2:	Bacteria; Firmicutes; Clostridia; Peptostreptococcaceae; Peptostreptococcus_anaerobius; Clostridium_bifermentans; Unclassified; otu_1213
D392P31FB4:	Bacteria; Nitrospirae; Leptospirillaceae; Leptospirillum; Unclassified; otu_1427
D392P31FB5:	Bacteria; Nitrospirae; Leptospirillaceae; Leptospirillum; Unclassified; otu_1427
D392P31FB9:	Bacteria; Proteobacteria; Gammaproteobacteria; Xanthomonadales; Xanthomonadales; gamma_proteobacterium_WJ2; otu_2136
D392P31FC11:	Bacteria; Nitrospirae; Leptospirillaceae; Leptospirillum; Unclassified; otu_1427
D392P31FC12:	Bacteria; Proteobacteria; Gammaproteobacteria; Betaproteobacteria; Burkholderiales; Unclassified; otu_1890
D392P31FC13:	Bacteria; Cyanobacteria; Chloroplasts; Euglena; Unclassified; otu_763
D392P31FC15:	Bacteria; Proteobacteria; Gammaproteobacteria; CCD24; Ellin339; RCP1-57; otu_1973
D392P31FC16:	Bacteria; Proteobacteria; Epsilonproteobacteria; Arcobacteraceae; Unclassified; otu_1823
D392P31FC17:	Bacteria; Cyanobacteria; Chloroplasts; Euglena; Unclassified; otu_763
D392P31FC18:	Bacteria; Firmicutes; Alicyclobacillaceae; Alicyclobacillus; mixotrophic_iron-oxidizing_bacterium; otu_858
D392P31FC19:	Bacteria; Firmicutes; Clostridia; Peptostreptococcaceae; Peptostreptococcus_anaerobius; Clostridium_bifermentans; Unclassified; otu_1213
D392P31FC1:	Bacteria; Firmicutes; Clostridia; Clostridiaceae; Clostridium; Clostridium_quinii; otu_990
D392P31FC20:	Bacteria; Proteobacteria; Gammaproteobacteria; Legionellales; Legionella; otu_2021
D392P31FC21:	Bacteria; Nitrospirae; Leptospirillaceae; Leptospirillum; Unclassified; otu_1427
D392P31FC22:	Bacteria; Cyanobacteria; Chloroplasts; Euglena; Unclassified; otu_763
D392P31FC23:	Bacteria; Cyanobacteria; Chloroplasts; Unclassified; otu_755
D392P31FC24:	Bacteria; Planctomycetes; WPS-1; CL500-3; CL120-56; DE613; otu_1549
D392P31FC2:	Bacteria; Nitrospirae; Leptospirillaceae; Leptospirillum; Unclassified; otu_1427
D392P31FC3:	Bacteria; Cyanobacteria; Chloroplasts; Euglena; Unclassified; otu_763
D392P31FC4:	Bacteria; Proteobacteria; Gammaproteobacteria; Xanthomonadales; Xanthomonadales; gamma_proteobacterium_WJ2; otu_2136
D392P31FC5:	Bacteria; Nitrospirae; Leptospirillaceae; Leptospirillum; Unclassified; otu_1427
D392P31FC6:	Bacteria; Proteobacteria; Gammaproteobacteria; Acidithiobacillaceae; Acidithiobacillus; otu_1857
D392P31FC7:	Bacteria; Proteobacteria; Gammaproteobacteria; Acidithiobacillaceae; Acidithiobacillus; otu_1857
D392P31FC8:	Bacteria; Proteobacteria; Alphaproteobacteria; Acetobacterales; Acetobacteraceae; Acidiphilium; otu_1560
D392P31FC9:	Bacteria; Proteobacteria; Gammaproteobacteria; Acidithiobacillaceae; Acidithiobacillus; otu_1857
D392P31FD10:	Bacteria; Proteobacteria; Alphaproteobacteria; Acetobacterales; Acetobacteraceae; Acidiphilium; otu_1560
D392P31FD11:	Bacteria; Proteobacteria; Gammaproteobacteria; Acidithiobacillaceae; Acidithiobacillus; otu_1857
D392P31FD13:	Bacteria; Cyanobacteria; Chloroplasts; Euglena; Unclassified; otu_763
D392P31FD14:	Bacteria; Proteobacteria; Gammaproteobacteria; Acidithiobacillaceae; Acidithiobacillus; otu_1857
D392P31FD15:	Bacteria; Nitrospirae; Leptospirillaceae; Leptospirillum; Unclassified; otu_1427
D392P31FD16:	Bacteria; Proteobacteria; Alphaproteobacteria; Acetobacterales; Acetobacteraceae; Acidiphilium; otu_1560
D392P31FD19:	Bacteria; Proteobacteria; Alphaproteobacteria; Acetobacterales; Acetobacteraceae; Acidiphilium; otu_1560
D392P31FD1:	Bacteria; Proteobacteria; Gammaproteobacteria; Acidithiobacillaceae; Acidithiobacillus; otu_1857

Sequence	Hugenholtz Taxonomic String
D392P31FD20:	Bacteria; Nitrospirae; Leptospirillaceae; Leptospirillum; Unclassified; otu_1427
D392P31FD21:	Bacteria; Cyanobacteria; Chloroplasts; Unclassified; otu_755
D392P31FD22:	Bacteria; Proteobacteria; Gammaproteobacteria; Acidithiobacillaceae; Acidithiobacillus; otu_1857
D392P31FD23:	Bacteria; Nitrospirae; Leptospirillaceae; Leptospirillum; Unclassified; otu_1427
D392P31FD2:	Bacteria; Proteobacteria; Alphaproteobacteria; Acetobacterales; Acetobacteraceae; Acidocella; otu_1562
D392P31FD3:	Bacteria; Proteobacteria; Gammaproteobacteria; Acidithiobacillaceae; Acidithiobacillus; otu_1857
D392P31FD4:	Bacteria; Cyanobacteria; Chloroplasts; Euglena; Unclassified; otu_763
D392P31FD5:	Bacteria; Cyanobacteria; Chloroplasts; Unclassified; otu_755
D392P31FD6:	Bacteria; Nitrospirae; Leptospirillaceae; Leptospirillum; Unclassified; otu_1427
D392P31FD8:	Bacteria; Proteobacteria; Gammaproteobacteria; Acidithiobacillaceae; Acidithiobacillus; otu_1857
D392P31FD9:	Bacteria; Nitrospirae; Leptospirillaceae; Leptospirillum; Unclassified; otu_1427
D392P31FE10:	Bacteria; Proteobacteria; Gammaproteobacteria; Xanthomonadales; Xanthomonadales; gamma_proteobacterium_WJ2; otu_2136
D392P31FE11:	Bacteria; Proteobacteria; Gammaproteobacteria; Acidithiobacillaceae; Acidithiobacillus; otu_1857
D392P31FE12:	Bacteria; Proteobacteria; Gammaproteobacteria; Xanthomonadales; Xanthomonadales; gamma_proteobacterium_WJ2; otu_2136
D392P31FE13:	Bacteria; Proteobacteria; Alphaproteobacteria; Acetobacterales; Acetobacteraceae; Acidiphilium; otu_1560
D392P31FE14:	Bacteria; Proteobacteria; Gammaproteobacteria; Acidithiobacillaceae; Acidithiobacillus; otu_1857
D392P31FE15:	Bacteria; Nitrospirae; Leptospirillaceae; Leptospirillum; Unclassified; otu_1427
D392P31FE16:	Bacteria; Nitrospirae; Leptospirillaceae; Leptospirillum; Unclassified; otu_1427
D392P31FE17:	Bacteria; Nitrospirae; Leptospirillaceae; Leptospirillum; Unclassified; otu_1427
D392P31FE18:	Bacteria; Firmicutes; Clostridia; Clostridiaceae; Clostridium; Clostridium_quinii; otu_990
D392P31FE19:	Bacteria; Nitrospirae; Leptospirillaceae; Leptospirillum; Unclassified; otu_1427
D392P31FE1:	Bacteria; Proteobacteria; Gammaproteobacteria; CCD24; Ellin339; RCP1-57; otu_1973
D392P31FE20:	Bacteria; Proteobacteria; Gammaproteobacteria; Acidithiobacillaceae; Acidithiobacillus; otu_1857
D392P31FE21:	Bacteria; Nitrospirae; Leptospirillaceae; Leptospirillum; Unclassified; otu_1427
D392P31FE22:	Bacteria; Proteobacteria; Gammaproteobacteria; Acidithiobacillaceae; Acidithiobacillus; otu_1857
D392P31FE23:	Bacteria; Proteobacteria; Gammaproteobacteria; CCD24; Ellin339; RCP1-57; otu_1973
D392P31FE24:	Bacteria; Proteobacteria; Gammaproteobacteria; Xanthomonadales; Xanthomonadales; gamma_proteobacterium_WJ2; otu_2136
D392P31FE2:	Bacteria; Proteobacteria; Gammaproteobacteria; Acidithiobacillaceae; Acidithiobacillus; otu_1857
D392P31FE3:	Bacteria; Firmicutes; Clostridia; Peptostreptococcaceae; Peptostreptococcus_anaerobius; Clostridium_bifermentans; Unclassified; otu_1213
D392P31FE4:	Bacteria; Proteobacteria; Gammaproteobacteria; Xanthomonadales; Xanthomonadales; gamma_proteobacterium_WJ2; otu_2136
D392P31FE5:	Bacteria; Firmicutes; Alicyclobacillaceae; Alicyclobacillus; mixotrophic iron-oxidizing bacterium; otu_858
D392P31FE6:	Bacteria; Proteobacteria; Alphaproteobacteria; Acetobacterales; Acetobacteraceae; Unclassified; otu_1559
D392P31FE7:	Bacteria; Nitrospirae; Leptospirillaceae; Leptospirillum; Unclassified; otu_1427
D392P31FE8:	Bacteria; Nitrospirae; Leptospirillaceae; Leptospirillum; Unclassified; otu_1427
D392P31FF10:	Bacteria; Nitrospirae; Leptospirillaceae; Leptospirillum; Unclassified; otu_1427
D392P31FF11:	Bacteria; Cyanobacteria; Chloroplasts; Euglena; Unclassified; otu_763
D392P31FF12:	Bacteria; Cyanobacteria; Chloroplasts; Chlorella; otu_757
D392P31FF14:	Bacteria; Proteobacteria; Gammaproteobacteria; Xanthomonadales; Xanthomonadales; gamma_proteobacterium_WJ2; otu_2136
D392P31FF15:	Bacteria; Nitrospirae; Leptospirillaceae; Leptospirillum; Unclassified; otu_1427
D392P31FF16:	Bacteria; Proteobacteria; Gammaproteobacteria; B2M28; otu_1880
D392P31FF17:	Bacteria; Proteobacteria; Gammaproteobacteria; Xanthomonadales; Xanthomonadales; gamma_proteobacterium_WJ2; otu_2136
D392P31FF18:	Bacteria; Proteobacteria; Gammaproteobacteria; CCD24; Ellin339; RCP1-57; otu_1973
D392P31FF19:	Bacteria; Firmicutes; Clostridia; Peptostreptococcaceae; Peptostreptococcus_anaerobius; Clostridium_bifermentans; Unclassified; otu_1213
D392P31FF1:	Bacteria; Proteobacteria; Gammaproteobacteria; CCD24; Ellin339; RCP1-57; otu_1973
D392P31FF20:	Bacteria; Proteobacteria; Gammaproteobacteria; Acidithiobacillaceae; Acidithiobacillus; otu_1857
D392P31FF23:	Bacteria; Proteobacteria; Alphaproteobacteria; Acetobacterales; Acetobacteraceae; Unclassified; otu_1559
D392P31FF24:	Bacteria; Cyanobacteria; Chloroplasts; Euglena; Unclassified; otu_763
D392P31FF2:	Bacteria; Planctomycetes; WPS-1; CL500-3; CL120-56; DE613; otu_1549
D392P31FF4:	Bacteria; Cyanobacteria; Chloroplasts; Euglena; Unclassified; otu_763
D392P31FF5:	Bacteria; Proteobacteria; Alphaproteobacteria; Acetobacterales; Acetobacteraceae; Acidiphilium; otu_1560
D392P31FF6:	Bacteria; Nitrospirae; Leptospirillaceae; Leptospirillum; Unclassified; otu_1427
D392P31FF7:	Bacteria; Cyanobacteria; Chloroplasts; Unclassified; otu_755
D392P31FF8:	Bacteria; Proteobacteria; Alphaproteobacteria; Acetobacterales; Acetobacteraceae; Unclassified; otu_1559
D392P31FF9:	Bacteria; Proteobacteria; Gammaproteobacteria; Xanthomonadales; Xanthomonadales; gamma_proteobacterium_WJ2; otu_2136
D392P31FG10:	Archaea; Thermoplasmata_Eury; Thermoplasmatales; Thermoplasmatales; Ferroplasmaceae; Ferroplasma; otu_118
D392P31FG12:	Bacteria; Nitrospirae; Leptospirillaceae; Leptospirillum; Unclassified; otu_1427
D392P31FG13:	Bacteria; Firmicutes; Clostridia; Peptostreptococcaceae; Peptostreptococcus_anaerobius; Clostridium_bifermentans; Unclassified; otu_1213
D392P31FG14:	Bacteria; Proteobacteria; Gammaproteobacteria; Acidithiobacillaceae; Acidithiobacillus; otu_1857
D392P31FG15:	Bacteria; Proteobacteria; Gammaproteobacteria; Acidithiobacillaceae; Acidithiobacillus; otu_1857
D392P31FG16:	Bacteria; Proteobacteria; Gammaproteobacteria; Acidithiobacillaceae; Acidithiobacillus; otu_1857
D392P31FG17:	Bacteria; Firmicutes; Clostridia; Peptostreptococcaceae; Peptostreptococcus_anaerobius; Clostridium_bifermentans; Unclassified; otu_1213
D392P31FG18:	Bacteria; Proteobacteria; Gammaproteobacteria; Xanthomonadales; Xanthomonadales; gamma_proteobacterium_WJ2; otu_2136
D392P31FG19:	Bacteria; Proteobacteria; Gammaproteobacteria; CCD24; Ellin339; RCP1-57; otu_1973
D392P31FG1:	Bacteria; Proteobacteria; Gammaproteobacteria; Acidithiobacillaceae; Acidithiobacillus; otu_1857
D392P31FG20:	Bacteria; Proteobacteria; Gammaproteobacteria; Xanthomonadales; Xanthomonadales; gamma_proteobacterium_WJ2; otu_2136
D392P31FG21:	Bacteria; Proteobacteria; Gammaproteobacteria; Xanthomonadales; Xanthomonadales; gamma_proteobacterium_WJ2; otu_2136
D392P31FG22:	Bacteria; Proteobacteria; Alphaproteobacteria; Acetobacterales; Acetobacteraceae; Unclassified; otu_1559
D392P31FG23:	Bacteria; Proteobacteria; Alphaproteobacteria; Acetobacterales; Acetobacteraceae; Unclassified; otu_1559
D392P31FG24:	Bacteria; Nitrospirae; Leptospirillaceae; Leptospirillum; Unclassified; otu_1427
D392P31FG2:	Bacteria; Proteobacteria; Alphaproteobacteria; Acetobacterales; Acetobacteraceae; Unclassified; otu_1559
D392P31FG3:	Bacteria; Proteobacteria; Gammaproteobacteria; Xanthomonadales; Xanthomonadales; gamma_proteobacterium_WJ2; otu_2136
D392P31FG4:	Bacteria; Firmicutes; Clostridia; Peptostreptococcaceae; Peptostreptococcus_anaerobius; Clostridium_bifermentans; Unclassified; otu_1213
D392P31FG5:	Bacteria; Firmicutes; Clostridia; Peptostreptococcaceae; Peptostreptococcus_anaerobius; Clostridium_bifermentans; Unclassified; otu_1213
D392P31FG6:	Bacteria; Cyanobacteria; Chloroplasts; Unclassified; otu_755
D392P31FG7:	Bacteria; Nitrospirae; Leptospirillaceae; Leptospirillum; Unclassified; otu_1427
D392P31FG8:	Bacteria; Proteobacteria; Gammaproteobacteria; CCD24; Ellin339; RCP1-57; otu_1973
D392P31FG9:	Bacteria; Proteobacteria; Gammaproteobacteria; Acidithiobacillaceae; Acidithiobacillus; otu_1857

Sequence	Hugenholtz Taxonomic String
D392P31FH10:	Bacteria; Proteobacteria; Gammaproteobacteria; Acidithiobacillaceae; Acidithiobacillus; otu_1857
D392P31FH13:	Bacteria; Proteobacteria; Gammaproteobacteria; Xanthomonadales; Xanthomonadales; gamma_proteobacterium_WJ2; otu_2136
D392P31FH14:	Bacteria; Proteobacteria; Gammaproteobacteria; Acidithiobacillaceae; Acidithiobacillus; otu_1857
D392P31FH15:	Bacteria; Proteobacteria; Gammaproteobacteria; Acidithiobacillaceae; Acidithiobacillus; otu_1857
D392P31FH16:	Bacteria; Proteobacteria; Gammaproteobacteria; Xanthomonadales; Xanthomonadales; gamma_proteobacterium_WJ2; otu_2136
D392P31FH17:	Bacteria; Nitrospirae; Leptospirillaceae; Leptospirillum; Unclassified; otu_1427
D392P31FH18:	Bacteria; Nitrospirae; Leptospirillaceae; Leptospirillum; Unclassified; otu_1427
D392P31FH19:	Bacteria; Cyanobacteria; Chloroplasts; Euglena; Unclassified; otu_763
D392P31FH20:	Bacteria; Nitrospirae; Leptospirillaceae; Leptospirillum; Unclassified; otu_1427
D392P31FH23:	Bacteria; Acidobacteria; Acidobacteriales; Acidobacterium; otu_180
D392P31FH24:	Bacteria; Proteobacteria; Gammaproteobacteria; Xanthomonadales; Xanthomonadales; gamma_proteobacterium_WJ2; otu_2136
D392P31FH2:	Bacteria; Nitrospirae; Leptospirillaceae; Leptospirillum; Unclassified; otu_1427
D392P31FH3:	Bacteria; Nitrospirae; Leptospirillaceae; Leptospirillum; Unclassified; otu_1427
D392P31FH4:	Bacteria; Proteobacteria; Gammaproteobacteria; Acidithiobacillaceae; Acidithiobacillus; otu_1857
D392P31FH5:	Bacteria; Proteobacteria; Alphaproteobacteria; Acetobacterales; Acetobacteraceae; Acidiphilium; otu_1560
D392P31FH6:	Bacteria; Cyanobacteria; Chloroplasts; Euglena; Unclassified; otu_763
D392P31FH7:	Bacteria; Proteobacteria; Gammaproteobacteria; Xanthomonadales; Xanthomonadales; gamma_proteobacterium_WJ2; otu_2136
D392P31FH8:	Bacteria; Proteobacteria; Gammaproteobacteria; Acidithiobacillaceae; Acidithiobacillus; otu_1857
D392P31RA10:	Bacteria; Cyanobacteria; Chloroplasts; Unclassified; otu_755
D392P31RA11:	Bacteria; Firmicutes; Clostridia; Peptostreptococcaceae; Peptostreptococcus_anaerobius; Clostridium_bifermentans; Unclassified; otu_1213
D392P31RA12:	Bacteria; Proteobacteria; Alphaproteobacteria; Bradyrhizobiales; Methylobacteriaceae; otu_1587
D392P31RA13:	Archaea; Thermoplasmata_Eury; Thermoplasmatales; Thermoplasmatales; Ferroplasmaceae; Ferroplasma; otu_118
D392P31RA14:	Archaea; Thermoplasmata_Eury; Thermoplasmatales; Thermoplasmatales; Ferroplasmaceae; Ferroplasma; otu_118
D392P31RA15:	Bacteria; Proteobacteria; Gammaproteobacteria; Acidithiobacillaceae; Acidithiobacillus; otu_1857
D392P31RA16:	Bacteria; Nitrospirae; Leptospirillaceae; Leptospirillum; Unclassified; otu_1427
D392P31RA17:	Bacteria; Proteobacteria; Gammaproteobacteria; Acidithiobacillaceae; Acidithiobacillus; otu_1857
D392P31RA18:	Bacteria; Proteobacteria; Gammaproteobacteria; Acidithiobacillaceae; Acidithiobacillus; otu_1857
D392P31RA19:	Bacteria; Proteobacteria; Alphaproteobacteria; Acetobacterales; Acetobacteraceae; Acidiphilium; otu_1560
D392P31RA20:	Archaea; Thermoplasmata_Eury; Thermoplasmatales; Thermoplasmatales; Ferroplasmaceae; Ferroplasma; otu_118
D392P31RA21:	Bacteria; Proteobacteria; Gammaproteobacteria; Acidithiobacillaceae; Acidithiobacillus; otu_1857
D392P31RA22:	Bacteria; Proteobacteria; Gammaproteobacteria; Xanthomonadales; Xanthomonadales; gamma_proteobacterium_WJ2; otu_2136
D392P31RA23:	Bacteria; Acidobacteria; Acidobacteriales; Unclassified; otu_179
D392P31RA24:	Bacteria; Proteobacteria; Gammaproteobacteria; Xanthomonadales; Xanthomonadales; gamma_proteobacterium_WJ2; otu_2136
D392P31RA2:	Bacteria; Nitrospirae; Leptospirillaceae; Leptospirillum; Unclassified; otu_1427
D392P31RA3:	Bacteria; Nitrospirae; Leptospirillaceae; Leptospirillum; Unclassified; otu_1427
D392P31RA4:	Bacteria; Proteobacteria; Alphaproteobacteria; Acetobacterales; Acetobacteraceae; Unclassified; otu_1559
D392P31RA5:	Bacteria; Proteobacteria; Gammaproteobacteria; Acidithiobacillaceae; Acidithiobacillus; otu_1857
D392P31RA6:	Bacteria; Proteobacteria; Gammaproteobacteria; Acidithiobacillaceae; Acidithiobacillus; otu_1857
D392P31RA7:	Bacteria; Nitrospirae; Leptospirillaceae; Leptospirillum; Unclassified; otu_1427
D392P31RA8:	Bacteria; Firmicutes; Clostridia; Clostridiales; Unclassified; otu_1006
D392P31RA9:	Bacteria; Nitrospirae; Leptospirillaceae; Leptospirillum; Unclassified; otu_1427
D392P31RB10:	Bacteria; Proteobacteria; Gammaproteobacteria; Acidithiobacillaceae; Acidithiobacillus; otu_1857
D392P31RB11:	Bacteria; Nitrospirae; Leptospirillaceae; Leptospirillum; Unclassified; otu_1427
D392P31RB12:	Bacteria; Proteobacteria; Alphaproteobacteria; Acetobacterales; Acetobacteraceae; Acidiphilium; otu_1560
D392P31RB13:	Bacteria; Nitrospirae; Leptospirillaceae; Leptospirillum; Unclassified; otu_1427
D392P31RB14:	Bacteria; Nitrospirae; Leptospirillaceae; Leptospirillum; Unclassified; otu_1427
D392P31RB15:	Bacteria; Proteobacteria; Gammaproteobacteria; Acidithiobacillaceae; Acidithiobacillus; otu_1857
D392P31RB17:	Bacteria; Nitrospirae; Leptospirillaceae; Leptospirillum; Unclassified; otu_1427
D392P31RB18:	Bacteria; Proteobacteria; Gammaproteobacteria; CCD24; Ellin339; RCP1-57; otu_1973
D392P31RB19:	Bacteria; Nitrospirae; Leptospirillaceae; Leptospirillum; Unclassified; otu_1427
D392P31RB1:	Bacteria; Firmicutes; Clostridia; Peptostreptococcaceae; Peptostreptococcus_anaerobius; Clostridium_bifermentans; Unclassified; otu_1213
D392P31RB20:	Archaea; Thermoplasmata_Eury; Thermoplasmatales; Thermoplasmatales; Ferroplasmaceae; Ferroplasma; otu_118
D392P31RB21:	Bacteria; Proteobacteria; Gammaproteobacteria; Acidithiobacillaceae; Acidithiobacillus; otu_1857
D392P31RB22:	Bacteria; Firmicutes; Clostridia; Peptostreptococcaceae; Peptostreptococcus_anaerobius; Clostridium_bifermentans; Unclassified; otu_1213
D392P31RB24:	Bacteria; Proteobacteria; Gammaproteobacteria; Xanthomonadales; Xanthomonadales; gamma_proteobacterium_WJ2; otu_2136
D392P31RB2:	Bacteria; Firmicutes; Clostridia; Peptostreptococcaceae; Peptostreptococcus_anaerobius; Clostridium_bifermentans; Unclassified; otu_1213
D392P31RB4:	Bacteria; Nitrospirae; Leptospirillaceae; Leptospirillum; Unclassified; otu_1427
D392P31RB5:	Bacteria; Nitrospirae; Leptospirillaceae; Leptospirillum; Unclassified; otu_1427
D392P31RB9:	Bacteria; Proteobacteria; Gammaproteobacteria; Xanthomonadales; Xanthomonadales; gamma_proteobacterium_WJ2; otu_2136
D392P31RC10:	Bacteria; Cyanobacteria; Chloroplasts; Euglena; Unclassified; otu_763
D392P31RC11:	Bacteria; Nitrospirae; Leptospirillaceae; Leptospirillum; Unclassified; otu_1427
D392P31RC12:	Bacteria; Proteobacteria; Gammaproteobacteria; Betaproteobacteria; Burkholderiales; Unclassified; otu_1890
D392P31RC13:	Bacteria; Cyanobacteria; Chloroplasts; Euglena; Unclassified; otu_763
D392P31RC15:	Bacteria; Proteobacteria; Gammaproteobacteria; CCD24; Ellin339; RCP1-57; otu_1973
D392P31RC16:	Bacteria; Proteobacteria; Epsilonproteobacteria; Arcobacteraceae; Unclassified; otu_1823
D392P31RC17:	Bacteria; Cyanobacteria; Chloroplasts; Unclassified; otu_755
D392P31RC18:	Bacteria; Firmicutes; Alicyclobacillaceae; Alicyclobacillus; Alicyclobacillus_acidocaldarius; Unclassified; otu_854
D392P31RC19:	Bacteria; Firmicutes; Clostridia; Peptostreptococcaceae; Peptostreptococcus_anaerobius; Clostridium_bifermentans; Unclassified; otu_1213
D392P31RC1:	Bacteria; Firmicutes; Clostridia; Clostridiaceae; Clostridium; Clostridium_quinii; otu_990
D392P31RC20:	Bacteria; Proteobacteria; Gammaproteobacteria; Legionellales; Unclassified; otu_2019
D392P31RC21:	Bacteria; Nitrospirae; Leptospirillaceae; Leptospirillum; Unclassified; otu_1427
D392P31RC22:	Bacteria; Cyanobacteria; Chloroplasts; Unclassified; otu_755
D392P31RC23:	Bacteria; Cyanobacteria; Chloroplasts; Euglena; Unclassified; otu_763
D392P31RC24:	Bacteria; Planctomycetes; WPS-1; CL500-3; CL120-56; Unclassified; otu_1546
D392P31RC2:	Bacteria; Nitrospirae; Leptospirillaceae; Leptospirillum; Unclassified; otu_1427
D392P31RC3:	Bacteria; Cyanobacteria; Chloroplasts; Unclassified; otu_755
D392P31RC4:	Bacteria; Proteobacteria; Gammaproteobacteria; Xanthomonadales; Xanthomonadales; gamma_proteobacterium_WJ2; otu_2136

Sequence	Hugenholtz Taxonomic String
D392P31RC5:	Bacteria; Nitrospirae; Leptospirillaceae; Leptospirillum; Unclassified; otu_1427
D392P31RC6:	Bacteria; Proteobacteria; Gammaproteobacteria; Acidithiobacillaceae; Acidithiobacillus; otu_1857
D392P31RC7:	Bacteria; Proteobacteria; Gammaproteobacteria; Acidithiobacillaceae; Acidithiobacillus; otu_1857
D392P31RC8:	Bacteria; Proteobacteria; Alphaproteobacteria; Acetobacterales; Acetobacteraceae; Acidiphilium; otu_1560
D392P31RC9:	Bacteria; Proteobacteria; Gammaproteobacteria; Acidithiobacillaceae; Acidithiobacillus; otu_1857
D392P31RD10:	Bacteria; Proteobacteria; Alphaproteobacteria; Acetobacterales; Acetobacteraceae; Acidiphilium; otu 1560
D392P31RD11:	Bacteria; Proteobacteria; Gammaproteobacteria; Acidithiobacillaceae; Acidithiobacillus; otu_1857
D392P31RD13:	Bacteria; Cyanobacteria; Chloroplasts; Unclassified; otu_755
D392P31RD14:	Bacteria; Proteobacteria; Gammaproteobacteria; Acidithiobacillaceae; Acidithiobacillus; otu_1857
D392P31RD15:	Bacteria; Nitrospirae; Leptospirillaceae; Leptospirillum; Unclassified; otu_1427
D392P31RD16:	Bacteria; Proteobacteria; Alphaproteobacteria; Acetobacterales; Acetobacteraceae; Acidiphilium; otu_1560
D392P31RD19:	Bacteria; Proteobacteria; Alphaproteobacteria; Acetobacterales; Acetobacteraceae; Acidiphilium; otu_1560
D392P31RD1:	Bacteria; Proteobacteria; Gammaproteobacteria; Acidithiobacillaceae; Acidithiobacillus; otu 1857
D392P31RD20:	Bacteria; Nitrospirae; Leptospirillaceae; Leptospirillum; Unclassified; otu 1427
D392P31RD21:	Bacteria; Cyanobacteria; Chloroplasts; Euglena; Unclassified; otu_763
D392P31RD22:	Bacteria; Proteobacteria; Gammaproteobacteria; Acidithiobacillaceae; Acidithiobacillus; otu_1857
D392P31RD23:	Bacteria; Nitrospirae; Leptospirillaceae; Leptospirillum; Unclassified; otu_1427
D392P31RD2:	Bacteria; Proteobacteria; Alphaproteobacteria; Acetobacterales; Acetobacteraceae; Acidocella; otu_1562
D392P31RD3:	Bacteria; Proteobacteria; Gammaproteobacteria; Acidithiobacillaceae; Acidithiobacillus; otu_1857
D392P31RD4:	Bacteria; Cyanobacteria; Chloroplasts; Unclassified; otu_755
D392P31RD5:	Bacteria; Cyanobacteria; Chloroplasts; Euglena; Unclassified; otu_763
D392P31RD6:	Bacteria; Nitrospirae; Leptospirillaceae; Leptospirillum; Unclassified; otu_1427
D392P31RD8:	Bacteria; Proteobacteria; Gammaproteobacteria; Acidithiobacillaceae; Acidithiobacillus; otu_1857
D392P31RD9:	Bacteria; Nitrospirae; Leptospirillaceae; Leptospirillum; Unclassified; otu 1427
D392P31RE10:	Bacteria; Proteobacteria; Gammaproteobacteria; Xanthomonadales; Xanthomonadales; gamma_proteobacterium_WJ2; otu_2136
D392P31RE11:	Bacteria; Proteobacteria; Gammaproteobacteria; Acidithiobacillaceae; Acidithiobacillus; otu_1857
D392P31RE12:	Bacteria; Proteobacteria; Gammaproteobacteria; Xanthomonadales; Xanthomonadales; gamma_proteobacterium_WJ2; otu_2136
D392P31RE13:	Bacteria; Proteobacteria; Alphaproteobacteria; Acetobacterales; Acetobacteraceae; Acidiphilium; otu_1560
D392P31RE14:	Bacteria; Proteobacteria; Gammaproteobacteria; Acidithiobacillaceae; Acidithiobacillus; otu_1857
D392P31RE15:	Bacteria; Nitrospirae; Leptospirillaceae; Leptospirillum; Unclassified; otu_1427
D392P31RE16:	Bacteria; Nitrospirae; Leptospirillaceae; Leptospirillum; Unclassified; otu 1427
D392P31RE17:	Bacteria; Nitrospirae; Leptospirillaceae; Leptospirillum; Unclassified; otu 1427
D392P31RE18:	Bacteria; Firmicutes; Clostridia; Clostridiaceae; Clostridium; Clostridium_quinii; otu_990
D392P31RE19:	Bacteria; Nitrospirae; Leptospirillaceae; Leptospirillum; Unclassified; otu_1427
D392P31RE1:	Bacteria; Proteobacteria; Gammaproteobacteria; CCD24; Ellin339; RCP1-57; otu_1973
D392P31RE20:	Bacteria; Proteobacteria; Gammaproteobacteria; Acidithiobacillaceae; Acidithiobacillus; otu_1857
D392P31RE21:	Bacteria; Nitrospirae; Leptospirillaceae; Leptospirillum; Unclassified; otu_1427
D392P31RE22:	Bacteria; Proteobacteria; Gammaproteobacteria; Acidithiobacillaceae; Acidithiobacillus; otu 1857
D392P31RE23:	Bacteria; Proteobacteria; Gammaproteobacteria; CCD24; Ellin339; RCP1-57; otu 1973
D392P31RE24:	Bacteria; Proteobacteria; Gammaproteobacteria; Xanthomonadales; Xanthomonadales; gamma_proteobacterium_WJ2; otu_2136
D392P31RE2:	Bacteria; Proteobacteria; Gammaproteobacteria; Acidithiobacillaceae; Acidithiobacillus; otu_1857
D392P31RE3:	Bacteria; Firmicutes; Clostridia; Peptostreptococcaceae; Peptostreptococcus_anaerobius; Clostridium_bifermentans; Unclassified; otu_1213
D392P31RE4:	Bacteria; Proteobacteria; Gammaproteobacteria; Xanthomonadales; Xanthomonadales; gamma_proteobacterium_WJ2; otu_2136
D392P31RE5:	Bacteria; Firmicutes; Alicyclobacillaceae; Alicyclobacillus; mixotrophic_iron-oxidizing_bacterium; otu_858
D392P31RE6:	Bacteria; Proteobacteria; Alphaproteobacteria; Acetobacterales; Acetobacteraceae; Unclassified; otu_1559
D392P31RE7:	Bacteria; Nitrospirae; Leptospirillaceae; Leptospirillum; Unclassified; otu 1427
D392P31RE8:	Bacteria; Nitrospirae; Leptospirillaceae; Leptospirillum; Unclassified; otu_1427
D392P31RF10:	Bacteria; Nitrospirae; Leptospirillaceae; Leptospirillum; Unclassified; otu_1427
D392P31RF11:	Bacteria; Cyanobacteria; Chloroplasts; Unclassified; otu_755
D392P31RF12:	Bacteria; Cyanobacteria; Chloroplasts; Chlorella; otu_757
D392P31RF14:	Bacteria; Proteobacteria; Gammaproteobacteria; Xanthomonadales; Xanthomonadales; gamma_proteobacterium_WJ2; otu_2136
D392P31RF15:	Bacteria; Nitrospirae; Leptospirillaceae; Leptospirillum; Unclassified; otu_1427
D392P31RF16:	Bacteria; Proteobacteria; Gammaproteobacteria; B2M28; otu 1880
D392P31RF17:	Bacteria; Proteobacteria; Gammaproteobacteria; Xanthomonadales; Xanthomonadales; gamma proteobacterium WJ2; otu 2136
D392P31RF18:	Bacteria; Proteobacteria; Gammaproteobacteria; CCD24; Ellin339; RCP1-57; otu_1973
D392P31RF19:	Bacteria; Firmicutes; Clostridia; Peptostreptococcaceae; Peptostreptococcus_anaerobius; Clostridium_bifermentans; Unclassified; otu_1213
D392P31RF1:	Bacteria; Proteobacteria; Gammaproteobacteria; CCD24; Ellin339; RCP1-57; otu_1973
D392P31RF20:	Bacteria; Proteobacteria; Gammaproteobacteria; Acidithiobacillaceae; Acidithiobacillus; otu_1857
D392P31RF21:	Bacteria; Acidobacteria; Acidobacteriales; bacterium_Ellin337; otu_181
D392P31RF22:	Bacteria; Acidobacteria; Acidobacteriales; bacterium_Ellin337; otu_181
D392P31RF23:	Bacteria; Proteobacteria; Alphaproteobacteria; Acetobacterales; Acetobacteraceae; Unclassified; otu_1559
D392P31RF24:	Bacteria; Cyanobacteria; Chloroplasts; Unclassified; otu_755
D392P31RF2:	Bacteria; Planctomycetes; WPS-1; CL500-3; CL120-56; DE613; otu_1549
D392P31RF4:	Bacteria; Cyanobacteria; Chloroplasts; Euglena; Euglena stellata; otu 764
D392P31RF5:	Bacteria; Proteobacteria; Alphaproteobacteria; Acetobacterales; Acetobacteraceae; Acidiphilium; otu_1560
D392P31RF6:	Bacteria; Nitrospirae; Leptospirillaceae; Leptospirillum; Unclassified; otu_1427
D392P31RF7:	Bacteria; Cyanobacteria; Chloroplasts; Euglena; Unclassified; otu_763
D392P31RF8:	Bacteria; Proteobacteria; Alphaproteobacteria; Acetobacterales; Acetobacteraceae; Unclassified; otu_1559
D392P31RF9:	Bacteria; Proteobacteria; Gammaproteobacteria; Xanthomonadales; Xanthomonadales; gamma_proteobacterium_WJ2; otu_2136
D392P31RG10:	Archaea; Thermoplasmata_Eury; Thermoplasmatales; Thermoplasmatales; Ferroplasmaceae; Ferroplasma; otu_118
D392P31RG11:	Bacteria; Nitrospirae; Leptospirillaceae; Leptospirillum; Unclassified; otu 1427
D392P31RG12:	Bacteria; Nitrospirae; Leptospirillaceae; Leptospirillum; Unclassified; otu 1427
D392P31RG13:	Bacteria; Firmicutes; Clostridia; Peptostreptococcaceae; Peptostreptococcus_anaerobius; Clostridium_bifermentans; Unclassified; otu_1213
D392P31RG14:	Bacteria; Proteobacteria; Gammaproteobacteria; Acidithiobacillaceae; Acidithiobacillus; otu_1857
D392P31RG15:	Bacteria; Proteobacteria; Gammaproteobacteria; Acidithiobacillaceae; Acidithiobacillus; otu_1857
D392P31RG16:	Bacteria; Proteobacteria; Gammaproteobacteria; Acidithiobacillaceae; Acidithiobacillus; otu_1857
D392P31RG17:	Bacteria; Firmicutes; Clostridia; Clostridiales; Ruminococcus; SJTU; RL245_aai81e03; RL176_aah44h04; otu_1149

Sequence	Hugenholtz Taxonomic String
D392P31RG18:	Bacteria; Proteobacteria; Gammaproteobacteria; Xanthomonadales; Xanthomonadales; gamma_proteobacterium_WJ2; otu_2136
D392P31RG19:	Bacteria; Proteobacteria; Gammaproteobacteria; CCD24; Ellin339; RCP1-57; otu_1973
D392P31RG1:	Bacteria; Proteobacteria; Gammaproteobacteria; Acidithiobacillaceae; Acidithiobacillus; otu_1857
D392P31RG20:	Bacteria; Proteobacteria; Gammaproteobacteria; Xanthomonadales; Xanthomonadales; gamma_proteobacterium_WJ2; otu_2136
D392P31RG21:	Bacteria; Proteobacteria; Gammaproteobacteria; Xanthomonadales; Xanthomonadales; gamma_proteobacterium_WJ2; otu_2136
D392P31RG22:	Bacteria; Proteobacteria; Alphaproteobacteria; Acetobacterales; Acetobacteraceae; Unclassified; otu_1559
D392P31RG23:	Bacteria; Proteobacteria; Alphaproteobacteria; Acetobacterales; Acetobacteraceae; Unclassified; otu_1559
D392P31RG24:	Bacteria; Nitrospirae; Leptospirillaceae; Leptospirillum; Unclassified; otu_1427
D392P31RG2:	Bacteria; Proteobacteria; Alphaproteobacteria; Acetobacterales; Acetobacteraceae; Unclassified; otu_1559
D392P31RG3:	Bacteria; Proteobacteria; Gammaproteobacteria; Xanthomonadales; Xanthomonadales; gamma_proteobacterium_WJ2; otu_2136
D392P31RG4:	Bacteria; Firmicutes; Clostridia; Peptostreptococcaceae; Peptostreptococcus_anaerobius; Clostridium_bifermentans; Unclassified; otu_1213
D392P31RG5:	Bacteria; Firmicutes; Clostridia; Peptostreptococcaceae; Peptostreptococcus_anaerobius; Clostridium_bifermentans; Unclassified; otu_1213
D392P31RG6:	Bacteria; Cyanobacteria; Chloroplasts; Euglena; Unclassified; otu_763
D392P31RG7:	Bacteria; Nitrospirae; Leptospirillaceae; Leptospirillum; Unclassified; otu_1427
D392P31RG8:	Bacteria; Proteobacteria; Gammaproteobacteria; CCD24; Ellin339; RCP1-57; otu_1973
D392P31RG9:	Bacteria; Proteobacteria; Gammaproteobacteria; Acidithiobacillaceae; Acidithiobacillus; otu_1857
D392P31RH10:	Bacteria; Proteobacteria; Gammaproteobacteria; Acidithiobacillaceae; Acidithiobacillus; otu_1857
D392P31RH13:	Bacteria; Proteobacteria; Gammaproteobacteria; Xanthomonadales; Xanthomonadales; gamma_proteobacterium_WJ2; otu_2136
D392P31RH14:	Bacteria; Proteobacteria; Gammaproteobacteria; Acidithiobacillaceae; Acidithiobacillus; otu_1857
D392P31RH15:	Bacteria; Proteobacteria; Gammaproteobacteria; Acidithiobacillaceae; Acidithiobacillus; otu_1857
D392P31RH16:	Bacteria; Proteobacteria; Gammaproteobacteria; Xanthomonadales; Xanthomonadales; gamma_proteobacterium_WJ2; otu_2136
D392P31RH17:	Bacteria; Nitrospirae; Leptospirillaceae; Leptospirillum; Unclassified; otu_1427
D392P31RH18:	Bacteria; Nitrospirae; Leptospirillaceae; Leptospirillum; Unclassified; otu_1427
D392P31RH19:	Bacteria; Cyanobacteria; Chloroplasts; Unclassified; otu_755
D392P31RH1:	Bacteria; Proteobacteria; Gammaproteobacteria; Xanthomonadales; Xanthomonadales; gamma_proteobacterium_WJ2; otu_2136
D392P31RH20:	Bacteria; Nitrospirae; Leptospirillaceae; Leptospirillum; Unclassified; otu_1427
D392P31RH23:	Bacteria; Acidobacteria; Acidobacteriales; Acidobacterium; otu_180
D392P31RH24:	Bacteria; Proteobacteria; Gammaproteobacteria; Xanthomonadales; Xanthomonadales; gamma_proteobacterium_WJ2; otu_2136
D392P31RH2:	Bacteria; Nitrospirae; Leptospirillaceae; Leptospirillum; Unclassified; otu_1427
D392P31RH3:	Bacteria; Nitrospirae; Leptospirillaceae; Leptospirillum; Unclassified; otu_1427
D392P31RH4:	Bacteria; Proteobacteria; Gammaproteobacteria; Acidithiobacillaceae; Acidithiobacillus; otu_1857
D392P31RH5:	Bacteria; Proteobacteria; Alphaproteobacteria; Acetobacterales; Acetobacteraceae; Acidiphilium; otu_1560
D392P31RH6:	Bacteria; Cyanobacteria; Chloroplasts; Euglena; Euglena_stellata; otu_764
D392P31RH7:	Bacteria; Proteobacteria; Gammaproteobacteria; Xanthomonadales; Xanthomonadales; gamma_proteobacterium_WJ2; otu_2136
D392P31RH8:	Bacteria; Proteobacteria; Gammaproteobacteria; Acidithiobacillaceae; Acidithiobacillus; otu_1857
D392P31FI10:	Bacteria; Nitrospirae; Leptospirillaceae; Leptospirillum; Unclassified; otu_1427
D392P31FI11:	Bacteria; Proteobacteria; Alphaproteobacteria; Acetobacterales; Acetobacteraceae; Acidiphilium; otu_1560
D392P31FI12:	Bacteria; Proteobacteria; Gammaproteobacteria; Acidithiobacillaceae; Acidithiobacillus; otu_1857
D392P31FI13:	Bacteria; Sulfobacillus; Sulfobacillus_thermosulfidooxidans; otu_2205
D392P31FI14:	Bacteria; Proteobacteria; Gammaproteobacteria; Xanthomonadales; Xanthomonadales; gamma_proteobacterium_WJ2; otu_2136
D392P31FI15:	Bacteria; Nitrospirae; Leptospirillaceae; Leptospirillum; Unclassified; otu_1427
D392P31FI16:	Bacteria; Proteobacteria; Gammaproteobacteria; Xanthomonadales; Xanthomonadales; gamma_proteobacterium_WJ2; otu_2136
D392P31FI17:	Bacteria; Proteobacteria; Gammaproteobacteria; Acidithiobacillaceae; Acidithiobacillus; otu_1857
D392P31FI18:	Bacteria; Proteobacteria; Alphaproteobacteria; Acetobacterales; Acetobacteraceae; Acidocella; otu_1562
D392P31FI19:	Bacteria; Cyanobacteria; Chloroplasts; Euglena; Unclassified; otu_763
D392P31FI20:	Bacteria; Proteobacteria; Gammaproteobacteria; Acidithiobacillaceae; Acidithiobacillus; otu_1857
D392P31FI21:	Bacteria; Proteobacteria; Gammaproteobacteria; CCD24; Ellin339; RCP1-57; otu_1973
D392P31FI22:	Bacteria; Proteobacteria; Gammaproteobacteria; Acidithiobacillaceae; Acidithiobacillus; otu_1857
D392P31FI24:	Bacteria; Proteobacteria; Gammaproteobacteria; CCD24; Ellin339; RCP1-57; otu_1973
D392P31FI2:	Bacteria; Nitrospirae; Leptospirillaceae; Leptospirillum; Unclassified; otu_1427
D392P31FI3:	Bacteria; Proteobacteria; Gammaproteobacteria; CCD24; Ellin339; RCP1-57; otu_1973
D392P31FI4:	Bacteria; Firmicutes; Clostridia; Peptostreptococcaceae; Peptostreptococcus_anaerobius; Clostridium_bifermentans; Unclassified; otu_1213
D392P31FI5:	Bacteria; Nitrospirae; Leptospirillaceae; Leptospirillum; Unclassified; otu_1427
D392P31FI6:	Bacteria; Proteobacteria; Gammaproteobacteria; Xanthomonadales; Xanthomonadales; gamma_proteobacterium_WJ2; otu_2136
D392P31FI7:	Bacteria; Proteobacteria; Gammaproteobacteria; Xanthomonadales; Xanthomonadales; gamma_proteobacterium_WJ2; otu_2136
D392P31FI8:	Bacteria; Proteobacteria; Gammaproteobacteria; Xanthomonadales; Xanthomonadales; gamma_proteobacterium_WJ2; otu_2136
D392P31FI9:	Bacteria; Cyanobacteria; Chloroplasts; Euglena; Unclassified; otu_763
D392P31FJ10:	Bacteria; Cyanobacteria; Chloroplasts; Euglena; Unclassified; otu_763
D392P31FJ11:	Bacteria; Proteobacteria; Gammaproteobacteria; CCD24; Ellin339; RCP1-57; otu_1973
D392P31FJ12:	Bacteria; Cyanobacteria; Chloroplasts; Euglena; Euglena_stellata; otu_764
D392P31FJ13:	Bacteria; Proteobacteria; Gammaproteobacteria; Acidithiobacillaceae; Acidithiobacillus; otu_1857
D392P31FJ14:	Bacteria; Nitrospirae; Leptospirillaceae; Leptospirillum; Unclassified; otu_1427
D392P31FJ15:	Bacteria; Proteobacteria; Gammaproteobacteria; Xanthomonadales; Xanthomonadales; gamma_proteobacterium_WJ2; otu_2136
D392P31FJ16:	Bacteria; Planctomycetes; WPS-1; CL500-3; CL120-56; DE613; otu_1549
D392P31FJ17:	Bacteria; Nitrospirae; Leptospirillaceae; Leptospirillum; Unclassified; otu_1427
D392P31FJ18:	Bacteria; Proteobacteria; Alphaproteobacteria; Acetobacterales; Acetobacteraceae; Acidiphilium; otu_1560
D392P31FJ19:	Bacteria; Nitrospirae; Leptospirillaceae; Leptospirillum; Unclassified; otu_1427
D392P31FJ1:	Bacteria; Cyanobacteria; Chloroplasts; Euglena; Unclassified; otu_763
D392P31FJ20:	Bacteria; Acidobacteria; Acidobacteriales; bacterium_Ellin337; otu_181
D392P31FJ21:	Bacteria; Cyanobacteria; Chloroplasts; Euglena; Euglena_stellata; otu_764
D392P31FJ22:	Bacteria; Proteobacteria; Gammaproteobacteria; Xanthomonadales; Xanthomonadales; gamma_proteobacterium_WJ2; otu_2136
D392P31FJ23:	Bacteria; Proteobacteria; Gammaproteobacteria; Acidithiobacillaceae; Acidithiobacillus; otu_1857
D392P31FJ24:	Bacteria; Planctomycetes; WPS-1; CL500-3; CL120-56; DE613; otu_1549
D392P31FJ2:	Bacteria; Proteobacteria; Gammaproteobacteria; Xanthomonadales; Xanthomonadales; gamma_proteobacterium_WJ2; otu_2136
D392P31FJ3:	Bacteria; Proteobacteria; Gammaproteobacteria; Acidithiobacillaceae; Acidithiobacillus; otu_1857
D392P31FJ4:	Bacteria; Proteobacteria; Alphaproteobacteria; Acetobacterales; Acetobacteraceae; Acidiphilium; otu_1560
D392P31FJ5:	Bacteria; Firmicutes; Alicyclobacillaceae; Alicyclobacillus; mixotrophic_iron-oxidizing_bacterium; otu_858

Sequence	Hugenholtz Taxonomic String
D392P31FJ7:	Bacteria; Proteobacteria; Gammaproteobacteria; Acidithiobacillaceae; Acidithiobacillus; otu_1857
D392P31FJ8:	Bacteria; Nitrospirae; Leptospirillaceae; Leptospirillum; Unclassified; otu_1427
D392P31FK10:	Bacteria; Nitrospirae; Leptospirillaceae; Leptospirillum; Unclassified; otu_1427
D392P31FK11:	Bacteria; Cyanobacteria; Chloroplasts; Euglena; Unclassified; otu_763
D392P31FK12:	Bacteria; Acidobacteria; Acidobacteriales; bacterium_Ellin337; otu_181
D392P31FK13:	Bacteria; Nitrospirae; Leptospirillaceae; Leptospirillum; Unclassified; otu_1427
D392P31FK14:	Archaea; Thermoplasmata_Eury; Thermoplasmatales; Thermoplasmatales; Ferroplasmaceae; Ferroplasma; otu_118
D392P31FK15:	Bacteria; Proteobacteria; Gammaproteobacteria; Acidithiobacillaceae; Acidithiobacillus; otu_1857
D392P31FK16:	Bacteria; Proteobacteria; Gammaproteobacteria; Xanthomonadales; Xanthomonadales; gamma_proteobacterium_WJ2; otu_2136
D392P31FK17:	Bacteria; Proteobacteria; Gammaproteobacteria; Xanthomonadales; Xanthomonadales; gamma_proteobacterium_WJ2; otu_2136
D392P31FK18:	Bacteria; Proteobacteria; Alphaproteobacteria; Acetobacterales; Acetobacteraceae; Unclassified; otu_1559
D392P31FK1:	Bacteria; Nitrospirae; Leptospirillaceae; Leptospirillum; Unclassified; otu_1427
D392P31FK20:	Bacteria; Proteobacteria; Gammaproteobacteria; Acidithiobacillaceae; Acidithiobacillus; otu_1857
D392P31FK21:	Bacteria; Planctomycetes; WPS-1; CL500-3; CL120-56; DE613; otu_1549
D392P31FK22:	Bacteria; Nitrospirae; Leptospirillaceae; Leptospirillum; Unclassified; otu_1427
D392P31FK23:	Bacteria; Proteobacteria; Gammaproteobacteria; Acidithiobacillaceae; Acidithiobacillus; otu_1857
D392P31FK24:	Bacteria; Proteobacteria; Alphaproteobacteria; Acetobacterales; Acetobacteraceae; Acidiphilium; otu_1560
D392P31FK2:	Bacteria; Proteobacteria; Gammaproteobacteria; Xanthomonadales; Xanthomonadales; gamma_proteobacterium_WJ2; otu_2136
D392P31FK3:	Bacteria; Proteobacteria; Gammaproteobacteria; Xanthomonadales; Xanthomonadales; gamma_proteobacterium_WJ2; otu_2136
D392P31FK4:	Bacteria; Proteobacteria; Gammaproteobacteria; Acidithiobacillaceae; Acidithiobacillus; otu_1857
D392P31FK5:	Bacteria; Cyanobacteria; Chloroplasts; Euglena; Unclassified; otu_763
D392P31FK6:	Bacteria; Proteobacteria; Gammaproteobacteria; Acidithiobacillaceae; Acidithiobacillus; otu_1857
D392P31FK8:	Bacteria; Firmicutes; Clostridia; Peptostreptococcaceae; Peptostreptococcus_anaerobius; Clostridium_bifermentans; Unclassified; otu_1213
D392P31FK9:	Bacteria; Cyanobacteria; Chloroplasts; Euglena; Unclassified; otu_763
D392P31FL10:	Bacteria; Acidobacteria; Acidobacteriales; bacterium_Ellin337; otu_181
D392P31FL12:	Bacteria; Proteobacteria; Gammaproteobacteria; Acidithiobacillaceae; Acidithiobacillus; otu_1857
D392P31FL13:	Bacteria; Proteobacteria; Alphaproteobacteria; Acetobacterales; Acetobacteraceae; Unclassified; otu_1559
D392P31FL14:	Bacteria; Firmicutes; Clostridia; Clostridiales; Ruminococcus; SJTU; Unclassified; otu_1146
D392P31FL15:	Bacteria; Proteobacteria; Alphaproteobacteria; Acetobacterales; Acetobacteraceae; Acidiphilium; otu_1560
D392P31FL16:	Bacteria; Proteobacteria; Gammaproteobacteria; Acidithiobacillaceae; Acidithiobacillus; otu_1857
D392P31FL17:	Bacteria; Proteobacteria; Alphaproteobacteria; Acetobacterales; Acetobacteraceae; Unclassified; otu_1559
D392P31FL18:	Bacteria; Nitrospirae; Leptospirillaceae; Leptospirillum; Unclassified; otu_1427
D392P31FL19:	Bacteria; Cyanobacteria; Chloroplasts; Unclassified; otu_755
D392P31FL1:	Bacteria; Nitrospirae; Leptospirillaceae; Leptospirillum; Unclassified; otu_1427
D392P31FL20:	Bacteria; Cyanobacteria; Chloroplasts; Euglena; Unclassified; otu_763
D392P31FL21:	Bacteria; Cyanobacteria; Chloroplasts; Euglena; Unclassified; otu_763
D392P31FL22:	Bacteria; Nitrospirae; Leptospirillaceae; Leptospirillum; Unclassified; otu_1427
D392P31FL23:	Bacteria; Proteobacteria; Gammaproteobacteria; Xanthomonadales; Xanthomonadales; gamma_proteobacterium_WJ2; otu_2136
D392P31FL24:	Bacteria; Proteobacteria; Gammaproteobacteria; Acidithiobacillaceae; Acidithiobacillus; otu_1857
D392P31FL2:	Bacteria; Firmicutes; Clostridia; Peptostreptococcaceae; Peptostreptococcus_anaerobius; Clostridium_bifermentans; AKIW475; otu_1214
D392P31FL3:	Bacteria; Cyanobacteria; Chloroplasts; Unclassified; otu_755
D392P31FL5:	Bacteria; Nitrospirae; Leptospirillaceae; Leptospirillum; Unclassified; otu_1427
D392P31FL6:	Bacteria; Nitrospirae; Leptospirillaceae; Leptospirillum; Unclassified; otu_1427
D392P31FL7:	Bacteria; Proteobacteria; Gammaproteobacteria; CCD24; Ellin339; RCP1-57; otu_1973
D392P31FL8:	Bacteria; Firmicutes; Clostridia; Peptostreptococcaceae; Peptostreptococcus_anaerobius; Clostridium_bifermentans; Unclassified; otu_1213
D392P31FL9:	Bacteria; Proteobacteria; Gammaproteobacteria; CCD24; Ellin339; RCP1-57; otu_1973
D392P31FM10:	Bacteria; Firmicutes; Alicyclobacillaceae; Alicyclobacillus; Alicyclobacillus_acidocaldarius; Unclassified; otu_854
D392P31FM11:	Bacteria; Nitrospirae; Leptospirillaceae; Leptospirillum; Unclassified; otu_1427
D392P31FM12:	Bacteria; Proteobacteria; Gammaproteobacteria; Acidithiobacillaceae; Acidithiobacillus; otu_1857
D392P31FM13:	Bacteria; Nitrospirae; Leptospirillaceae; Leptospirillum; Unclassified; otu_1427
D392P31FM14:	Bacteria; Proteobacteria; Gammaproteobacteria; Acidithiobacillaceae; Acidithiobacillus; otu_1857
D392P31FM15:	Bacteria; Proteobacteria; Gammaproteobacteria; Xanthomonadales; Xanthomonadales; gamma_proteobacterium_WJ2; otu_2136
D392P31FM16:	Bacteria; Planctomycetes; WPS-1; CL500-3; CL120-56; DE613; otu_1549
D392P31FM17:	Bacteria; Cyanobacteria; Chloroplasts; Chlorella; otu_757
D392P31FM18:	Bacteria; Cyanobacteria; Chloroplasts; Chlorella; otu_757
D392P31FM19:	Bacteria; Proteobacteria; Gammaproteobacteria; Acidithiobacillaceae; Acidithiobacillus; otu_1857
D392P31FM1:	Bacteria; Proteobacteria; Gammaproteobacteria; Acidithiobacillaceae; Acidithiobacillus; otu_1857
D392P31FM20:	Bacteria; Nitrospirae; Leptospirillaceae; Leptospirillum; Unclassified; otu_1427
D392P31FM23:	Bacteria; Proteobacteria; Alphaproteobacteria; Acetobacterales; Acetobacteraceae; Unclassified; otu_1559
D392P31FM24:	Bacteria; Proteobacteria; Gammaproteobacteria; Acidithiobacillaceae; Acidithiobacillus; otu_1857
D392P31FM2:	Bacteria; Cyanobacteria; Chloroplasts; Euglena; Unclassified; otu_763
D392P31FM6:	Bacteria; Proteobacteria; Gammaproteobacteria; Xanthomonadales; Xanthomonadales; gamma_proteobacterium_WJ2; otu_2136
D392P31FM7:	Bacteria; Proteobacteria; Gammaproteobacteria; Acidithiobacillaceae; Acidithiobacillus; otu_1857
D392P31FM8:	Bacteria; Proteobacteria; Gammaproteobacteria; Xanthomonadales; Xanthomonadales; gamma_proteobacterium_WJ2; otu_2136
D392P31FM9:	Bacteria; Proteobacteria; Gammaproteobacteria; Unclassified; otu_1854
D392P31FN10:	Bacteria; Nitrospirae; Leptospirillaceae; Leptospirillum; Unclassified; otu_1427
D392P31FN11:	Bacteria; Proteobacteria; Gammaproteobacteria; Acidithiobacillaceae; Acidithiobacillus; otu_1857
D392P31FN12:	Bacteria; Nitrospirae; Leptospirillaceae; Leptospirillum; Unclassified; otu_1427
D392P31FN13:	Bacteria; Firmicutes; Clostridia; Clostridiaceae; Clostridium; Clostridium_quinii; otu_990
D392P31FN14:	Bacteria; Proteobacteria; Gammaproteobacteria; Acidithiobacillaceae; Acidithiobacillus; otu_1857
D392P31FN15:	Bacteria; Acidobacteria; Acidobacteriales; bacterium_Ellin337; otu_181
D392P31FN16:	Bacteria; Nitrospirae; Leptospirillaceae; Leptospirillum; Unclassified; otu_1427
D392P31FN17:	Bacteria; Firmicutes; Clostridia; Clostridiaceae; Clostridium; Clostridium_quinii; otu_990
D392P31FN18:	Bacteria; Nitrospirae; Leptospirillaceae; Leptospirillum; Unclassified; otu_1427
D392P31FN19:	Bacteria; Nitrospirae; Leptospirillaceae; Leptospirillum; Unclassified; otu_1427
D392P31FN1:	Bacteria; Proteobacteria; Gammaproteobacteria; B2M28; otu_1880
D392P31FN20:	Bacteria; Proteobacteria; Gammaproteobacteria; Xanthomonadales; Xanthomonadales; gamma_proteobacterium_WJ2; otu_2136

Sequence	Hugenholtz Taxonomic String
D392P31FN23:	Bacteria; Proteobacteria; Gammaproteobacteria; Acidithiobacillaceae; Acidithiobacillus; otu_1857
D392P31FN24:	Bacteria; Firmicutes; Clostridia; Peptostreptococcaceae; Peptostreptococcus_anaerobius; Clostridium_bifermentans; Unclassified; otu_1213
D392P31FN2:	Bacteria; Proteobacteria; Gammaproteobacteria; Acidithiobacillaceae; Acidithiobacillus; otu_1857
D392P31FN3:	Bacteria; Proteobacteria; Alphaproteobacteria; Acetobacterales; Acetobacteraceae; Acidocella; otu_1562
D392P31FN4:	Bacteria; Cyanobacteria; Chloroplasts; Unclassified; otu_755
D392P31FN7:	Bacteria; Proteobacteria; Alphaproteobacteria; Acetobacterales; Acetobacteraceae; Acidiphilium; otu_1560
D392P31FN8:	Bacteria; Cyanobacteria; Chloroplasts; Euglena; Unclassified; otu_763
D392P31FN9:	Bacteria; Proteobacteria; Gammaproteobacteria; Acidithiobacillaceae; Acidithiobacillus; otu_1857
D392P31FO10:	Bacteria; Nitrospirae; Leptospirillaceae; Leptospirillum; Unclassified; otu_1427
D392P31FO11:	Bacteria; Proteobacteria; Gammaproteobacteria; Acidithiobacillaceae; Acidithiobacillus; otu_1857
D392P31FO12:	Bacteria; Proteobacteria; Gammaproteobacteria; Xanthomonadales; Xanthomonadales; gamma_proteobacterium_WJ2; otu_2136
D392P31FO13:	Bacteria; Proteobacteria; Alphaproteobacteria; Acetobacterales; Acetobacteraceae; Unclassified; otu_1559
D392P31FO14:	Bacteria; Proteobacteria; Gammaproteobacteria; Acidithiobacillaceae; Acidithiobacillus; otu_1857
D392P31FO15:	Bacteria; Proteobacteria; Gammaproteobacteria; Acidithiobacillaceae; Acidithiobacillus; otu_1857
D392P31FO17:	Bacteria; Proteobacteria; Gammaproteobacteria; Acidithiobacillaceae; Acidithiobacillus; otu_1857
D392P31FO18:	Bacteria; Nitrospirae; Leptospirillaceae; Leptospirillum; Unclassified; otu_1427
D392P31FO19:	Bacteria; Cyanobacteria; Chloroplasts; Euglena; Unclassified; otu_763
D392P31FO1:	Bacteria; Proteobacteria; Gammaproteobacteria; Betaproteobacteria; Burkholderiales; Comamonadaceae; Unclassified; otu_1899
D392P31FO20:	Bacteria; Nitrospirae; Leptospirillaceae; Leptospirillum; Unclassified; otu_1427
D392P31FO21:	Bacteria; Proteobacteria; Gammaproteobacteria; Acidithiobacillaceae; Acidithiobacillus; otu_1857
D392P31FO22:	Bacteria; Proteobacteria; Gammaproteobacteria; Acidithiobacillaceae; Acidithiobacillus; otu_1857
D392P31FO23:	Bacteria; Nitrospirae; Leptospirillaceae; Leptospirillum; Unclassified; otu_1427
D392P31FO24:	Bacteria; Proteobacteria; Gammaproteobacteria; Xanthomonadales; Xanthomonadales; gamma_proteobacterium_WJ2; otu_2136
D392P31FO2:	Bacteria; Proteobacteria; Gammaproteobacteria; CCD24; Ellin339; RCP1-57; otu_1973
D392P31FO3:	Bacteria; Proteobacteria; Alphaproteobacteria; Acetobacterales; Acetobacteraceae; Acidiphilium; otu_1560
D392P31FO4:	Bacteria; Firmicutes; Clostridia; Clostridiaceae; Clostridium; Clostridium_quinii; otu_990
D392P31FO6:	Bacteria; Proteobacteria; Gammaproteobacteria; Xanthomonadales; Xanthomonadales; gamma_proteobacterium_WJ2; otu_2136
D392P31FO7:	Bacteria; Proteobacteria; Gammaproteobacteria; CCD24; Ellin339; RCP1-57; otu_1973
D392P31FO8:	Bacteria; Nitrospirae; Leptospirillaceae; Leptospirillum; Unclassified; otu_1427
D392P31FO9:	Bacteria; Proteobacteria; Gammaproteobacteria; CCD24; Ellin339; RCP1-57; otu_1973
D392P31FP10:	Bacteria; Proteobacteria; Gammaproteobacteria; Acidithiobacillaceae; Acidithiobacillus; otu_1857
D392P31FP11:	Archaea; Thermoplasmata_Eury; Thermoplasmatales; Thermoplasmatales; Ferroplasmaceae; Ferroplasma; otu_118
D392P31FP12:	Bacteria; Acidobacteria; Acidobacteriales; bacterium_Ellin337; otu_181
D392P31FP13:	Bacteria; Cyanobacteria; Chloroplasts; Euglena; Euglena_stellata; otu_764
D392P31FP14:	Bacteria; Proteobacteria; Gammaproteobacteria; Acidithiobacillaceae; Acidithiobacillus; otu_1857
D392P31FP15:	Bacteria; Proteobacteria; Gammaproteobacteria; B2M28; otu_1880
D392P31FP16:	Bacteria; Nitrospirae; Leptospirillaceae; Leptospirillum; Unclassified; otu_1427
D392P31FP18:	Bacteria; Proteobacteria; Gammaproteobacteria; Acidithiobacillaceae; Acidithiobacillus; otu_1857
D392P31FP19:	Bacteria; Proteobacteria; Gammaproteobacteria; Xanthomonadales; Xanthomonadales; gamma_proteobacterium_WJ2; otu_2136
D392P31FP20:	Bacteria; Nitrospirae; Leptospirillaceae; Leptospirillum; Unclassified; otu_1427
D392P31FP21:	Bacteria; Proteobacteria; Alphaproteobacteria; Acetobacterales; Acetobacteraceae; Acidiphilium; otu_1560
D392P31FP22:	Bacteria; Proteobacteria; Gammaproteobacteria; Xanthomonadales; Xanthomonadales; gamma_proteobacterium_WJ2; otu_2136
D392P31FP23:	Bacteria; Nitrospirae; Leptospirillaceae; Leptospirillum; Unclassified; otu_1427
D392P31FP24:	Bacteria; Proteobacteria; Gammaproteobacteria; Acidithiobacillaceae; Acidithiobacillus; otu_1857
D392P31FP3:	Bacteria; Cyanobacteria; Chloroplasts; Unclassified; otu_755
D392P31FP5:	Bacteria; Proteobacteria; Gammaproteobacteria; Acidithiobacillaceae; Acidithiobacillus; otu_1857
D392P31FP6:	Bacteria; Proteobacteria; Gammaproteobacteria; Xanthomonadales; Xanthomonadales; gamma_proteobacterium_WJ2; otu_2136
D392P31FP8:	Bacteria; Nitrospirae; Leptospirillaceae; Leptospirillum; Unclassified; otu_1427
D392P31FP9:	Bacteria; Proteobacteria; Alphaproteobacteria; Acetobacterales; Acetobacteraceae; Acidocella; otu_1562
D392P31RI10:	Bacteria; Nitrospirae; Leptospirillaceae; Leptospirillum; Unclassified; otu_1427
D392P31RI11:	Bacteria; Proteobacteria; Alphaproteobacteria; Acetobacterales; Acetobacteraceae; Acidiphilium; otu_1560
D392P31RI12:	Bacteria; Proteobacteria; Gammaproteobacteria; Acidithiobacillaceae; Acidithiobacillus; otu_1857
D392P31RI13:	Bacteria; Sulfobacillus; Sulfobacillus_thermosulfidooxidans; otu_2205
D392P31RI14:	Bacteria; Proteobacteria; Gammaproteobacteria; Xanthomonadales; Xanthomonadales; gamma_proteobacterium_WJ2; otu_2136
D392P31RI15:	Bacteria; Nitrospirae; Leptospirillaceae; Leptospirillum; Unclassified; otu_1427
D392P31RI16:	Bacteria; Proteobacteria; Gammaproteobacteria; Xanthomonadales; Xanthomonadales; gamma_proteobacterium_WJ2; otu_2136
D392P31RI17:	Bacteria; Proteobacteria; Gammaproteobacteria; Acidithiobacillaceae; Acidithiobacillus; otu_1857
D392P31RI18:	Bacteria; Proteobacteria; Alphaproteobacteria; Acetobacterales; Acetobacteraceae; Acidocella; otu_1562
D392P31RI19:	Bacteria; Cyanobacteria; Chloroplasts; Unclassified; otu_755
D392P31RI20:	Bacteria; Proteobacteria; Gammaproteobacteria; Acidithiobacillaceae; Acidithiobacillus; otu_1857
D392P31RI21:	Bacteria; Proteobacteria; Gammaproteobacteria; CCD24; Ellin339; RCP1-57; otu_1973
D392P31RI22:	Bacteria; Proteobacteria; Gammaproteobacteria; Acidithiobacillaceae; Acidithiobacillus; otu_1857
D392P31RI24:	Bacteria; Proteobacteria; Gammaproteobacteria; CCD24; Ellin339; RCP1-57; otu_1973
D392P31RI3:	Bacteria; Proteobacteria; Gammaproteobacteria; CCD24; Ellin339; RCP1-57; otu_1973
D392P31RI4:	Bacteria; Firmicutes; Clostridia; Peptostreptococcaceae; Peptostreptococcus_anaerobius; Clostridium_bifermentans; Unclassified; otu_1213
D392P31RI5:	Bacteria; Nitrospirae; Leptospirillaceae; Leptospirillum; Unclassified; otu_1427
D392P31RI6:	Bacteria; Proteobacteria; Gammaproteobacteria; Xanthomonadales; Xanthomonadales; gamma_proteobacterium_WJ2; otu_2136
D392P31RI7:	Bacteria; Proteobacteria; Gammaproteobacteria; Xanthomonadales; Xanthomonadales; gamma_proteobacterium_WJ2; otu_2136
D392P31RI8:	Bacteria; Proteobacteria; Gammaproteobacteria; Xanthomonadales; Xanthomonadales; gamma_proteobacterium_WJ2; otu_2136
D392P31RI9:	Bacteria; Cyanobacteria; Chloroplasts; Unclassified; otu_755
D392P31RJ10:	Bacteria; Cyanobacteria; Chloroplasts; Euglena; Unclassified; otu_763
D392P31RJ11:	Bacteria; Proteobacteria; Gammaproteobacteria; CCD24; Ellin339; RCP1-57; otu_1973
D392P31RJ12:	Bacteria; Cyanobacteria; Chloroplasts; Euglena; Euglena_stellata; otu_764
D392P31RJ13:	Bacteria; Proteobacteria; Gammaproteobacteria; Acidithiobacillaceae; Acidithiobacillus; otu_1857
D392P31RJ14:	Bacteria; Nitrospirae; Leptospirillaceae; Leptospirillum; Unclassified; otu_1427
D392P31RJ15:	Bacteria; Proteobacteria; Gammaproteobacteria; Xanthomonadales; Xanthomonadales; gamma_proteobacterium_WJ2; otu_2136
D392P31RJ16:	Bacteria; Planctomycetes; WPS-1; CL500-3; CL120-56; DE613; otu_1549

Sequence	Hugenholtz Taxonomic String
D392P31RJ17:	Bacteria; Nitrospirae; Leptospirillaceae; Leptospirillum; Unclassified; otu_1427
D392P31RJ18:	Bacteria; Proteobacteria; Alphaproteobacteria; Acetobacterales; Acetobacteraceae; Acidiphilium; otu_1560
D392P31RJ19:	Bacteria; Nitrospirae; Leptospirillaceae; Leptospirillum; Unclassified; otu_1427
D392P31RJ1:	Bacteria; Cyanobacteria; Chloroplasts; Unclassified; otu_755
D392P31RJ20:	Bacteria; Acidobacteria; Acidobacteriales; bacterium_Ellin337; otu_181
D392P31RJ21:	Bacteria; Cyanobacteria; Chloroplasts; Unclassified; otu_755
D392P31RJ22:	Bacteria; Proteobacteria; Gammaproteobacteria; Xanthomonadales; Xanthomonadales; gamma_proteobacterium_WJ2; otu_2136
D392P31RJ23:	Bacteria; Proteobacteria; Gammaproteobacteria; Acidithiobacillaceae; Acidithiobacillus; otu_1857
D392P31RJ24:	Bacteria; Planctomycetes; WPS-1; CL500-3; CL120-56; DE613; otu_1549
D392P31RJ2:	Bacteria; Proteobacteria; Gammaproteobacteria; Xanthomonadales; Xanthomonadales; gamma_proteobacterium_WJ2; otu_2136
D392P31RJ3:	Bacteria; Proteobacteria; Gammaproteobacteria; Acidithiobacillaceae; Acidithiobacillus; otu_1857
D392P31RJ4:	Bacteria; Proteobacteria; Alphaproteobacteria; Acetobacterales; Acetobacteraceae; Acidiphilium; otu_1560
D392P31RJ5:	Bacteria; Firmicutes; Alicyclobacillaceae; Alicyclobacillus; Alicyclobacillus_acidocaldarius; Unclassified; otu_854
D392P31RJ6:	Bacteria; Cyanobacteria; Chloroplasts; Unclassified; otu_755
D392P31RJ7:	Bacteria; Proteobacteria; Gammaproteobacteria; Acidithiobacillaceae; Acidithiobacillus; otu_1857
D392P31RJ8:	Bacteria; Nitrospirae; Leptospirillaceae; Leptospirillum; Unclassified; otu_1427
D392P31RK10:	Bacteria; Nitrospirae; Leptospirillaceae; Leptospirillum; Unclassified; otu_1427
D392P31RK11:	Bacteria; Cyanobacteria; Chloroplasts; Unclassified; otu_755
D392P31RK12:	Bacteria; Acidobacteria; Acidobacteriales; bacterium_Ellin337; otu_181
D392P31RK13:	Bacteria; Nitrospirae; Leptospirillaceae; Leptospirillum; Unclassified; otu_1427
D392P31RK14:	Archaea; Thermoplasmata_Eury; Thermoplasmatales; Thermoplasmatales; Ferroplasmaceae; Ferroplasma; otu_118
D392P31RK15:	Bacteria; Proteobacteria; Gammaproteobacteria; Acidithiobacillaceae; Acidithiobacillus; otu_1857
D392P31RK16:	Bacteria; Proteobacteria; Gammaproteobacteria; Xanthomonadales; Xanthomonadales; gamma_proteobacterium_WJ2; otu_2136
D392P31RK17:	Bacteria; Proteobacteria; Gammaproteobacteria; Xanthomonadales; Xanthomonadales; gamma_proteobacterium_WJ2; otu_2136
D392P31RK18:	Bacteria; Proteobacteria; Alphaproteobacteria; Acetobacterales; Acetobacteraceae; Acidiphilium; otu_1560
D392P31RK1:	Bacteria; Nitrospirae; Leptospirillaceae; Leptospirillum; Unclassified; otu_1427
D392P31RK20:	Bacteria; Proteobacteria; Gammaproteobacteria; Acidithiobacillaceae; Acidithiobacillus; otu_1857
D392P31RK21:	Bacteria; Planctomycetes; WPS-1; CL500-3; CL120-56; DE613; otu_1549
D392P31RK22:	Bacteria; Nitrospirae; Leptospirillaceae; Leptospirillum; Unclassified; otu_1427
D392P31RK23:	Bacteria; Proteobacteria; Gammaproteobacteria; Acidithiobacillaceae; Acidithiobacillus; otu_1857
D392P31RK24:	Bacteria; Proteobacteria; Alphaproteobacteria; Acetobacterales; Acetobacteraceae; Acidiphilium; otu_1560
D392P31RK2:	Bacteria; Proteobacteria; Gammaproteobacteria; Xanthomonadales; Xanthomonadales; gamma_proteobacterium_WJ2; otu_2136
D392P31RK3:	Bacteria; Proteobacteria; Gammaproteobacteria; Xanthomonadales; Xanthomonadales; gamma_proteobacterium_WJ2; otu_2136
D392P31RK4:	Bacteria; Proteobacteria; Gammaproteobacteria; Acidithiobacillaceae; Acidithiobacillus; otu_1857
D392P31RK6:	Bacteria; Proteobacteria; Gammaproteobacteria; Acidithiobacillaceae; Acidithiobacillus; otu_1857
D392P31RK8:	Bacteria; Firmicutes; Clostridia; Peptostreptococcaceae; Peptostreptococcus_anaerobius; Clostridium_bifermentans; Unclassified; otu_1213
D392P31RK9:	Bacteria; Cyanobacteria; Chloroplasts; Euglena; Unclassified; otu_763
D392P31RL10:	Bacteria; Acidobacteria; Acidobacteriales; bacterium_Ellin337; otu_181
D392P31RL12:	Bacteria; Proteobacteria; Gammaproteobacteria; Acidithiobacillaceae; Acidithiobacillus; otu_1857
D392P31RL13:	Bacteria; Proteobacteria; Alphaproteobacteria; Acetobacterales; Acetobacteraceae; Unclassified; otu_1559
D392P31RL14:	Bacteria; Firmicutes; Clostridia; Clostridiales; Ruminococcus; SJTU; AP10R262; otu_1147
D392P31RL15:	Bacteria; Proteobacteria; Alphaproteobacteria; Acetobacterales; Acetobacteraceae; Acidiphilium; otu_1560
D392P31RL16:	Bacteria; Proteobacteria; Gammaproteobacteria; Acidithiobacillaceae; Acidithiobacillus; otu_1857
D392P31RL17:	Bacteria; Proteobacteria; Alphaproteobacteria; Acetobacterales; Acetobacteraceae; Unclassified; otu_1559
D392P31RL18:	Bacteria; Nitrospirae; Leptospirillaceae; Leptospirillum; Unclassified; otu_1427
D392P31RL19:	Bacteria; Cyanobacteria; Chloroplasts; Euglena; Unclassified; otu_763
D392P31RL1:	Bacteria; Nitrospirae; Leptospirillaceae; Leptospirillum; Unclassified; otu_1427
D392P31RL20:	Bacteria; Cyanobacteria; Chloroplasts; Unclassified; otu_755
D392P31RL21:	Bacteria; Cyanobacteria; Chloroplasts; Euglena; Unclassified; otu_763
D392P31RL22:	Bacteria; Nitrospirae; Leptospirillaceae; Leptospirillum; Unclassified; otu_1427
D392P31RL23:	Bacteria; Proteobacteria; Gammaproteobacteria; Xanthomonadales; Xanthomonadales; gamma_proteobacterium_WJ2; otu_2136
D392P31RL24:	Bacteria; Proteobacteria; Gammaproteobacteria; Acidithiobacillaceae; Acidithiobacillus; otu_1857
D392P31RL2:	Bacteria; Firmicutes; Clostridia; Peptostreptococcaceae; Peptostreptococcus_anaerobius; Clostridium_bifermentans; Unclassified; otu_1213
D392P31RL3:	Bacteria; Cyanobacteria; Chloroplasts; Euglena; Unclassified; otu_763
D392P31RL4:	Bacteria; Nitrospirae; Leptospirillaceae; Leptospirillum; Unclassified; otu_1427
D392P31RL7:	Bacteria; Proteobacteria; Gammaproteobacteria; CCD24; Ellin339; RCP1-57; otu_1973
D392P31RL8:	Bacteria; Firmicutes; Clostridia; Peptostreptococcaceae; Peptostreptococcus_anaerobius; Clostridium_bifermentans; AKIW475; otu_1214
D392P31RL9:	Bacteria; Proteobacteria; Gammaproteobacteria; CCD24; Ellin339; RCP1-57; otu_1973
D392P31RM10:	Bacteria; Firmicutes; Alicyclobacillaceae; Alicyclobacillus; Alicyclobacillus_acidocaldarius; Unclassified; otu_854
D392P31RM11:	Bacteria; Nitrospirae; Leptospirillaceae; Leptospirillum; Unclassified; otu_1427
D392P31RM12:	Bacteria; Proteobacteria; Gammaproteobacteria; Acidithiobacillaceae; Acidithiobacillus; otu_1857
D392P31RM13:	Bacteria; Nitrospirae; Leptospirillaceae; Leptospirillum; Unclassified; otu_1427
D392P31RM14:	Bacteria; Proteobacteria; Gammaproteobacteria; Acidithiobacillaceae; Acidithiobacillus; otu_1857
D392P31RM15:	Bacteria; Proteobacteria; Gammaproteobacteria; Xanthomonadales; Xanthomonadales; gamma_proteobacterium_WJ2; otu_2136
D392P31RM16:	Bacteria; Planctomycetes; WPS-1; CL500-3; CL120-56; DE613; otu_1549
D392P31RM17:	Bacteria; Cyanobacteria; Chloroplasts; Chlorella; otu_757
D392P31RM18:	Bacteria; Cyanobacteria; Chloroplasts; Chlorella; otu_757
D392P31RM19:	Bacteria; Proteobacteria; Gammaproteobacteria; Acidithiobacillaceae; Acidithiobacillus; otu_1857
D392P31RM1:	Bacteria; Proteobacteria; Gammaproteobacteria; Acidithiobacillaceae; Acidithiobacillus; otu_1857
D392P31RM20:	Bacteria; Nitrospirae; Leptospirillaceae; Leptospirillum; Unclassified; otu_1427
D392P31RM21:	Bacteria; Proteobacteria; Gammaproteobacteria; Acidithiobacillaceae; Acidithiobacillus; otu_1857
D392P31RM23:	Bacteria; Proteobacteria; Alphaproteobacteria; Acetobacterales; Acetobacteraceae; Unclassified; otu_1559
D392P31RM24:	Bacteria; Proteobacteria; Gammaproteobacteria; Acidithiobacillaceae; Acidithiobacillus; otu_1857
D392P31RM2:	Bacteria; Cyanobacteria; Chloroplasts; Euglena; Unclassified; otu_763
D392P31RM3:	Bacteria; Nitrospirae; Leptospirillaceae; Leptospirillum; Unclassified; otu_1427
D392P31RM4:	Bacteria; Proteobacteria; Gammaproteobacteria; Acidithiobacillaceae; Acidithiobacillus; otu_1857
D392P31RM5:	Bacteria; Proteobacteria; Gammaproteobacteria; Acidithiobacillaceae; Acidithiobacillus; otu_1857

Sequence	Hugenholtz Taxonomic String
D392P31RM6:	Bacteria; Nitrospirae; Leptospirillaceae; Leptospirillum; Unclassified; otu_1427
D392P31RM7:	Bacteria; Proteobacteria; Gammaproteobacteria; Acidithiobacillaceae; Acidithiobacillus; otu_1857
D392P31RM8:	Bacteria; Proteobacteria; Gammaproteobacteria; Xanthomonadales; Xanthomonadales; gamma_proteobacterium_WJ2; otu_2136
D392P31RM9:	Bacteria; Proteobacteria; Gammaproteobacteria; B2M28; otu_1880
D392P31RN10:	Bacteria; Nitrospirae; Leptospirillaceae; Leptospirillum; Unclassified; otu_1427
D392P31RN11:	Bacteria; Proteobacteria; Gammaproteobacteria; Acidithiobacillaceae; Acidithiobacillus; otu_1857
D392P31RN12:	Bacteria; Nitrospirae; Leptospirillaceae; Leptospirillum; Unclassified; otu_1427
D392P31RN13:	Bacteria; Firmicutes; Clostridia; Clostridiaceae; Clostridium; Clostridium quinii; otu 990
D392P31RN14:	Bacteria; Proteobacteria; Gammaproteobacteria; Acidithiobacillaceae; Acidithiobacillus; otu 1857
D392P31RN15:	Bacteria; Acidobacteria; Acidobacteriales; bacterium_Ellin337; otu_181
D392P31RN16:	Bacteria; Nitrospirae; Leptospirillaceae; Leptospirillum; Unclassified; otu_1427
D392P31RN17:	Bacteria; Firmicutes; Clostridia; Clostridiaceae; Clostridium; Clostridium_quinii; otu_990
D392P31RN18:	Bacteria; Nitrospirae; Leptospirillaceae; Leptospirillum; Unclassified; otu_1427
D392P31RN19:	Bacteria; Nitrospirae; Leptospirillaceae; Leptospirillum; Unclassified; otu_1427
D392P31RN1:	Bacteria; Proteobacteria; Gammaproteobacteria; B2M28; otu_1880
D392P31RN20:	Bacteria; Proteobacteria; Gammaproteobacteria; Xanthomonadales; Xanthomonadales; gamma_proteobacterium_WJ2; otu_2136
D392P31RN21:	Bacteria; Proteobacteria; Gammaproteobacteria; Acidithiobacillaceae; Acidithiobacillus; otu 1857
D392P31RN23:	Bacteria; Proteobacteria; Gammaproteobacteria; Acidithiobacillaceae; Acidithiobacillus; otu 1857
D392P31RN24:	Bacteria; Firmicutes; Clostridia; Peptostreptococcaceae; Peptostreptococcus_anaerobius; Clostridium_bifermentans; Unclassified; otu_1213
D392P31RN2:	Bacteria; Proteobacteria; Gammaproteobacteria; Acidithiobacillaceae; Acidithiobacillus; otu_1857
D392P31RN3:	Bacteria; Proteobacteria; Alphaproteobacteria; Acetobacterales; Acetobacteraceae; Acidocella; otu_1562
D392P31RN4:	Bacteria; Cyanobacteria; Chloroplasts; Euglena; Unclassified; otu 763
D392P31RN6:	Archaea; Thermoplasmata Eury; Thermoplasmatales; Thermoplasmatales; Ferroplasmaceae; Ferroplasma; otu 118
D392P31RN7:	Bacteria; Proteobacteria; Alphaproteobacteria; Acetobacterales; Acetobacteraceae; Acidiphilium; otu_1560
D392P31RN8:	Bacteria; Cyanobacteria; Chloroplasts; Euglena; Euglena_stellata; otu_764
D392P31RN9:	Bacteria; Proteobacteria; Gammaproteobacteria; Acidithiobacillaceae; Acidithiobacillus; otu_1857
D392P31RO10:	Bacteria; Nitrospirae; Leptospirillaceae; Leptospirillum; Unclassified; otu_1427
D392P31RO11:	Bacteria; Proteobacteria; Gammaproteobacteria; Acidithiobacillaceae; Acidithiobacillus; otu_1857
D392P31RO12:	Bacteria; Proteobacteria; Gammaproteobacteria; Xanthomonadales; Xanthomonadales; gamma_proteobacterium_WJ2; otu_2136
D392P31RO13:	Bacteria; Proteobacteria; Alphaproteobacteria; Acetobacterales; Acetobacteraceae; Unclassified; otu_1559
D392P31RO14:	Bacteria; Proteobacteria; Gammaproteobacteria; Acidithiobacillaceae; Acidithiobacillus; otu 1857
D392P31RO15:	Bacteria; Proteobacteria; Gammaproteobacteria; Acidithiobacillaceae; Acidithiobacillus; otu 1857
D392P31RO17:	Bacteria; Proteobacteria; Gammaproteobacteria; Acidithiobacillaceae; Acidithiobacillus; otu_1857
D392P31RO18:	Bacteria; Nitrospirae; Leptospirillaceae; Leptospirillum; Unclassified; otu_1427
D392P31RO19:	Bacteria; Cyanobacteria; Chloroplasts; Euglena; Unclassified; otu_763
D392P31RO1:	Bacteria; Proteobacteria; Gammaproteobacteria; Betaproteobacteria; Burkholderiales; Comamonadaceae; Unclassified; otu_1899
D392P31RO20:	Bacteria; Nitrospirae; Leptospirillaceae; Leptospirillum; Unclassified; otu_1427
D392P31RO21:	Bacteria; Proteobacteria; Gammaproteobacteria; Acidithiobacillaceae; Acidithiobacillus; otu_1857
D392P31RO22:	Bacteria; Proteobacteria; Gammaproteobacteria; Acidithiobacillaceae; Acidithiobacillus; otu_1857
D392P31RO23:	Bacteria; Nitrospirae; Leptospirillaceae; Leptospirillum; Unclassified; otu_1427
D392P31RO24:	Bacteria; Proteobacteria; Gammaproteobacteria; Xanthomonadales; Xanthomonadales; gamma proteobacterium WJ2; otu 2136
D392P31RO2:	Bacteria; Proteobacteria; Gammaproteobacteria; CCD24; Ellin339; RCP1-57; otu 1973
D392P31RO3:	Bacteria; Proteobacteria; Alphaproteobacteria; Acetobacterales; Acetobacteraceae; Acidiphilium; otu_1560
D392P31RO4:	Bacteria; Firmicutes; Clostridia; Clostridiaceae; Clostridium; Clostridium_quinii; otu_990
D392P31RO5:	Bacteria; Planctomycetes; WPS-1; CL500-3; CL120-56; DE613; otu_1549
D392P31RO6:	Bacteria; Proteobacteria; Gammaproteobacteria; Xanthomonadales; Xanthomonadales; gamma_proteobacterium_WJ2; otu_2136
D392P31RO7:	Bacteria; Proteobacteria; Gammaproteobacteria; CCD24; Ellin339; RCP1-57; otu_1973
D392P31RO8:	Bacteria; Nitrospirae; Leptospirillaceae; Leptospirillum; Unclassified; otu_1427
D392P31RO9:	Bacteria; Proteobacteria; Gammaproteobacteria; CCD24; Ellin339; RCP1-57; otu_1973
D392P31RP10:	Bacteria; Proteobacteria; Gammaproteobacteria; Acidithiobacillaceae; Acidithiobacillus; otu_1857
D392P31RP11:	Archaea; Thermoplasmata Eury; Thermoplasmatales; Thermoplasmatales; Ferroplasmaceae; Ferroplasma; otu 118
D392P31RP12:	Bacteria; Acidobacteria; Acidobacteriales; Ephadobacter; Acidobacteriaceae bacterium Thars1; otu 186
D392P31RP13:	Bacteria; Cyanobacteria; Chloroplasts; Euglena; Unclassified; otu_763
D392P31RP14:	Bacteria; Proteobacteria; Gammaproteobacteria; Acidithiobacillaceae; Acidithiobacillus; otu_1857
D392P31RP15:	Bacteria; Proteobacteria; Gammaproteobacteria; B2M28; otu_1880
D392P31RP16:	Bacteria; Nitrospirae; Leptospirillaceae; Leptospirillum; Unclassified; otu_1427
D392P31RP18:	Bacteria; Proteobacteria; Gammaproteobacteria; Acidithiobacillaceae; Acidithiobacillus; otu_1857
D392P31RP19:	Bacteria; Proteobacteria; Gammaproteobacteria; Xanthomonadales; Xanthomonadales; gamma_proteobacterium_WJ2; otu_2136
D392P31RP1:	Bacteria; Nitrospirae; Leptospirillaceae; Leptospirillum; Unclassified; otu_1427
D392P31RP20:	Bacteria; Nitrospirae; Leptospirillaceae; Leptospirillum; Unclassified; otu_1427
D392P31RP21:	Bacteria; Proteobacteria; Alphaproteobacteria; Acetobacterales; Acetobacteraceae; Acidiphilium; otu_1560
D392P31RP22:	Bacteria; Proteobacteria; Gammaproteobacteria; Xanthomonadales; Xanthomonadales; gamma_proteobacterium_WJ2; otu_2136
D392P31RP23:	Bacteria; Nitrospirae; Leptospirillaceae; Leptospirillum; Unclassified; otu_1427
D392P31RP24:	Bacteria; Proteobacteria; Gammaproteobacteria; Acidithiobacillaceae; Acidithiobacillus; otu_1857
D392P31RP2:	Bacteria; Proteobacteria; Gammaproteobacteria; Acidithiobacillaceae; Acidithiobacillus; otu 1857
D392P31RP3:	Bacteria; Cyanobacteria; Chloroplasts; Euglena; Unclassified; otu 763
D392P31RP5:	Bacteria; Proteobacteria; Gammaproteobacteria; Acidithiobacillaceae; Acidithiobacillus; otu_1857
D392P31RP6:	Bacteria; Proteobacteria; Gammaproteobacteria; Xanthomonadales; Xanthomonadales; gamma_proteobacterium_WJ2; otu_2136
D392P31RP8:	Bacteria; Nitrospirae; Leptospirillaceae; Leptospirillum; Unclassified; otu_1427
D392P31RP9:	Bacteria; Proteobacteria; Alphaproteobacteria; Acetobacterales; Acetobacteraceae; Acidocella; otu_1562
D392P32FA10:	Bacteria; Proteobacteria; Alphaproteobacteria; Acetobacterales; Acetobacteraceae; Acidiphilium; otu_1560
D392P32FA12:	Bacteria; Cyanobacteria; Chloroplasts; Euglena; Euglena_stellata; otu_764
D392P32FA13:	Bacteria; Proteobacteria; Gammaproteobacteria; Moraxellaceae; Unclassified; otu_2039
D392P32FA14:	Bacteria; Proteobacteria; Deltaproteobacteria; BA18; otu_1735
D392P32FA15:	Bacteria; Bacteroidetes; Cardiniaceae; Candidatus Cardinium; Ixodes scapularis endosymbiont; otu 508
D392P32FA16:	Bacteria; Proteobacteria; Gammaproteobacteria; Acidithiobacillaceae; Acidithiobacillus; otu 1857
D392P32FA17:	Bacteria; Proteobacteria; Gammaproteobacteria; Xanthomonadales; Xanthomonadales; gamma_proteobacterium_WJ2; otu_2136

Sequence	Hugenholtz Taxonomic String
D392P32FA18:	Bacteria; Proteobacteria; Gammaproteobacteria; Acidithiobacillaceae; Acidithiobacillus; otu_1857
D392P32FA19:	Bacteria; Firmicutes; Alicyclobacillaceae; Alicyclobacillus; Alicyclobacillus_acidocaldarius; Unclassified; otu_854
D392P32FA1:	Bacteria; Nitrospirae; Leptospirillaceae; Leptospirillum; Unclassified; otu_1427
D392P32FA21:	Bacteria; Firmicutes; Clostridia; Clostridiaceae; Clostridium; Clostridium_quinii; otu_990
D392P32FA23:	Bacteria; Proteobacteria; Alphaproteobacteria; Acetobacterales; Acetobacteraceae; Acidiphilium; otu_1560
D392P32FA3:	Bacteria; Proteobacteria; Gammaproteobacteria; Xanthomonadales; Xanthomonadales; gamma_proteobacterium_WJ2; otu_2136
D392P32FA4:	Bacteria; Proteobacteria; Gammaproteobacteria; CCD24; Ellin339; RCP1-57; otu_1973
D392P32FA5:	Bacteria; Proteobacteria; Alphaproteobacteria; Acetobacterales; Acetobacteraceae; Acidiphilium; otu_1560
D392P32FA6:	Bacteria; Proteobacteria; Gammaproteobacteria; CCD24; Ellin339; RCP1-57; otu_1973
D392P32FA7:	Bacteria; Proteobacteria; Gammaproteobacteria; Xanthomonadales; Xanthomonadales; gamma_proteobacterium_WJ2; otu_2136
D392P32FA8:	Bacteria; Nitrospirae; Leptospirillaceae; Leptospirillum; Unclassified; otu_1427
D392P32FA9:	Archaea; Thermoplasmata_Eury; Thermoplasmatales; Thermoplasmatales; Ferroplasmaceae; Ferroplasma; otu_118
D392P32FC10:	Archaea; Thermoplasmata_Eury; Thermoplasmatales; Thermoplasmatales; Ferroplasmaceae; Ferroplasma; otu_118
D392P32FC11:	Bacteria; Nitrospirae; Leptospirillaceae; Leptospirillum; Unclassified; otu_1427
D392P32FC13:	Bacteria; Proteobacteria; Gammaproteobacteria; CCD24; Ellin339; RCP1-57; otu_1973
D392P32FC14:	Bacteria; Proteobacteria; Gammaproteobacteria; Acidithiobacillaceae; Acidithiobacillus; otu_1857
D392P32FC15:	Bacteria; Cyanobacteria; Chloroplasts; Chlorella; otu_757
D392P32FC16:	Bacteria; Cyanobacteria; Chloroplasts; Euglena; Unclassified; otu_763
D392P32FC18:	Bacteria; Cyanobacteria; Chloroplasts; Euglena; Unclassified; otu_763
D392P32FC19:	Bacteria; Nitrospirae; Leptospirillaceae; Leptospirillum; Unclassified; otu_1427
D392P32FC1:	Bacteria; Proteobacteria; Alphaproteobacteria; Acetobacterales; Acetobacteraceae; Acidiphilium; otu_1560
D392P32FC21:	Bacteria; Cyanobacteria; Chloroplasts; Chlorella; otu_757
D392P32FC23:	Archaea; Thermoplasmata_Eury; Thermoplasmatales; Thermoplasmatales; Ferroplasmaceae; Ferroplasma; otu_118
D392P32FC4:	Bacteria; Proteobacteria; Gammaproteobacteria; Acidithiobacillaceae; Acidithiobacillus; otu_1857
D392P32FC6:	Bacteria; Proteobacteria; Gammaproteobacteria; Acidithiobacillaceae; Acidithiobacillus; otu_1857
D392P32FC7:	Bacteria; Proteobacteria; Gammaproteobacteria; Xanthomonadales; Xanthomonadales; gamma_proteobacterium_WJ2; otu_2136
D392P32FC8:	Bacteria; Cyanobacteria; Chloroplasts; Euglena; Unclassified; otu_763
D392P32FC9:	Bacteria; Cyanobacteria; Chloroplasts; Unclassified; otu_755
D392P32FE10:	Bacteria; Proteobacteria; Gammaproteobacteria; Acidithiobacillaceae; Acidithiobacillus; otu_1857
D392P32FE11:	Bacteria; Proteobacteria; Gammaproteobacteria; CCD24; Ellin339; RCP1-57; otu_1973
D392P32FE12:	Bacteria; Cyanobacteria; Chloroplasts; Euglena; Unclassified; otu_763
D392P32FE13:	Bacteria; Proteobacteria; Gammaproteobacteria; Xanthomonadales; Xanthomonadales; gamma_proteobacterium_WJ2; otu_2136
D392P32FE14:	Bacteria; Proteobacteria; Gammaproteobacteria; Xanthomonadales; Xanthomonadales; gamma_proteobacterium_WJ2; otu_2136
D392P32FE15:	Bacteria; Proteobacteria; Gammaproteobacteria; CCD24; Ellin339; RCP1-57; otu_1973
D392P32FE16:	Bacteria; Proteobacteria; Gammaproteobacteria; Unclassified; otu_1854
D392P32FE17:	Bacteria; Proteobacteria; Gammaproteobacteria; CCD24; Ellin339; RCP1-57; otu_1973
D392P32FE18:	Bacteria; Proteobacteria; Gammaproteobacteria; CCD24; Ellin339; RCP1-57; otu_1973
D392P32FE19:	Bacteria; Proteobacteria; Alphaproteobacteria; Acetobacterales; Acetobacteraceae; Acidiphilium; otu_1560
D392P32FE1:	Bacteria; Proteobacteria; Gammaproteobacteria; CCD24; Ellin339; RCP1-57; otu_1973
D392P32FE21:	Bacteria; Cyanobacteria; Chloroplasts; Euglena; Unclassified; otu_763
D392P32FE23:	Bacteria; Proteobacteria; Gammaproteobacteria; Xanthomonadales; Xanthomonadales; gamma_proteobacterium_WJ2; otu_2136
D392P32FE2:	Bacteria; Proteobacteria; Gammaproteobacteria; Acidithiobacillaceae; Acidithiobacillus; otu_1857
D392P32FE3:	Bacteria; Nitrospirae; Leptospirillaceae; Leptospirillum; Unclassified; otu_1427
D392P32FE4:	Bacteria; Proteobacteria; Alphaproteobacteria; Acetobacterales; Acetobacteraceae; Acidiphilium; otu_1560
D392P32FE5:	Bacteria; Proteobacteria; Gammaproteobacteria; Acidithiobacillaceae; Acidithiobacillus; otu_1857
D392P32FE6:	Archaea; Thermoplasmata_Eury; Thermoplasmatales; Thermoplasmatales; Ferroplasmaceae; Ferroplasma; otu_118
D392P32FE7:	Bacteria; Cyanobacteria; Chloroplasts; Chlorella; otu_757
D392P32FE8:	Bacteria; Proteobacteria; Gammaproteobacteria; Xanthomonadales; Xanthomonadales; gamma_proteobacterium_WJ2; otu_2136
D392P32FE9:	Bacteria; Proteobacteria; Alphaproteobacteria; Acetobacterales; Acetobacteraceae; Acidiphilium; otu_1560
D392P32FG10:	Bacteria; Proteobacteria; Gammaproteobacteria; Acidithiobacillaceae; Acidithiobacillus; otu_1857
D392P32FG11:	Bacteria; Proteobacteria; Gammaproteobacteria; Xanthomonadales; Xanthomonadales; gamma_proteobacterium_WJ2; otu_2136
D392P32FG12:	Bacteria; Nitrospirae; Leptospirillaceae; Leptospirillum; Unclassified; otu_1427
D392P32FG13:	Bacteria; Nitrospirae; Leptospirillaceae; Leptospirillum; Unclassified; otu_1427
D392P32FG14:	Bacteria; Proteobacteria; Alphaproteobacteria; Acetobacterales; Acetobacteraceae; Acidiphilium; otu_1560
D392P32FG15:	Bacteria; Proteobacteria; Alphaproteobacteria; Acetobacterales; Acetobacteraceae; Acidiphilium; otu_1560
D392P32FG16:	Bacteria; Proteobacteria; Alphaproteobacteria; Acetobacterales; Acetobacteraceae; Acidiphilium; otu_1560
D392P32FG17:	Bacteria; Nitrospirae; Leptospirillaceae; Leptospirillum; Unclassified; otu_1427
D392P32FG18:	Bacteria; Proteobacteria; Gammaproteobacteria; Acidithiobacillaceae; Acidithiobacillus; otu_1857
D392P32FG19:	Bacteria; Proteobacteria; Gammaproteobacteria; Xanthomonadales; Xanthomonadales; gamma_proteobacterium_WJ2; otu_2136
D392P32FG1:	Bacteria; Nitrospirae; Leptospirillaceae; Leptospirillum; Unclassified; otu_1427
D392P32FG21:	Bacteria; Proteobacteria; Gammaproteobacteria; Acidithiobacillaceae; Acidithiobacillus; otu_1857
D392P32FG23:	Bacteria; Proteobacteria; Gammaproteobacteria; Acidithiobacillaceae; Acidithiobacillus; otu_1857
D392P32FG2:	Bacteria; Cyanobacteria; Chloroplasts; Euglena; Unclassified; otu_763
D392P32FG3:	Bacteria; Nitrospirae; Leptospirillaceae; Leptospirillum; Unclassified; otu_1427
D392P32FG4:	Bacteria; Nitrospirae; Leptospirillaceae; Leptospirillum; Unclassified; otu_1427
D392P32FG5:	Bacteria; Planctomycetes; WPS-1; CL500-3; CL120-56; DE613; otu_1549
D392P32FG6:	Bacteria; Nitrospirae; Leptospirillaceae; Leptospirillum; Unclassified; otu_1427
D392P32FG7:	Bacteria; Proteobacteria; Gammaproteobacteria; Acidithiobacillaceae; Acidithiobacillus; otu_1857
D392P32FG8:	Bacteria; Nitrospirae; Leptospirillaceae; Leptospirillum; Unclassified; otu_1427
D392P32FG9:	Bacteria; Proteobacteria; Gammaproteobacteria; Betaproteobacteria; Burkholderiales; Comamonadaceae; Variovorax; Unclassified; otu_1917
D392P32RA10:	Bacteria; Proteobacteria; Alphaproteobacteria; Acetobacterales; Acetobacteraceae; Acidiphilium; otu_1560
D392P32RA12:	Bacteria; Cyanobacteria; Chloroplasts; Euglena; Unclassified; otu_763
D392P32RA13:	Bacteria; Proteobacteria; Gammaproteobacteria; Moraxellaceae; Unclassified; otu_2039
D392P32RA14:	Bacteria; Proteobacteria; Deltaproteobacteria; BA18; otu_1735
D392P32RA15:	Bacteria; Bacteroidetes; Cardiniaceae; Candidatus_Cardinium; Ixodes_scapularis_endosymbiont; otu_508
D392P32RA16:	Bacteria; Proteobacteria; Gammaproteobacteria; Acidithiobacillaceae; Acidithiobacillus; otu_1857
D392P32RA17:	Bacteria; Proteobacteria; Gammaproteobacteria; Xanthomonadales; Xanthomonadales; gamma_proteobacterium_WJ2; otu_2136

Sequence	Hugenholtz Taxonomic String
D392P32RA18:	Bacteria; Proteobacteria; Gammaproteobacteria; Acidithiobacillaceae; Acidithiobacillus; otu_1857
D392P32RA19:	Bacteria; Firmicutes; Alicyclobacillaceae; Alicyclobacillus; Alicyclobacillus_acidocaldarius; Unclassified; otu_854
D392P32RA1:	Bacteria; Nitrospirae; Leptospirillaceae; Leptospirillum; Unclassified; otu_1427
D392P32RA21:	Bacteria; Firmicutes; Clostridia; Clostridiaceae; Clostridium; Clostridium_quinii; otu_990
D392P32RA23:	Bacteria; Proteobacteria; Alphaproteobacteria; Acetobacterales; Acetobacteraceae; Acidiphilium; otu_1560
D392P32RA3:	Bacteria; Proteobacteria; Gammaproteobacteria; Xanthomonadales; Xanthomonadales; gamma_proteobacterium_WJ2; otu_2136
D392P32RA5:	Bacteria; Proteobacteria; Alphaproteobacteria; Acetobacterales; Acetobacteraceae; Acidiphilium; otu_1560
D392P32RA6:	Bacteria; Proteobacteria; Gammaproteobacteria; CCD24; Ellin339; RCP1-57; otu_1973
D392P32RA7:	Bacteria; Proteobacteria; Gammaproteobacteria; Xanthomonadales; Xanthomonadales; gamma_proteobacterium_WJ2; otu_2136
D392P32RA8:	Bacteria; Nitrospirae; Leptospirillaceae; Leptospirillum; Unclassified; otu_1427
D392P32RA9:	Archaea; Thermoplasmata_Eury; Thermoplasmatales; Thermoplasmatales; Ferroplasmaceae; Ferroplasma; otu_118
D392P32RC10:	Archaea; Thermoplasmata_Eury; Thermoplasmatales; Thermoplasmatales; Ferroplasmaceae; Ferroplasma; otu_118
D392P32RC11:	Bacteria; Nitrospirae; Leptospirillaceae; Leptospirillum; Unclassified; otu_1427
D392P32RC13:	Bacteria; Proteobacteria; Gammaproteobacteria; CCD24; Ellin339; RCP1-57; otu_1973
D392P32RC14:	Bacteria; Proteobacteria; Gammaproteobacteria; Acidithiobacillaceae; Acidithiobacillus; otu_1857
D392P32RC15:	Bacteria; Cyanobacteria; Chloroplasts; Chlorella; otu_757
D392P32RC16:	Bacteria; Cyanobacteria; Chloroplasts; Unclassified; otu_755
D392P32RC18:	Bacteria; Cyanobacteria; Chloroplasts; Unclassified; otu_755
D392P32RC19:	Bacteria; Nitrospirae; Leptospirillaceae; Leptospirillum; Unclassified; otu_1427
D392P32RC1:	Bacteria; Proteobacteria; Alphaproteobacteria; Acetobacterales; Acetobacteraceae; Acidiphilium; otu_1560
D392P32RC21:	Bacteria; Cyanobacteria; Chloroplasts; Chlorella; otu_757
D392P32RC23:	Archaea; Thermoplasmata_Eury; Thermoplasmatales; Thermoplasmatales; Ferroplasmaceae; Ferroplasma; otu_118
D392P32RC4:	Bacteria; Proteobacteria; Gammaproteobacteria; Acidithiobacillaceae; Acidithiobacillus; otu_1857
D392P32RC6:	Bacteria; Proteobacteria; Gammaproteobacteria; Acidithiobacillaceae; Acidithiobacillus; otu_1857
D392P32RC7:	Bacteria; Proteobacteria; Gammaproteobacteria; Xanthomonadales; Xanthomonadales; gamma_proteobacterium_WJ2; otu_2136
D392P32RC8:	Bacteria; Cyanobacteria; Chloroplasts; Unclassified; otu_755
D392P32RC9:	Bacteria; Cyanobacteria; Chloroplasts; Euglena; Unclassified; otu_763
D392P32RE10:	Bacteria; Proteobacteria; Gammaproteobacteria; Acidithiobacillaceae; Acidithiobacillus; otu_1857
D392P32RE11:	Bacteria; Proteobacteria; Gammaproteobacteria; CCD24; Ellin339; RCP1-57; otu_1973
D392P32RE12:	Bacteria; Cyanobacteria; Chloroplasts; Euglena; Unclassified; otu_763
D392P32RE13:	Bacteria; Proteobacteria; Gammaproteobacteria; Xanthomonadales; Xanthomonadales; gamma_proteobacterium_WJ2; otu_2136
D392P32RE14:	Bacteria; Proteobacteria; Gammaproteobacteria; Xanthomonadales; Xanthomonadales; gamma_proteobacterium_WJ2; otu_2136
D392P32RE15:	Bacteria; Proteobacteria; Gammaproteobacteria; CCD24; Ellin339; RCP1-57; otu_1973
D392P32RE16:	Bacteria; Proteobacteria; Gammaproteobacteria; B2M28; otu_1880
D392P32RE17:	Bacteria; Proteobacteria; Gammaproteobacteria; CCD24; Ellin339; RCP1-57; otu_1973
D392P32RE18:	Bacteria; Proteobacteria; Gammaproteobacteria; CCD24; Ellin339; RCP1-57; otu_1973
D392P32RE19:	Bacteria; Proteobacteria; Alphaproteobacteria; Acetobacterales; Acetobacteraceae; Acidiphilium; otu_1560
D392P32RE1:	Bacteria; Proteobacteria; Gammaproteobacteria; CCD24; Ellin339; RCP1-57; otu_1973
D392P32RE21:	Bacteria; Cyanobacteria; Chloroplasts; Unclassified; otu_755
D392P32RE23:	Bacteria; Proteobacteria; Gammaproteobacteria; Xanthomonadales; Xanthomonadales; gamma_proteobacterium_WJ2; otu_2136
D392P32RE2:	Bacteria; Proteobacteria; Gammaproteobacteria; Acidithiobacillaceae; Acidithiobacillus; otu_1857
D392P32RE3:	Bacteria; Nitrospirae; Leptospirillaceae; Leptospirillum; Unclassified; otu_1427
D392P32RE4:	Bacteria; Proteobacteria; Alphaproteobacteria; Acetobacterales; Acetobacteraceae; Acidiphilium; otu_1560
D392P32RE5:	Bacteria; Proteobacteria; Gammaproteobacteria; Acidithiobacillaceae; Acidithiobacillus; otu_1857
D392P32RE6:	Archaea; Thermoplasmata_Eury; Thermoplasmatales; Thermoplasmatales; Ferroplasmaceae; Ferroplasma; otu_118
D392P32RE7:	Bacteria; Cyanobacteria; Chloroplasts; Chlorella; otu_757
D392P32RE8:	Bacteria; Proteobacteria; Gammaproteobacteria; Xanthomonadales; Xanthomonadales; gamma_proteobacterium_WJ2; otu_2136
D392P32RE9:	Bacteria; Proteobacteria; Alphaproteobacteria; Acetobacterales; Acetobacteraceae; Acidiphilium; otu_1560
D392P32RG10:	Bacteria; Proteobacteria; Gammaproteobacteria; Acidithiobacillaceae; Acidithiobacillus; otu_1857
D392P32RG11:	Bacteria; Proteobacteria; Gammaproteobacteria; Xanthomonadales; Xanthomonadales; gamma_proteobacterium_WJ2; otu_2136
D392P32RG12:	Bacteria; Nitrospirae; Leptospirillaceae; Leptospirillum; Unclassified; otu_1427
D392P32RG13:	Bacteria; Nitrospirae; Leptospirillaceae; Leptospirillum; Unclassified; otu_1427
D392P32RG14:	Bacteria; Proteobacteria; Alphaproteobacteria; Acetobacterales; Acetobacteraceae; Acidiphilium; otu_1560
D392P32RG15:	Bacteria; Proteobacteria; Alphaproteobacteria; Acetobacterales; Acetobacteraceae; Acidiphilium; otu_1560
D392P32RG16:	Bacteria; Proteobacteria; Alphaproteobacteria; Acetobacterales; Acetobacteraceae; Acidiphilium; otu_1560
D392P32RG17:	Bacteria; Nitrospirae; Leptospirillaceae; Leptospirillum; Unclassified; otu_1427
D392P32RG18:	Bacteria; Proteobacteria; Gammaproteobacteria; Acidithiobacillaceae; Acidithiobacillus; otu_1857
D392P32RG19:	Bacteria; Proteobacteria; Gammaproteobacteria; Xanthomonadales; Xanthomonadales; gamma_proteobacterium_WJ2; otu_2136
D392P32RG1:	Bacteria; Nitrospirae; Leptospirillaceae; Leptospirillum; Unclassified; otu_1427
D392P32RG21:	Bacteria; Proteobacteria; Gammaproteobacteria; Acidithiobacillaceae; Acidithiobacillus; otu_1857
D392P32RG23:	Bacteria; Proteobacteria; Gammaproteobacteria; Acidithiobacillaceae; Acidithiobacillus; otu_1857
D392P32RG2:	Bacteria; Cyanobacteria; Chloroplasts; Unclassified; otu_755
D392P32RG3:	Bacteria; Nitrospirae; Leptospirillaceae; Leptospirillum; Unclassified; otu_1427
D392P32RG4:	Bacteria; Nitrospirae; Leptospirillaceae; Leptospirillum; Unclassified; otu_1427
D392P32RG5:	Bacteria; Planctomycetes; WPS-1; CL500-3; CL120-56; DE613; otu_1549
D392P32RG6:	Bacteria; Nitrospirae; Leptospirillaceae; Leptospirillum; Unclassified; otu_1427
D392P32RG7:	Bacteria; Proteobacteria; Gammaproteobacteria; Acidithiobacillaceae; Acidithiobacillus; otu_1857
D392P32RG8:	Bacteria; Nitrospirae; Leptospirillaceae; Leptospirillum; Unclassified; otu_1427
D392P32RG9:	Bacteria; Proteobacteria; Gammaproteobacteria; Betaproteobacteria; Burkholderiales; Comamonadaceae; Variovorax; Unclassified; otu_1917
D392P32FI10:	Archaea; Thermoplasmata_Eury; Thermoplasmatales; Thermoplasmatales; Ferroplasmaceae; Ferroplasma; otu_118
D392P32FI11:	Bacteria; Nitrospirae; Leptospirillaceae; Leptospirillum; Unclassified; otu_1427
D392P32FI12:	Bacteria; Nitrospirae; Leptospirillaceae; Leptospirillum; Unclassified; otu_1427
D392P32FI14:	Bacteria; Proteobacteria; Alphaproteobacteria; Acetobacterales; Acetobacteraceae; Acidocella; otu_1562
D392P32FI15:	Bacteria; Firmicutes; Clostridia; Peptostreptococcaceae; Peptostreptococcus_anaerobius; Clostridium_bifermentans; Unclassified; otu_1213
D392P32FI16:	Bacteria; Proteobacteria; Gammaproteobacteria; Xanthomonadales; Xanthomonadales; gamma_proteobacterium_WJ2; otu_2136
D392P32FI17:	Bacteria; Proteobacteria; Gammaproteobacteria; Xanthomonadales; Xanthomonadales; gamma_proteobacterium_WJ2; otu_2136
D392P32FI18:	Bacteria; Nitrospirae; Leptospirillaceae; Leptospirillum; Unclassified; otu_1427

Sequence	Hugenholtz Taxonomic String
D392P32FI19:	Bacteria; Proteobacteria; Alphaproteobacteria; Acetobacterales; Acetobacteraceae; Acidiphilium; otu_1560
D392P32FI1:	Bacteria; Nitrospirae; Leptospirillaceae; Leptospirillum; Unclassified; otu_1427
D392P32FI21:	Bacteria; Planctomycetes; WPS-1; CL500-3; CL120-56; DE613; otu_1549
D392P32FI23:	Bacteria; Proteobacteria; Gammaproteobacteria; Acidithiobacillaceae; Acidithiobacillus; otu_1857
D392P32FI3:	Bacteria; Acidobacteria; Acidobacteriales; Unclassified; otu_179
D392P32FI4:	Bacteria; Proteobacteria; Gammaproteobacteria; Acidithiobacillaceae; Acidithiobacillus; otu_1857
D392P32FI5:	Bacteria; Proteobacteria; Gammaproteobacteria; Acidithiobacillaceae; Acidithiobacillus; otu_1857
D392P32FI6:	Bacteria; Proteobacteria; Gammaproteobacteria; B2M28; otu_1880
D392P32FI7:	Bacteria; Firmicutes; Clostridia; Peptostreptococcaceae; Peptostreptococcus_anaerobius; Clostridium_bifermentans; Unclassified; otu_1213
D392P32FI8:	Bacteria; Cyanobacteria; Chloroplasts; Euglena; Unclassified; otu_763
D392P32FK10:	Bacteria; Proteobacteria; Gammaproteobacteria; Xanthomonadales; Xanthomonadales; gamma_proteobacterium_WJ2; otu_2136
D392P32FK11:	Bacteria; Nitrospirae; Leptospirillaceae; Leptospirillum; Unclassified; otu_1427
D392P32FK12:	Bacteria; Firmicutes; Clostridia; Peptostreptococcaceae; Peptostreptococcus_anaerobius; Clostridium_bifermentans; Unclassified; otu_1213
D392P32FK14:	Bacteria; Proteobacteria; Gammaproteobacteria; Acidithiobacillaceae; Acidithiobacillus; otu_1857
D392P32FK15:	Bacteria; Cyanobacteria; Chloroplasts; Euglena; Euglena_stellata; otu_764
D392P32FK16:	Bacteria; Nitrospirae; Leptospirillaceae; Leptospirillum; Unclassified; otu_1427
D392P32FK17:	Bacteria; Acidobacteria; Acidobacteriales; Unclassified; otu_179
D392P32FK19:	Bacteria; Proteobacteria; Gammaproteobacteria; Acidithiobacillaceae; Acidithiobacillus; otu_1857
D392P32FK1:	Bacteria; Proteobacteria; Gammaproteobacteria; Xanthomonadales; Xanthomonadales; gamma_proteobacterium_WJ2; otu_2136
D392P32FK21:	Bacteria; Proteobacteria; Alphaproteobacteria; Acetobacterales; Acetobacteraceae; Acidiphilium; otu_1560
D392P32FK23:	Bacteria; Nitrospirae; Leptospirillaceae; Leptospirillum; Unclassified; otu_1427
D392P32FK2:	Bacteria; Proteobacteria; Gammaproteobacteria; Xanthomonadales; Xanthomonadales; gamma_proteobacterium_WJ2; otu_2136
D392P32FK3:	Bacteria; Nitrospirae; Leptospirillaceae; Leptospirillum; Unclassified; otu_1427
D392P32FK5:	Bacteria; Nitrospirae; Leptospirillaceae; Leptospirillum; Unclassified; otu_1427
D392P32FK6:	Bacteria; Firmicutes; Clostridia; Clostridiaceae; Clostridium; Clostridium_quinii; otu_990
D392P32FK7:	Bacteria; Cyanobacteria; Chloroplasts; Euglena; Euglena_stellata; otu_764
D392P32FK8:	Bacteria; Nitrospirae; Leptospirillaceae; Leptospirillum; Unclassified; otu_1427
D392P32FK9:	Bacteria; Proteobacteria; Gammaproteobacteria; Xanthomonadales; Xanthomonadales; gamma_proteobacterium_WJ2; otu_2136
D392P32FM10:	Bacteria; Proteobacteria; Gammaproteobacteria; Xanthomonadales; Xanthomonadales; gamma_proteobacterium_WJ2; otu_2136
D392P32FM11:	Bacteria; Planctomycetes; WPS-1; CL500-3; CL120-56; DE613; otu_1549
D392P32FM12:	Bacteria; Proteobacteria; Gammaproteobacteria; Xanthomonadales; Xanthomonadales; gamma_proteobacterium_WJ2; otu_2136
D392P32FM13:	Bacteria; Nitrospirae; Leptospirillaceae; Leptospirillum; Unclassified; otu_1427
D392P32FM14:	Bacteria; Nitrospirae; Leptospirillaceae; Leptospirillum; Unclassified; otu_1427
D392P32FM15:	Bacteria; Cyanobacteria; Chloroplasts; Euglena; Unclassified; otu_763
D392P32FM16:	Bacteria; Proteobacteria; Gammaproteobacteria; Xanthomonadales; Xanthomonadales; gamma_proteobacterium_WJ2; otu_2136
D392P32FM17:	Bacteria; Proteobacteria; Gammaproteobacteria; Acidithiobacillaceae; Acidithiobacillus; otu_1857
D392P32FM19:	Bacteria; Nitrospirae; Leptospirillaceae; Leptospirillum; Unclassified; otu_1427
D392P32FM1:	Bacteria; Proteobacteria; Gammaproteobacteria; Xanthomonadales; Xanthomonadales; gamma_proteobacterium_WJ2; otu_2136
D392P32FM21:	Bacteria; Cyanobacteria; Chloroplasts; Unclassified; otu_755
D392P32FM23:	Bacteria; Proteobacteria; Gammaproteobacteria; Xanthomonadales; Xanthomonadales; gamma_proteobacterium_WJ2; otu_2136
D392P32FM2:	Bacteria; Proteobacteria; Alphaproteobacteria; Acetobacterales; Acetobacteraceae; Acidiphilium; otu_1560
D392P32FM3:	Bacteria; Proteobacteria; Gammaproteobacteria; B2M28; otu_1880
D392P32FM4:	Bacteria; Cyanobacteria; Chloroplasts; Euglena; Euglena_stellata; otu_764
D392P32FM5:	Bacteria; Proteobacteria; Gammaproteobacteria; Acidithiobacillaceae; Acidithiobacillus; otu_1857
D392P32FM7:	Bacteria; Proteobacteria; Gammaproteobacteria; Xanthomonadales; Xanthomonadales; gamma_proteobacterium_WJ2; otu_2136
D392P32FM8:	Bacteria; Proteobacteria; Gammaproteobacteria; Xanthomonadales; Xanthomonadales; gamma_proteobacterium_WJ2; otu_2136
D392P32FM9:	Bacteria; Nitrospirae; Leptospirillaceae; Leptospirillum; Unclassified; otu_1427
D392P32FO10:	Bacteria; Cyanobacteria; Chloroplasts; Euglena; Unclassified; otu_763
D392P32FO11:	Bacteria; Nitrospirae; Leptospirillaceae; Leptospirillum; Unclassified; otu_1427
D392P32FO12:	Bacteria; Proteobacteria; Gammaproteobacteria; Acidithiobacillaceae; Acidithiobacillus; otu_1857
D392P32FO13:	Bacteria; Cyanobacteria; Chloroplasts; Unclassified; otu_755
D392P32FO14:	Bacteria; Proteobacteria; Gammaproteobacteria; CCD24; Ellin339; RCP1-57; otu_1973
D392P32FO15:	Bacteria; Proteobacteria; Alphaproteobacteria; Acetobacterales; Acetobacteraceae; Acidiphilium; otu_1560
D392P32FO16:	Bacteria; Proteobacteria; Gammaproteobacteria; Acidithiobacillaceae; Acidithiobacillus; otu_1857
D392P32FO17:	Bacteria; Proteobacteria; Gammaproteobacteria; Acidithiobacillaceae; Acidithiobacillus; otu_1857
D392P32FO19:	Bacteria; Proteobacteria; Gammaproteobacteria; B2M28; otu_1880
D392P32FO1:	Bacteria; Proteobacteria; Gammaproteobacteria; Xanthomonadales; Xanthomonadales; gamma_proteobacterium_WJ2; otu_2136
D392P32FO21:	Bacteria; Acidobacteria; Acidobacteriales; Unclassified; otu_179
D392P32FO23:	Bacteria; Proteobacteria; Gammaproteobacteria; Acidithiobacillaceae; Acidithiobacillus; otu_1857
D392P32FO2:	Bacteria; Proteobacteria; Gammaproteobacteria; Acidithiobacillaceae; Acidithiobacillus; otu_1857
D392P32FO3:	Bacteria; Proteobacteria; Gammaproteobacteria; Acidithiobacillaceae; Acidithiobacillus; otu_1857
D392P32FO4:	Bacteria; Proteobacteria; Gammaproteobacteria; Acidithiobacillaceae; Acidithiobacillus; otu_1857
D392P32FO5:	Bacteria; Proteobacteria; Gammaproteobacteria; Acidithiobacillaceae; Acidithiobacillus; otu_1857
D392P32FO6:	Bacteria; Proteobacteria; Gammaproteobacteria; Acidithiobacillaceae; Acidithiobacillus; otu_1857
D392P32FO7:	Bacteria; Proteobacteria; Gammaproteobacteria; Xanthomonadales; Xanthomonadales; gamma_proteobacterium_WJ2; otu_2136
D392P32FO8:	Bacteria; Nitrospirae; Leptospirillaceae; Leptospirillum; Unclassified; otu_1427
D392P32FO9:	Bacteria; Nitrospirae; Leptospirillaceae; Leptospirillum; Unclassified; otu_1427
D392P32RI10:	Archaea; Thermoplasmata_Eury; Thermoplasmatales; Thermoplasmatales; Ferroplasmaceae; Ferroplasma; otu_118
D392P32RI11:	Bacteria; Nitrospirae; Leptospirillaceae; Leptospirillum; Unclassified; otu_1427
D392P32RI12:	Bacteria; Nitrospirae; Leptospirillaceae; Leptospirillum; Unclassified; otu_1427
D392P32RI14:	Bacteria; Proteobacteria; Alphaproteobacteria; Acetobacterales; Acetobacteraceae; Acidocella; otu_1562
D392P32RI15:	Bacteria; Firmicutes; Clostridia; Peptostreptococcaceae; Peptostreptococcus_anaerobius; Clostridium_bifermentans; Unclassified; otu_1213
D392P32RI16:	Bacteria; Proteobacteria; Gammaproteobacteria; Xanthomonadales; Xanthomonadales; gamma_proteobacterium_WJ2; otu_2136
D392P32RI17:	Bacteria; Proteobacteria; Gammaproteobacteria; Xanthomonadales; Xanthomonadales; gamma_proteobacterium_WJ2; otu_2136
D392P32RI18:	Bacteria; Nitrospirae; Leptospirillaceae; Leptospirillum; Unclassified; otu_1427
D392P32RI19:	Bacteria; Proteobacteria; Alphaproteobacteria; Acetobacterales; Acetobacteraceae; Acidiphilium; otu_1560
D392P32RI1:	Bacteria; Nitrospirae; Leptospirillaceae; Leptospirillum; Unclassified; otu_1427

Sequence	Hugenholtz Taxonomic String
D392P32RI21:	Bacteria; Planctomycetes; WPS-1; CL500-3; CL120-56; DE613; otu_1549
D392P32RI23:	Bacteria; Proteobacteria; Gammaproteobacteria; Acidithiobacillaceae; Acidithiobacillus; otu_1857
D392P32RI2:	Bacteria; Firmicutes; Clostridia; Ruminococcus; Ruminococcus_bromii; Unclassified; otu_1257
D392P32RI3:	Bacteria; Acidobacteria; Acidobacteriales; Unclassified; otu_179
D392P32RI4:	Bacteria; Proteobacteria; Gammaproteobacteria; Acidithiobacillaceae; Acidithiobacillus; otu_1857
D392P32RI5:	Bacteria; Proteobacteria; Gammaproteobacteria; Acidithiobacillaceae; Acidithiobacillus; otu_1857
D392P32RI6:	Bacteria; Proteobacteria; Gammaproteobacteria; B2M28; otu_1880
D392P32RI7:	Bacteria; Firmicutes; Clostridia; Peptostreptococcaceae; Peptostreptococcus anaerobius; Clostridium bifermentans; AKIW475; otu 1214
D392P32RI8:	Bacteria; Cyanobacteria; Chloroplasts; Unclassified; otu 755
D392P32RK10:	Bacteria; Proteobacteria; Gammaproteobacteria; Xanthomonadales; Xanthomonadales; gamma_proteobacterium_WJ2; otu_2136
D392P32RK11:	Bacteria; Nitrospirae; Leptospirillaceae; Leptospirillum; Unclassified; otu_1427
D392P32RK12:	Bacteria; Firmicutes; Clostridia; Peptostreptococcaceae; Peptostreptococcus_anaerobius; Clostridium_bifermentans; Unclassified; otu_1213
D392P32RK14:	Bacteria; Proteobacteria; Gammaproteobacteria; Acidithiobacillaceae; Acidithiobacillus; otu_1857
D392P32RK15:	Bacteria; Cyanobacteria; Chloroplasts; Euglena; Unclassified; otu_763
D392P32RK16:	Bacteria; Nitrospirae; Leptospirillaceae; Leptospirillum; Unclassified; otu_1427
D392P32RK17:	Bacteria; Acidobacteria; Acidobacteriales; Unclassified; otu_179
D392P32RK19:	Bacteria; Proteobacteria; Gammaproteobacteria; Acidithiobacillaceae; Acidithiobacillus; otu 1857
D392P32RK1:	Bacteria; Proteobacteria; Gammaproteobacteria; Xanthomonadales; Xanthomonadales; gamma proteobacterium WJ2; otu 2136
D392P32RK21:	Bacteria; Proteobacteria; Alphaproteobacteria; Acetobacterales; Acetobacteraceae; Acidiphilium; otu_1560
D392P32RK23:	Bacteria; Nitrospirae; Leptospirillaceae; Leptospirillum; Unclassified; otu_1427
D392P32RK2:	Bacteria; Proteobacteria; Gammaproteobacteria; Xanthomonadales; Xanthomonadales; gamma_proteobacterium_WJ2; otu_2136
D392P32RK3:	Bacteria; Nitrospirae; Leptospirillaceae; Leptospirillum; Unclassified; otu_1427
D392P32RK5:	Bacteria; Nitrospirae; Leptospirillaceae; Leptospirillum; Unclassified; otu_1427
D392P32RK6:	Bacteria; Firmicutes; Clostridia; Clostridiaceae; Clostridium; Clostridium_quinii; otu_990
D392P32RK7:	Bacteria; Cyanobacteria; Chloroplasts; Euglena; Unclassified; otu_763
D392P32RK8:	Bacteria; Nitrospirae; Leptospirillaceae; Leptospirillum; Unclassified; otu_1427
D392P32RK9:	Bacteria; Proteobacteria; Gammaproteobacteria; Xanthomonadales; Xanthomonadales; gamma proteobacterium WJ2; otu 2136
D392P32RM10:	Bacteria; Proteobacteria; Gammaproteobacteria; Xanthomonadales; Xanthomonadales; gamma proteobacterium WJ2; otu 2136
D392P32RM11:	Bacteria; Planctomycetes; WPS-1; CL500-3; CL120-56; DE613; otu_1549
D392P32RM12:	Bacteria; Proteobacteria; Gammaproteobacteria; Xanthomonadales; Xanthomonadales; gamma_proteobacterium_WJ2; otu_2136
D392P32RM13:	Bacteria; Nitrospirae; Leptospirillaceae; Leptospirillum; Unclassified; otu_1427
D392P32RM14:	Bacteria; Nitrospirae; Leptospirillaceae; Leptospirillum; Unclassified; otu_1427
D392P32RM15:	Bacteria; Cyanobacteria; Chloroplasts; Unclassified; otu 755
D392P32RM16:	Bacteria; Proteobacteria; Gammaproteobacteria; Xanthomonadales; Xanthomonadales; gamma proteobacterium WJ2; otu 2136
D392P32RM17:	Bacteria; Proteobacteria; Gammaproteobacteria; Acidithiobacillaceae; Acidithiobacillus; otu_1857
D392P32RM19:	Bacteria; Nitrospirae; Leptospirillaceae; Leptospirillum; Unclassified; otu_1427
D392P32RM1:	Bacteria; Proteobacteria; Gammaproteobacteria; Xanthomonadales; Xanthomonadales; gamma_proteobacterium_WJ2; otu_2136
D392P32RM21:	Bacteria; Cyanobacteria; Chloroplasts; Euglena; Unclassified; otu_763
D392P32RM23:	Bacteria; Proteobacteria; Gammaproteobacteria; Xanthomonadales; Xanthomonadales; gamma_proteobacterium_WJ2; otu_2136
D392P32RM2:	Bacteria; Proteobacteria; Alphaproteobacteria; Acetobacterales; Acetobacteraceae; Acidiphilium; otu_1560
D392P32RM3:	Bacteria; Proteobacteria; Gammaproteobacteria; B2M28; otu_1880
D392P32RM4:	Bacteria; Cyanobacteria; Chloroplasts; Euglena; Unclassified; otu 763
D392P32RM5:	Bacteria; Proteobacteria; Gammaproteobacteria; Acidithiobacillaceae; Acidithiobacillus; otu 1857
D392P32RM6:	Bacteria; Proteobacteria; Gammaproteobacteria; CCD24; Ellin339; Unclassified; otu_1972
D392P32RM7:	Bacteria; Proteobacteria; Gammaproteobacteria; Xanthomonadales; Xanthomonadales; gamma_proteobacterium_WJ2; otu_2136
D392P32RM8:	Bacteria; Proteobacteria; Gammaproteobacteria; Xanthomonadales; Xanthomonadales; gamma_proteobacterium_WJ2; otu_2136
D392P32RM9:	Bacteria; Nitrospirae; Leptospirillaceae; Leptospirillum; Unclassified; otu_1427
D392P32RO10:	Bacteria; Cyanobacteria; Chloroplasts; Euglena; Unclassified; otu_763
D392P32RO11:	Bacteria; Nitrospirae; Leptospirillaceae; Leptospirillum; Unclassified; otu_1427
D392P32RO12:	Bacteria; Proteobacteria; Gammaproteobacteria; Acidithiobacillaceae; Acidithiobacillus; otu_1857
D392P32RO13:	Bacteria; Cyanobacteria; Chloroplasts; Unclassified; otu_755
D392P32RO14:	Bacteria; Proteobacteria; Gammaproteobacteria; CCD24; Ellin339; RCP1-57; otu 1973
D392P32RO15:	Bacteria; Proteobacteria; Alphaproteobacteria; Acetobacterales; Acetobacteraceae; Acidiphilium; otu 1560
D392P32RO16:	Bacteria; Proteobacteria; Gammaproteobacteria; Acidithiobacillaceae; Acidithiobacillus; otu_1857
D392P32RO17:	Bacteria; Proteobacteria; Gammaproteobacteria; Acidithiobacillaceae; Acidithiobacillus; otu_1857
D392P32RO19:	Bacteria; Proteobacteria; Gammaproteobacteria; B2M28; otu_1880
D392P32RO1:	Bacteria; Proteobacteria; Gammaproteobacteria; Xanthomonadales; Xanthomonadales; gamma_proteobacterium_WJ2; otu_2136
D392P32RO21:	Bacteria; Acidobacteria; Acidobacteriales; Unclassified; otu_179
D392P32RO23:	Bacteria; Proteobacteria; Gammaproteobacteria; Acidithiobacillaceae; Acidithiobacillus; otu_1857
D392P32RO2:	Bacteria; Proteobacteria; Gammaproteobacteria; Acidithiobacillaceae; Acidithiobacillus; otu_1857
D392P32RO3:	Bacteria; Proteobacteria; Gammaproteobacteria; Acidithiobacillaceae; Acidithiobacillus; otu_1857
D392P32RO4:	Bacteria; Proteobacteria; Gammaproteobacteria; Acidithiobacillaceae; Acidithiobacillus; otu 1857
D392P32RO5:	Bacteria; Proteobacteria; Gammaproteobacteria; Acidithiobacillaceae; Acidithiobacillus; otu 1857
D392P32RO6:	Bacteria; Proteobacteria; Gammaproteobacteria; Acidithiobacillaceae; Acidithiobacillus; otu_1857
D392P32RO7:	Bacteria; Proteobacteria; Gammaproteobacteria; Xanthomonadales; Xanthomonadales; gamma_proteobacterium_WJ2; otu_2136
D392P32RO8:	Bacteria; Nitrospirae; Leptospirillaceae; Leptospirillum; Unclassified; otu_1427
D392P32RO9:	Bacteria; Nitrospirae; Leptospirillaceae; Leptospirillum; Unclassified; otu_1427

Appendix Table 6.1 Taxonomic identifications with Hugenholtz nomenclature from the Greengenes classification tool (http://greengenes.lbl.gov) [*DeSantis, et al.*, 2006].

Forward and Reverse sequences are denoted by “F” and “R” within the sequence names.

[THIS PAGE INTENTIONALLY LEFT BLANK]

Chapter 7

Conclusion

7.1 Review of results and future work

As with most completed dissertations, the preceding chapters raise more questions than they answer, or even acknowledge. A few such questions, however, are so closely related to the results presented herein, and so ripe for immediate scientific inquiry, that they merit special attention.

The results presented in Chapters 2 and 3 show high sulfur solubility and significant sulfur-induced greenhouse warming on early Mars from investigating aspects of the mantle and atmosphere. Although this work does not delve into the wide range of sulfur-related geochemical interactions at the surface-atmosphere interface on ancient Mars, investigations in this realm nicely complement this work. Aspects of geochemical research involving sulfur are already underway [*Halevy, et al.*, 2007], with results indicating that an important SO_2 climate feedback may have been at play during the late Noachian. Intriguingly, the ChemCam Laser Induced Breakdown Spectrometer (LIBS) on the 2009 Mars Science Laboratory Rover will be able to remotely probe and quantify sulfur in various samples on the Martian surface, offering a unique opportunity to test hypotheses about ancient aqueous processes and the geochemical history of atmosphere/soil interactions [*Clegg*, 2007].

Chapter 4's findings about lipid biomarker preservation in the modern acid salt lake system on the Yilgarn Craton in Western Australia call for further studies of acid lakebeds preserved in the geologic record, particularly the ancient acid saline pans of the Opeche Shale in Williston Basin. The Opeche Shale dates to the Permian and consists of bedded evaporites and red-bed siliciclastics, with deposition having taken place in halite-dominated shallow perennial and ephemeral saline lakes [*Benison and Goldstein*, 2000]. Data on the sedimentology and mineralogy of the lithified strata at Merdiani Planum suggest that both ancient Mars and these ancient terrestrial sites precipitated a unique suite of evaporitic minerals under an arid climatic regime [*Benison, et al.*, 2007; *Benison*, 1998]; the discovery of lipid biomarkers in the Opeche Shale would galvanize and inform the search for remnant organic matter on Mars.

The long-term survival of bacteria within frozen environments in Chapter 5 also presents intriguing possibilities for future work, particularly regarding DNA maintenance and recovery from subsurface environments. The enduring metabolic activity observed in *Actinobacteria* warrants investigation as components of these repair pathways could be enlisted for medical or industrial applications requiring maintenance of DNA integrity for extended periods of time. This study also demonstrates that frozen environs, such as permafrost, may serve as an archival store of viable bacteria adapted to past paleoenvironments. This work calls for further inquiry into subsurface microbiology,

with opportunities to inform the search for life at subzero temperatures in subsurface conditions on Mars and Europa.

Even more broadly, the study of sulfur in the Martian atmosphere may reveal unexpected properties and processes, some with possible applications for our own atmosphere. Because of its similarities to Earth, Mars is a rare body in planetary science. It offers us a comparison and a contrast to the Earth, and an opportunity to understand how a planet once so similar to our own took a dramatically different path. Much can and has been learned from comparative planetology; for instance, Sherwood Rowland and Mario Molina realized that chlorine acts as a catalyst in the destruction of ozone while studying the chemistry of the Venusian atmosphere, which in turn led them to the pivotal discovery that manmade chlorofluorocarbons destroy the ozone in the Earth's stratosphere. In the case of sulfur, sulfur species can be studied as dominant players in the Martian atmosphere, while they are presently at low levels on Earth. Because our terrestrial climate has so much oxygen, sulfur dioxide is quickly oxidized into sulfate aerosols, which have a tendency to cool our climate by reflecting light back to space (a process that also happens on Mars, albeit much more slowly). For this reason, and because there is much less sulfur on Earth, industrial sulfur dioxide emissions have been subject to local regulation, where pollution leads to acid rain, but not international regulation. However, sulfur's ability to heat and cool different layers of the atmosphere may have implications for climate instabilities. This line of research may be particularly timely as climate engineering strategies are beginning to emerge, many of which that

involve injecting sulfur into the stratosphere as a way to abate to anthropogenic greenhouse warming [*Crutzen*, 2006; *Dickinson*, 1996; *Keith*, 2000]. It bears mention that the careful identification and continued study of Mars analog sites on Earth will be central to the pursuit of comparative planetology in the future.

Finally, future work could also include the ultimate experiment: sending a life detection platform to Mars. The SETG instrument is being developed as a prototype to be ready for launch as part of a NASA Mars mission during a 2016 or 2018 opportunity. SETG's approach may enable us to find life forms that are deeply divergent from or even difficult to imagine within the confines of our current biological thinking. Such a discovery would not only transform the field of biology, it would inspire the human imagination as much as any discovery in the history of modern science.

This dissertation has addressed the prospects for habitability in the late Noachian epoch of Martian history. The first half analyzed the ancient Martian climate, positing that sulfur-induced greenhouse warming may have been significant in both magnitude and duration, thereby promoting the creation of a warm, wet surface environment. The second half investigated the persistence and detection of life in Mars-like environments on Earth, in acid salt lakes, soil samples from permafrost, and an iron- and sulfur-rich acidic river, and concluded that life and its traces may survive longer in harsher environments than

previously believed and may be present in smaller, more-difficult-to-detect amounts that previously known.

The primary thrust of this dissertation, the work it builds on, and the work that one day may be built upon it, is to assist the planetary science and biology communities in understanding Mars and, eventually, searching for life there. Unquestionably, the search for life on Mars is an ambitious goal, one that, perhaps, will never be attained. But even if life is never found on Mars, the technologies developed for Mars have numerous potential applications elsewhere in the solar system, including many on our own planet. Following the dawn of the space age, satellite images and other remotely sensed data were generated from projects originally developed for the exploration of space. Society reaped countless terrestrial benefits from these extraterrestrial efforts: among them, a staggering array of technologies and techniques that allowed us to acquire data from the most inhospitable environments on Earth. At present, biology is poised for a similar revolution. The studies performed and recommended in this dissertation – the development of instruments like SETG, the study of Mars analog sites, the attempts to integrate the evidence from Mars rovers into our understanding of planetary science – although all pursued with space exploration in mind, will each contribute to our understanding of biology by deepening our ability to observe and understand these environments. With continued attention to this work, with the continued integration of innovations in genetic and biosignature analysis, we will come closer to unlocking the

mysteries of our most inaccessible parts of our biosphere: deserts and glaciers, the deep ocean, and our planet's subsurface.

7.2 References

Benison, K. C., et al. (2007), Sedimentology of Acid Saline Lakes in Southern Western Australia: Newly Described Processes and Products of an Extreme Environment, *Journal of Sedimentary Research*, *77*, 366-388.

Benison, K. C., and R. H. Goldstein (2000), Sedimentology of Ancient Saline Pans: An Example from the Permian Opeche Shale, Williston Basin, North Dakota, U.S.A, *Journal of Sedimentary Research*, *70*, 159-169.

Benison, K. C., R.H. Goldstein, B. Wopenka, R.C. Burruss, and J.D. Pasteris (1998), Extremely acid Permian lakes and ground waters in North America, *Nature*, *392*, 911-914.

Clegg, S. M., R.C. Wiens, M.D. Dyar, D.T. Vaniman, J.R. Thompson, E.C. Sklute, J.E. Barefield, B. Salle_, J.-B. Sirven, P. Mauchien, J.-L. Lacour, and S. Maurice (2007), Sulfur geochemical analysis with remote laser induced breakdown spectroscopy on the 2009 Mars Science Laboratory Rover, *38th Lunar and Planetary Science Conference,(Lunar and Planetary Science XXXVIII), held March 12-16, 2007 in League City, Texas. LPI Contribution No. 1960.*

Crutzen, P. J. (2006), Albedo Enhancement by Stratospheric Sulfur Injections: A Contribution to Resolve a Policy Dilemma?, *Climatic Change*, *77*, 211-220.

Dickinson, R. E. (1996), Climate engineering: a review of aerosol approaches to changing the global energy balance, *Climatic Change*, *33*, 279-290.

Halevy, I., et al. (2007), A Sulfur Dioxide Climate Feedback on Early Mars, *Science*, *318*, 1903-1907.

Keith, D. W. (2000), Geoengineering the climate: history and prospect, *Annual Review of Energy and the Environment*, *25*, 245-284.

[THIS PAGE INTENTIONALLY LEFT BLANK]